Morphological and architectural control of hydroxyapatite growth

Walsh, Dominic

Award date:
1995

Awarding institution:
University of Bath

MORPHOLOGICAL AND ARCHITECTURAL CONTROL OF HYDROXYAPATITE GROWTH

submitted by Dominic Walsh

for the degree of Doctor of Philosophy

of the University of Bath

1995

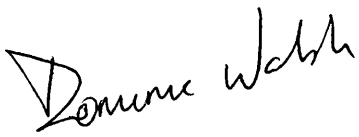

ProQuest LLC
789 East Eisenhower Parkway
P.O. Box 1346
Ann Arbor, MI 48106-1346

For my family and Baoxiu

Acknowledgements

My thanks are first due to my supervisor Professor Stephen Mann for giving me the opportunity to carry out research in the area of bio-inorganic chemistry and for his guidance throughout this study. My thanks also go to Dr. Brigid Heywood for advice during the initial stages of this study.

Secondly I wish to thank members of the bio-inorganic group, including Dr. Doug Archibald, Jeremy Hopwood, Dr. Jon Didymus and others and the staff of the Electron Optics Unit for providing training and advice on many occasions. I also wish to thank Alan Carver and Barry Chapman for running X-ray diffractions and Robert Stevens for great assistance in obtaining apparatus and chemicals.

My thanks also go to Drs. Stuart Carr and Andy Waller of Unilever Research, Port Sunlight for helpful discussions and financial support for this study. The co-funding of this studentship by the Science and Engineering Research Council is gratefully acknowledged.

CONTENTS

Foreword

Central to this thesis is the modification of the morphology of the mineral hydroxyapatite (HAP). This mineral is the model compound for the inorganic component of bones and teeth, in which it exhibits two distinct morphological types, i.e. plates or hexagonal rods. HAP with suitable properties is an ideal material for implantation in dentistry and orthopaedics and is also used in chromatography, catalysis and ion-exchange. Thus the ability to tailor its characteristics by control of the crystal size, shape, porosity and surface area could have applications in industry.

Because of its biological role there has been much interest in the mineral in the field of biomineralization. Many studies involving HAP and its growth kinetics with and without the presence of additives have been undertaken. Research has also been conducted on how biological systems are able to exert control over nucleation, growth and morphology of HAP by the utilization of specialised proteins.

Overview of thesis

This thesis begins with a discussion on some fundamental aspects of crystal growth, biomineralization, calcium phosphate phases and morphology. The first experimental work (Chapter 3) is concerned with a study of simple monosaccharides and hydroxylated additives on the morphology of HAP. The additives served as simple mimics of the extensively glycosylated molecules associated with calcification processes. Following this, chapter 4 describes a short study of the effect of the lithium ion on HAP morphology. The small size of the ion facilitates lattice incorporation and has previously been shown to produce morphological effects with other minerals such as calcium carbonate. Chapter 5 concerns a different approach to HAP morphological

modification on a macroscopic scale. Self-organized bicontinuous microemulsions constructed using a surfactant,oil and mineralizing solution were used as a medium to construct macroscopic reticulated HAP structures, the porous nature of which suggests a use as a biomaterial. Chapter 6 goes on to describe the application of this method with polymorphs of calcium carbonate and other inorganic materials. Chapter 7 describes an alternative approach in which the outer surface of self-organized galactocerebroside lipid tubules was coated with a layer of HAP. The thesis ends with some general conclusions and recommendations for future work.

CHAPTER 1

CRYSTAL GROWTH AND MORPHOLOGY OF CALCIUM PHOSPHATES

1 Crystals

1.1 Ions in solution

Ions in solution will only begin to form crystalline structures when they are at a concentration that exceeds the solubility product constant. Often in practice it is also necessary for a nucleation centre to be present in the solution. The solubility product can be defined as the thermodynamic product of the activities of the ions in a solution that is in equilibrium with a pure solid (C_nA_m) and can be expressed as:

$$K_{sp}=[C^+]^n[A^-]^m(f_{C+}f_{A-})$$

in which $[C^+]$ and $[A^-]$ are ion concentration and $f_{C+}f_{A-}$ is the product of the mean activity coefficients of the ions (Clark 1948). This assumes a homogeneous environment containing only the relevant ions. Note that it is the product of the ions, so if the concentration of either ion is raised beyond the product of the two ions this is sufficient in itself to produce crystallization (Simkiss and Wilbur 1989).

Another point to note is that the solubility product constants are specific to a particular arrangement of ions in a crystal, for crystals that can have different arrangements or polymorphs such as calcium carbonate or calcium phosphate each polymorph will have its own solubility product constant.

When the solubility product is exceeded precipitation is thermodynamically feasible and the solution is said to be supersaturated with respect to that particular phase. Thus supersaturation may be expressed by (Wong and Czernuska 1993):

$$\text{Supersaturation} = \frac{[C+]\,[A-]\,(f_C.f_A)}{Ksp} = \frac{IP}{Ksp} > 1 = ß$$

where ß = supersaturation (supersaturation when ß>1)
IP = ionic product
K_{sp} =solubility product

1.2 Nucleation

As the concentration of ions increase, assuming a homogeneous environment the ions repeatedly, possibly by stepwise reactions, associate into small clusters. They then rapidly dissociate because the energy required to form the relatively large surface area in relation to their size is too great (Simkiss and Wilbur 1989). For the clusters to grow and become stable an energy input is required, which is provided by bond formation. This may be expressed by:

$$G_N = G_{surface} + G_{solid}$$

where: G_N= energy required for formation of nucleus
$G_{surface}$= free energy at the solid-liquid interface
G_{solid}= negative energy change in the energy released by bond formation in the solid phase

With increasing ion cluster size a critical point is reached at which G_N reaches a maximum. Clusters smaller than the critical size tend to dissolve, above this size growth is energetically favoured (fig.1.0).

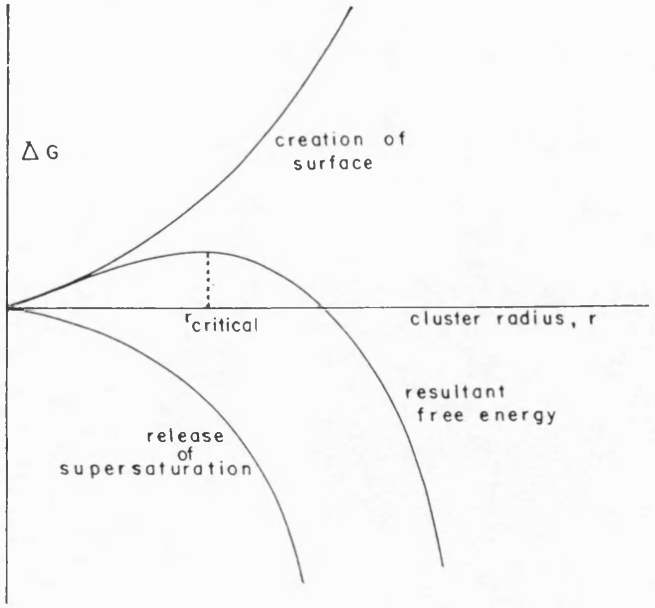

Fig. 1.0. Free energy of nucleation, ΔG, plotted as a function of cluster radius.

Thus the level of supersaturation with its concomitant tendency to release energy by precipitation determines the nuclei population initially (Nancollas 1989). If supersaturation is at too low a level the nucleation rate is at an insufficient rate to allow crystal growth. Within a range where it is possible the solution is said to be metastable. If the supersaturation is at a sufficient level or if the solution is seeded with crystals the rate of nuclei formation greatly increases and crystal growth proceeds (fig. 1.1) (Simkiss and Wilbur 1989).

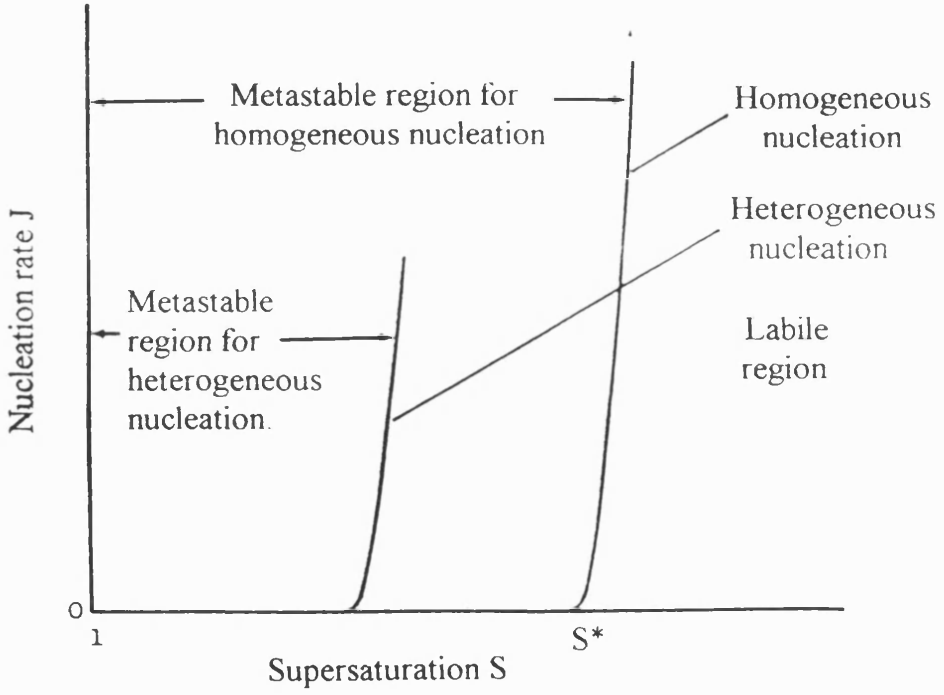

Fig.1.1. Relationship between supersaturation of the solution and the rate of crystal nucleation for homogeneous and heterogeneous nucleation.

1.3 Crystal growth

The nuclei continue to add ions onto their surfaces and form repeating identical units in three dimensions. The addition of ions to faces is not necessarily uniform however. A face can develop kinks or steps, subsequent growth is more energetically favourable to

occur at these sites (Grigor'ev 1965). Thus kinks have a tendency to become filled in leaving a step. If growth occurs along a step at a uniform rate, the step winds itself into a spiral which gives rise to a continuous source of growth sites on the crystal surface (Simkiss and Wilbur 1989). If the saturation is very high many surface nuclei will form on the crystal face and spread over the surface. With this polynucleation mechanism the crystal surface is covered by islands or surface nuclei, with many steps and kinks available for the addition of ions (Nancollas 1989).

In practice crystal growth may occur by a variety of mechanisms and the rate of growth can be determined by the rate of mass transport of ions to the crystal surfaces and/or by the surface growth mechanisms. These mechanisms can vary according to particle size, solution concentration and surface properties of the crystallites (Nielsen 1984; Mullin 1971).

1.4 Biomineralization

Biomineralization is the process by which organisms change ions in solution into solid material. It evolved abruptly in 40 to 50 million years of the Cambrian period from the processes of active transport that are necessary to maintain the osmotic balance of a lipid bound cell with its surroundings. Among divalent cations calcium is actively expelled across a membrane, whilst magnesium is accumulated intracellularly. Bicarbonate and phosphate ions are actively transported across the cell membranes and act as inorganic buffers of cells (Simkiss and Wilbur 1989).In can be envisaged that natural selection led to the exploitation of existing cell transport processes to produce a variety of mineralized products composed of the available, non-toxic and sparingly soluble ions involved in active transport processes.

In living systems various ions, molecules and bodies are abundant and will have an influence upon crystal nucleation and growth processes. Under cellular conditions *heterogeneous nucleation* conditions are present and deposition on existing surfaces can occur at lower supersaturations than with homogeneous nucleation. The activation energy is reduced by a factor Φ:

$$\Delta G_{Heterogeneous} = \Phi \Delta G_{Homogeneous}$$

The factor is related to the interaction between the foreign substrate and the growing crystal. The most effective nucleators have two surface properties in common; a moderately strong affinity for the ions which form the nucleus, and a suitable structural and electrical topography that will allow adsorbed ions to arrange themselves into a stable cluster (Eanes 1992).

1.5 Calcium phosphate

Calcium phosphate are found in very many biological minerals and this has led to great interest in the study of mechanisms of crystallization and dissolution of calcium phosphate phases. It is now widely accepted that many sparingly soluble salts crystallize via a number of precursor phases which dissolve then reprecipitate. Calcium phosphates are able to pass through a large number of phases until the least soluble hydroxyapatite ($Ca_{10}(PO_4)_6(OH)_2$, HAP) is reached. Thus an initial formation of amorphous calcium phosphate (ACP) may convert to tricalcium phosphate ($Ca_3(PO_4)_2$, TCP) or octacalcium phosphate ($Ca_8H_2(PO_4).5H_2O$, OCP) then to HAP. The similarity between HAP and OCP structures has led to the suggestion that OCP serves as a template for HAP overgrowth (Tung et al 1977). Under slightly acidic conditions a further phase dicalcium phosphate dihydrate ($CaHPO_4.2H_20$, DCPD) may be precipitated (Brown and Lehr 1959; DeRooij et al 1984).

The formation of calcium phosphate phases may be expressed as Gibbs free energy transfer between a supersaturated to a saturated solution (Nancollas 1989):

$$-\Delta G_g = (RT/\nu)\ln(IP/K_{sp}) = (RT/\nu)\ln S$$

where IP=ionic product in the supersaturated solution
K_{sp}=ionic product at equilibrium
ν=number of ions in molecule

E.g. the ionic product for HAP is given by:

$$IP=[Ca^{2+}]^{10}[PO_4^{3-}]^6[OH^-]^2 f_1^2 f_2^{10} f_3^6$$

in which the molar concentrations of the ionic species are enclosed in square brackets.

Another expression for the driving force of crystallization is given by (Nancollas 1989)

Relative supersaturation $\sigma = (IP^{1/\nu} - K_{sp}^{1/\nu})/Ksp^{1/\nu} = S-1$ where

S=supersaturation ratio

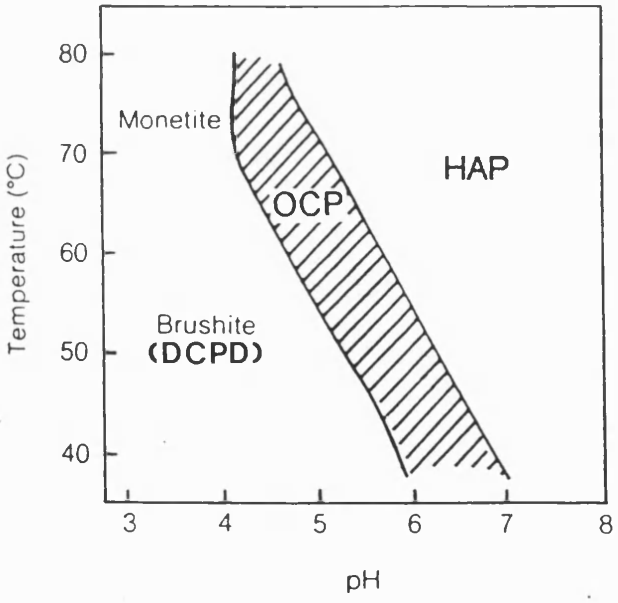

Fig. 1.2. Precipitated calcium phosphate as a function of temperature and pH.

The formation of the precursor phases may be governed by Ostwald rule of stages for the precipitation of sparingly soluble ionic salts (Ostwald 1897). This predicts that the

least stable phase having the highest solubility is formed preferentially, however it is now known that kinetic factors may override purely thermodynamic considerations. Thermodynamic calculations may also ignore the role played by existing phases which allow the epitaxial growth of further phases at much lower supersaturations than necessary by homogeneous precipitation.

A recent attempt at a model for heterogeneous precipitation has been derived making use of the Avrami-Johnson-Mehl formulae (Avrami 1939), this model takes into consideration the thermodynamic and kinetic factors present during heterogeneous precipitation (Wong and Czernuska 1993). A function for the strain energy due to lattice mismatch between crystal and substrate is included. Due to the similarity of crystal structures along certain planes (Brown et al 1962, 1981) the strain function is minimal at an OCP-HAP interface. However the greater lattice distortion between DCPD-OCP and DCPD-HAP increases the strain function accordingly.

A revised Avrami equation was constructed which has been shown to accurately predict the precipitation sequence of calcium phosphate solutions at different pH, temperature and concentration in vitro (Wong and Czernuska 1993).
This work may not however accurately predict precipitation behaviour in the presence of foreign ions and molecules, as found in vivo, due to distortion of terms in the Avrami equation.

1.6 Calcium phosphate phases

1.7 Amorphous calcium phosphate

Amorphous calcium phosphate (ACP) is an unstable precursor phase which was shown by X-ray radial distribution to consist of approximately 9.5Å spherical clusters of $Ca_9(PO_4)_6$ units (Betts and Posner 1974). The 15-20 % water present in dried ACP exists in the interstices between particles. These clusters associate to form 300-1000Å spheroids which have a characteristic, non-beam stable appearance under TEM. The $Ca_9(PO_4)_6$ unit of ACP is thought as similar or identical to the critical nucleus of HAP. Conversion to less soluble phases is believed to take place by an autocatalytic dissolution and reprecipitation process (Termine and Posner 1966).

It is possible to isolate ACP by freeze-drying and to stabilize the phase in solution when in the presence of some foreign substances. Mg^{2+} is thought to inhibit transformation by entering prenuclei structures, distorting them such that a structural mismatch is created which prevents further epitaxial growth (Posner et al 1984). Phosphorylated macromolecules such as adenosine triphosphate (ATP) are believed to prevent transformation by being adsorbed at active growth sites on embryonic nuclei, blocking further growth.

1.8 Tricalcium phosphate

Tricalcium phosphate $Ca_3(PO_4)_2$ exists as four types, two α forms and one ß form that are only stable at high pressure or temperature. A remaining ß-$Ca_3(PO_4)_2$ is made in magnesium containing aqueous solutions at room temperature. A small proportion of calcium vacancy sites exist which Mg^{2+} occupy to stabilize the structure. The mineral whitlockite $(Ca,Mg)_9(PO_4)_6$ has a similar structure to that of ß-TCP (Calvo

and Gopal 1975). Magnesium containing ß-TCP is stable and does not hydrolyze to HAP (Boskey and Posner 1974).

1.9 Octacalcium phosphate

Octacalcium phosphate ($Ca_8H_2(PO_4)_6.5H_2O$, OCP) has structural similarities to HAP and has been shown to be a precursor or at least important phase in the formation of HAP in vitro under physiological conditions (Eanes and Mayer 1987; Cheng 1987). Because of the structural similarity and the calcium deficient nature of biological apatites, OCP has been suggested as a precursor of biological calcification processes present in enamel, dentine and bone (Brown et al 1962 and 1981). Indeed the close resemblance enables interlayered mixtures of OCP and HAP to be formed epitaxially with low interfacial energy (Verbeeck et al 1992).

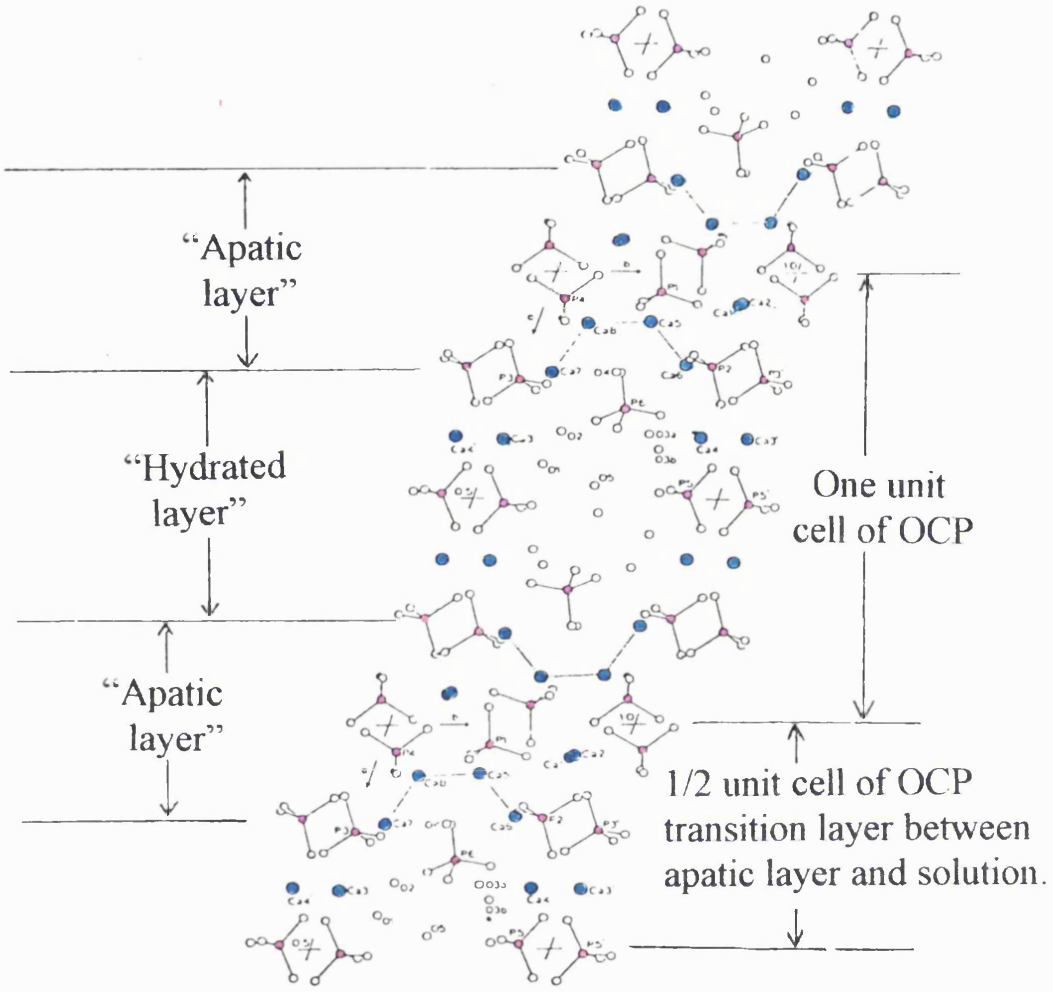

Fig. 1.4. Crystal structure of octacalcium phosphate projected down the c axis. Two unit cells are shown together with the proposed apatic and hydrated transition layer between the apatic and aqueous phase. (Adapted from *Biological Mineralization and Demineralization* (1982), Nancollas G.H. Ed.)

1.10 Hydroxyapatite

Hydroxyapatite (HAP) is generally accepted to be a model compound for biological apatites. The study of HAP and modification of its crystal habit and morphology are central to this study.

1.11 Structure of hydroxyapatite

Initially it was believed that HAP occurred only with hexagonal crystal symmetry, however a monoclinic phase has been identified (Elliot 1973).This form is made in high temperature preparations (1000-1200 ^{o}C) and is pure and defect free. It differs from hexagonal HAP in that the hydroxyl ions arranged in columns are arranged head to tail with very few reversal points. This form has the space group $P2_1/b$.

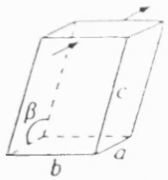

MONOCLINIC

Monoclinic system of HAP prepared at high temperature

HAP prepared by precipitation (as in this study) is of the space group $P6_3/m$ the unit cell is a rhombic prism with a width along the edge of the basal plane of a=b=9.432Å and a thickness of c=6.881Å (Kay et al 1964). The unit cell contents cannot be specified with less atoms than a formula of $Ca_{10}(PO_4)_6(OH)_2$, though the simplest formula $Ca_5(PO_4)_3OH$ is sometimes used. The hydroxyls present occur at the corners of the rhomb in columns parallel to the c axis at z=1/2. It is now known that the oxygen centres of the hydroxyls are displaced by 0.37Å from the centres of the calcium triangles rotated at 60^{o} about c at z=1/4 and 3/4 (Kay et al 1964). The calcium ions

present at these sites are known as Ca_{II} atoms and have an irregular sevenfold co-ordination with six oxygens of five phosphate groups plus the hydroxyl ion. The four remaining calcium ions of a unit cell, known as Ca_{I} atoms, occur at the acute corners at z=0 and 1/2 and are completely co-ordinated by six surrounding oxygens from orthophosphate tetrahedra.

The unit cell bound by calcium phosphate chains which form the edges of the rhomb and bisect its middle thus linking the calcium triangles (Fig. 1.5). The hydroxyl channels provide a good diffusion path for a variety of cations and anions which will substitute for existing components.

Infra red spectroscopy data have suggested that carbonate will substitute for tetrahedral phosphate in HAP prepared by precipitation at lower temperatures, as in this study (LeGeros et al 1971). In high temperature (>1000 C) HAP preparations it is believed carbonate substitutes for the column hydroxyls with a specific orientation (Elliot 1973). The HAP prepared in the study contains approximately 3% carbonate by weight despite measures to exclude CO_2. Biological apatites contain at least 4% carbonate by weight. The presence of the larger carbonate ions in the phosphate positions give rise to structural distortion which decrease their chemical stability (Nelson and Featherstone 1982).A decrease in the *a* axis and an increase in the *c* axis takes place (LeGeros et al 1967). Infra red studies have also shown (Stutman et al 1962) that hydrogen bonds occur between oxygen of adjacent orthophophate in precipitated HAP.

Thus a more accurate formula for HAP prepared by precipitation at lower temperatures is $Ca_{10-x}H_x(PO_4)_{6-y}(OH)_{2-x}.(CO_3)_y$ with x=0-2 and y=0-0.02.

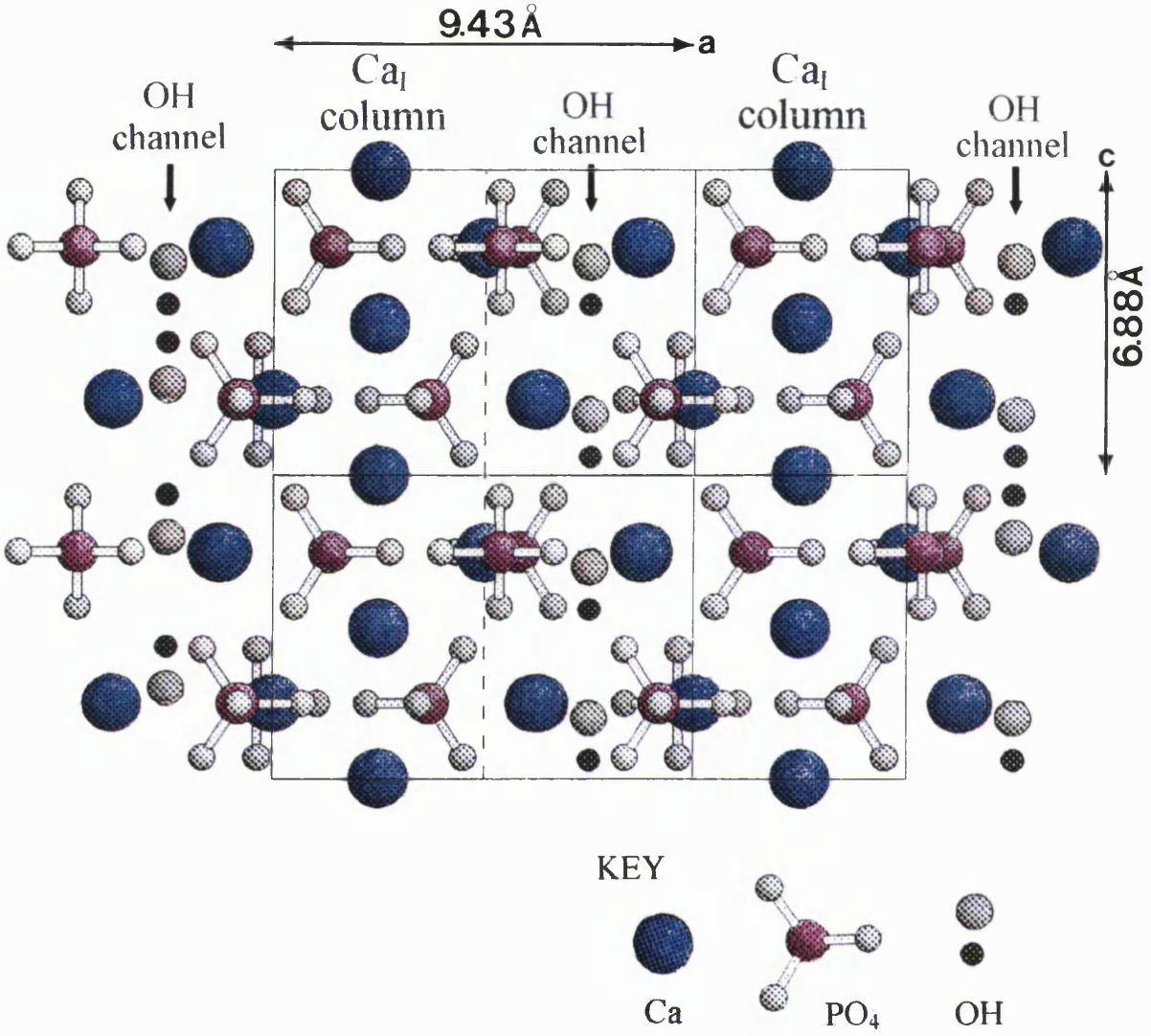

Fig.1.5. (a) Projection of the HAP structure viewed along the [100] direction.

(Diagram constructed using Atoms™ (V2.2) program, Dowty 1992)

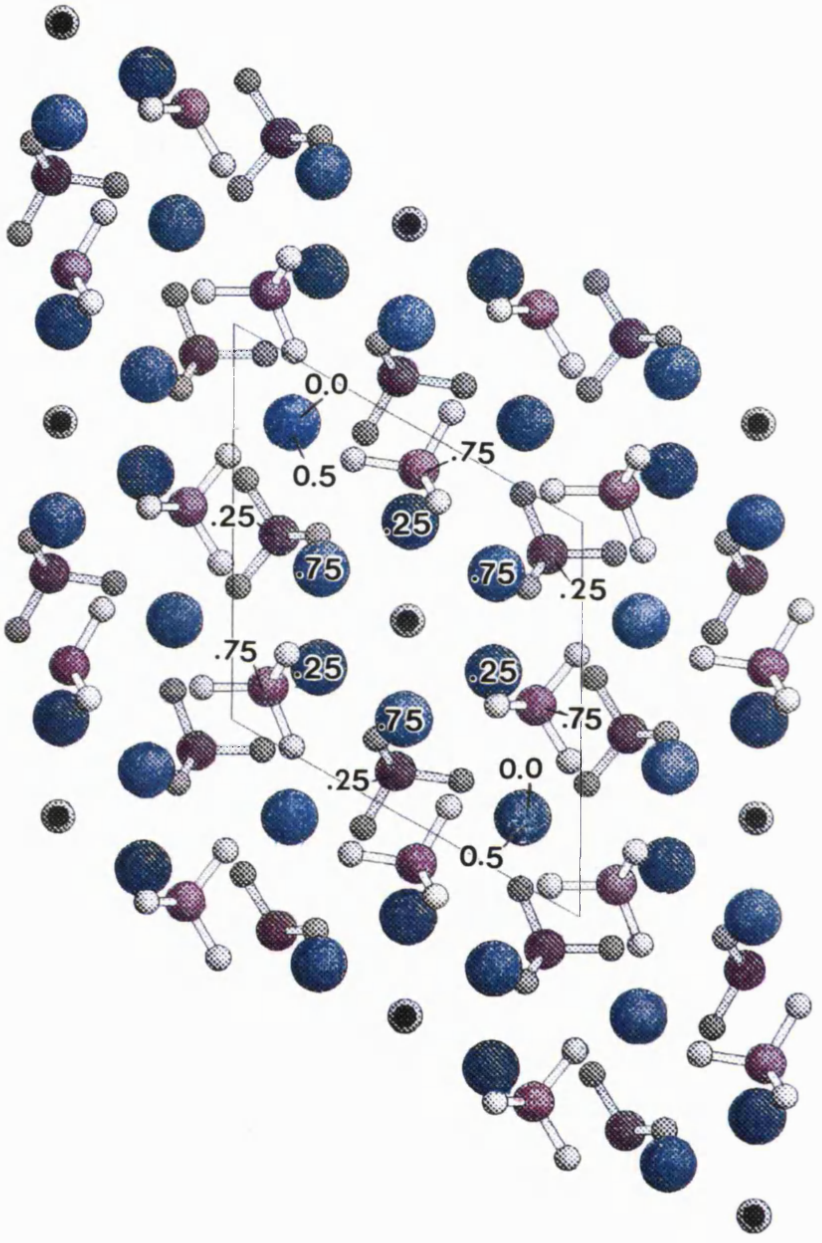

Fig. 1.5. (b) Projection of the HAP structure viewed along the [001] direction.

(Diagram constructed using Atoms™ (V2.2) program, Dowty 1992)

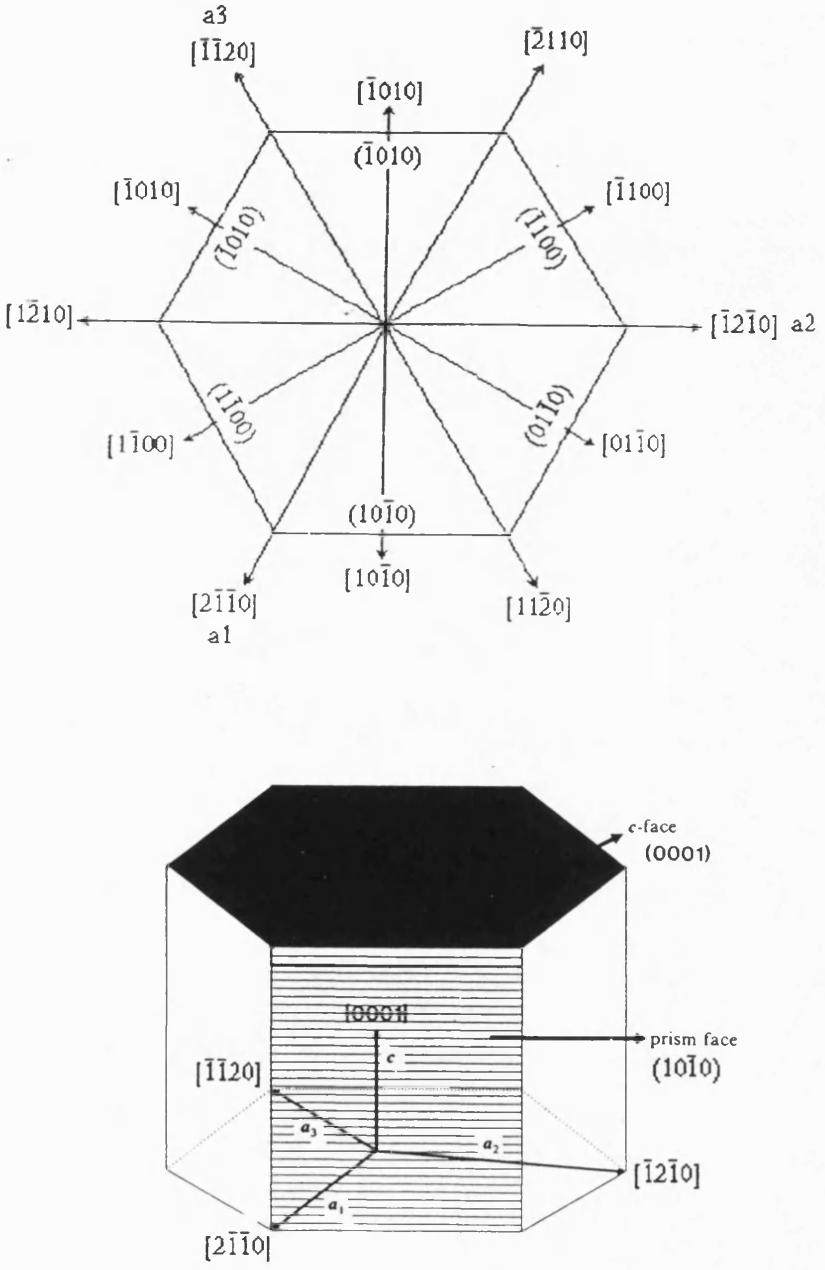

Fig. 1.6. Diagram of hexagonal system showing Miller-Bravais axes and prismatic faces. (For derivation of planes and zones see Appendix 1).

1.12 Biological apatites

Calcium phosphates are present in a variety of organisms and have a variety of functions (table 1.1) (Mann 1993; Lowenstam and Weiner 1989).The biological apatites bone, enamel, dentine and cementum are composed of calcium phosphates, principally an HAP like mineral together with an assemblage of other macromolecules the largest component being collagen.

Formula	Organism	Location	Mineral	Function
$Ca_{10}(PO_4)_6(OH)_2$	Vertebrates	Bone	Hydroxyapatite	Endoskelton /ion store
	Mammals	Teeth		Cutting/ grinding
	Fish	Scales		Protection
$Ca_8H_2(PO_4)_6$	Vertebrates	Bone/ teeth	OCP	Precursor phase
------	Chitons	Teeth	Amorphous	Precursor phase
	Gastropoda	Gizzard		Crushing
	Bivalves	Gills		Ion store
	Mammalia	Mitocondria		Ion store
	Cow	Milk		Ion store

Table 1.1. Table of calcium phosphates present in living organisms.

A large variety of trace constituents such as Mg^{2+}, Na^{+}, CO_3^{2-}, Cl^{-}, (LeGeros 1981), Sr^{2+} (Nancollas and Koutsoukos 1981), F^{-} (Baud and Bangs 1975) and $P_2O_7^{4-}$ (Fleisch and Bisaz 1962) can also be present. Some of these ions can enter the crystal lattice whilst others remain adsorbed only at surface sites. Chloride and fluoride anions substitute for hydroxyls.

The chloride ions are situated further from the mirror planes perpendicular to the c axis than are hydroxyls (LeGeros 1974). Chloride containing apatites have been shown to be less stable than normal apatite (LeGeros 1974). The average chloride content of human enamel is about 0.25 wt.%, bone and dentine contain less than 0.01wt % (LeGeros 1967 and 1974). Biological fluids contain significant concentrations of Cl^- ions but only very small quantities are incorporated . Even in aqueous systems the maximum incorporation is only 3wt.% (LeGeros 1974 and 1981). This suggests that there is discrimination against Cl^- incorporation, it may be that in biological systems the environment of forming apatite is particularly effective in discriminating against Cl^- .

Conversely there is a marked discrimination in favour of fluoride incorporation. The presence of fluoride results in increased crystal size, decrease in strain, contraction of the *a* axis and increased chemical and thermal stability (Baud et al 1975). Fluoride can compensate for the paracrystalline disorder brought about by the presence of carbonate. The fluoride ions lie in the plane of the calcium triangles and co-ordination between the fluorides is thus greater. The diffusion of acidic substances along the channels formed by fluoride containing calcium triangles is retarded and this is probably why the presence of fluoride allows dental enamel to be more resistant to acid attack (Baud et al 1975, Eanes 1979).

The presence of extraneous ions may play an important role in determining the nucleation, crystal growth, morphology, aggregation, ion-exchange, adsorption and dissolution properties of HAP. Bone tissue contains a large proportion of ACP that

represents the beginnings of the calcification process. The ACP is in a zone between osteoblast cells and crystal rich matrix (Molnar 1959).

An essential component in the deposition of calcium phosphates to form bone is the role played by collagen. The basic structural unit, called tropocollagen (285kd) consists of three polypeptide chains of the same size. The composition of the chains depends on the type of collagen. Type I collagen, present in bone, consists of two chains of one kind (a1(I)) and one of another (a2(I)). Collagen contains two amino acids found in very few other proteins i.e. 5-hydroxylysine and 4-hydroxyproline. The hydroxylysine units of collagen are covalently bound to carbohydrate units. A disaccharide of glucose and galactose is often present (Stryer 1988).

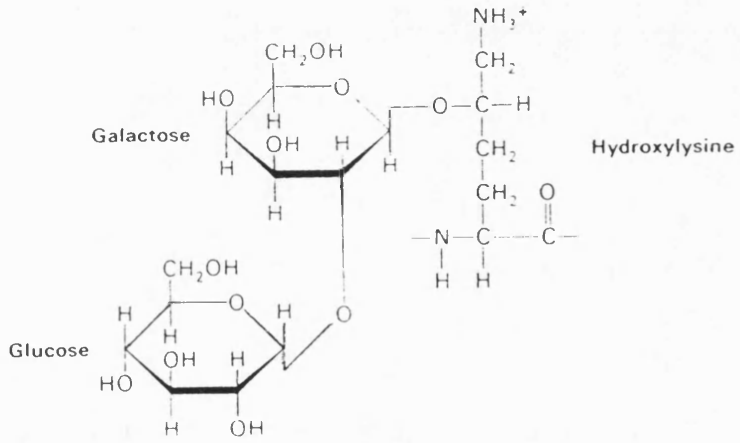

Fig.1.7. A carbohydrate unit in collagen.

At the sites of bone and teeth formation, cartilage and dentine, proteoglycans and glycosaminoglycans are believed to play a role in the regulation of calcification processes. Proteoglycans are believed to confer cartilage with its cation binding and anion excluding properties. The polysaccharide chains in proteoglycans are made up disaccharide repeating units containing a derivative of an amino sugar, either glucosamine or galactosamine (Stryer 1988, p276). Thus the presence of sugar units feature prominently in the organic assemblies governing calcification processes.

1.13 Bone and enamel

Bone HAP when examined by TEM appears as broad platelets up to 400Å in length,nearly as wide and 50Å thick. This morphology is consistent with the appearance of plates together with dense ridges, (previously mistaken for needles), which correspond to the view of the plate edge-on. The platy character of bone crystallites has also been investigated by tilting the specimen to produce stereo-micrographs. The morphology of HAP crystals that form dental enamel differ markedly from bone crystals. Mature enamel crystallites can be described as flattened hexagonal prisms, average thickness values for human crystallites have been given as 263±22Å and 683±135Å width, the average width to thickness ratio being 2.59±0.4 (Daculsi and Kerebel 1978). Heywood et al (1991) has shown that bone plate-like HAP is brought about by suppression of growth along the [001] direction and enhancement of the prismatic (-110) and (1-10) faces and the expression of a (110) plane (fig. 1.8).

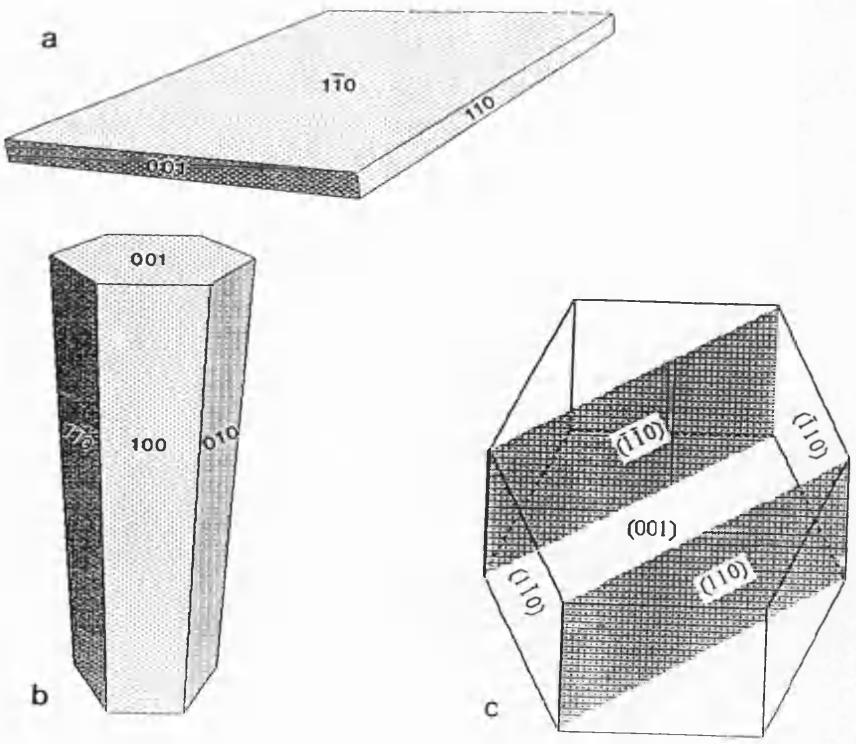

Fig. 1.8. Diagram of (a) plate-like, (b) needle-like HAP crystals and (c) needle-like HAP showing (110) planes expressed in plates.

1.14 Morphology

The shape or morphology that a crystal develops in a supersaturated solution can be related to the arrangement and processes occurring at its surface. Gibbs (Gibbs 1906) showed that for a crystal in equilibrium with its surroundings the sum of the specific surface free energy of a particular face and the area of that face will be at a minimum. Thus the crystal structure can be used (very approximately) to predict crystal morphology on an energy basis.

Wulff (Wulff 1901), Liebmann (Liebmann 1914) and later von Laue (von Laue 1943) showed the Gibbs condition to be equivalent to the statement that a point can be located in the crystal (the Wulff point) from which the distances to the different crystal faces are proportional to the specific surface free energies. Therefore, the surface area of a crystal face, and consequently its morphological importance, decreases with increasing surface free energy. In order to greatly simplify the application of the theory to practical problems the surface free energy term was replaced by surface energies as defined by Born (Born 1923). This means that only bond energies were taken into account.

Later Harman and Perdok (Hartman and Perdok 1955) devised the use of an 'attachment energy' which was defined as the bond energy released when one building unit is attached to the surface of a crystal. This approach assumes that as bond energy increases the time needed for bond formation decreases. Therefore with increasing attachment energy of a particular crystal face the less it will be expressed as it moves away from the growth centre. This approach was found to give a very reasonable guide to the morphological importance (MI) of a particular face when compared to observed

morphologies. Hartman and Perdok came to three general conclusions regarding there technique;

1) For crystal growth to follow a direction of a strong bond, the bonds must exist as an uninterrupted chain through the structure.

2) If a chain of bonds contains a weak bond, this bond determines the influence of the chain on the crystal shape.

3) Important zones are parallel to bond chains containing only strong bonds.

Strong bonds are taken as bonds that release a high amount of energy in the crystallization process. Such a chain of strong bonds is called a complete periodic bond chain (PBC), periodic because the chains are connected at regular intervals to a structurally equivalent one.

To obtain a general morphological picture of a crystal species the crystal faces were divided into three classes depending on their positions with respect to the PBC vectors;

F-faces or flat faces containing two or more coplanar PBC vectors, the attachment of a building unit to this face evolves only a small amount of bond energy.

S-faces or stepped faces containing one PBC vector, when a building unit attaches to this face at least one more strong bond is formed than with an F-face.

K-faces or kinked faces containing no PBC vector, attachment to this face will result in at least one more strong bond than an S-face.

Hence the displacement velocity for the F-face is smallest and these faces will become the larger final faces, other faces are most likely to be S-faces and K-faces are usually not observed. In practice when the model is applied to specific cases the S and K faces

are considered to grow so relatively rapidly that they are not expected to be expressed and are thus not usually determined.

Two versions of the PBC concept have been used more recently; primitive PBC and complete PBC. In the latter case side branches are added to one or more primitive PBC's so that a complete PBC is obtained having a stoichiometric composition. The whole crystal can then be partitioned into equal complete PBC's. An F face can also be defined as a crystallographic face (*hkl*) parallel to a two-dimensional slice where all the points are connected to each other by paths of bonds. Such a slice is known as a connected net or F slice. The Hartman Perdok theory has been further developed by Strom (Strom 1980, 1981) using graph theory. This made computerized determination of connected nets possible. As available computational power has greatly increased the sophistication of model systems has also increased, however they are all based on the premise that the slowest growing face has the least number of vacant co-ordination sites.

1.15 Morphological development of amorphous material

When growth initiates from a point there is likely to be a high level of supersaturation in its environment. Thus there will be a plentiful supply of material so that a building unit, once attached to the points surface will very rapidly be overgrown before it can detach and return to the disordered phase. At this time many zones grow out from the centre at approximately the same rate. The attachment energy is not yet an important factor. Thus a poorly ordered amorphous material with overall isotropy will grow as a *spherical* particle. As time proceeds the degree of supersaturation decreases and the attachment energy can begin to control the development of the particle, which starts to

develop faces and become anisotropic. If the growth conditions remain constant no new faces can be formed which were not originally present.

1.16 Effect of solvent

Studies have shown that crystal habit can be altered greatly depending on the solvent (Wells 1946). Molecules of solvent may adsorb to certain faces of the developing crystal so that the formation of a new bond in the structure involves the breaking of the adsorption bond. Thus the overall amount of energy released in the crystallisation process may be lowered to the extent that the normal development of morphology is altered.

1.17 Determination of growth forms

In order to determine the relative growth rate of different crystallographic forms (*hkl*) E^{slice}_{hkl} and E^{att}_{hkl} terms are calculated (Hartman 1973). E^{slice}_{hkl} is the energy of a molecule or stoichoimetric unit within the connected net under consideration. E^{att}_{hkl} is the energy to remove a stoichoimetric unit from its crystallographic position on the connected net. The terms are related by:

$$E^{cr} = E^{att}_{hkl} + E^{slice}_{hkl}$$

where E^{cr} is the crystallization energy, which is a bulk property independent of the connected net under consideration. In order to construct growth forms it is assumed that the rate of growth R_{hkl} of a face (*hkl*) of a crystallographic form {*hkl*} is proportional to E^{att}_{hkl}. Using this proportional relationship growth forms can be predicted which are in good agreement with observed growth forms (Weissbuch et al 1983).

1.18 F-slices of HAP

The F-slices (where there are two or more interconnected PBC's) have previously been determined for HAP (Terpstra et al 1986) and are shown in fig. 1.9).

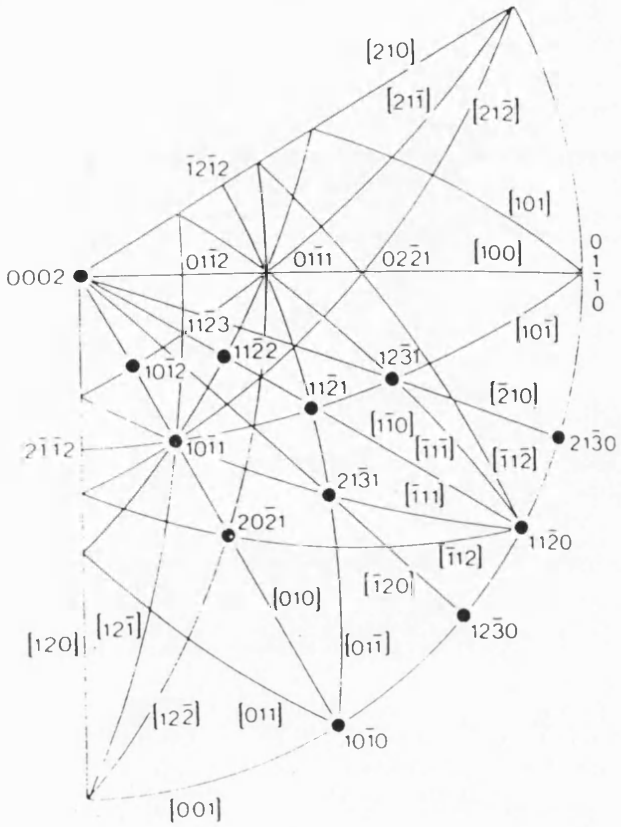

Fig. 1.9. Stereographic projection of HAP. The points of intersection of the zones parallel to a periodic bond chain (PBC) direction are potential F faces. The dots are F faces that were found on observation. (Adapted from Terpstra et al 1986).

1.19 Effect of additives on morphology

If an additive is present in a solution in which a crystal is developing it may have an influence on the morphological development of the crystal if it shows any affinity to the developing crystal surface. If the affinity is with all of the crystal faces equally the growth may be inhibited but the overall morphology will not be altered significantly. If the additive has a interaction with a specific face which inhibits its development that face will tend to increase in relative size as growth proceeds. This can have significant

consequences on the development of morphology (fig.1.10). Additives may chosen that are similar in structure to host molecular crystal molecules so that the additive or guest molecules can be incorporated into the lattice and give rise to a localized disruption which may in turn produce a change in morphological development (Weissbuch et al 1991).

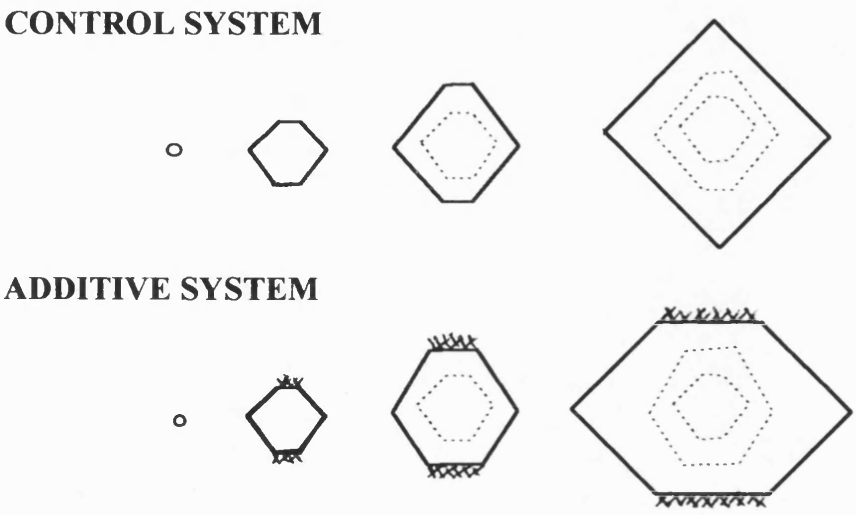

Fig. 1.10. Effect of a face specific additive on the development of morphology.

REFERENCES

Avrami, M. (1939) , J. Chem. Phys., **7**, 1103.

Baud C.A., Bangs S. Very J.M. (1977), *Minor Elements in Bone Mineral and their Effects in its Solubility*. J. Biol. Buccale **5**, 105-202.

Betts F., Posner A.F. (1974), *A Structural Model for Amorphous Calcium Phosphate*, Trans. Am. Cryst. Assoc., **10**, 73-84.

Boskey A.L., Posner A.S. (1974), *Magnesium Stabilization of Amorphous Calcium Phosphates: a Kinetic Study*, Mater. Res. Bull., **9**, 907-914.

Brown W.E., Lehr J.R. (1959), *Application of Phases Rule to the Chemical Behaviour of Monocalcium Phosphate Monohydrate in Soils*, Soil Sci. Soc. Amer. Proc., **23**, 7-12.

Brown W.E., Smith J.P., Lehr J.R., Frazer A.W. (1962), *Crystallographic and Chemical Relations Between OCP and HAP*, Nature, **196**, 1050-1054.

Brown W.E. (1966), *Crystal Growth of Bone Mineral*, Clin. Orth.Rel.Res., **44**, 205-220.

Brown W.E., Mathew M., Tung M.S. (1981), *Crystal Chemistry of OCP*, Prog. Crystal Growth Charact. **4**, 59-87.

Calvo C., Gopal R. (1975), *The Crystal Structure of Whitlockite from the Palermo Quarry*, Am. Min., **60**, 120-133.

Cheng P.T. (1987), *Formation of Octacalcium phosphate and Subsequent Transformation to Hydroxyapatite at Low Supersaturation-A Model for Cartilage Calcification.*, Calcif. Tissue. Int., **40(6)**, 339-343.

Clark W.M. (1948), *Topics In Physical Chemistry*, Williams and Wilkins, Baltimore, Maryland.

Daculsi G., Kerebel B. (1978), *High-Resolution Electron Microscope Study of Human Enamel Crystallites:Size, Shape and Growth*, Jr. of Ultrastruc. Res.,**65**,163-172.

DeRooij J.F., Heughebaert J.C., Nancollas G.H. (1984), *A pH Study of Calcium Phosphate Seeded Precipitation*, J. Coll. Int. Sci., **100**, 350-358.

Eanes E.D., Meyer J.L. (1977), *The Maturation of Crystalline Calcium Phosphates in Aqueous Suspensions at Physiological pH*, Calcif. Tissue Res., **23**, 259-269.

Eanes E.D. (1979), *Enamel Apatite:Chemistry, Structure and Properties.*, J. Dent. Res., **58**, 829-834.

Elliot J.C., Mackie P.E., Young R.A. (1973), *Monoclininc Hydroxyapatite*, Science, **180**, 1055-1057.

Fleisch H, Bisaz S. (1962), *Role of Collagen, Pyrophosphate and Pyrophosphatase in Calcification*, Bone Tooth Proc. European Symp. 1st., Oxford, 249-256.

Gibbs J.W. (1906), *On the Equilibrium of Heterogeneous Substances*, Scientific Papers, vol. 1., 315-316, 320-322, 324-326.

Grigor`ev D.P. (1965), *Ontogeny of Minerals*, Israel Program for Scientific Translations, Jerusalem.

Hartman P., Perdok W.G. (1955),*On the Relations Between Structure and Morphology of Crystals I and II,* Acta. Cryst., **8**, 49-52, 521-529.

Hartman P. (1973), *Structure and Morphology in: Crystal Growth: An Introduction*, Ed. Hartman P., North Holland, Amsterdam, p367.

Heywood B.R., Sparks N.H.C., Shellis R.P, Weiner S., Mann S. (1990), *Ultrastructure, Morphology and Crystal Growth of Biogenic and Synthetic Apatites*, Conn. Tiss. Res, **25**, 1-17.

Kay M.I., Young R.A., Posner A.S. (1964), *Crystal Structure of Hydroxyapatite*, Nature, **204**, 1050-1052.

Koutsoukos P.G., Nancollas G.H. (1981), *The Morphology of Hydroxyapatite Grown in Aqueous Solution at 37°C*, J. Cryst. Growth, **55**, 369-375.

Laue M. von (1943), *The Wulff Theorem for the Equilibrium Form of Crystals,* Z. Kristallogr, **105**, 124-133.

Liebmann H. (1914), Z. Kristallogr, **53**, 171.

LeGeros R.Z. (1967), *Apatite crystalline: Effects of Carbonate on Morphology*, Science, **155**, 1409-1411.

LeGeros R.Z., Trautz O.R., LeGeros J.P., Klein E. (1967), *Carbonate Substitution in Apatite Structure*, Collern Int. Sur Les Phosphates Mineraux Solides, Toulose, pp66-72.

LeGeros R.Z., LeGeros J.P., Trautz O.R., Slurra W.P. (1971), *Conversion of Monetite, $CaHPO_4$, to Apatites: Effect of Carbonate on th Morphology of Apatite Crystallites*, Advances in X-Ray Analysis, **14**, 57-66.

LeGeros R.Z. (1974), *The Unit-Cell Dimensions of Human Enamel Apatite: Effect of Chloride Incorporation*, Arch. Oral Biol. **20**, 63-71.

LeGeros R.Z. (1981) *Apatites in Biological Systems*. Prog. Crystal Growth Charact., **4**, 1-45.

Molnar Z. (1959), Development of *Parietal Bone of Young Mice. I. Crystals of Bone Mineral in Frozen-dried Preparations*, J. Ultrastruct. Res., **3**, 39-45.

Nancollas G.H, Koutsoukos P.G. (1981), *Influence of the Strontium Ion on the Crystallization of Hydroxyapatite from Aqueous Solution*, J. Am. Chem. Soc., **85**, 2403-2408.

Nancollas G.H. (1989), *Calcium Phosphate Crystallization*, in Biomineralization-Chemical and Biochemical Perspectives, Mann S., Webb J., Williams R.J.P. (Eds), pp 157-186, Weinheim:VCH.

Nelson D.G.A., Featherstone J.D.R. (1982), *Preparation Analysis and Characterization of Carbonated Hydroxyapatites*, Calcif. Tissue Int, **34**, S69-S81.

Nielsen A.E. (1984), *Electrolyte Crystal Growth Mechanisms*, J. Cryst. Growth, **67**, 289-310.

Ostwald W. (1897), *Die Wissenschaftlichen Grunlagen der Analytischen Chemie*, Z. Phys. Chem, **22**, 289.

Posner A.S., Blumenthal N.C., Betts F. (1984), in *Phosphate Minerals*, Nriagu F.O., Moore P.B. (Eds), pp330-350, Springer, New York.

Simkiss K, Wilbur K.M. (1984), *The Deposition of Minerals, in Biomineralization-Cell Biology and Mineral Deposition*, pp11-20, Academic Press Inc, San Diego, California.

Stutman J.M., Posner A.S., Lippincott E.R. (1962), *Hydrogen Bonding in the Calcium Phosphates*, Nature, **193**, 368-369.

Strom C.S. (1980), Z. Krist., **153**, 99.
Strom C.S. (1981), Z. Krist., **154**, 31.

Stryer L. (1988), in *Biochemistry 3rd Ed.*, Freeman, San Francisco.

Termine J.D., Posner A.S. (1966), *Infra-red analysis of Rat Bone: Age Dependancy of Amorphous and Crystalline Mineral Fractions*, Science, **153**, 1523-1525.

Terpstra R.A., Bennema P., Hartman P., Woensdergt C.F., Perdok W.G., Senechal M.L.(1986), *F Faces of Apatite and its Morphologicy: Theory and Observation*, J. Cryst. Growth, **78**, 468-478.

Tung M.S., Brown W.E. (1977), *Characterisation and Modification of Permaselective Properties of Apatite Membranes*, Calcif. Tiss. Res., **35**, 783- .

Verbeeck M.R.H., Devenys J.A.H. (1992), *The Kinetics of Dissolution of Octacalcium Phosphate. 2. The Combined Effects of pH and Solution Calcium/Phosphate ratio.*, J. Cryst. Growth, **121**, 335-348.

Weissbach I., Addadi L., Berkovitch-Yellin Z., Gati E., Weinstein S., Lahar M., Leiserowitz L. (1983), J. Am. Chem. Soc., **105**, 6615.

Weissbach L, Addadi L., Lahav M., Leisrowitz L. (1991), *Molecular Recognition at Crystal Interfaces*, Science, **253**, 637-645.

Wong A.T.-C., Czernuska J.T. (1993), *Transformaion Behaviour of Calcium Phosphate 1. Theory and Modelling*, Colloids and Surfaces A- Physicochemical and Engineering Aspects, **78**, 245-253.

Wulff G. (1901), *On the Question of the Rate of Growth and of Dissolution of Crystal Faces*, Z. Krist., **34**, 449.

CHAPTER 2.

INSTRUMENTAL AND EXPERIMENTAL METHODS

2.0 INSTRUMENTAL AND EXPERIMENTAL METHODS

2.1 Water purification

Tapwater of fairly high hardness (320mg/l $CaCO_3$) was distilled using an Aquatron A4D commercial still with dual boilers to produce double-distilled water. This water was then fed through a Purite Standard Stillplus incorporating a 0.2μm bacterial filter and activated carbon cartridge and twin mixed bed ion-exchange columns. High quality water of conductivity 0.5-1.0μS was obtained.

2.2 Preparation of control hydroxyapatite

Hydroxyapatite was prepared under N_2 at 40° and 70°C by the pulse addition of 100 cm^3 (3.5 cm^3 aliquots at 4 minute intervals) of 0.1 M $CaCl_2$ to 100 cm^3 of 0.06 M Na_2HPO_4. The reaction vessel was stirred continuously and the pH monitored with a pH electrode (fig 2.1). Following an addition of calcium solution the pH was readjusted to between 9.3-9.8 by the addition of small quantities of 1.5 M NaOH. After *ca.*120 min. the mixture was allowed to cool, and the white precipitate filtered and washed several times with distilled water to remove residual anions. The sample was then washed with acetone, dried under vacuum and oven dried at 80°C. The precipitates were stored at room temperature in vials under N_2. Some filtered and washed samples were refluxed for 18 hours before analysis.

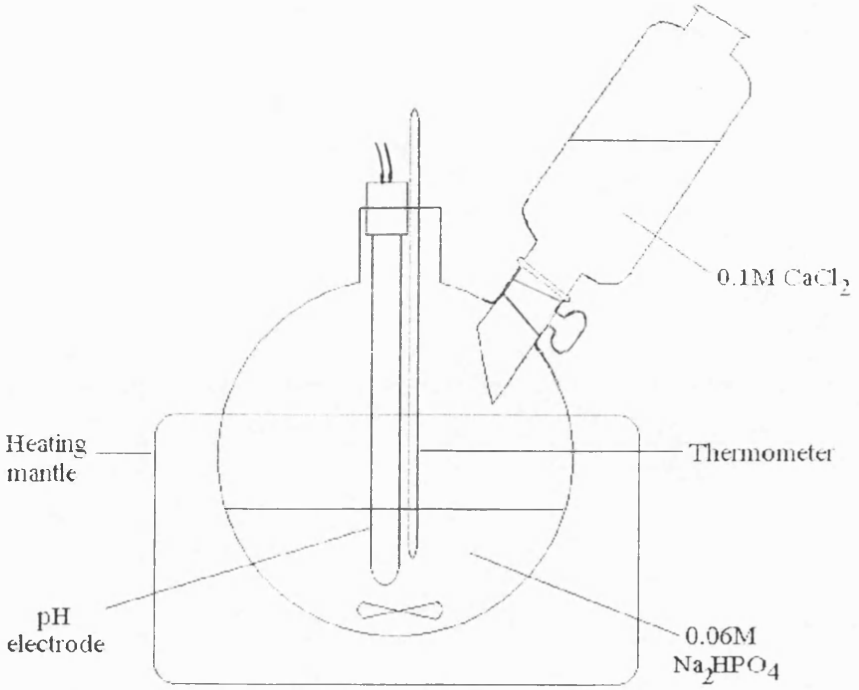

Fig. 2.1. Diagram of apparatus used for precipitation of HAP.

2.3 Calcium electrode measurements

In some preparations the concentration of calcium in the reaction vessel was monitored using a Radiometer calcium electrode. The upper operating temperature limit for the electrode was found to be 55^{o}C, therefore its use was limited to preparations at 40^{o}C only. When a pulse addition method was employed the large changes in concentration obtained on each addition produced unreliable readings. Therefore a dropwise addition method was used, pH was maintained close to 9.5 with 0.05M NaOH, employing a ABU 80 autoburrete, TTT 80 titrator, PHM 82 standard pH meter and LKB 2120 Varioperpex II peristaltic pump. A continuous plot of the calcium electrode reading in the reaction vessel as calcium solution was added was recorded. Calibration experiments with the electrode in additive and non-additive containing standard solutions produced virtually identical results, indicating that interaction of the additive with the electrode was negligible.

2.4 Analysis of Crystal Products

2.5 Transmission electron microscopy

Samples for electron microscopy were prepared by air-drying a drop of a briefly sonicated suspension of the dried precipitate in ethanol onto carbon-coated, formvar-covered copper electron microscope grids. Examination was conducted with a Jeol 2000EX high resolution transmission electron microscope operating at 200kV, this instrument has lattice resolution of 1.4Å and a point to point resolution of 2.8Å. Additionally, a Jeol 1200FX transmission electron microscope operating at 120kV was used, having a lattice resolution of 2.0Å and a point to point resolution of 4.5Å. The samples were characterized by bright field imaging and selected area electron diffraction (SAED). SAED could be conducted using field limiting apertures of 20,100 and 300μm and camera length between 13-270cm, the goniometer could be tilted along X to ±30 degrees to bring a crystal into diffraction. The corresponding TEM image could be recorded immediately after a diffraction pattern was taken.

Lattice imaging was conducted on the 2000FX, this requires that the instrument is correctly aligned and a series of micrographs taken at Gaussian (ideal focus) through to Schertzer (optimum under focus). Lattice fringes can be measured from blow-up prints calibrated using fringes from a standard graphite sample (3.36Å (002)).

Micrographic data was recorded on Agfa-Gevaert Scientia photographic plates of 100x80mm.

2.6 Sectioning studies

A small quantity of the crystals was embedded in 100% TAAB premix resin The resin was then poured into tapered moulds held upright so that the crystals would migrate to the pointed end and have a tendency to be oriented vertically. The resin was then polymerized at 60°C for 24 hours. Thin sections (60-100nm) were cut using a diamond blade and mounted onto carbon-coated mesh grids for high resolution TEM examination using a Jeol 2000FX electron microscope.

2.7 Energy dispersive X-ray analysis (EDXA)

Elemental analysis was conducted conducted on 2000FX and 1200EX microscopes (TEM mode) by energy dispersive X-ray analysis. The detector was a Link Li-drifted, silicon type and was windowless. Elements with mass greater than nitrogen are detectable in the order of 0.5%w/w, the peak areas give a good indication of relative quantity. A Link AN10000 X-ray computer microanalysis system processed the data.

2.8 Scanning electron microscopy

Samples were mounted by placing a drop of sample suspended in acetone onto a sample holder and allowing the acetone to evaporate. The mount was then gold coated for 3 minutes to prevent charging using an Edwards S150B sputter coater. Examination was then made using an Scanning Imaging Device (ASID) unit of a Jeol 1200EX electron microscope operating at 120kV. This gives much greater resolution than a standard scanning electron microscope but has the disadvantage of a relatively small area available for examination.

2.9 Fourier transform infrared spectroscopy

Samples of the dried precipitates were hand ground and mixed with KBr at approximately 5%w/w solid and then pressed into KBr disks. The spectra were recorded at $4cm^{-1}$ resolution on a Nicolet 510P fourier transform infra-red (FTIR) spectrometer. Characteristic bands for stoichiometric HAP are shown in table 2.1 (Fowler, Moreno and Brown 1966, Nelson and Featherstone 1982).

Assignment	Wavenumber (cm^{-1})
ν_s OH stretch (weakly H bonded)	3570 (shp)
ν_3 CO_3^{2-}	1660-1370 (b)
ν_3 PO_4^{3-}	1030-1090 (b)
V_L OH librational	630 (shp)
ν_4''' PO_4^{3-}	605 (shp)
ν_4' PO_4^{3-}	565 (shp)

Table 2.1. Table of infrared assignments of carbonated hydroxyapatite

The bands at $3570cm^{-1}$ and $630cm^{-1}$ have been assigned to the hydroxyl stretch and librational mode of the hydroxyl ion.The hydroxyl stretch at $3570cm^{-1}$ is somewhat lower than might be expected and generally the lowering of the ν_s(OH) frequency is regarded as strong evidence for hydrogen bonding. There is evidence that this lowering is due to a weak hydrogen bond of the O-H..OPO_3 type. The band at $630cm^{-1}$ has been shown to shift on deuteration, also this particular band is absent in the spectrum of fluoroapatite.The librational mode is envisaged as a complex motion that closely resembles rotation. Neutron diffraction studies (Kay, Young and Posner 1964) have

shown that the hydrogen atom of the hydroxyl ion is not localized, and a librational movement feasible.

The v_2 and v_4 vibrations of the tetrahedral PO_4 ion at 363cm^{-1} and 565 cm^{-1} are infra-red active, the infrared inactive modes v_1 and v_3 at 980 and 1080cm^{-1} become active and degenerate modes split by distortion of the PO_4 groups through lack of symmetry in the lattice sites (Fowler, Moreno and Brown 1966).

2.10 X-ray diffraction (XRD)

X-ray powder diffraction patterns of HAP samples were recorded on a Philips PW-1130 X-ray diffractometer fitted with a Debye-Scherrer camera (diameter =11.4592 cm) and CuKa radiation (a_1=1.54050 Å, a_2=1.54434 Å, weighted mean=1.5418 Å) at 40KV, 20mA for 3 hours. Samples were sonicated and placed into Lidemann capillary tubes made of highly amorphous lithium glass for analysis. The distance between entrance and exit holes is equal to 180^o 2ϕ. The d-spacings were calculated using the Bragg equation $n\lambda = 2d\sin\phi$. Lattice parameters of HAP samples were obtained from diffractograms using a Philips PW 1730 diffractometer fitted with a 4KW X-ray generator and a long fine focus 2KW copper target tube. Lattice parameters were calculated using the equation of interplanar spacings of (hkl) in hexagonal systems as follows:

$$\frac{1}{d^2hkl} = \frac{4}{3a^2}(h^2+k^2+hk) + \frac{l^2}{c^2}$$

Taking the (002) plane

d=3.4486Å h=0, k=0, l=2

$$\frac{1}{(3.4486)^2} = \frac{4}{c^2} \quad \text{therefore } c^2 = \frac{4}{\frac{1}{(3.4486)^2}} = 47.57$$

Lattice parameter c =6.89Å±0.01

Similarly (004) d=1.7229 Å gives c=6.89Å±0.01Å

Taking the (300) plane

d=2.7241Å h=3, k=0, l=0

$$\frac{1}{(2.7241)^2} = \frac{4}{3a^2} \cdot 9 = \frac{36}{3a^2} = \frac{12}{a^2}$$

$$a^2 = \frac{12}{\frac{1}{(2.72341)^2}} = 89.049$$

Lattice parameter a =9.44Å±0.01

Similarly (410) d=1.7835Å gives a=9.44Å±0.01

REFERENCES

Fowler B.O., Moreno E.C., Brown W.E. (1966), *Infra-red Spectra of Hydroxyapatite, Octacalcium Phosphate and Pyrolyzed Octacalcium Phosphate*, Arch. Oral. Biol., **11**, 477-492.

Kay M.I., Young R.A., Posner A.S. (1964), *Crystal Structure of Hydroxyapatite*, Nature, **204**, 1050-1052.

Nelson D.G.A., Featherstone J.D.R. (1982), *Preparation Analysis and Characterization of Carbonated Hydroxyapatites*, Calcif. Tissue Int, **34**, S69-S81.

CHAPTER 3.

INFLUENCE OF MONOSACCHARIDES AND RELATED MOLECULES ON THE MORPHOLOGY OF HYDROXYAPATITE

3.0 INFLUENCE OF MONOSACCHARIDES AND RELATED MOLECULES ON THE MORPHOLOGY OF HYROXYAPATITE

3.1 Introduction

Mineralized structures are believed to be formed by the growth of mineral (usually calcium carbonate or HAP) in an extracellular matrix composed largely of protein (Lowenstam 1981; Weiner, Traub and Lowenstam 1983). It has been suggested that the protein matrix contains regularly spaced calcium nucleation sites, composed of repeating points on the polypeptide chain that contain acidic amino acid side chains. Subsequent development of the mineral is also guided by the matrix (Weiner, Traub 1984; Weiner, Talmon and Traub 1983).

A number of kinetic studies of HAP crystal growth in the absence and presence of additives such as Mg^{2+} (Bigi et al 1993), CO_3^{2-} (LeGeros 1967), citrate (Werness et al 1981), pyrophosphate (Francis et al 1973), polyphosphates and polyphosphonates (Moreno 1981), albumin (Garnett et al 1990), proteoglycans (Chen et al 1984;Dziewiatkowski 1987), glysosaminoglycans (Hunter et al 1987), osteocalcin and osteonectin (Romberg et al 1986), and ATP (Christoffersen et al 1984) have been reported. Among inorganic ions Cl^- (Koutsoukos et al 1981), F^- (Okazaki 1992), CO_3^{2-} (LeGeros et al 1971), Li^+ (Nancollas et al 1986) and Sr^{2+} (Nancollas et al 1981) when present during precipitation have been shown to produce needle-like, hexagonal rod or plate-like morphologies depending on concentration. This morphological change is brought about by suppression of growth along the [001] direction and enhancement of the (1-10) face.

However there have been few counterpart studies involving soluble organic additives. This seems to overlook a probable role of organic assemblies in bringing about the significantly different HAP morphology present in contrasting biological tissue.

3.2 EXPERIMENTAL

Control HAP was prepared by pulse addition precipitation of $CaCl_2$ and $NaHPO_4$ solutions as described in chapter 2.2. Examination of the product by TEM revealed the presence of thin irregular plate-like material at both 40° and 70°C of mean dimensions, length=500nm, width=350nm and thickness=5nm (fig. 3.2a). EDXA analysis revealed the presence of calcium, phosphate and oxygen. Electron diffraction studies of crystals viewed face on produced a pattern corresponding to the [110] zone suggesting that that the plate-like particles were single crystals of HAP with two well-developed (1-10) faces (fig. 3.2b), this crystal morphology matches that reported for biological and synthetic plate-like HAP (Selvig 1970; Moradian-Oldak et al 1991; Bres, Barry and Hutchinson 1985; Cuisinier et al 1987; Heywood et al 1990).On refluxing the washed sample for 18 hours a transformation into more regular shaped crystals takes place (fig. 3.3a). Electron diffraction studies showed that the slight elongation of the crystals was along the c-axis (fig. 3.3b).

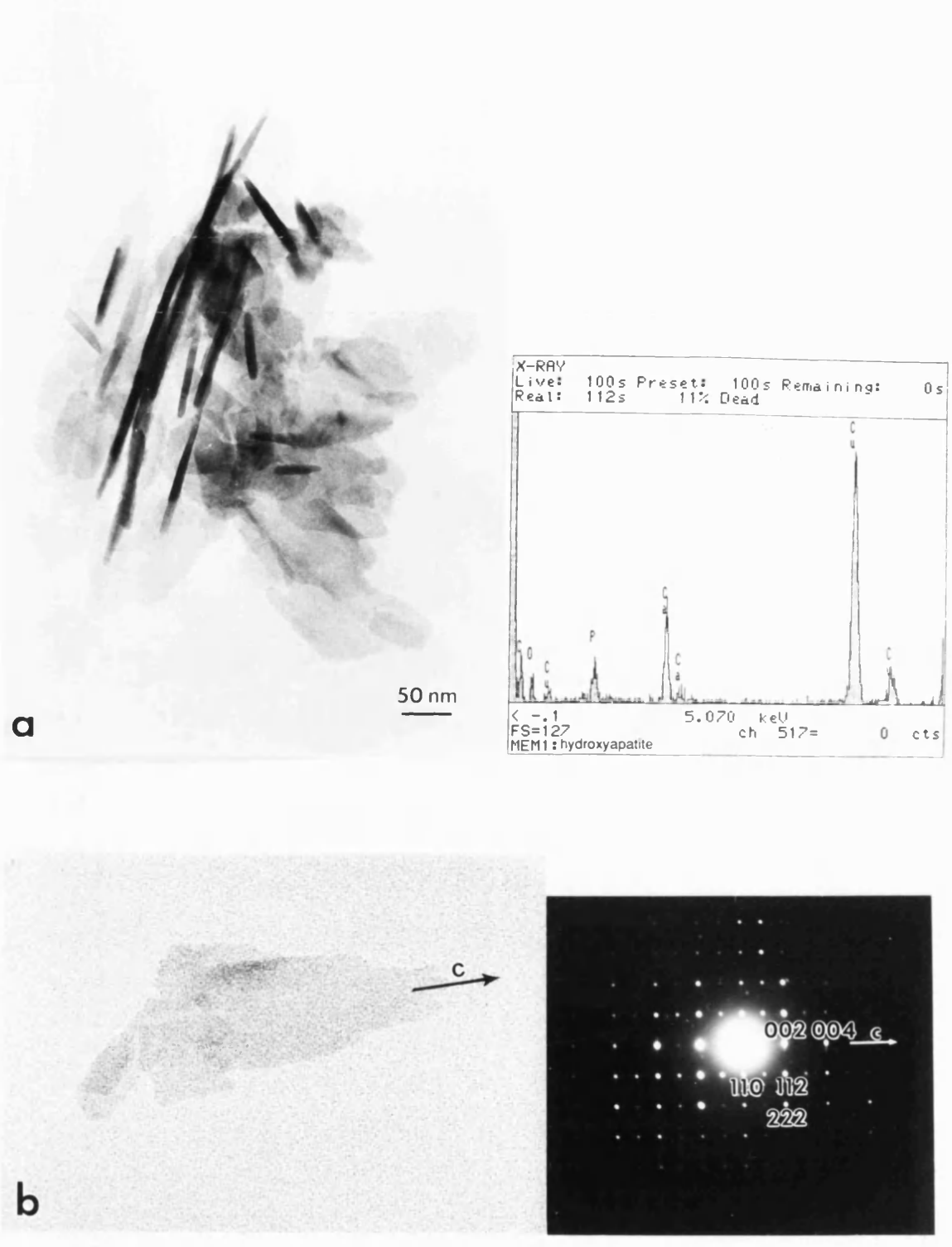

Fig. 3.2 (a) TEM micrograph of plate-like HAP precipitated in the presence in the presence of Cl⁻ at 70°C and EDXA of precipitate; (b) ED of single HAP plate showing slight elongation along the *c* or [001] axis, the pattern corresponds to the [110] zone

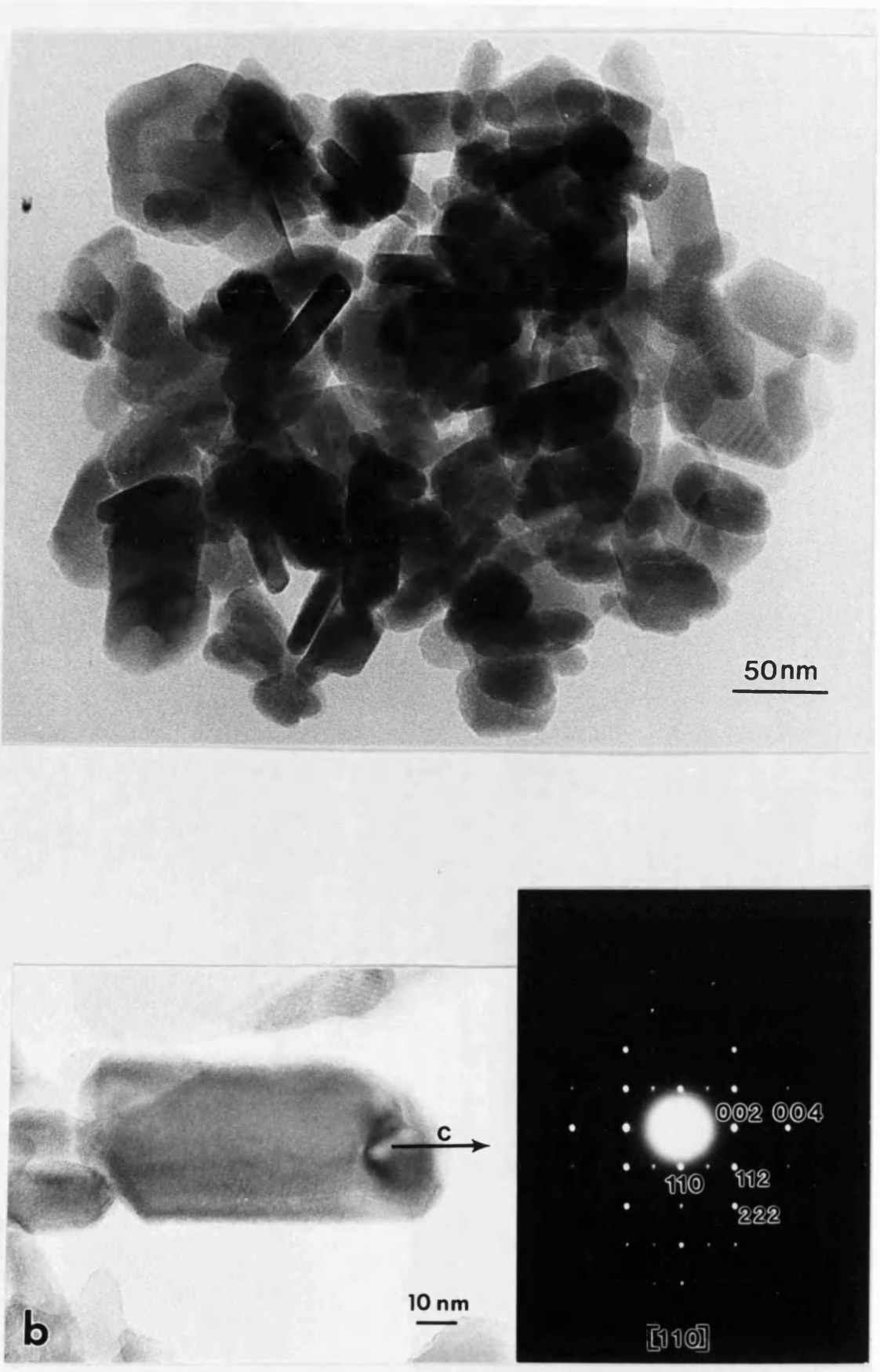

Fig. 3.3. (a) TEM micrograph of plate-like HAP after reflux for 12 hours; (b) ED of single crystal showing slight elongation along *c* axis.

The FT-IR spectra of the unrefluxed and refluxed samples are shown in fig. 3.4a and are characteristic of the hexagonal HAP structure (see chapter 2.9, table 2.1). Carbonate bands were present indicating that although the crystals were prepared under N_2 incorporation of carbonate readily takes place during exposure of the crystals to atmospheric CO_2. A measure of the carbonate content is given by the $\nu 3$ peaks 1370-1660 cm^{-1}, the $\nu 2$ CO_3^{2-} peak at 870 cm^{-1} and the degree of splitting of the $\nu 4$ PO_4^{3-} peaks (LeGeros et al 1989). The relative size of the bands in the sample indicated a carbonate content of about 3%. An increase in the intensity of the hydroxyl stretch at 3570cm^{-1} and hydroxyl librational mode at 630cm^{-1} was evident in the refluxed sample.

The sample gave an XRD reflection entirely characteristic of HAP (fig.3.4c). Calculation of the a and c cell parameters (see chapter 2.10) gave measurements consistent with stoichiometric HAP within experimental error (Table 3.1). Chloride inclusion into HAP is known to expand a and contract c (LeGeros 1974). Conversely carbonate inclusion contracts a and expands c (LeGeros et al 1971). The results suggests that there is no or negligible inclusion of these ions into the lattice. Inclusion of these ions would promote the formation of plate like HAP (Koutsoukos et al 1981; LeGeros et al 1971).

	Stoichiometric HAP	Precipitated HAP
a axis (Å)	9.432	9.43 ±0.01
c axis (Å)	6.881	6.89 ±0.01

Table 3.1. Unit cell parameters of HAP precipitated at 70°C in the presence of Cl^- compared with stoichiometric HAP.

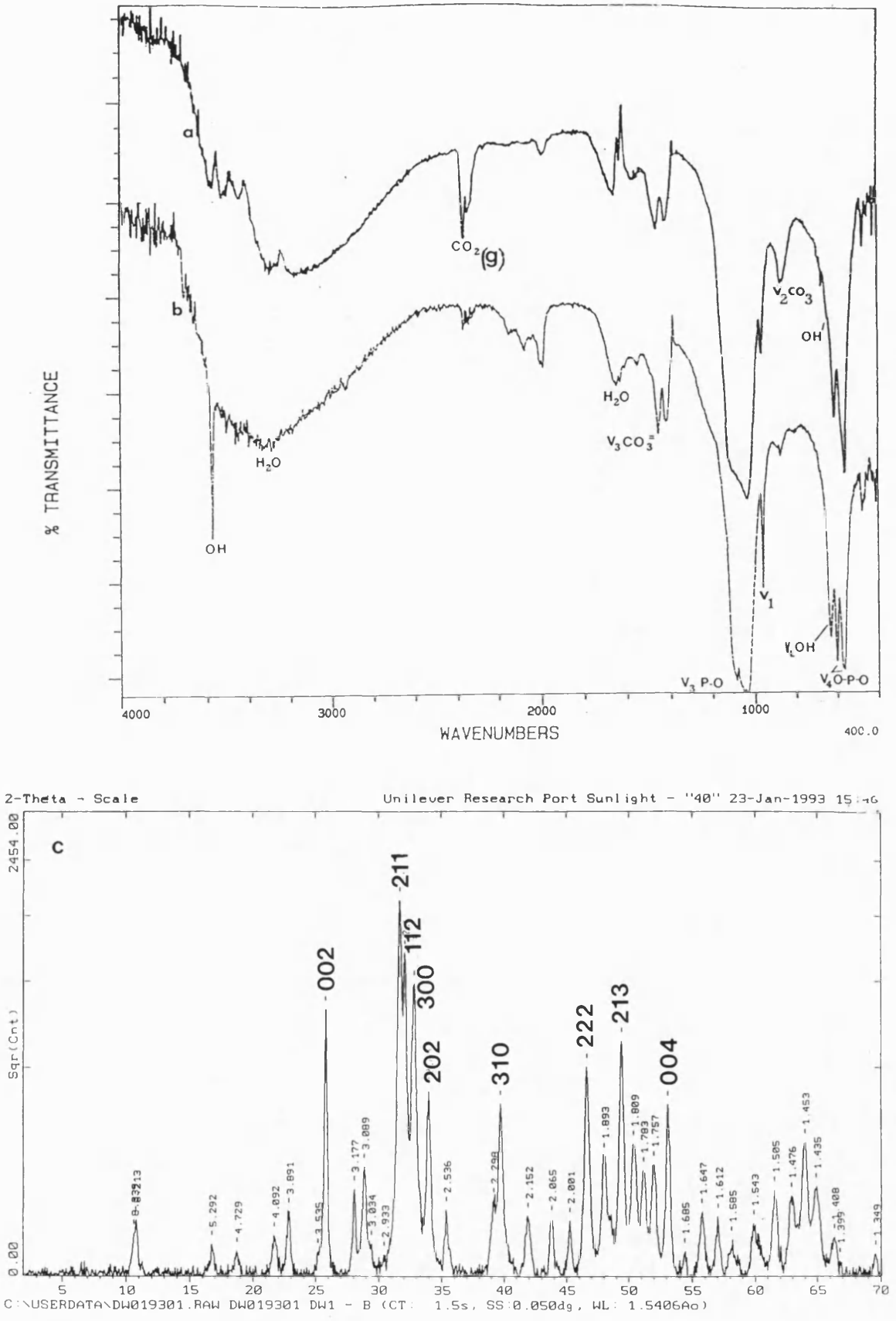

Fig. 3.4. (a) FT-IR spectra of unrefluxed HAP; (b) FT-IR spectra after reflux; (c) XRD of HAP precipitated in the presence of Cl^- at 70°C.

3.3 CRYSTALLIZATION IN THE PRESENCE OF CHLORIDE AND ADDITIVES

3.4 Additive materials

The additives D-glucose, D(+)-galactose, D-glucuronic acid, N-acetylglucosamine, glucose-6-phosphate, glucose-6-sulphate, ascorbic acid, 1,2-butanediol, 1,2-cyclohexanediol, 1,3 cis/trans cyclohexanediol, polyvinyl alcohol, ethylene glycol, 2,5-hexanediol and acetonitrile were obtained from Aldrich Chem Co. and were used as supplied. The additives D(-)-fructose, D-sorbitol (D-glucitol) and D(+)-mannose were obtained from Sigma Chemical Co. and were used as supplied. Table 3.1 shows the molecular structures of the additives employed.

D- Glucose	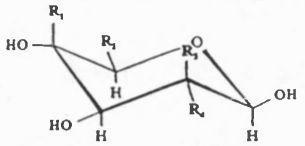 R_1=H, R_2=CH_2OH, R_3=H, R_4=OH
D(+)-Galactose	R_1=OH, R_2=CH_2OH, R_3=H, R_4=OH
D(+)-Mannose	R_1=H, R_2=CH_2OH, R_3=OH, R_4=H
D- Glucuronic acid	R_1=H, R_2=COOH, R_3=H, R_4=OH
N-acetyl glucosamine	R_1=H, R_2=CH_2OH, R_3=H, R_4=$NHCOCH_3$
Glucose-6-phosphate	R_1=H, R_2=$CH_2PO_4^{2-}$, R_3=H, R_4=OH
Glucose-6-sulphate	R_1=H, R_2=$CH_2SO_4^{1-}$, R_3=H, R_4=OH
D(-)-fructose	R_1=H, R_2=OH, R_3=OH, R_4=H + 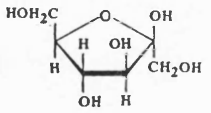

1,2-cyclohexanediol 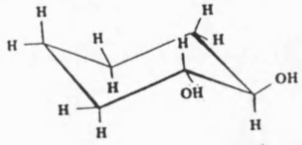

1,3 cis/trans cyclohexanediol 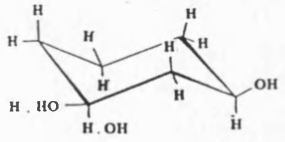

2,5-hexanediol 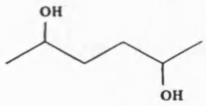

1,2-butanediol 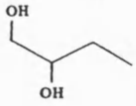

Sorbitol 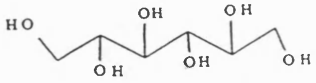

Ethylene glycol $HOCH_2CH_2OH$

Ascorbic acid 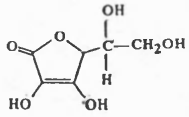

Polyvinyl alcohol $[-CH_2CH(OH)-]_n$

Acetonitrile CH_3CN

Table 3.2. Molecular structures of additives employed.

3.5 Materials and method

The HAP preparation procedure as described in chapter 2.2 was repeated except that a known weight of an additive was dissolved in the Na_2HPO_4 solution prior to addition of aqueous $CaCl_2$. Experiments were performed at total phosphate:additive mole ratios of 60:1, 6:1. or 0.6:1. In some experiments involving D-glucose, crystals were removed at various time intervals during the reaction and examined by transmission electron microscopy (TEM).

3.6 Calcium electrode measurements

HAP was prepared by a pulse addition method as described in chapter 2.2 with and without the presence of D-glucose additive. The concentration of calcium was monitored with a Ca^{2+} electrode as described in chapter 2.3. Plots of the calcium electrode readings are shown in fig.3.5. The initial ACP phase is formed almost immediately upon addition of a few ml of calcium solution with both additive and non-additive containing solutions. However the amplitude in the readings upon each drop added are less, boundaries more abrupt and the overall length of the initial phase longer with the additive containing reactions. This suggests that the additive inhibits the transformation of the ACP phase to a small degree, perhaps by absorption to the surface of the ACP clusters. In both cases the size of the amplitude decreases as the concentration of nuclei of a less soluble secondary phase increases with increasing supersaturation. The overall concentration of free calcium in solution then decreases indicating the precipitation of a less soluble phase. The free calcium then remains relatively stable as precipitation and rapid conversion to HAP on pre-existing crystallites takes place. The presence of only a single step in the graph indicates the formation of only two phases, ACP followed by HAP. A transient OCP phase may be present at the temperature used, but at levels too low to be detectable. The completion point, again slightly longer for the additive containing solution, gives a $Ca:PO_4$ ratio of 1.5±0.4, typical of precipitated HAP.

3.5 Materials and method

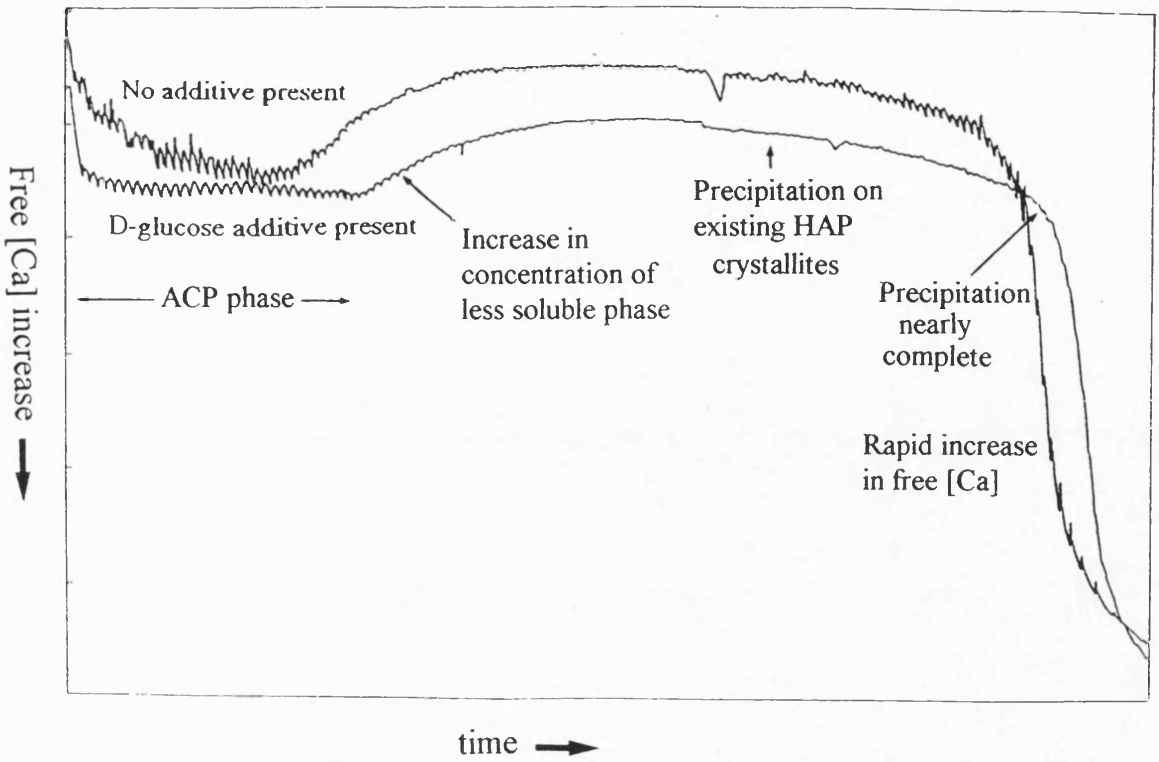

Fig. 3.5. Calcium electrode measurements of free Ca concentration during precipitation of HAP with and without additive at 40°C using drop addition.

3.7 HAP crystallization in the presence of chloride and additive

Addition of monosaccharides to the $CaCl_2$ reaction mixture had no influence on the crystal structure parameters of the HAP precipitated. X-ray diffraction patterns and infra-red spectra were essentially identical with control samples (fig. 3.6a). However, after reflux the HAP precipitated in the presence of D-glucose did not show an increase in intensity of the hydroxyl bands that was found with the control preparation without additive (fig. 3.6b).

Examination by TEM of a preparation made at 70°C revealed a dramatic morphological change in which the HAP plates of the control system were replaced by elongated needle-shaped crystals. Moreover, upon reflux no significant change in morphology took place. At a PO_4 : D-glucose ratio of 6:1, the HAP crystals were generally discrete and longer (550-750nm) than the plate-like control crystals (fig. 3.7a). A frequency histogram of crystal measurements is shown in figure 3.13. The average aspect ratio was approximately 10:1. This morphological effect was apparently

at or near the optimum at a PO_4 : additive ratio of 6:1 since a lower concentration of glucose (PO_4 : additive=60:1) was less effective, resulting in partially-elongated irregular plate-like crystals (fig. 3.7b), and an increased level of glucose (PO_4 : additive=0.6:1) gave ill-defined aggregates of elongated crystals (fig. 3.7c).

Preparation of HAP at 40°C with D-glucose (and other additives) was shown by TEM to produce HAP plates similar to the control preparations (fig. 3.7d) (with the exception of D-mannose which produced plates of much smaller dimensions).

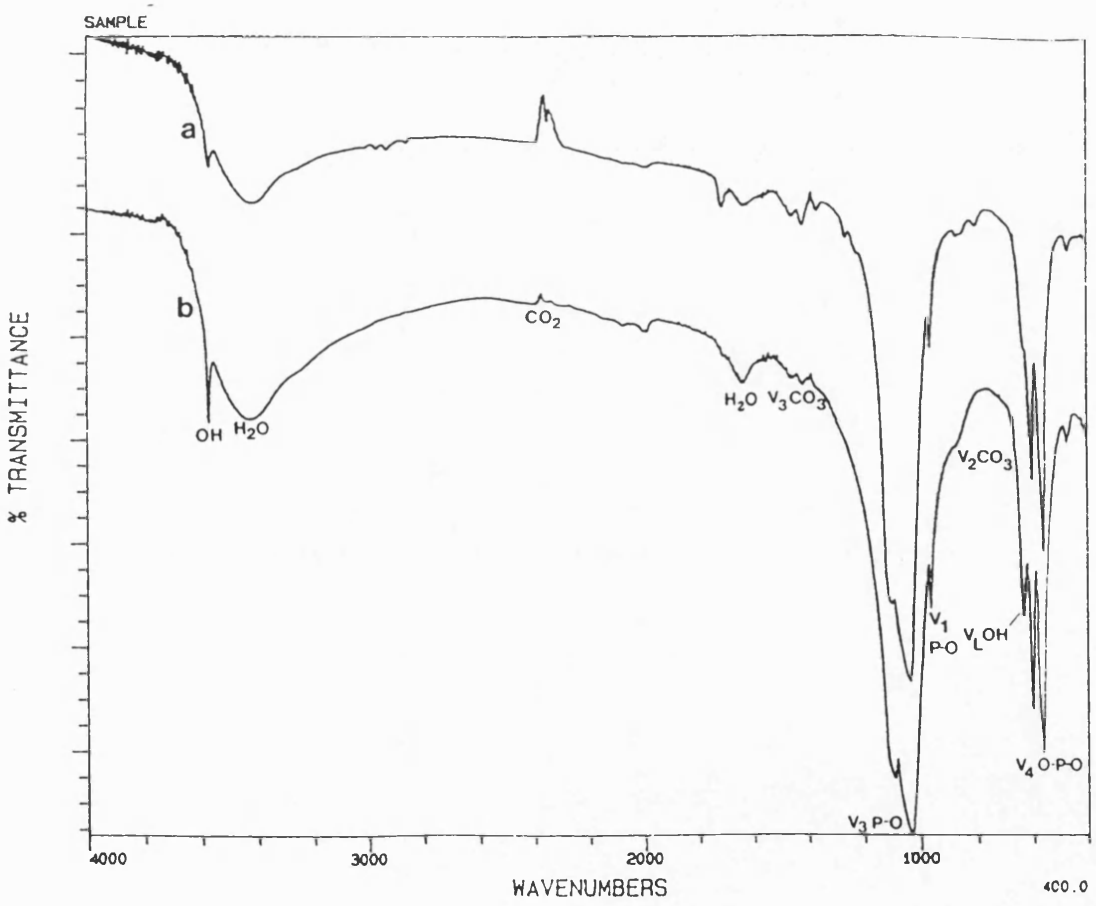

Fig. 3.6. (a) FT-IR spectrum of HAP prepared in the presence of Cl^- and D-glucose additive after reflux for 12hours; (b) FT-IR spectrum of HAP prepared in the presence of Cl^- after reflux for 12 hours.

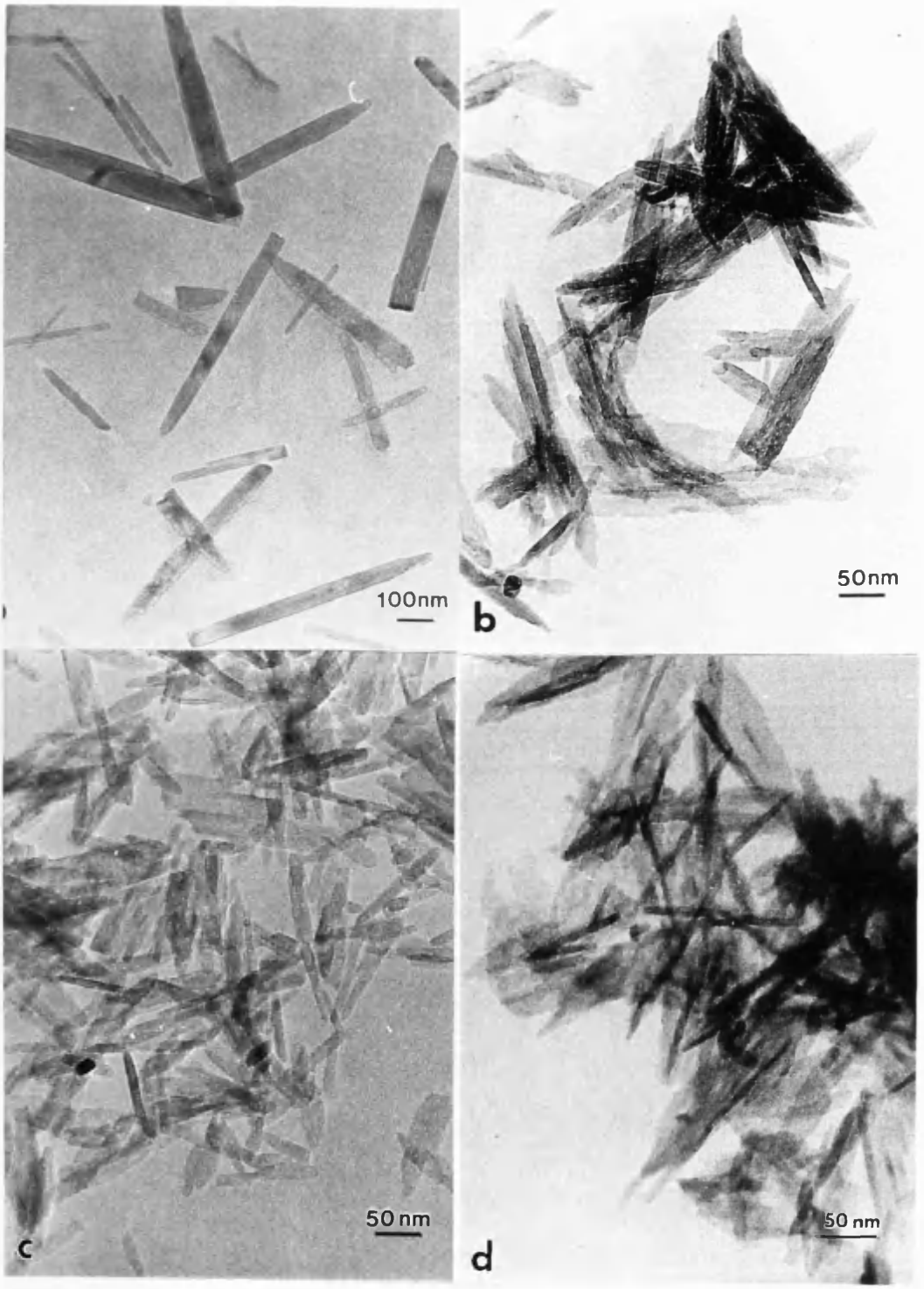

Fig. 3.7. TEM micrographs of HAP precipitated with D-glucose at 70°C with:
(a) PO_4: additive ratio of 6:1; (b) PO_4: additive ratio of 60:1; (c) PO_4: additive ratio of 0.6:1;
(d) TEM micrograph of HAP precipitated with D-glucose at 40°C.

Single crystal electron diffraction patterns of HAP were obtained from individual crystals in the presence of D-glucose (fig. 3.8). The patterns indicated that the needle axis was parallel to the crystallographic *c* ([001]) direction. Examination of the sectioned material by HRTEM showed the presence of hexagonal crystals with six well-defined prismatic faces which were oriented parallel to lattice fringes of 0.82 nm spacing (fig. 3.9). These results indicate that the HAP crystals grown in the presence of glucose were hexagonal prisms of {100} faces extensively elongated along the *c* axis. Many crystals were terminated at one end by a smooth flat edge whilst the other end was noticeably rounded. Theoretically the crystals should be completely symmetrical (HAP has a centrosymmetric space group); the asymmetry probably originates from the fracturing of individual needles present in larger aggregates during sample preparation. Indeed, florrete type aggregates were often observed by scanning electron microscopy (fig 3.10).

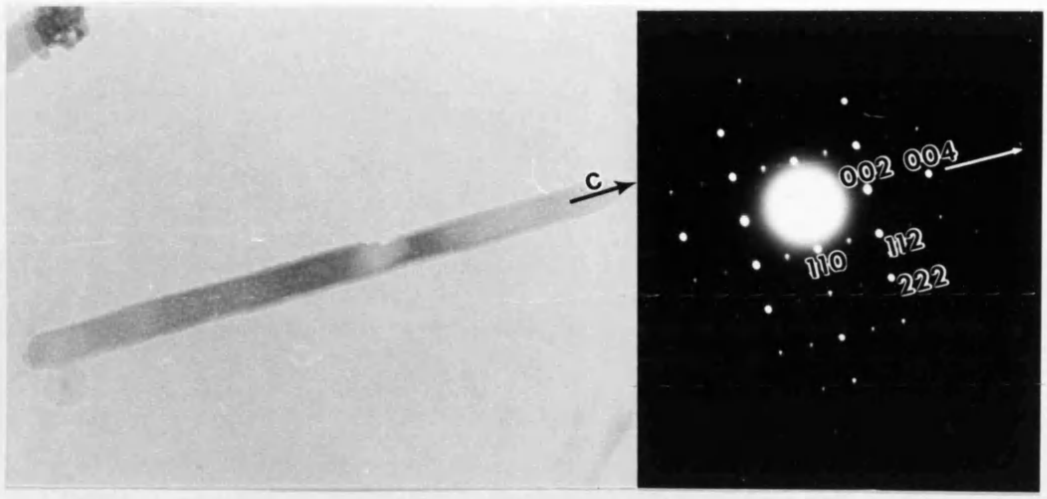

Fig.3.8. (a) TEM micrograph of needle-like HAP crystals showing elongation along the c axis; (b) single-crystal ED pattern of needle-like HAP crystal formed with D-glucose. The pattern corresponds to the [1 1 0] zone of the hexagonal unit cell.

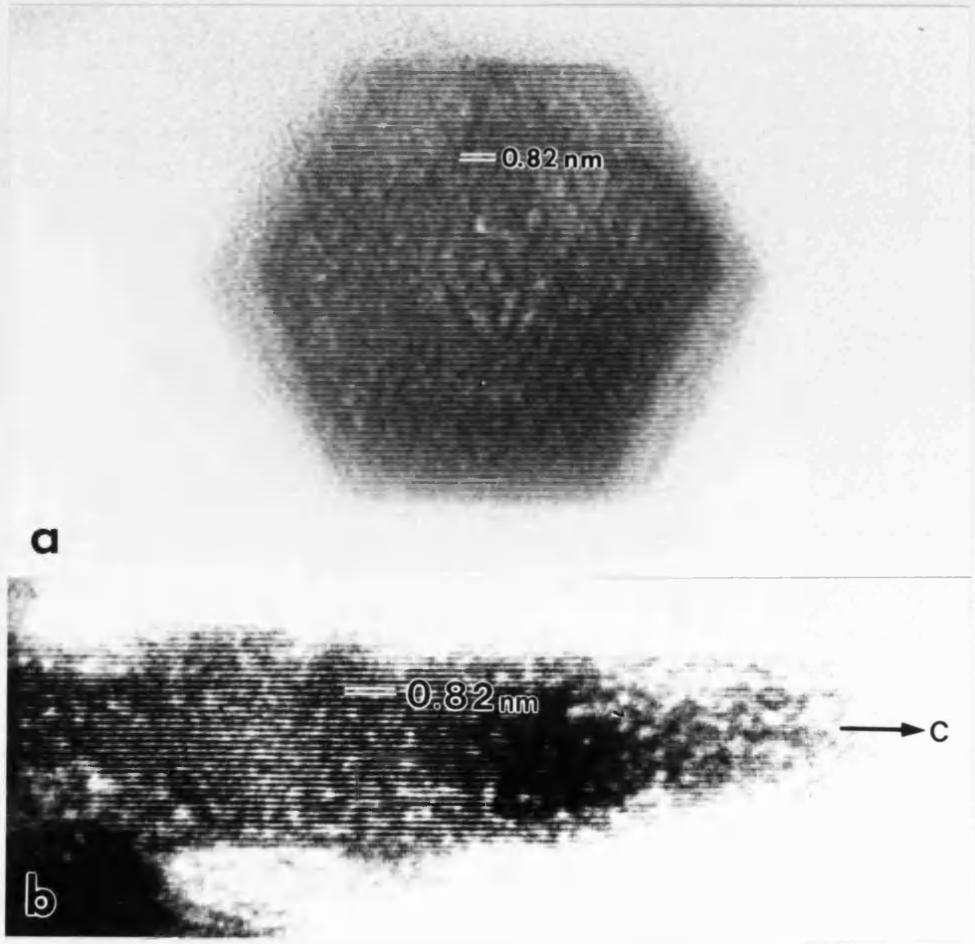

Fig.3.9.(a) high resolution TEM micrograph of the cross-section of an elongated crystal showing well defined hexagonal profile of {100} faces and {100} lattice spacing (0.82nm); (b) high resolution TEM micrograph of longitudinal-section showing {100} (0.82nm) spacing.

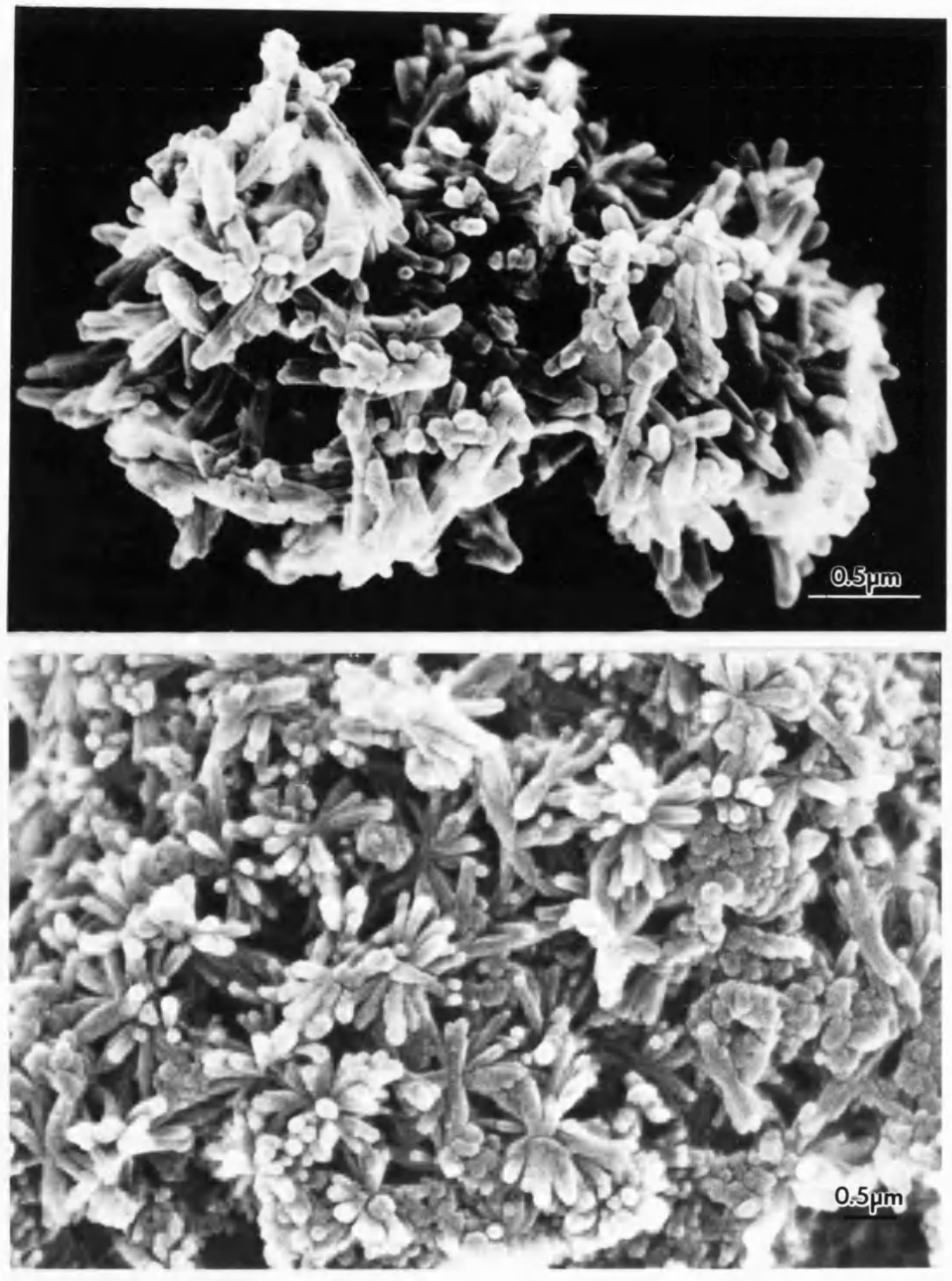

Fig. 3.10. SEM micrographs of HAP crystals precipitated with D-glucose. Florrete type aggregations are visible which are fractured during TEM preparation.

3.8 Effect of other monosaccharides on morphology of HAP

Experiments involving other monosaccharides indicated that the above morphological effects were general to this class of compounds. Crystallization in the presence of stereoisomers (epimers) of D-glucose, such as D-galactose and D-mannose, which differ in configuration at a single asymmetric carbon centre (C-4 and C-2, respectively), resulted in needle-like HAP single-crystals of similar size distribution as observed in the glucose-containing experiments (fig. 3.11a). Functionalized derivatives of D-glucose, glucuronic acid and N-acetyl glucosamine, produced crystals of marginally greater size (fig. 3.11b,c). Interestingly, the most effective monosaccharide studied was the ketohexose, D-fructose, (fig.3.11d) which resulted in needle-shaped crystals that were significantly longer (700-900nm) and had a higher average aspect ratio (20:1) than the corresponding hexoaldose additives. Frequency histograms of glucuronic acid and fructose crystal measurements are shown in fig 3.13. The results suggested that the presence of hydroxyl groups play an important role in producing morphological modification. Therefore experiments were conducted using a range of non-sugar additives. Sorbitol, which is an open chain molecule containing six OH groups, produced needle-like crystals that were similar in length (700-950 nm) to the crystals grown in the presence of fructose, but with a higher average aspect ratio (25:1) (3.12a). A frequency histogram of crystal measurements is shown in fig 3.13e. The linear diol, 1,2-butanediol, was similar in potency to sorbitol (fig. 3.12b) whereas the cyclic molecules, 1,2-cyclohexanediol and 1,3-cyclohexanediol were less effective than the hexoaldose additives. Ascorbic acid, which contains two adjacent -OH groups connected by a C=C double bond, was less effective than sorbitol, 1,2-butanediol or fructose but similar in activity to the hexoaldoses. Modifications in the spacing between hydroxyl groups had a significant effect for the linear molecules, for example, 2,5-hexanediol was inactive in producing needle-shaped HAP crystals (fig. 3.12d). One of the additives tested, polyvinylalcohol (PVA) was unusual in that its presence led to the formation of clusters of plates and needles apparently fused together in a manner not found with other additives (fig. 3.12c). The crystal dimensions were similar to control preparations however. Active and inactive additives tested are shown in Table 3.3.

a

Additive	Structure
D- Glucose	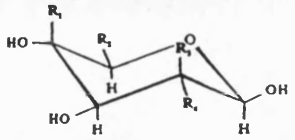 R_1=H, R_2=CH_2OH, R_3=H, R_4=OH
D(+)-Galactose	R_1=OH, R_2=CH_2OH, R_3=H, R_4=OH
D(+)-Mannose	R_1=H, R_2=CH_2OH, R_3=OH, R_4=H
D- Glucuronic acid	R_1=H, R_2=COOH, R_3=H, R_4=OH
N-acetyl glucosamine	R_1=H, R_2=CH_2OH, R_3=H, R_4=$NHCOCH_3$
Glucose-6-phosphate	R_1=H, R_2=$CH_2PO_4^{2-}$, R_3=H, R_4=OH
Glucose-6-sulphate	R_1=H, R_2=$CH_2SO_4^{1-}$, R_3=H, R_4=OH
D(-)-fructose	R_1=H, R_2=OH, R_3=OH, R_4=H + 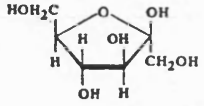
Ascorbic acid	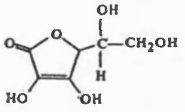
Sorbitol	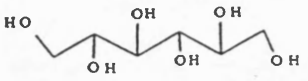
1,2-butanediol	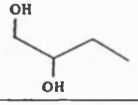
1,2-cyclohexanediol	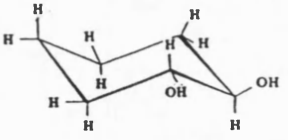
1,3 cis/trans cyclohexanediol	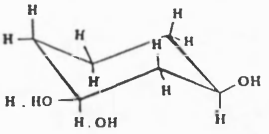

b

Additive	Structure
Polyvinyl alcohol	$[-CH_2CH(OH)-]_n$
Ethylene glycol	$HOCH_2CH_2OH$
2,5-hexanediol	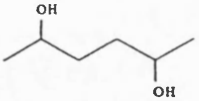
Acetonitrile	CH_3CN

Table. 3.3(a). Additives that promote needle-like HAP crystals; (b) non-active additives tested.

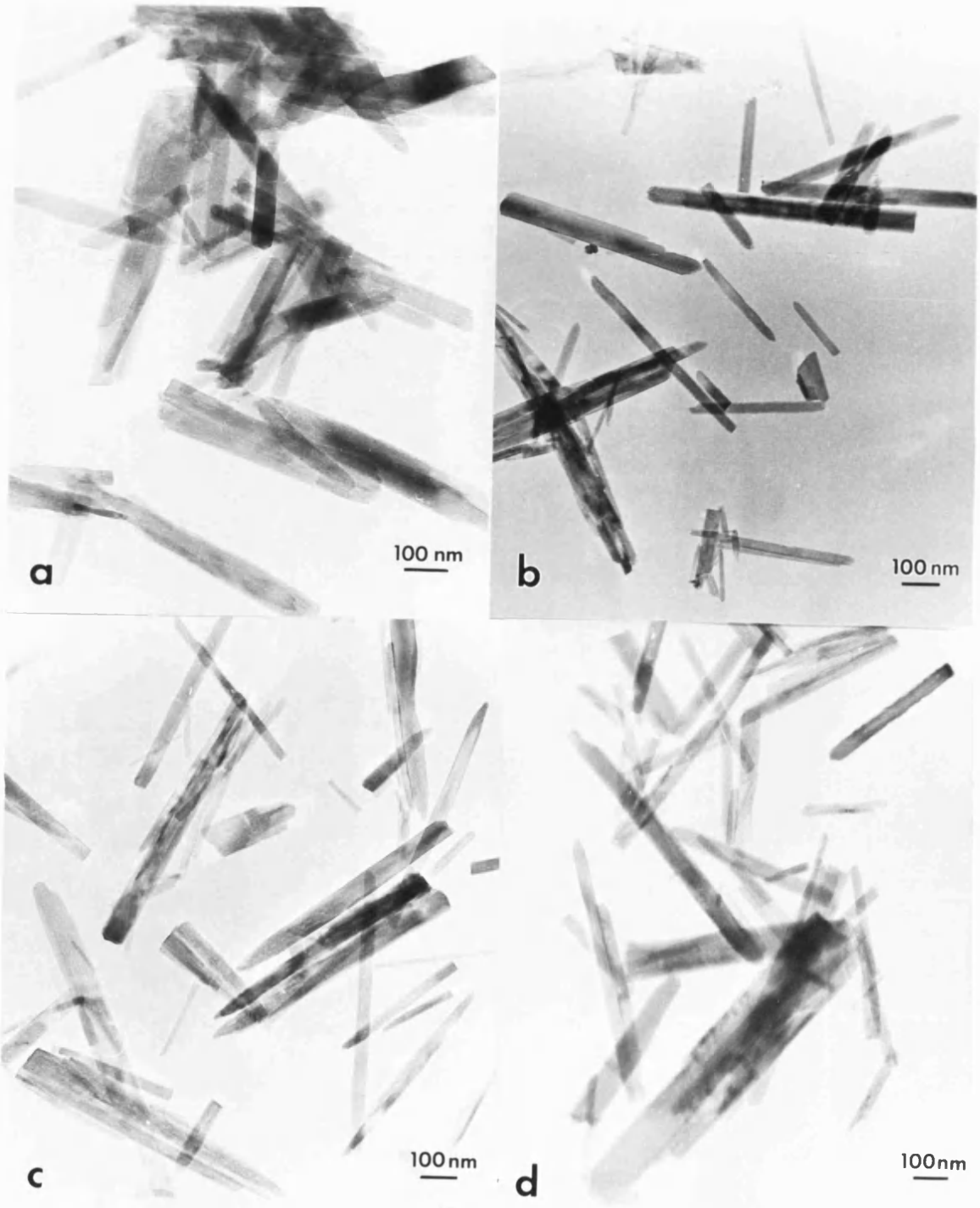

Fig.3.11. (a) TEM micrographs of HAP precipitated with monosaccharide additives (at PO4 additive ration of 6:1) (a)D-galactose; (b) glucuronic acid; (c) N-acetylglucosamine; (d) fructose.

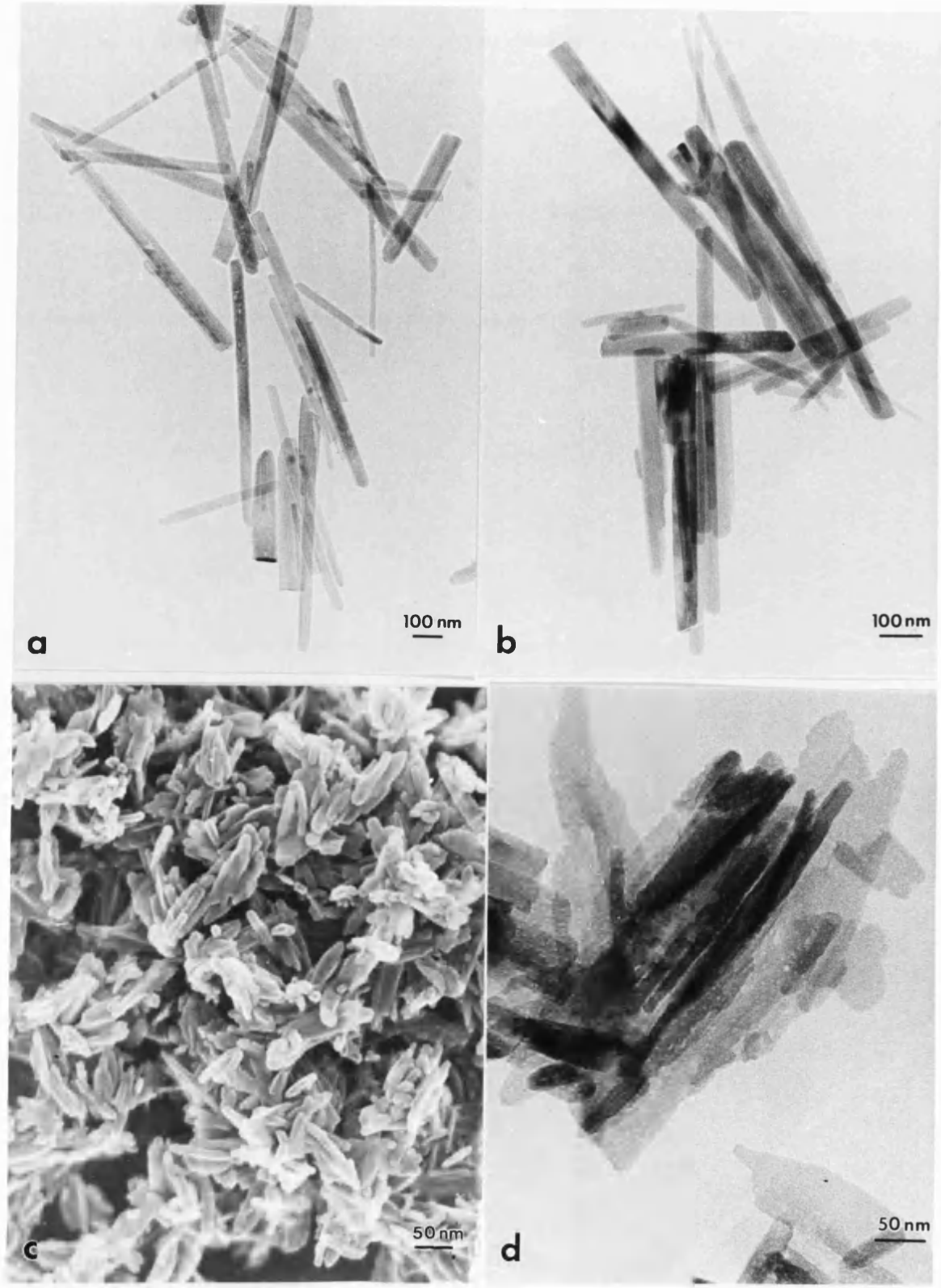

Fig.3.12. TEM micrographs of HAP precipitated with non-monosaccharide additives:(a) sorbitol, (b) 1,2-butanediol, (c) polyvinyl alcohol (SEM), (d) 2,5-hexanediol.

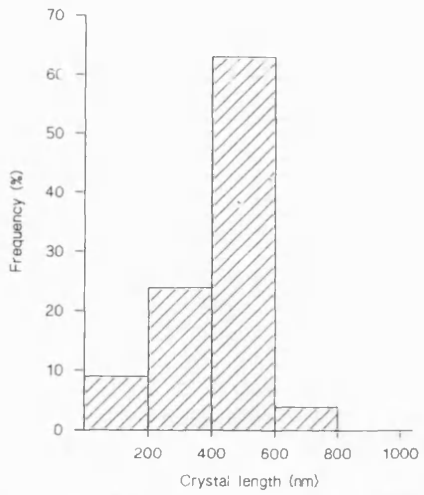

Fig. 3.13 (a) Histogram of control HAP plate length obtained in presence of Cl^-.

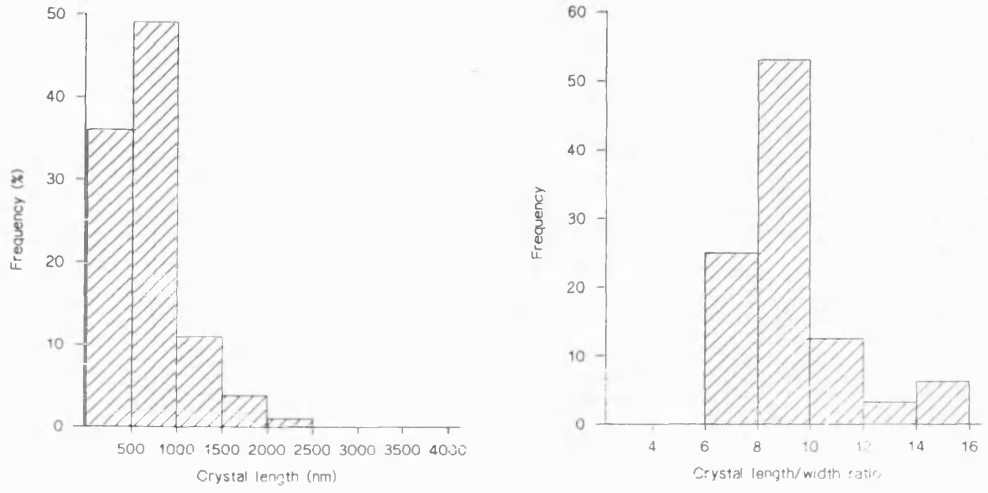

Fig. 3.13 (b) Histogram of crystal length/width ratio obtained with D-glucose at 6:1 PO_4 / additive ratio.

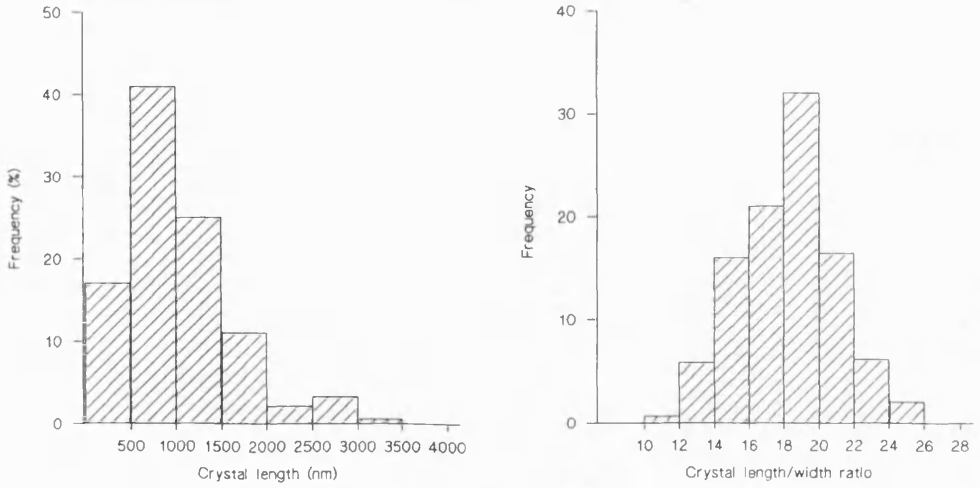

Fig. 3.13 (c) Histogram of crystal length and length/width ratio obtained with D-fructose at 6:1 PO_4 / additive ratio.

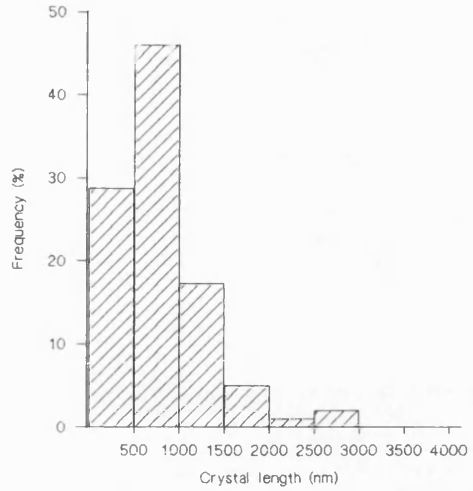

Fig. 3.13 (d) Histogram of crystal length obtained with glucuronic acid at 6:1 PO_4 / additive ratio.

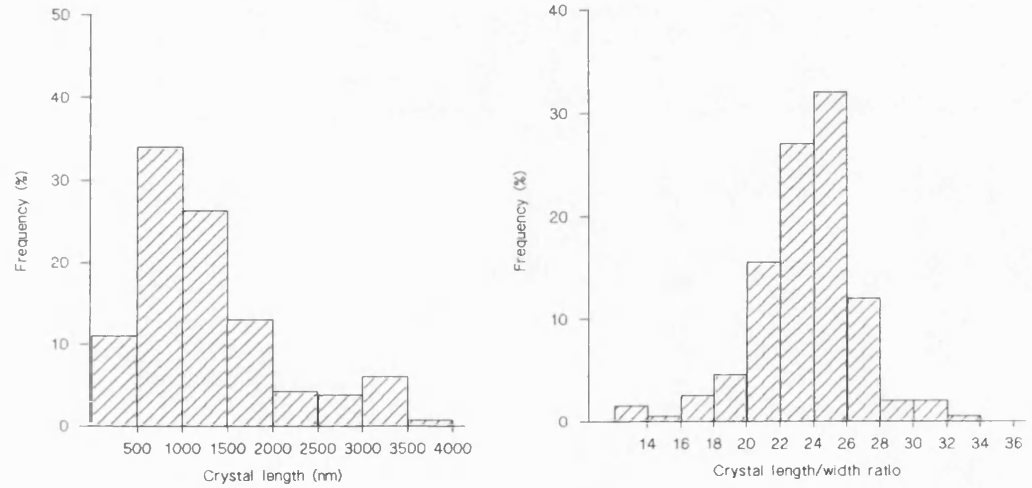

Fig. 3.13 (e) Histogram of crystal length and length/width ratio obtained with sorbitol at 6:1 PO_4 / additive ratio.

3.9 Development of HAP crystals in the presence of D-glucose.

Electron microscopy studies of HAP crystals, removed at various time intervals from an HAP preparation in the presence of D-glucose, indicated that the needle-like habit was established in the first few minutes after addition of only 3-5 cm ^{3} of aqueous $CaCl_2$. Samples removed and not washed at 1 min. show the presence of crystallites and ACP spherules with additive strongly adsorbed at the surface (fig. 3.14a). After 4 minutes needle-like crystallites a few hundred nm in length have developed, again additive is apparently adsorbed to the surfaces (fig. 3.14b). After 10 min. elongation of the crystallites to approximately 500nm has taken place and adsorbed additive is no longer in evidence (fig. 3.14c). Samples removed after 30s and washed show the presence of sheet-like gel structures of crystalline HAP (fig. 3.15a). At 4 min, the gel-like structures had transformed into regular elongated HAP crystals of pronounced striated texture consisting of linear arrays of nanometer-size spherical domains (fig. 3.15b). These particles subsequently developed within 10-15 min after the start of the reaction into smooth-edged filamentous HAP crystals (fig. 3.15c) which were comparable in maximum length but not width with fully mature particles. The remaining stages of the reaction (20-100 min) were associated with a progressive increase in the width and thickness of the filamentous crystals (fig. 3.15d).

X-ray diffractions of samples taken for analysis at various time intervals reflected the conversion from ACP into poorly crystalline HAP, which increased in ordering with time (3.16a). The characteristic (300) OCP reflection at 18.7Å and the (100), (020) and (110) reflections at 9.36Å and 9.05Å are all absent from the diffractions. Minor phases, such as OCP, could not be detected below 5 wt%. Infra-red spectra of developing samples showed some increase in the resolution of peaks with time, indicating an increase in ordering (fig.3.16b). Only peaks characteristic of HAP were present.

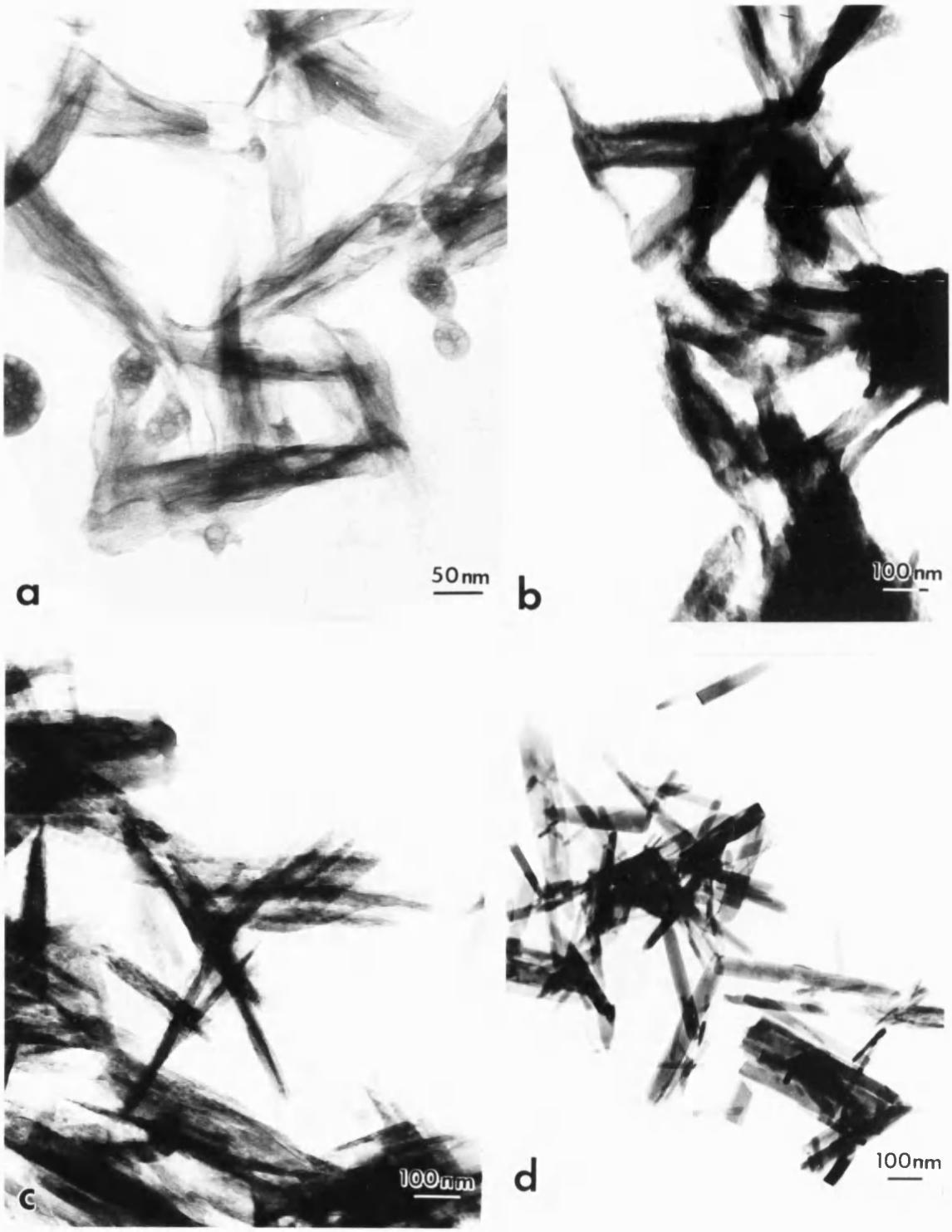

Fig. 3.14. TEM micrographs of samples removed at intervals from HAP precipitated in the presence of D-glucose (unwashed) after (a) 1min, (b) 4 min, (c) 10 min, (d) 100 min.

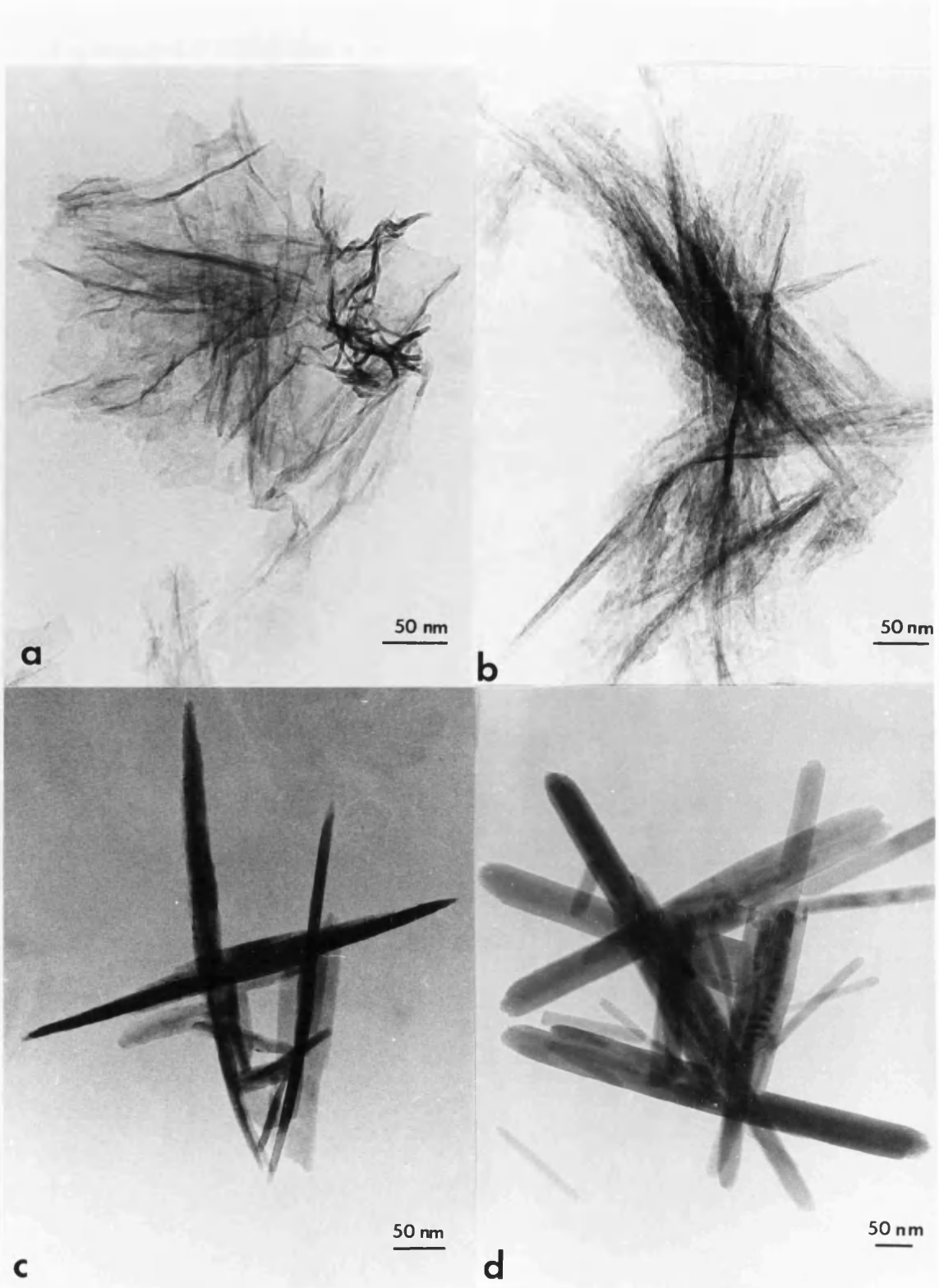

Fig. 3.15 . TEM micrograph of samples removed at intervals from HAP precipitated in the presence of D-glucose (washed) after (a) 30s.; (b) 4 min; (c) 10 min; (d) 100 min.

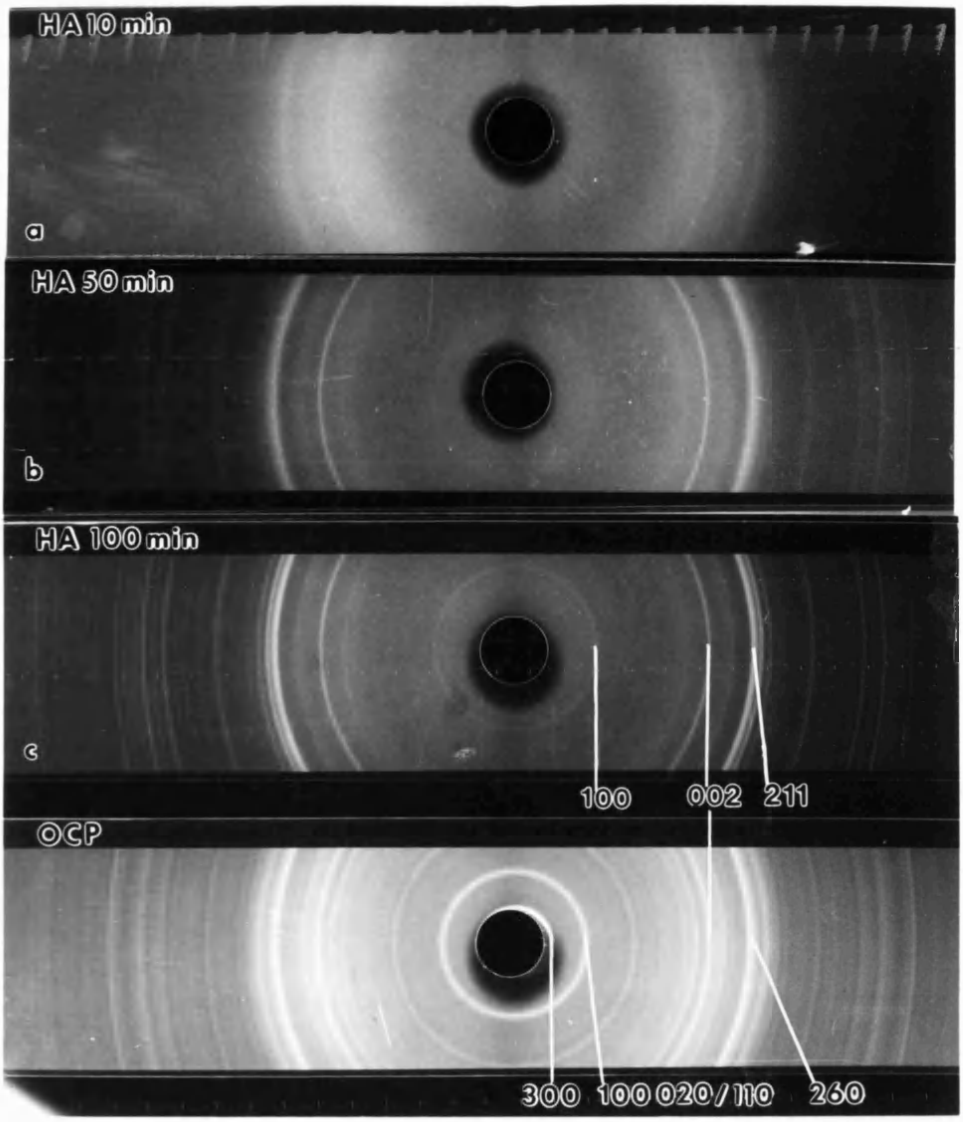

Fig. 3.16 (a) XRD of developing HAP after (a) 10 min; (b) 50 min; (c) 100 min.; (d) control OCP.

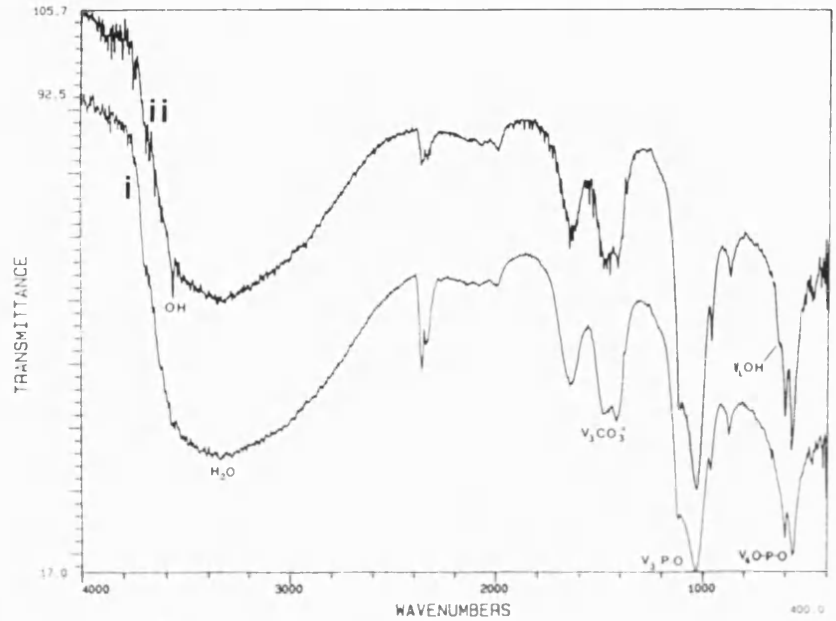

Fig. 3.16 (b) FT-IR spectrum of HAP precipitated in the presence of Cl^- and D-glucose after (I) 1 min; (ii) 40 min.

3.10 Effect of altering experimental procedure

HAP was prepared as in chapter 2.2 with the following modifications;
(i) D-glucose was added to the calcium solution prior to a pulse addition to the phosphate solution. (ii) D-glucose was added to the phosphate solution prior to addition to the calcium solution. (iii) Phosphate solution was added by pulse addition to calcium solution containing D-glucose.
Examination by TEM revealed that the HAP existed largely as needle-like HAP with small amounts of plate-like HAP. Phosphate deficient precipitates were characterized by poorly developed needles with highly tapered ends (fig. 3.17). Calcium deficient precipitates were similar to the control preparation except that the needles were of smaller overall dimensions.

3.12 HAP crystallization in the presence of nitrate

In order to help explain the role of the above additives on HAP crystallization in the presence of chloride, the HAP was prepared as in chapter 2.2 except that calcium nitrate was used in place of calcium chloride. X-ray diffraction patterns and infrared spectra were essentially identical to HAP precipitated in presence of chloride. However, unlike the chloride-derived crystals, the nitrate-containing solution produced HAP crystals that were needle-like (fig. 3.18). In general, the lengths of these needles (350-550 nm) were comparable with the length of HAP plates obtained in control preparations. The average aspect ratio (9:1) were reduced compared with those formed in the glucose-containing experiments. Electron diffraction studies indicated that the *c* axis was aligned with the morphological long axis.

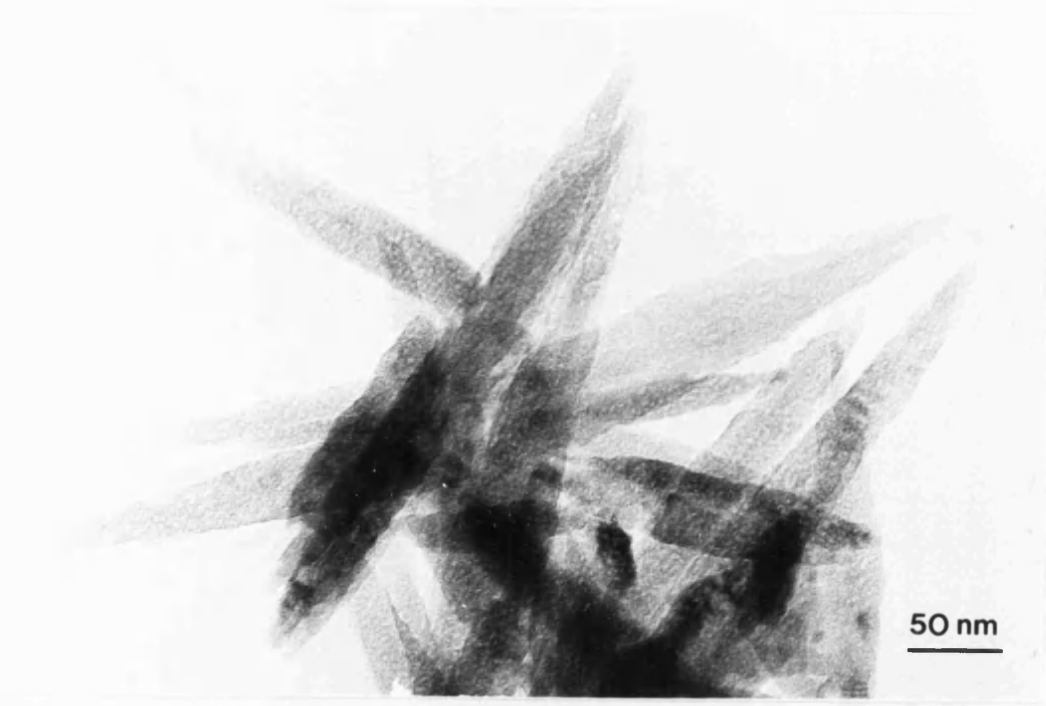

Fig. 3.17. TEM micrograph of HAP precipitated under phosphate deficient conditions.

Fig. 3.18. TEM micrograph of HAP precipitated in presence of nitrate.

3.13 ESCA analysis of plate-like HAP prepared in the presence of chloride and needle-like HAP prepared in presence of additive and chloride.

A sample of plate-like HAP prepared in the presence of chloride and a sample of needle-like HAP prepared in the presence of chloride and D-glucose additive were well washed with distilled water and submitted for ESCA analysis of chloride to Unilever Research , Port Sunlight Laboratory. ESCA analysis is concerned with the masurement of core-electron binding energies. A molecule or atom is bombarded with high-energy X rays, which cause the emission from sample atoms of inner-level electrons. All electrons whose binding energies are less than the energy of the exciting X rays are ejected. The kinetic energies of these photoelectrons are then measured by an energy analyzer. Although the incident X-ray photon may penetrate and excite photoelectrons to a depth of several hundred nanometers, only the photoelectrons from the outermost layers have any chance to escape from the material environment and subsequently be measured (Barr 1978). The ESCA measurement of the HAP sample generates information from the outer 2nm of the surface layer.

In both cases negligible (<0.2%) Cl^- composition in the surfaces of the crystals was found.

3.14 Crystallization of HAP using a continuous dropwise precipitation method

Hydroxyapatite was prepared in the presence of chloride as in chapter 2.2 except that a continuous dropwise addition rather than periodic pulse addition method was made. Examination by TEM of the HAP precipitated showed the presence of only needle-like HAP rather than the plate-like previously obtained (fig. 3.19).

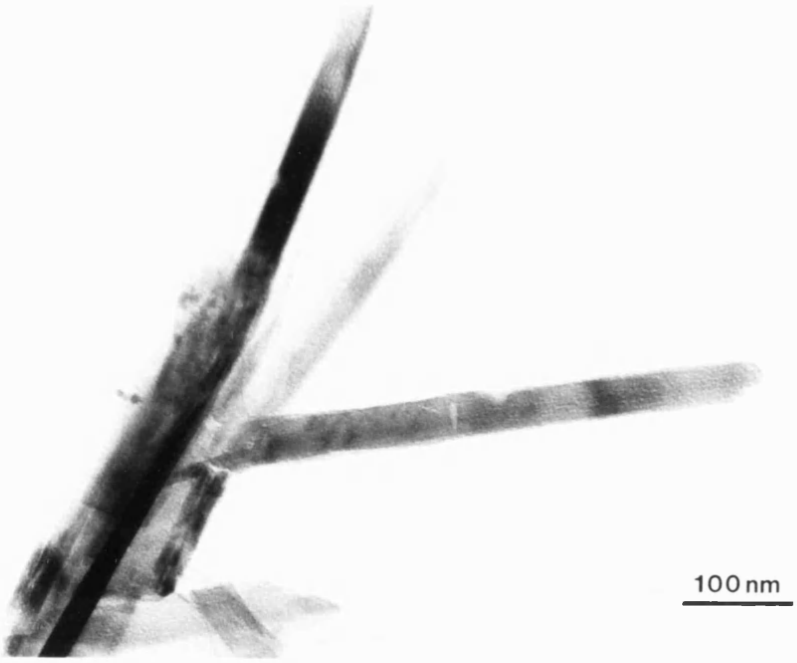

Fig. 3.19. TEM micrograph of HAP precipitated in the presence of Cl^- by a continuous dropwise method.

3.15 Effect of reaction conditions on additive

The supernatant liquor of the HAP preparations using D-glucose and D-fructose were decanted, filtered and calcium chloride added to precipitate any unreacted phosphate. The filtered solution was then roto-evaporated at room temperature and the material obtained examined by FTIR using KBr disks. The presence of a large carbonyl (-C=O) peak at 1640cm^{-1} is present in the spectrum of additive recovered from a D-glucose containing reaction suggesting that conversion of the D-glucose to ketoses had taken place (fig. 3.20). FTIR spectra of material recovered from a D-fructose reaction showed very little alteration. In neither case were peaks due to the presence of carboxyl groups (-COOH) found to be present.

Under the reaction conditions employed (70°C and pH 9.3-9.8) extensive isomerism of the monosaccharide between the epimeric aldoses and the correseponding ketoses probably through the formation of a 1,2-enediol occurs (fig. 3.21) . Conversion between all the various sugars of the same chain length and rearrangements into saccharinic acids from the isomerism and cleavage products may be possible (Pigman 1957; Ferrier and Collins 1972; Kennedy and White 1983).

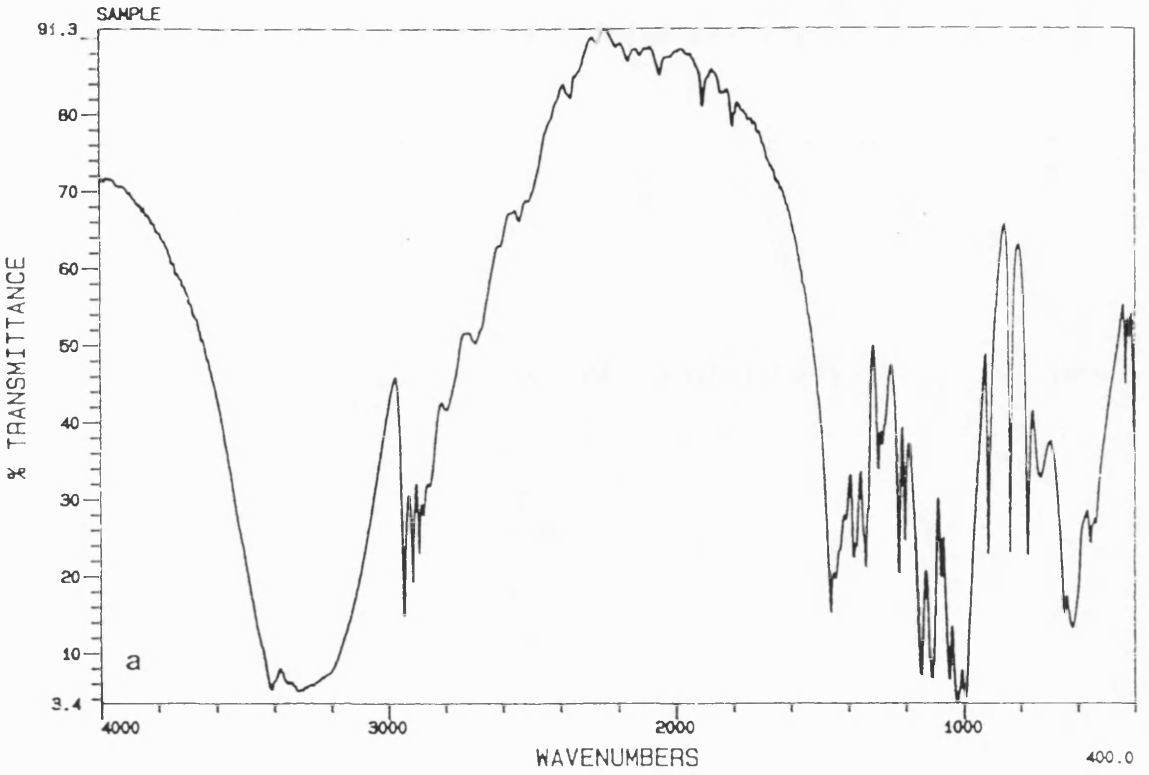

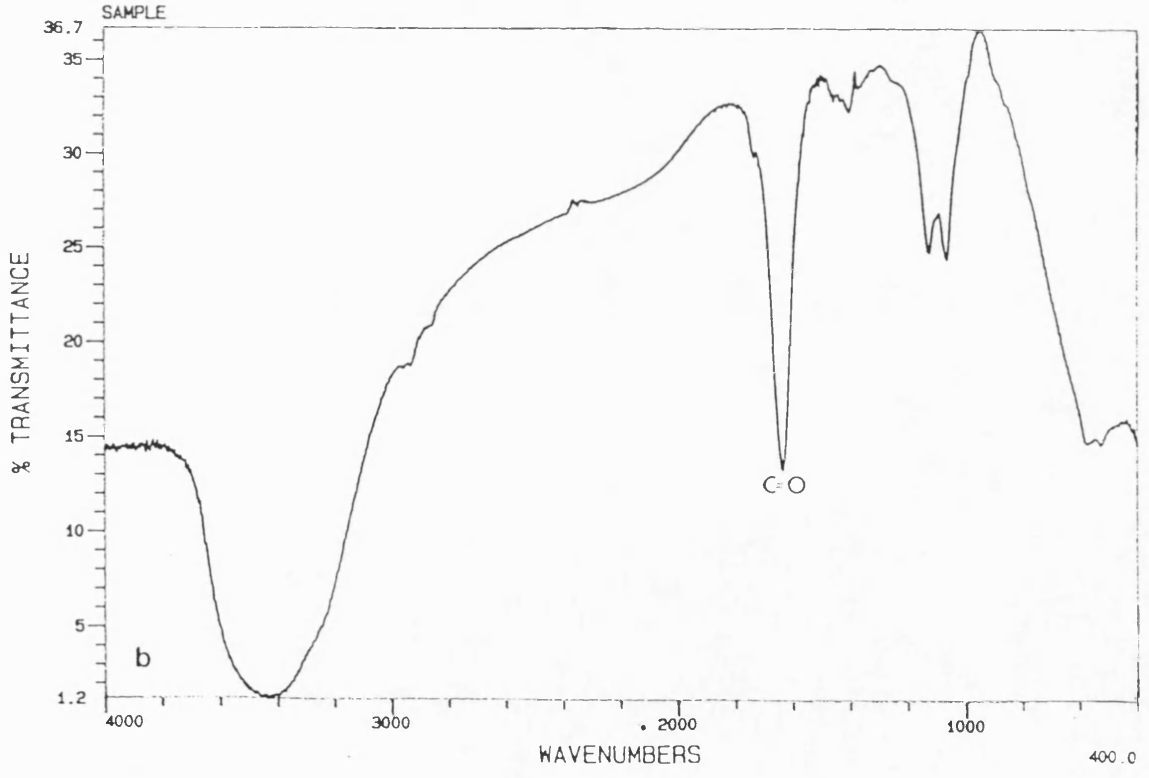

3.19. (a) FT-IR spectrum of D-glucose; (b) FT-IR spectrum of additive material recovered after completion of precipitation of HAP. Rearangements into ketoses is suggested by the prominant carbonyl peak.

Fig. 3.20. Diagram showing the ß-elimination and benzilic acid type re-arangements of D-glucose under alkaline conditions. (From Bioactive Carbohyrates, Kennedy J.F., White C.A., Ellis Horwood Ltd. 1985).

3.16 DISCUSSION

The results show that the introduction of monosaccharides into chloride-containing supersaturated calcium phosphate solutions dramatically influences the crystal morphology of the hexagonal polymorph of HAP. Interaction of the monosaccharides with the HAP lattice restricts growth perpendicular to the *c* axis such that thin hexagonal needle-like crystals are formed. Co-ordination between sugar molecules and Ca^{2+} are known to occur and binding via mono, bi or tridentate sites on the sugar is possible. The sugar is only very weakly bound if held by one or two sites only (Angyal 1972). A relatively strong calcium-carbohydrate interaction occurs when three are arranged in an axial-equatorial-axial sequence. This particular arrangement is not found with an anomer of glucose but a geometrical arrangement close to that does occur with the β-D-mannofuranose of D-mannose (Angyal 1972). This may explain the finding that particularly small plates were obtained with D-mannose. The co-ordination effect could be enhanced at the crystal surfaces of HAP by the high spatial charge density and possibility of H-bonding to the surface phosphate groups. Moreover, the stability constants for Ca polyhydroxyl complexes decrease in the order, D-sorbitol > D-fructose > D-glucose (Makinen and Soderling 1984). This is consistent with the sequence of the ability of active additives to induce morphological changes with HAP crystals, i.e:

Sorbitol =1,2-butanediol > D-fructose > glucuronic acid = N-acetyl glucosamine > D-glucose + anomers = ascorbic acid > 1,2 and 1,3 cyclohexanediol.

This suggests that the strength of interaction with surface Ca ions could be an important factor in determining the size and aspect ratio of the needle-like crystals formed from chloride-containing solutions

The expression of well-defined HAP {100} faces in the presence of sugar molecules indicates some selectivity in surface binding. But as these surfaces are also stable in the absence of additives, differences in the inherent growth kinetics of unrelated faces, rather than variations in the arrangement of surface calcium and phosphate groups, could be responsible for this apparent selectivity. This is borne out by the fact that changes in structure (ring verses open-chain), stereochemistry or functionalization often had negligible effect, suggesting that the extent of molecular recognition present at the crystal/additive interface is limited to multiple polar interactions involving co-operative binding of hydroxyl residues. Support for this is the finding that the most effective additive in terms of inducing morphological effects is sorbitol, which contains six hydroxyl groups. However, 1,2-butanediol was equally effective suggesting that the 1,2-diol moiety of a linear molecule interacts strongly with the crystal surfaces. PVA produced an anomalous effect which may be a result of its relatively great length. The polymer may too long and flexible to interact with individual crystal faces, but simultaneously adsorbs to adjacent prenuclei structures which then facilitates a fusion between them as they develop. The 1,2-diol group is less effective when present in a cyclic molecule, possibly due to increased steric hindrance arising from the ring conformation. This may explain why fructose was more effective than the hexaldoses since the greater conformational flexibility of the envelope form of the furanose ring, as compared with that of the $^4C_1$ chair form of the β-D-glucopyranose ring, would reduce the degree of steric hindrance associated with additive adsorption. In aqueous solution fructose cyclizes to form both furanose and pyranose rings. But, unlike the glucopyranose derivatives, the furanose and fructopyranose rings have one carbon centre (C-2) which is bifunctional (pendant CH_2OH and OH residues) and this could

also be a site capable of strong interaction with the HAP {100} faces. Increasing the separation between hydroxyls or a very high degree of free rotation around OH bonds is reflected in a decrease in additive effectiveness. With a high degree of free rotation the configurational energy barrier that has to be overcome is to allow a suitable orientation is too great.

Further support for a general kinetic, rather than structural mechanism for the modification of HAP crystallization in the presence of monosaccharides, is indicated by the formation of needle-like crystals in the presence of nitrate-containing solutions. Although these crystals were not as elongated as the additive-grown samples, their presence clearly indicates the important role of Cl^- in promoting the plate-like morphology of HAP. Thus, it appears that the potency of the polyhydroxyl additives in inducing high axial ratio crystals is dependent on their ability to override the effect of Cl^-. The morphological influence of Cl^- has been previously observed and can be attributed to surface incorporation at defect sites (Koutsoukos and Nancollas 1981). It is still unknown how the Cl^- interaction not only stabilize the (110) faces but reduce the crystal symmetry ($P6_3/m$ to $P2_1/b$) such that only two of the possible six {100} faces are expressed. Terpstra (Terpstra et al 1986, 1987) has calculated the E^{slice}_{hkl} and E^{att}_{hkl} for OCP and HAP F faces (see chapter 1.13-1.17). These values are here compared with the observed relative area of faces for needle-like (Cl^- absent) and plate-like (Cl^- present) HAP morphologies precipitated in this study in the absence of organic additives (Table 3.2).

Connected net (*kl*)	Morphological Importance OCP	HAP	Relative observed area for needle-like HAP	Relative observed area for plate-like HAP
(100)	1	1	{10}	---
(011)	10	2	---	---
(110)	8	3	---	1.5
(002)	4	4	1	1
(-110)	2	?	---	100

Table 3.2. Table of calculated morphological importance of crystal forms compared to observed relative areas for needle-like and plate-like HAP. Note that for HAP {10}=(100),(1-10), (010), (-100), (-110) and (010) faces, dash denotes non-expression.

Thus the (-110) face is predicted as a stable face in OCP and interestingly this face forms the large face in plate-like HAP. This suggests that the plate-like form of HAP is derived more fully from an OCP plate-like precursor than is the needle-like form.

A possible explanation of the role of Cl^- is that it destabilizes the ACP phase to some degree by undergoing a dynamic exchange at the surface of the ACP that exists transiently upon each pulse addition. Cl^- incorporation into the ACP cluster surface may produce a disruption that increases the solubility of the ACP phase at that site, this in turn would increase the supersaturation. In sufficient quantity the localized disturbances and associated higher supersaturation could kinetically favour the formation of thin plates of OCP which serve as templates for HAP overgrowth (Brown 1981) (fig. 3.21). This effect may have been assisted, when a pulse addition method was employed, by the short-term drop in pH to below 7 that occurred on each addition

before adjustment to pH 9.5 took place. The lower pH reduces the rate of hydrolysis of OCP nuclei into HAP (Nelson et al 1989). During a continuous dropwise addition of aqueous $CaCl_2$ to a phosphate solution at 70°C the pH could be maintained close to 9.5 by addition of alkali. It was observed that this method resulted in needle-like rather than plate-like HAP crystals.

When polyhydroxyl additives are present they may bind strongly to the surfaces of the relatively soluble initial ACP/embryonic nuclei phase, excluding Cl^- from surface sites and inhibiting the OCP plate-like precursor. Possible support for this is shown by the finding that unwashed samples removed at intervals from a precipitation showed additive to be adsorbed initially, but as the HAP developed adsorption rapidly became non-evident. Also, calcium electrode experiments indicated that a longer and more stable ACP phase was obtained in the presence of additives. Nucleation of needle-like HAP outgrowths from the ACP spherulites would then be followed by a normal growth pattern of elongation along the *c* axis and expression of six {100} faces.

Previous workers have shown that the interaction of sugars with mature HAP crystal faces is minimal (Makinen and Soderling 1984). However, differences in the lability of Ca-additive complexes could account for variation of aspect ratios of the HAP crystals grown with different additives due to changes in the affinity of polyhydroxyl additives at the *developing* crystal surfaces. It may be that the greater the interaction at the prismatic crystal faces the less the lateral expression and the higher the aspect ratio. It would seem likely that many open chain polyhydroxyl derivatives (such as sorbitol) will produce HAP crystals extensively elongated along the *c* axis.

A further possibility is that the observed differences in morphological potency could be due to differences in the thermal and chemical stability of the additives at 70 ^{o}C and pH 9.3-9.8. For example, α and β anomers, epimers, fructose, open-chain structures, disaccharides, polysaccharides and a variety of saccharinic acids are known to coexist in alkaline glucose solutions (Hough and Richardson 1979 p687-748; Machell and Richards 1960). Indeed, FTIR spectra of monosaccharides subjected to the reaction conditions were complex.

A series of analogous experiments in which HAP crystals were grown in the presence of monosaccharides but at 40 ^{o}C produced plate-like HAP crystals where no morphological effects were apparent. These results suggest that the rapid transformation of the initial gel-like precipitate into filamentous HAP crystals is kinetically inhibited at lower temperature, hydrolysis of OCP precursors into HAP is less rapid at this temperature. Presumably, adsorption of sugar molecules onto the primary precipitate can stabilise this phase unless sufficient thermal energy is provided to overcome the activation energy barriers associated with desorption and subsequent crystal growth in the presence of the additives. This could explain why P : additive ratios lower than 6:1 were not as selective in producing the needle-like habit at 70 ^{o}C, since an increased sugar concentration could stabilize the initial gel by extensive surface adsorption.

The first stage in the transformation of the gel-like structures involves the formation of linear arrays of spherical domains within the ill-defined matrix suggesting that this process is essentially an *in situ* transformation within the calcium phosphate/sugar

network. The subsequent rapid crystal growth along the *c* axis could be a consequence of both chemical and physical properties of the surrounding gel matrix. Growth perpendicular to the *c* axis becomes more pronounced as the reaction proceeds possibly because of increasing thermal degradation and transformation of the sugar molecules (fig. 3.21). Indeed, it was observed that the continuous addition of monosaccharide solutions to the reaction results in increased *c*-axis elongation of the HAP crystals compared with those in the above experiments.

When the reaction conditions were altered such that calcium was in large excess, particularly pointed needles were obtained. The hydration layer surrounding the developing crystal would contain a relatively higher proportion of calcium ions compared to that obtained with the normal experimental protocol. The higher positive charge may lead to more adsorption of additive through attraction of the hydroxyl groups. The increased level of additive further suppresses lateral development of the developing needle and results in highly pointed crystals.

The results obtained in this study may have significance in the field of biological calcification. Although the HAP crystals were grown under conditions far-removed from the physiological environment, there are striking similarities between the crystals produced in the presence of chloride and bone mineral, and the sugar-induced needle-shaped crystals and enamel HAP. Whilst the presence of regularly spaced organic structures could be responsible for extreme *c* axis elongation of enamel crystals, it is possible that the covalently-bound polysaccharide residues of the acidic enamelin proteins could act in a similar manner to the monosaccharides used in this study. The combination of polyhydroxyl and negatively charged glutamate and aspartate residues

might have a role in chloride exclusion from developing tooth enamel and augment the growth of needle shaped HAP crystals under conditions of physiological temperature and pH.

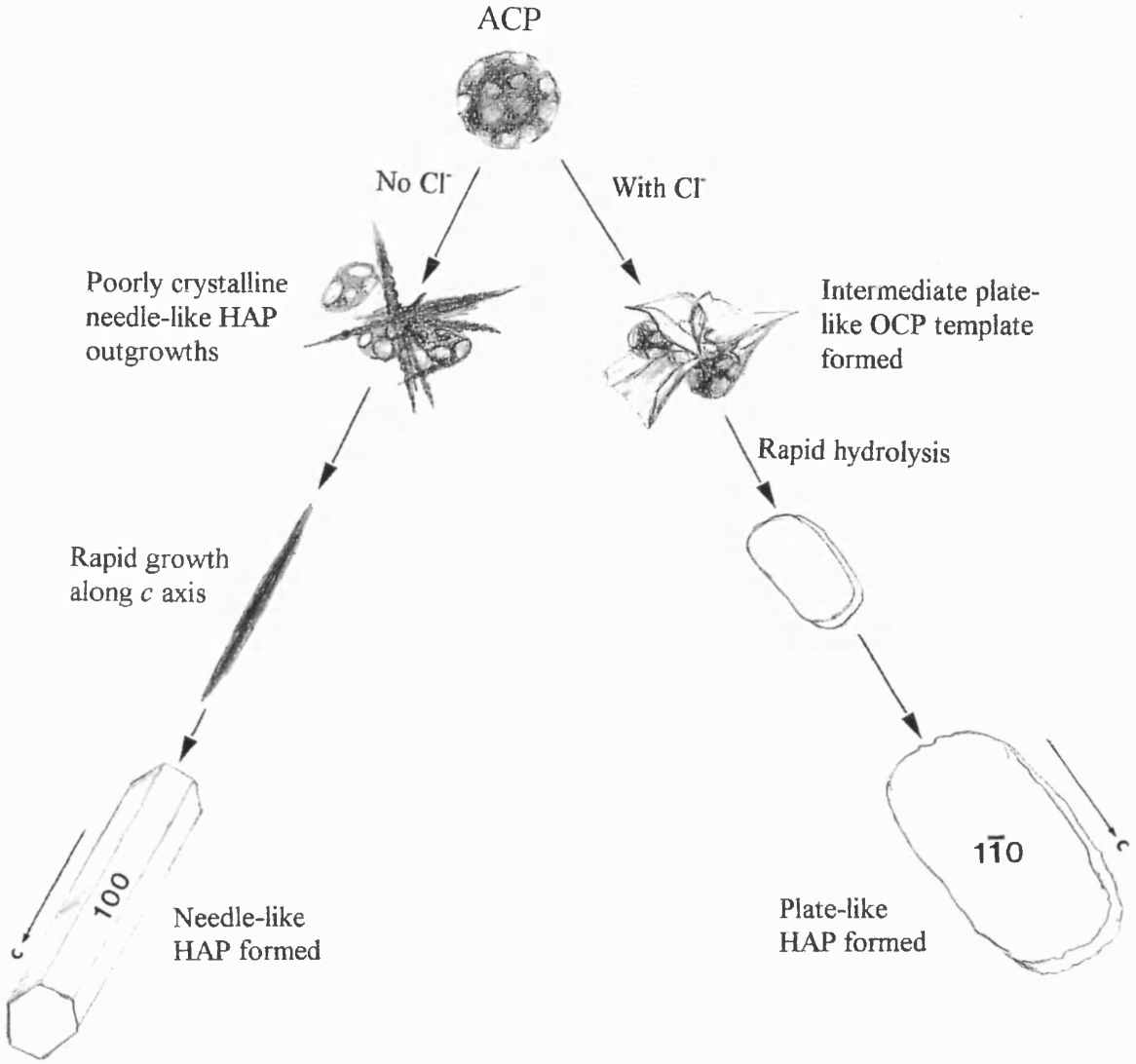

Fig. 3.21. Summary of possible pathways to needle-like and plate-like HAP morphologies.

REFERENCES

Angyal S.J. (1972), *Complexes of Carbohydrates with Metal Cations*, Australain J. Chem., **25**, 1957-1966.

Barr T.L. (1978), *Applications of ESCA in Industrial Research*, Am. Lab., **10(65)**, 40.

Bigi A., Falini G., Foresti E, Gazzano M.,Ripamonti A., Roveri N. (1993), *Magnesium Influence on Hydroxyapatite Crystallization*, J. of Inorg. Biochem., **49**, 69-78.

Bres E.F, Barry J.C., Hutchison J.L. (1985), *High-resolution Microscope and Computed Images of Human Tooth Enamel Crystals*, J. Ultrastruct Res., **90**, 261-274.

Chen C.C., Boskey A.L., Rosenberg L.C. (1984), *The Inhibitory Effect of Cartilage Proeoglycans on Hyroxyapatite Growth*, Calcif. Tissue. Int., **36**, 285-290.

Christoffersen M.R., Christofferesen J. (1984), *The Inhibitory Effect of ATP,ADP and AMP on the Rate of Dissolution of Calcium Hydroxyapatite*, Calcif. Tissue Int., **36**,659-661.

Cook W.J., Bugg C.E. (1973), *Calcium Binding to Galactose. Crystal Structure of a Hydrated α–Galactose-Calcium Bromide Complex*, J.Am. Chem Soc., **95** (19), 6442-6446.

Cuisinier F., Bres E.F, Hemmerle J., Voegel J-C, Frank R.M, (1987), *Transmission Electron Microscopy of Lattice Planes in Human Alveolar Bone Apatite Crystals.*, Calcif. Tiss. Int, **40**, 332-338.

Dziewiatkowski D.D. (1987), *Binding of Calcium by Proteoglycans in Vitro*, Calcif. Tissue Int., **40**, 265-269.

Francis M.D., Briner W.W., Gray J.A. (1973), in *Hard Tissue Growth,Repair and Remineralization*, Sognnanes R.F, Vaughn J.M. (Eds), Elsevier, Amsterdam.

Garnett J., Dieppe P. (1990), *The Effects of Serum and Human Albumin on Calcium Hydroxyapatite Crystal Growth*, Biochem J., **266**, 863-868.

Heywood B.R., Sparks N.H.C., Shellis R.P., Weiner S., Mann S. (1990), *Ultrastructure, morphology and crystal growth of biogenic and synthetic apatites*, Connect. Tiss. Res., **25**, 1-17.

Hunter G.K., Grynpas M.D., Cheng P.-T., Pritzer P.H., *Effect of Glycosamines on Calcium Pyrophosphate Crystal Growth in Collagen Gels*, Calcif. Tissue Int., **41**, 1164-1170.

Koutsoukos P.G., Nancollas G.H. (1981), *The Morphology of Hydroxyapatite Growth in Aqueous Solution at 37°C*, J. Cryst. Growth, **55**, 369-375.

LeGeros, Trautz O.R., LeGeros J.P., Klein E. (1967), *Carbonate Substitution in Apatite Structure*, Collern Int. Sur Les Phosphates Mineraux Solides, Toulose, pp66-72.

LeGeros R.Z., Le Geros J.P., Trautz O.R., Slurra W.P. (1971), *Conversion of Monetite, $CaHPO_4$, to Apatites:Effect of Carbonates on the Morphology of Apatite Crystallites,* Advances in X-ray Analysis, **14**, 57-66.

Lowenstam H.A. (1981), *Minerals Formed by Organisms*, Science, **211**, 1126-1131

Makinen K.K., Soderling E., (1984), *Solubility of Calcium Salts, Enamel and Hydroxyapatite in Aqueous Solutions of Simple Carbohydrates*, Calcif. Tissue Int., 36, 64-71.

Moreno E.C., Varoghese K. (1981), *Crystal Growth of Calcium Apatites from Dilute Solution*, J. of Cryst. Growth, **53**, 20-30.

Moridian-Oldak J., Weiner S. Addadi W.J., Landis W.J., Traub W. (1991), *Electron Imaging and Diffraction Study of Individual Crystals of Bone, Mineralized Tendon and Synthetic Carbonated Apatite*, Connnect Tiss. Res., **25**, 219-228.

Nelson D.G.A., Barry J.C., Shields C.P., Glena R., Featherstone J.D.B. (1989), *Crystal Morphology, Composition and Dissolution Behaviour of Carbonated Apatites Prepared at Controlled pH and Temperature*, Jr. of Coll. and Int. Sci, **130**(2), 467-479.

Nancollas G.H., Koutsoukos P.G. (1981), *Influence of the Strontium on the Crystallization of Hydroxyapatite from Aqueous Solution.*, J. Am. Chem. Soc., **85**, 2403-2408.

Nancollas G.H., Koutsoukos P.G. (1986), *The Effect of Lithium on the Precipitation of Hydroxyapatite from Aqueous Solution,* Colloids and Surfaces, **17**, 361-370.

Okazaki M. (1992), *Heterogeneous Synthesis of Fluoridated Hydroxyapatites*, Biomaterials, **13(11)**, 749-754.

Romberg R.W., Werness P.G., Riggs B.L., Mann K.G. (1986), *Inhibition of Hydroxyapatite Crystal Growth by Bone Specific and Other Calcium-Binding Proteins,* Biochemistry, **25**, 1176-1180.

Selvig K. (1970), *Periodic Lattice Images of Hydroxyapatite Crystals in Human Bone and Dental Hard Tissues*, Calcif. Tiss. Res., **6**, 227-238.

Terpstra R.A., Bennema P., Hartman P., Woensregt C.F., Perdok W.G., Senechal M.L. (1986), *F Faces of Apatite and its Morphology: Theory and Observation*, Jr. Crystal Growth, **78**, 468-478.

Terpstra R.A., Bennema P. (1987), *Crystal Morphology of Octacalcium Phosphate: theory and Observation*, Jr Crystal Growth, **82**, 416-426.

Weiner S, Talmon Y., Traub W. (1983), *Electron Diffraction of Mollusc Shell Organic Matrices and their Relationship to the Mineral Phase.*, Int. J. Biol. Macromol., **5**, 325-328.

Weiner S., Traub W. (1984), *Macromolecules in Mollusc Shells and their Functions in Biomineralization*, Philos. Trans. R. Soc. Lond. [Biol], **304**, 425-434.

Werness P.G., Bergert J.H., Lee K.E., *Urinary Crystal Growth: Effect of Inhibitor Mixtures*, Clin. Sci., **61**, 487-491.

CHAPTER 4.0

PRECIPITATION OF HAP IN PRESENCE OF LITHIUM

4.0 Precipitation of HAP in the presence of lithium

4.1 Introduction

The last chapter involved the use of organic additives in solution with developing HAP crystals, in which the Cl^- anion was found to promote the formation of plate-like rather than needle-like HAP. ESCA analysis suggested that this anion was not incorporated. However, the small size of the lithium cation has been found in many studies to allow incorporation into crystal structures. The incorporation is often reflected by large changes in the morphology of the crystals, e.g. a high proportion of lithium has been shown to change normal rhombohedral calcite into a tabular form with truncated hexagonal faces (Rajam and Mann 1990).

HAP precipitated with lithium at 40ppm in constant composition studies at pH 8.5 and 37°C produced marked changes in the HAP morphology. Strong inhibition of precipitation was also found which is thought to be caused by blocking of active crystallization sites through adsorption at crystal surfaces (Koutsoukos and Nancollas 1986).

The effect of the lithium cation on the morphology of HAP precipitated by the pulse addition method at 70°C used in the previous chapter was studied in an attempt to produce modification of HAP away from the apparently invariable plate or needle like morphology reported in literature.

4.2 Materials and methods

HAP was prepared using calcium nitrate as in chapter 2.2, lithium nitrate was added to the phosphate solution prior to calcium nitrate addition at a PO_4/Li molar ratio of 1:1 and 1:10. The experiment was then repeated using lithium chloride in place of lithium nitrate at a PO_4:Li molar ratio of 1:10.

4.3 Analysis of crystal products

Samples of the precipitate were removed at intervals and examined by TEM and SEM using a Jeol 1200EX operating at 120kV, SEM analysis was conducted using a ASID attachment. FT-IR spectra of the precipitates formed at both Li^+ concentrations and following reflux for 18 hours were recorded as KBr disks on a Nicolet 510P FT-IR spectrometer. XRD of the precipitates were recorded on a Philips PW 1730 diffractometer with a 4KW X-ray generator with collection made on a PM8203 chart recorder.

4.4 Results

When HAP was precipitated in the presence of lithium nitrate at a PO_4:Li molar ratio of 1:1 the rate of precipitation was observed to be markedly reduced, following the precipitation procedure the mixture was allowed to stand at room temperature. After 5 days the mass of the precipitate recovered was approximately 30% of that obtained in lithium free preparations. Upon examination of the precipitate by TEM and SEM plate-like HAP crystals of up to 300nm length, 100nm width and 20nm thickness were observed (fig.4.1). Electron diffraction studies showed that the c axis was aligned with the long axis of the plate (fig.4.2). Also present were a small number of truncated rod

like crystals which were shown by electron diffraction to be lithium phosphate. D-spacing measurements obtained form an electron diffraction pattern corresponding to the [110] zone of HAP show an increase compared to lithium free control preparations, which may be a reflection of poor crystallinity (table 4.1). An FT-IR spectrum taken after the mixture had been allowed to stand for five days shows an abnormal ν_4 phosphate band at around 600cm^{-1} and the ν_3 phosphate band at 1030cm^{-1} is barely split which is consistent with poorly crystalline HAP (fig. 4.3) (Fowler et al 1966). XRD analysis of the sample after standing for 3 months produced a diffractogram with well defined peaks which was virtually identical to control HAP.

Precipitation of HAP from a preparation made at XRD a PO_4:Li of 1:10 was observed to be very greatly inhibited and continued to occur on standing for several months. Upon examination by TEM aggregations of large plates are visible (fig. 4.4.). An FT-IR spectra recorded after six days again showed an abnormal ν_4 phosphate band around 600cm^{-1} and the ν_3 phosphate band at 1030cm^{-1} shows a complete absence of splitting and is consistent with amorphous/very poorly crystalline HAP (fig 4.5). This suggests that the higher lithium content further inhibits the development of the HAP. Upon removal, extensive washing and refluxing of the precipitate in water for 18 hours, the FT-IR spectrum now shows split phosphate band and is entirely consistent with control HAP (fig. 4.6). An XRD measurement of sample was taken after 3 months gave well defined peaks indicating that development into well crystalline HAP had taken place (fig. 4.7). The unit cell dimensions of the sample calculated using the XRD data (see chapter 2.10) show a slight enlargement (table 4.2). The diffractogram has very well defined sharp peaks suggesting that the increase is not due to poor crystallinity.

Fig.4.1TEM micrograph of HAP precipitated with $LiNO_3$ at PO4:Li molar ratio of 1:1

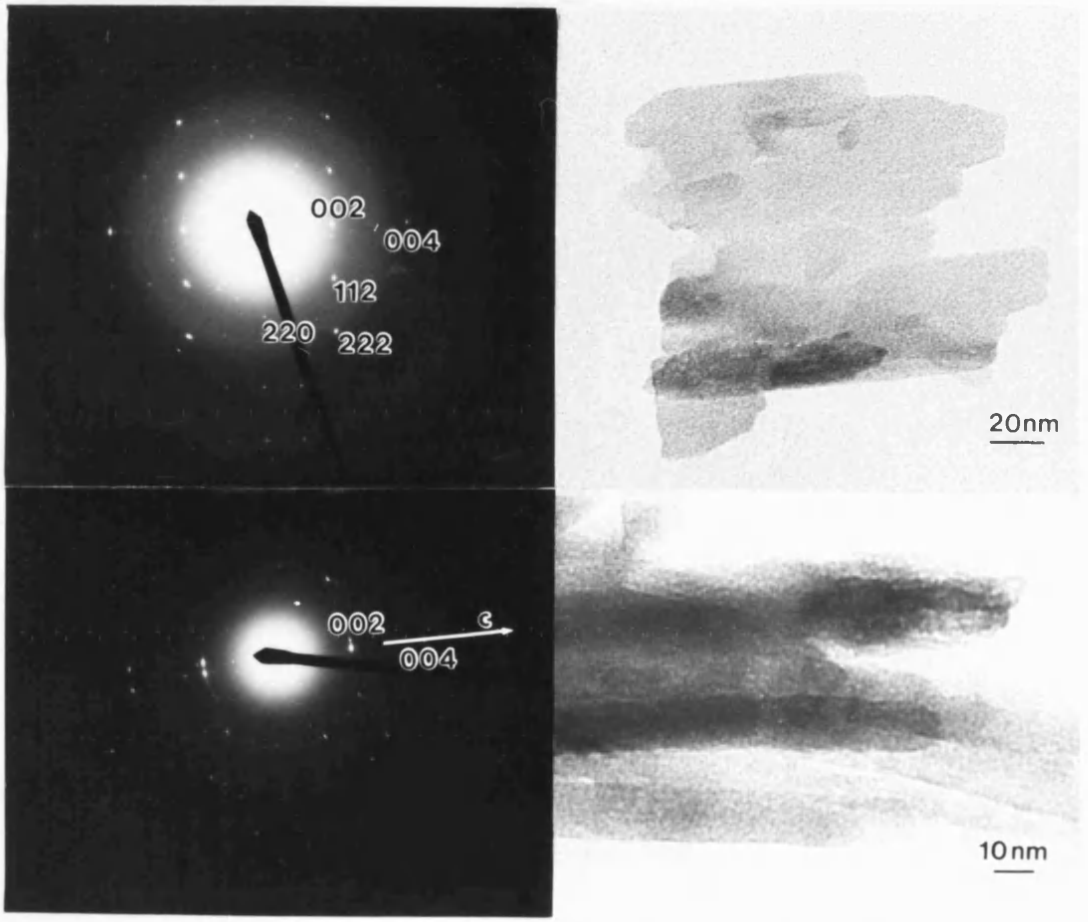

Fig. 4.2. (a) ED pattern of plate-like HAP formed with $LiNO_3$ at PO_4:Li of 1:1, the pattern corresponds to the [110] zone; (b) large (1-10) faces of plate-like HAP; (c) ED pattern corresponding to the [010] zone; (d) edge-on view of plate-like HAP.

d Å measured	d Å standard	hkl
3.53	3.44	002
2.85	2.77	112
4.01	3.88	111

Table 4.1. Measured d spacings for HAP prepared with $LiNO_3$ at a PO_4:Li molar ratio of 1:1 compared to standard. (Standard values obtained from ASTM (JCPDS) cards).

	c axis d Å	a axis dÅ
Standard HAP	6.88	9.43
Control HAP	6.89	9.44
HAP precipitated with Li	6.90	9.45

Table 4.2. Unit cell dimensions of HAP precipitated with $LiNO_3$ at PO_4:Li molar ratio of 1:10 (calculated from XRD) compared to standard and control HAP.

Examination of the precipitate formed with lithium chloride at a PO_4: Li molar ratio of 1:10 by TEM revealed the presence of plate-like HAP of length 500nm, width 200 nm and thickness 10 nm, the plates are somewhat thinner than those produced in the presence nitrate (fig.4.8), the FT-IR spectrum shows the same characteristics as the HAP preparations with lithium nitrate.

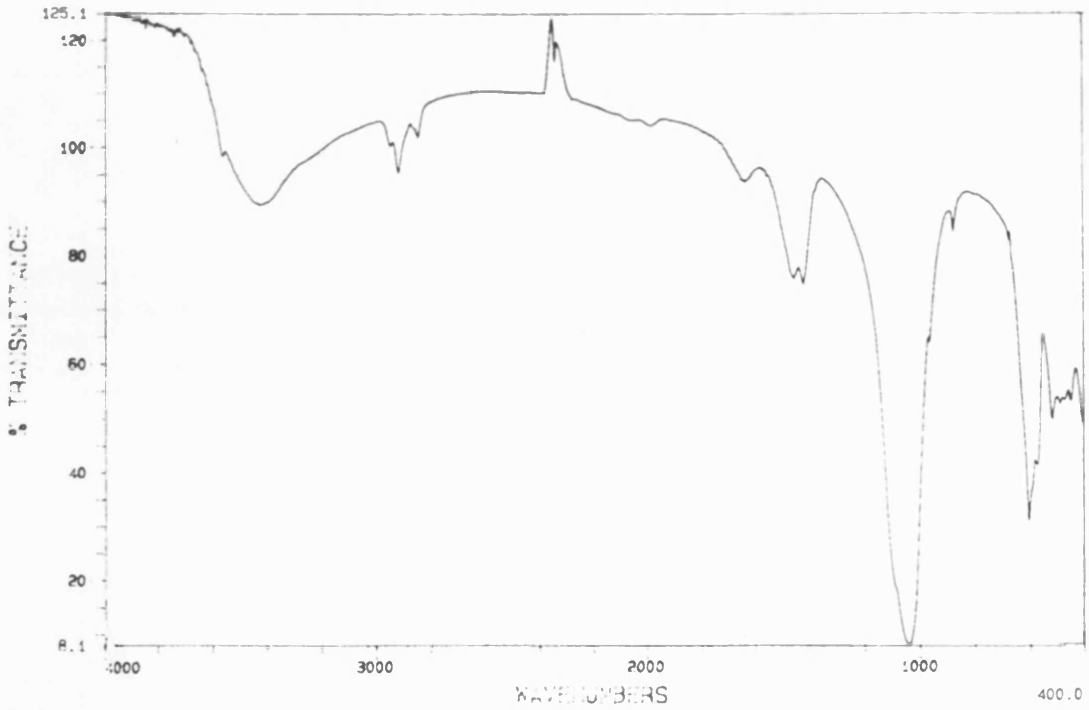

Fig. 4.3. FT-IR spectrum of poorly crystalline HAP precipitated with $LiNO_3$ at PO_4:Li molar ratio of 1:1after standing for 5 days.

Fig. 4.4. (a) TEM micrograph of HAP precipitated with $LiNO_3$ at PO_4:Li molar ratio of 1:10.

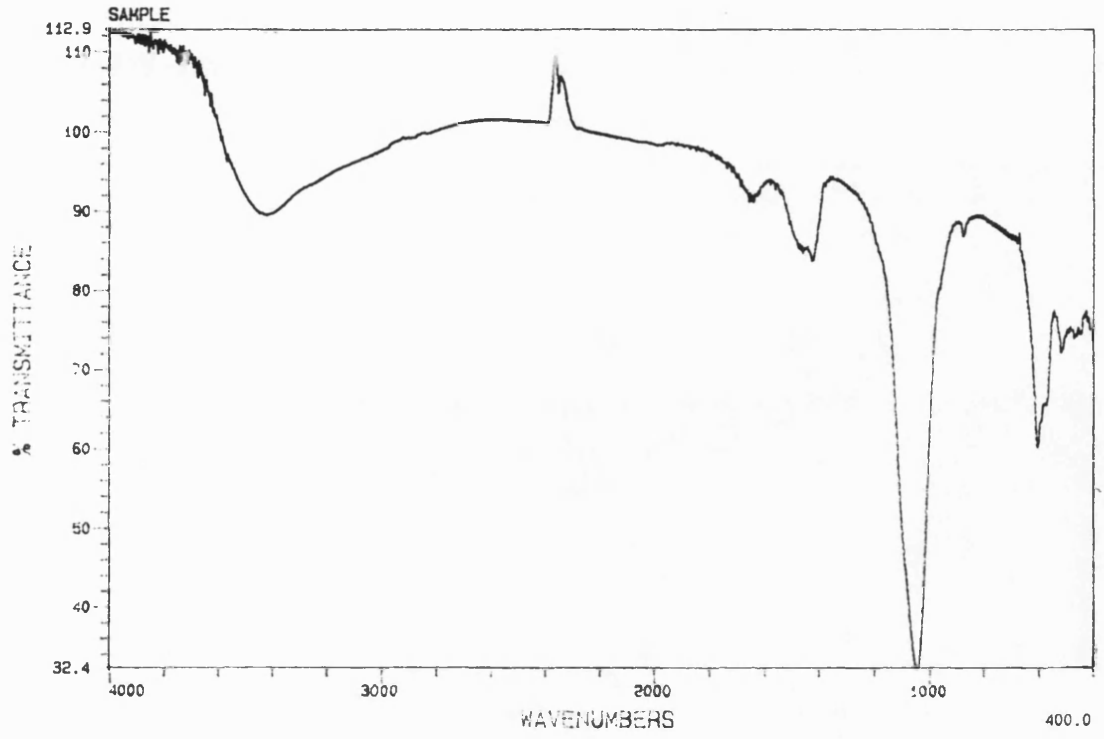

Fig. 4.5. FT-IR spectrum of poorly crystalline HAP precipitated with $LiNO_3$ at PO_4:Li molar ratio of 1:10 obtained after standing for 6 days.

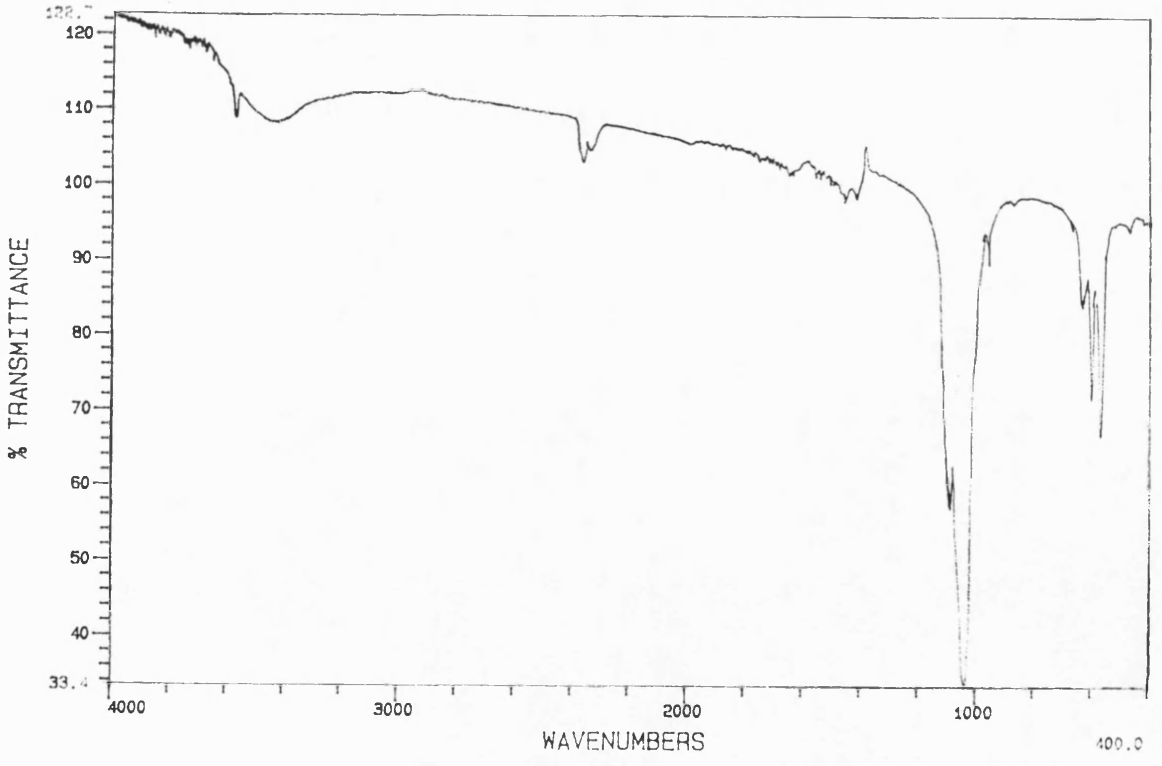

Fig.4.6. FT-IR spectrum of well crystalline HAP formed after reflux for 18 hours.

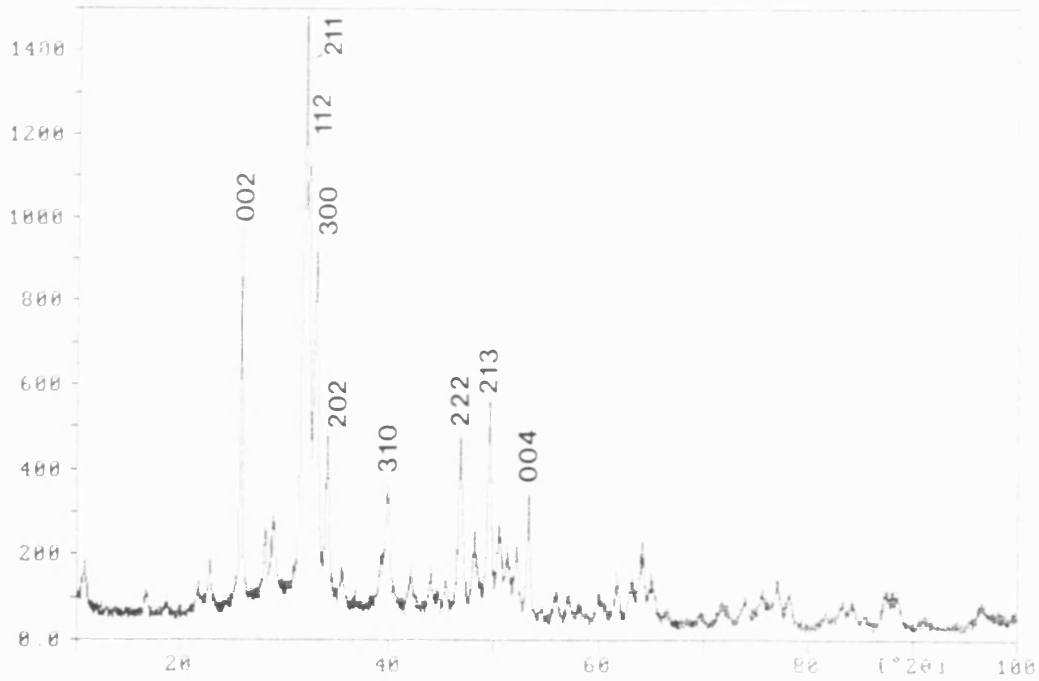

Fig. 4.7. XRD of well crystalline HAP precipitated with $LiNO_3$ at a PO_4:Li molar ratio of 1:10 after standing for 3 months.

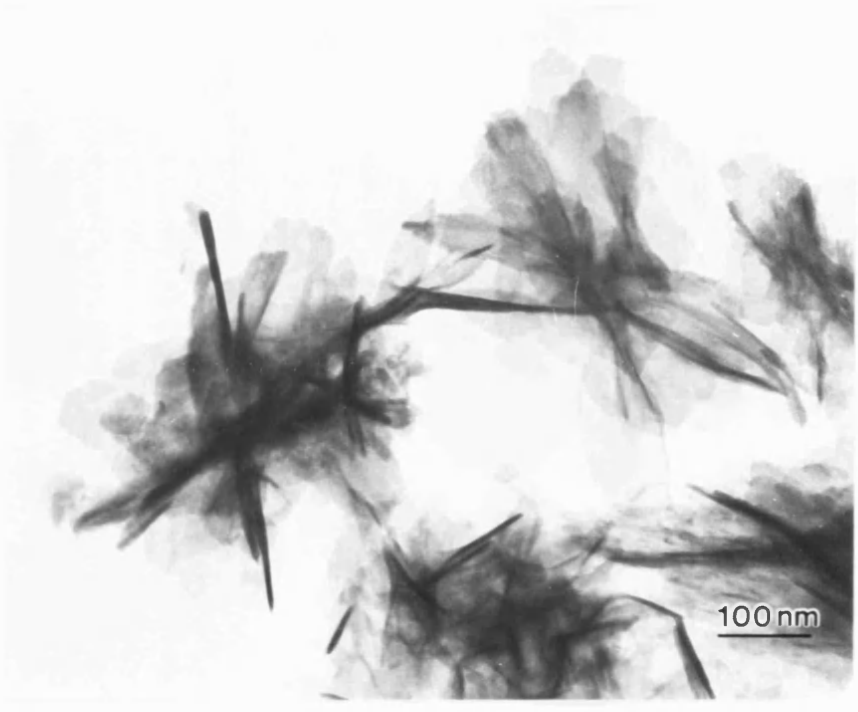

Fig. 4.8. TEM of plate like HAP precipitated with LiCl at PO_4:Li molar ratio of 1:10.

4.5 Discussion

A considerably reduced rate of precipitation of HAP was observed which was dependant on the concentration of Li^+. It was previously shown that nitrate had no morphological effect, therefore it is likely that the Li^+ is similar to Cl^- in possibly disrupting the surface of the ACP precursor which then promotes the plate-like HAP. The abnormal phosphate bands at around $600cm^{-1}$ in the IR spectrum and the increased d-spacing and slightly increased unit cell dimensions point toward a limited incorporation of Li^+ . The incorporation is facilitated by its small size (ionic radius 0.6Å), incorporation of the larger Cl^- ion (ionic radius 1.81Å) was not indicated in the previous chapter. Substitution into lattice sites would be likely to decrease the unit cell dimensions which suggests that the incorporation is occurring in interstitial sites rather than lattice sites. A suitable site may be in spaces surrounding the negatively charged oxygens of the phosphates, this may give rise to the alteration in the arrangement of P-O bonds of phosphate tetrahedra suggested by the IR spectrum.

A consequence of incorporation may be that the charge is balanced by the further incorporation of HPO_4^{2-} or CO_3^{2-} ions or possibly by calcium vacancies. Upon reflux the incorporated species are lost as a consequence of Ostwald ripening and fully ordered HAP is formed.

The results suggest that Li^+ can produce morphological effects similar to those found with Cl^- but the small size of the ion allows greater adsorption to the surfaces of the developing HAP and possibly its incorporation into interstitial sites surrounding phosphates. The presence of both Li^+ and Cl^- appear to have a combined effect that

accentuates the formation of plates. The lithium ion under the conditions used was not found to be absorbed to a specific face such that an unusual morphology was stabilized.

References

Fowler B.O., Moreno E.C., Brown W.E. 1966, *Infra-red Spectra of Hydroxyapatite, Octacalcium Phosphate and Pyrolysed Octacalcium Phosphate*, Arch. Oral. Biol., **11**, 477-492.

Koutsoukos P.G., Nancollas G.H. 1986, *The Effect of Lithium on the Precipitation of Hydroxyapatite from Aqueous Solutions*, Colloids and Surfaces, **17**, 361-370.

Rajam S., Mann S. 1990, *Selective Stabilisation of the (001) face of calcite in the presence of lithium*, J. Chem. Soc. Chem. Commun., **24**, 1789-1791.

CHAPTER 5.

CONSTRUCTION OF RETICULATED CALCIUM PHOSPHATE FRAMEWORKS IN BICONTINUOUS REVERSE MICROEMULSIONS

5.0 Construction of Reticulated Calcium Phosphate Frameworks in Bicontinuous Reverse Microemulsions

5.1 Introduction

Nature is able with apparent ease to produce elaborate structures composed of inorganic solids by the utilization of a protein matrix or vesicle. Until recently attempts at mimicking the biological strategies involved in biomineralization have involved essentially two-dimensional approaches. Organized assemblies of amphiphilic molecules have been used as templates for the production of inorganic-organic composites, as monolayers to provide recognition surfaces for the orientated nucleation of inorganic crystals and as vesicles to provide environments for inorganic materials synthesis. This approach can successfully imitate small aspects of biomineralization processes but has not so far led to the production of three-dimensional structures that can begin to mimic the architectures of biological tests and shells of creatures such as diatoms and sea urchins.

Recent interest in this area has been shown by a new development in the preparation of mesoporous silica-based composite structures of organic and inorganic compounds with lamellar (Sakata and Kunitake 1990, Dubois and Gulik-Kryzywickl 1993), hexagonal and cubic (Krege et al 1992, Beck et al 1992) topologies. This was achieved by the utilization of microemulsion based self-assembled organic aggregates as a framework to organize inorganic oxides. This discovery involves the use of liquid crystal surfactant aggregates to control the pore size (up to 10nm in diameter) of amorphous aluminosilicate materials formed from aqueous solution (Krege et al 1992, Monnier et al 1993).

The bicontinuous phase of a microemulsion system composed of interconnecting water and oil conduits, separated by a surfactant wall, is an elaborate structure which was found to be suitable for exploitation in the construction of nano-porous three-dimensional structures. The approach adopted in this study differed from previous studies with liquid-crystal aggregates in that the aqueous channels were targeted and reticulated frameworks of macro-porous inorganic crystals formed. Many of the physical properties of HAP will be affected by its crystal size, shape and surface area and the ability to modify these characteristics could have implications in its use in chromatography, catalysis and ion-exchange (Tiselius A. et al 1956), (Bernardi G. et al 1971), (Hjerten S. 1959), orthopaedics and dentistry (Makishima A. et al 1958).

5.2 Microemulsions

Microemulsions are thermodynamically stable fluid mixtures of water, oil and amphiphile, the water rich areas are separated from the oil rich by an amphiphilic layer. The mutual arrangement and shapes of these separated areas is related to proportion of the three components and is an area of much research.

Microemulsion structures have been observed by means of freeze fracture microscopy (FFEM) and direct imaging (DI). In FFEM the specimens are rapidly frozen, fractured, shadowed and replicated followed by examination by TEM (Jahn and Strey 1988). In DI a cryostage is used to study thin sections in the hydrated state (Talmon 1986). Techniques such as conductance (Chen 1986), viscosity and NMR (Blum 1985), small angle neutron scattering (SANS) fluorescent probes (Eastoe 1992) and X-ray scattering (Zemb 1987)

have been used to elucidate the microemulsion structure as the proportion of components is altered and three component phase diagrams constructed. From this work a general picture of the microemulsion and its changes in structure across its phase diagram has emerged, large variations due to the particular nature of the oil and surfactant can exist.

Microemulsions involving the cationic quaternary ammonium surfactant didodecyldimethyl ammonium bromide ($(C_{12}H_{25})_2(CH_3)_2NBr$, DDAB) and alkane oils have some unique features. The surfactant is insoluble in alkanes and almost insoluble in water and does not form reverse micelles at very low water. Many studies of the system have been made and it is believed that the addition of water to a mixture containing a mixture at fixed surfactant/oil ratio produces the following changes. The mixture of surfactant, oil, and water will become a clear microemulsion when sufficient water is added so that all the surfactant is solubilized at the oil-water interface, consistent with the degree of oil penetration and the need to solvate counterions. The predominant structures will be interconnected and rodlike, with a characteristic curvature set by the volume of water (Fig. 5.1).

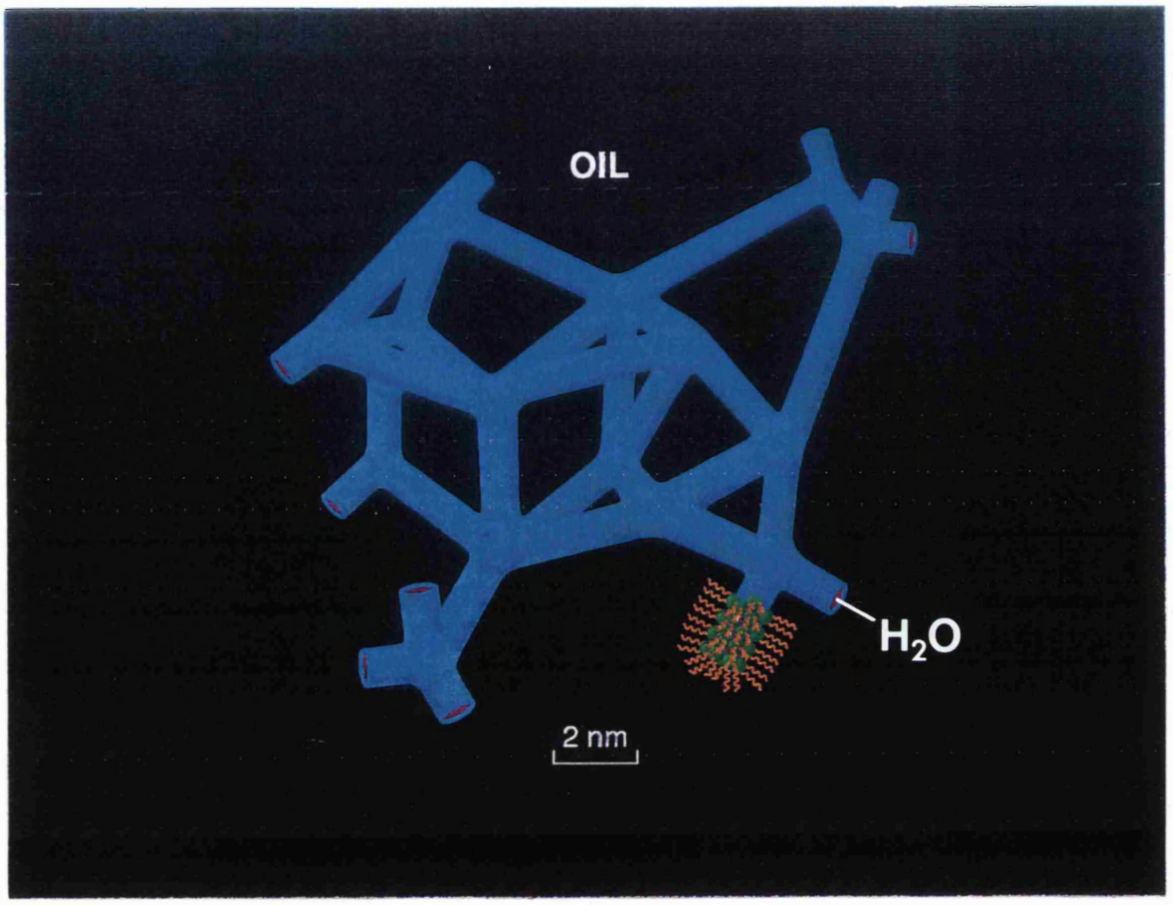

Fig. 5.1. Envisaged structure of bicontinuous microemulsions.

With addition of water the radii of these tubes increase and the average and gaussian curvature decreases, since interfacial area remains, within reasonable limits, fairly constant. With further increase in water the tubes grow and exceed optimal curvature as dictated by opposing head group interactions and oil penetration. The conduits begin to disconnect and a transition from a connected conducting network to nonconducting spheres occurs. This transition occurs in a way that the curvature remains essentially constant. At the percolation boundary the system has converted completely to spheres. Further addition of

water causes the spheres to grow, but when the curvature exceeds optimal, phase separation occurs (Zemb et al 1985). As well as being a function of the proportion of water present the degree of curvature shown by the water conduits and hence the 'pore-size', is determined by the degree of penetration of the alkane oil into the surfactant tails. Shorter chains penetrate more effectively and cause a greater degree of curvature than longer chains, indeed once the alkane chain length exceeds that of the surfactant tails the water conduits to do not convert to spheres over the entire single-phase region (Allen et al 1987). Thus a high degree of control over the structure of the microemulsion is possible by the choice of oil, surfactant and the proportion of the components.

Bicontinuous microemulsions obtained using DDAB have a networked microstructure that rapidly fluctuates in liquid media. In this study frozen oils were used to generate immobilized frameworks for the construction of inorganic architectures. Previous work has shown that upon rapid freezing the water contained in a microemulsion is supercooled and initially does not freeze, though after some time ice crystals form and the water becomes progressively more frozen (Becher 1985). The frozen mixture can also be stored below the melting point of the oil until crystal growth has proceeded greatly. It is likely that storage of a microemulsion mixture below the melting points of hexane through to decane would result in freezing of the water conduits before appreciable crystal growth had occured. With the shorter chain alkanes the low m.p. also presents some practical difficulties with storage. However the alkane dodecane ($C_{12}H_{26}$, m.p. -9.6°C) and particularly tetradecane ($C_{14}H_{30}$, +5.9°C) and higher oils are suitable. These oils have the advantage that the microemulsion can be stored below the oil m.p. but above 0°C, thus

5.3 Materials and methods

5.4 Surfactants and Oils

The cationic surfactant didodecyldimethylammonium bromide (DDAB) and the alkane oils dodecane ($C_{12}H_{26}$), tetradecane ($C_{14}H_{30}$) and hexadecane ($C_{16}H_{34}$) were obtained from Aldrich Chem Co. The oils were filtered through 0.2 μm filters before use. The non-ionic surfactant pentaethylene glycol dodecylether ($C_{12}H_{25}(OCH_2CH_2)_5OH$, $C_{12}E_5$) was obtained from Sigma Chemical Co. and used as supplied.

5.5 Preparation of reticulated HAP from bicontinuous microemulsions using DDAB and dodecane (C12)

A 4.8-5.7 mM solution of calcium nitrate and 3.0mM-3.9mM solution of dihydrogen potassium phosphate were prepared, equal volumes were then mixed and the pH rapidly adjusted using 0.15M NaOH solution to approximately 7.4. The supersaturation (S) using $Ksp=10^{-59}$ (McDowell et al 1977) is given by (see chapter 1.1):

$$S=(4.8\times10^{-3})^5 \times (3\times10^{-3})^3\times10^{-7.4}/10^{-59} = \underline{6.19\times10^{26.6}}$$

The onset of appreciable precipitation occurs within five minutes and the preparation procedure was completed within that time. The supersaturated calcium phosphate solution was then added dropwise to a rapidly stirred mixture of the oil and surfactant such that the final proportions were at a point on the phase diagram equivalent to bicontinuous conduits (fig. 5.2 point A and table 5.1). In a typical experiment 4g of dodecane was mixed with 4g of surfactant and 2ml of supersaturated solution.

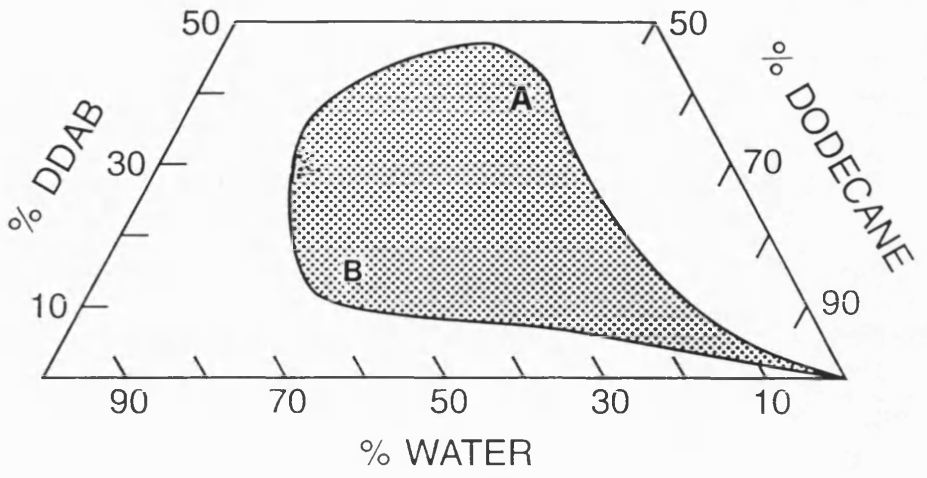

Fig. 5.2. Phase diagram of DDAB, dodecane and water microemulsion system at room temperature. Point A is area where bicontinuous cylinders predominate, point B is area where connected spheres predominate.

The onset of the single phase region was marked by the formation of an optically clear solution. When the required amount of supersaturated solution had been mixed into the microemulsion the clear mixture was poured into a container pre-cooled in liquid nitrogen to ensure rapid freezing. Rapid freezing was necessary to prevent a phase change from occurring before the oil component is frozen. The frozen mixture was stored at -25°C below the alkanes melting point of -9.6°C. It was found that the microemulsion transformed from a soft texture to hard after approximately one week, this was taken as indicating the freezing of the water component. At this time the mineral replica was extracted by centrifugation of the melted microemulsion at around 8000 rpm for 5-10 minutes. The supernatant was removed and the pellet washed extensively with hot hexane or acetone to remove residual DDAB and oil, followed by drying at room temperature. The effect of heating upon the recovered material was investigated by heating a sample to 200°C for 25 minutes followed by re-examination.

5.6 Analysis of Crystal Products

Samples were prepared for TEM and SEM by applying the unwashed pellet of white crystalline material directly to a grid or stub followed by washing in hot hexane and air drying. TEM examination was conducted using a Jeol 2000EX and a Jeol 1200EX transmission electron microscope operating at 200kV and 120kV respectively. SEM samples were gold coated using an Edwards S150B sputter coater prior to examination on a Jeol 1200EX transmission electron microscope using a Scanning Imaging Device (ASID) unit. A sample of the recovered solid was subjected to EDX analysis on a Jeol 2000FX TEM and XRD using a Philips PW-1130 X-ray diffractometer fitted witha Debye-Scherrer camera. Small quantities of the mineral were extracted by filtration of a few drops of the melted microemulsion on a 0.2μm polyester nucleopore membrane followed by washing with acetone or chloroform and air drying. The membrane was then gold coated and examined by SEM directly.

5.7 Results

After storage for ten days, centrifugation of the melted microemulsion produced a pellet of white crystalline material. Following extensive washing with hot chloroform, EDXA and XRD analysis showed the material was composed of HAP (fig. 5.3). Upon examination of the sample extracted by SEM a reticulated microstructure of interconnecting curved needle-like crystals of width 50nm and pore size up to 0.8μm was observed. (fig. 5.4). The reticulated structure is very similar to the envisaged structure of the bicontinuous microemulsion but the wall and pore size are considerably larger than the 1 nm channel size of an unchanged microemulsion (Hyde et al 1989). Upon heating of the recovered and washed material to 200°C for 25 mins. re-examination revealed that the reticulated network was unchanged (fig. 5.5). The heating temperature was much greater than the DDAB m.p. of 160°C thus indicating that the surfactant was removed completely prior to examination.

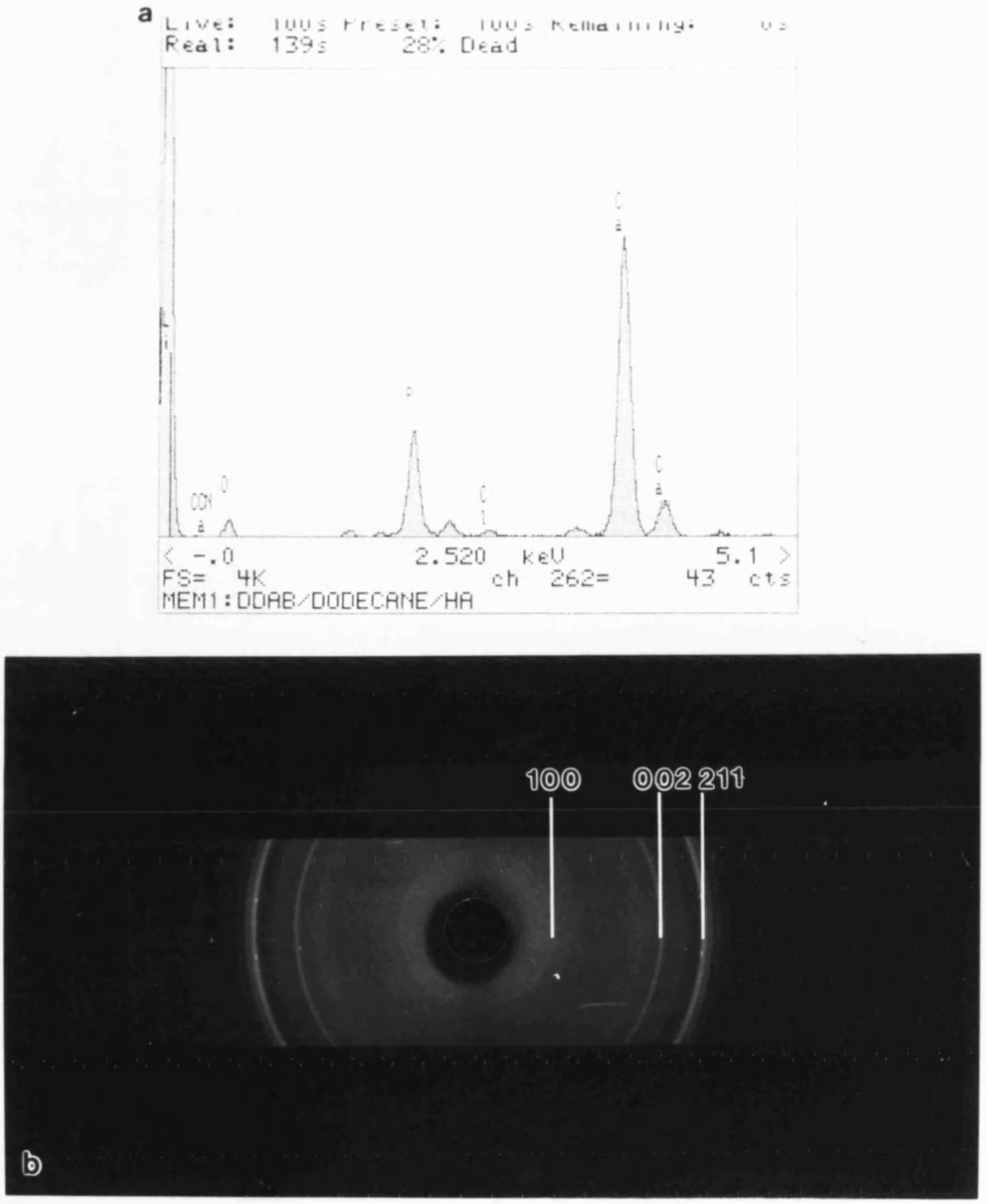

Fig. 5.3. (a) EDXA and (b) XRD of recovered crystalline material from bicontinuous microemulsion formed by DDAB/ dodecane and supersaturated calcium phosphate solution.

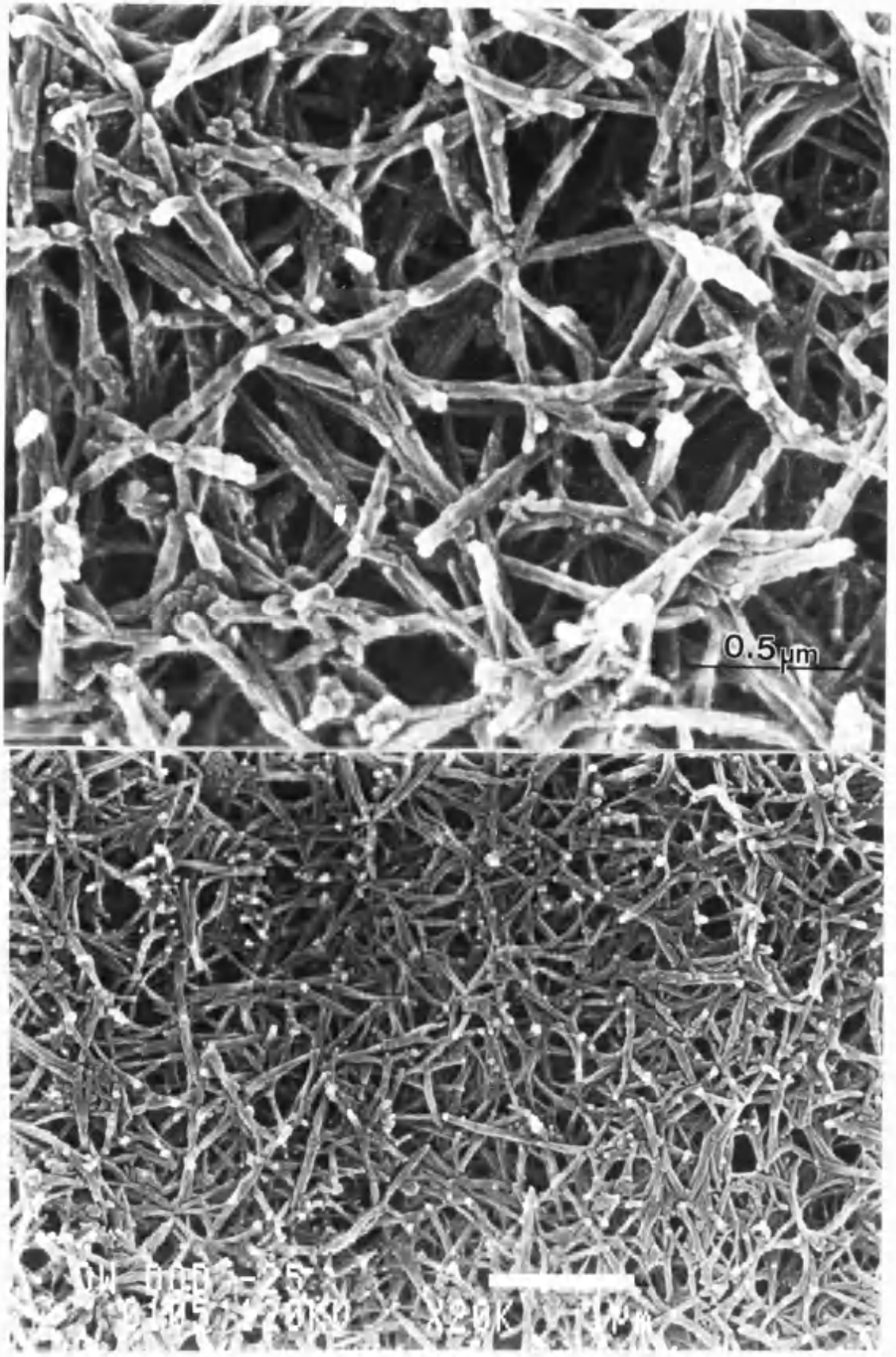

Fig 5.4. SEM micrographs of reticulated HAP structures recovered from mineralized microemulsion. (Stored at -25°C for 10 days).

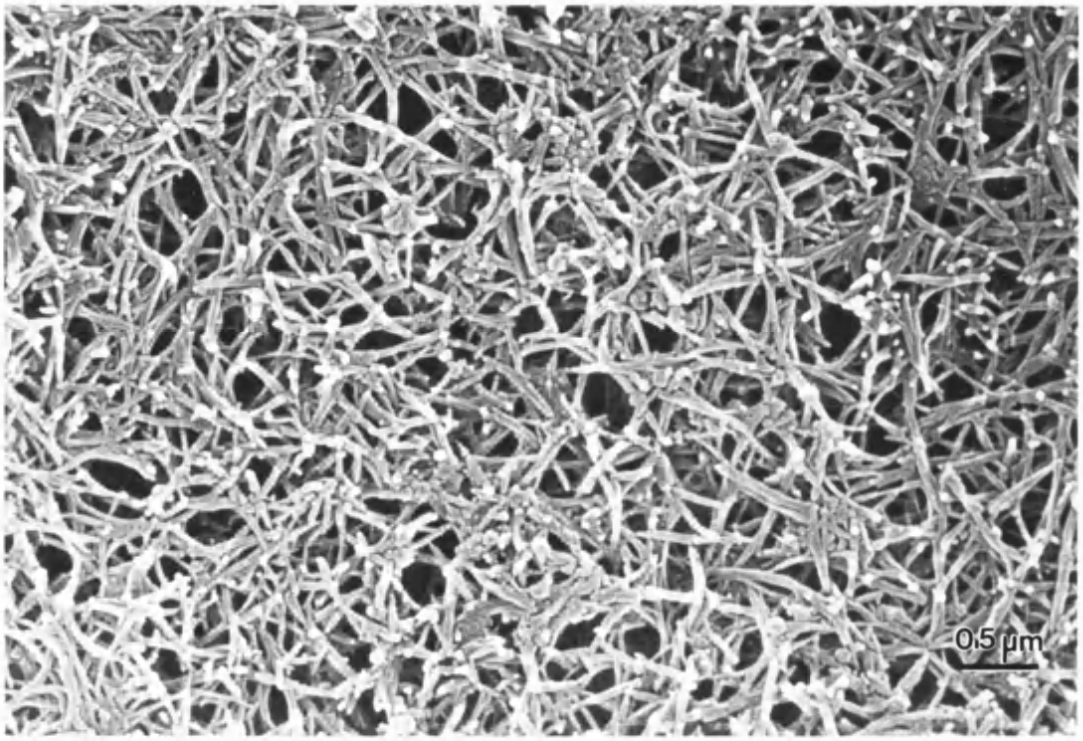

Fig 5.5 SEM micrograph of reticulated HAP structures recovered from mineralized microemulsion after heating to 200°C for 25 mins. The structure is identical to unheated samples showing that surfactant is removed during the washing procedure.

5.8 Preparation of control HAP

Method

A supersaturated solution of HAP was prepared as above and allowed to stand for one week, the precipitate was collected by filtration and examined by SEM directly. The precipitate was also added to a mixture of oil and surfactant and collected by centrifugation and filtration followed by washing with hot solvent, SEM examination was then conducted.

Result

Very similar characteristic aggregations of HAP crystals without any porous structure were visible (fig.5.6).

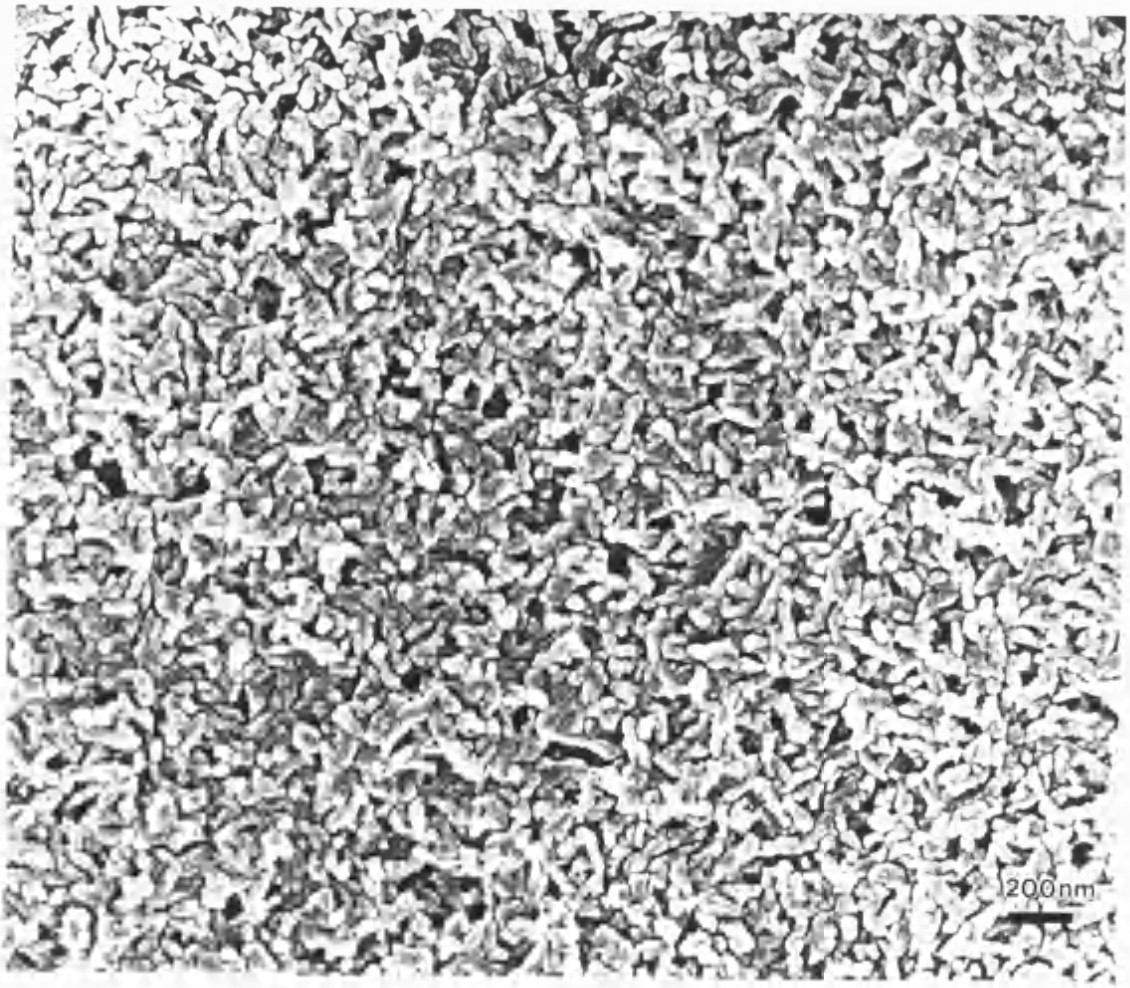

Fig 5 6 SEM micrograph of control HAP aggregations formed in aqueous system

5.9 Preparation of HAP at edge of bicontinuous region of microemulsion using DDAB and dodecane

Method

In order to elucidate the role of the microemulsion structure a microemulsion was prepared as above except that the oil proportion was increased and the surfactant proportion lowered (point B of fig. 5.2 and table 5.1). This corresponds to a point on the phase diagram on the edge of the single phase region where bicontinuity begins to breakdown and the water conduits disconnect into spheres before macroscopic phase separation. The pre-frozen mixture was then stored at -25°C. Samples where removed at intervals of 2, 5,10 and 15 days, the mineral extracted and examination by TEM and SEM and EDXA and XRD analysis conducted.

Results

Analysis of the product during the later stages of growth by XRD indicated the particles were composed of poorly crystalline HAP (fig. 5.7). TEM examination of a sample recovered after two days revealed the presence of a reticulated network of amorphous particles of wall diameter 10nm and pore size 100nm (fig.5.8 (a)). After 5 days chains of spherical particles of diameter up to 100nm are visible (fig.5.9 (b)). After 10 days the thickness of the extracted material does not allow TEM analysis, SEM showed interconnected particles of size 90-160nm that encircled pores up to 0.5μm. No further development was observed, this was probably due to freezing of the water component since the texture changed from soft to hard at this time.

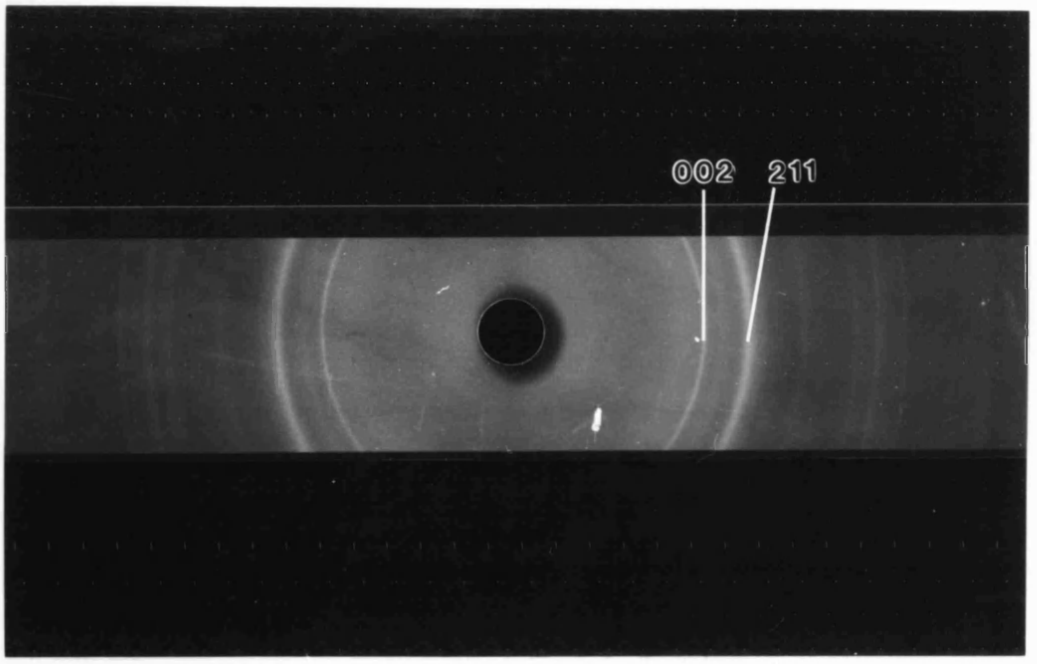

Fig. 5.7. XRD of HAP particles recovered from DDAB/ dodecane/ supersaturated solution at edge of bicontinuous region.

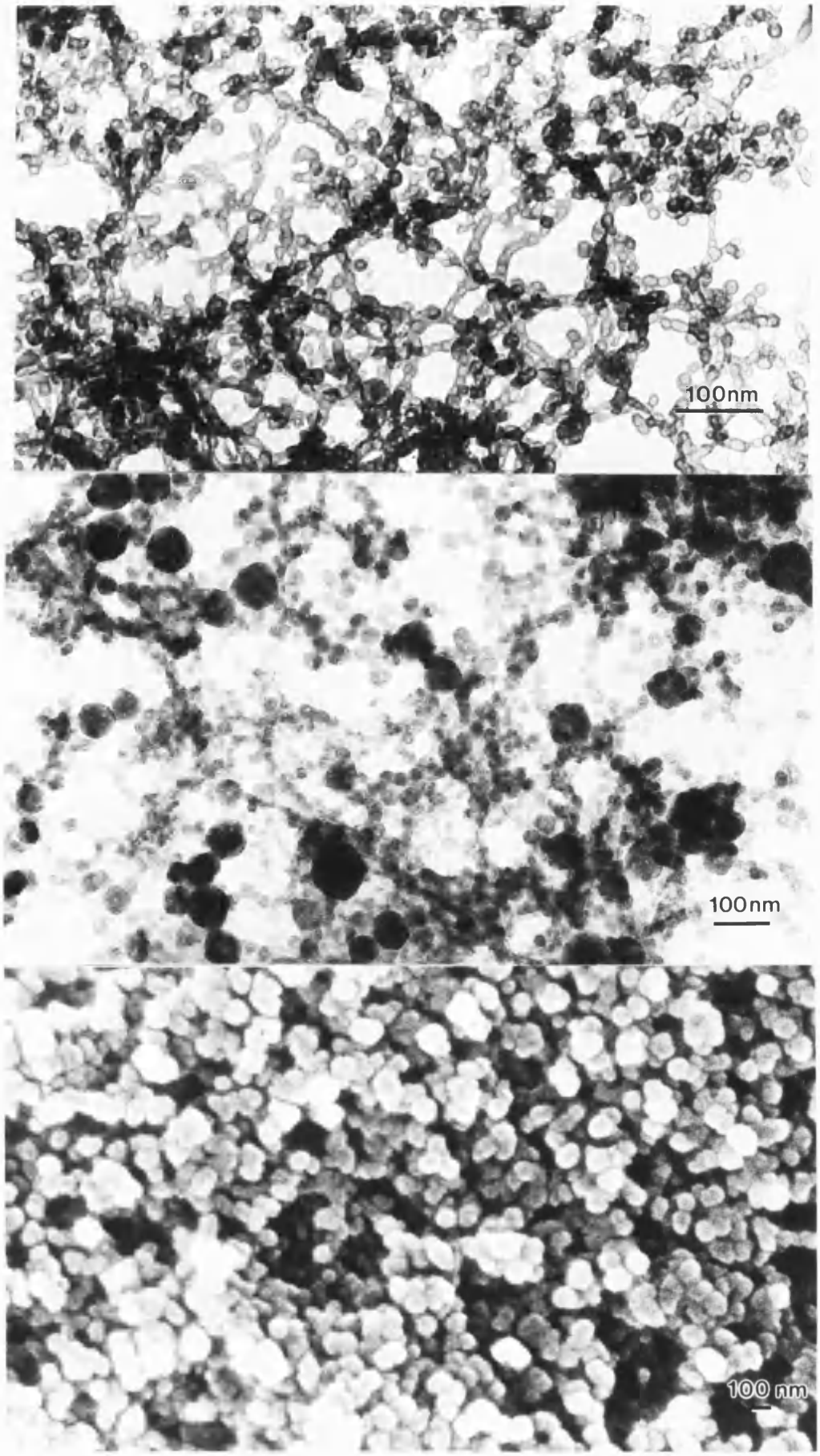

Fig 5.8 (a) TEM micrograph of mineralizing microemulsion at edge of bicontinuous region after 2 days; (b) 5 days; (c) SEM micrograph after 10 days.

5.10 Preparation of reticulated HAP from bicontinuous microemulsions using DDAB and tetradecane

Method

Microemulsions prepared using tetradecane differ from dodecane based ones in that the channels remain as bicontinuous conduits throughout the single phase region. Also the freezing point of +5.9°C allowed storage of the frozen microemulsion below the alkanes m.p. but above 0°C so avoiding problems with the freezing of the water component. The microemulsion was prepared using the previous method with suitable proportions of components (fig.5.9 point X and table 5.1). The pre-frozen mixture was then stored at +2-3°C for 2 weeks before extraction and cleaning. Examination of the recovered material was conducted by SEM and EDXA spectra recorded.

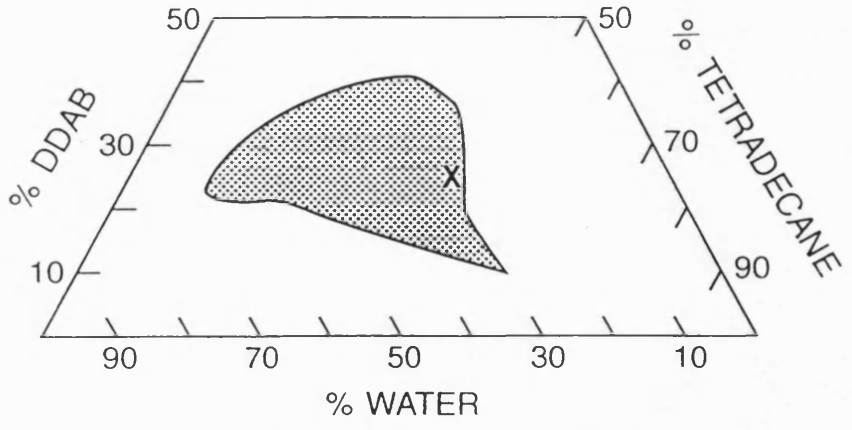

Fig.5.9. Phase diagram of DDAB, tetradecane and water microemulsion system at room temperature. Point X denotes composition of microemulsion.

Results

SEM examination of the material recovered after 14 days showed it to be composed of a reticulated network of bundles of several intergrown crystals of wall size 100-250 nm and pore size up to 2.5μm (fig.5.10). EDX analysis of the material was consistent with HAP. The formation of bundles rather than single crystals as obtained previously may be a reflection of the less rigid environment. The dodecane based microemulsions are stored well below the m.p. of the alkane component whereas the tetradecane microemulsion was stored close to m.p. of its oil component.

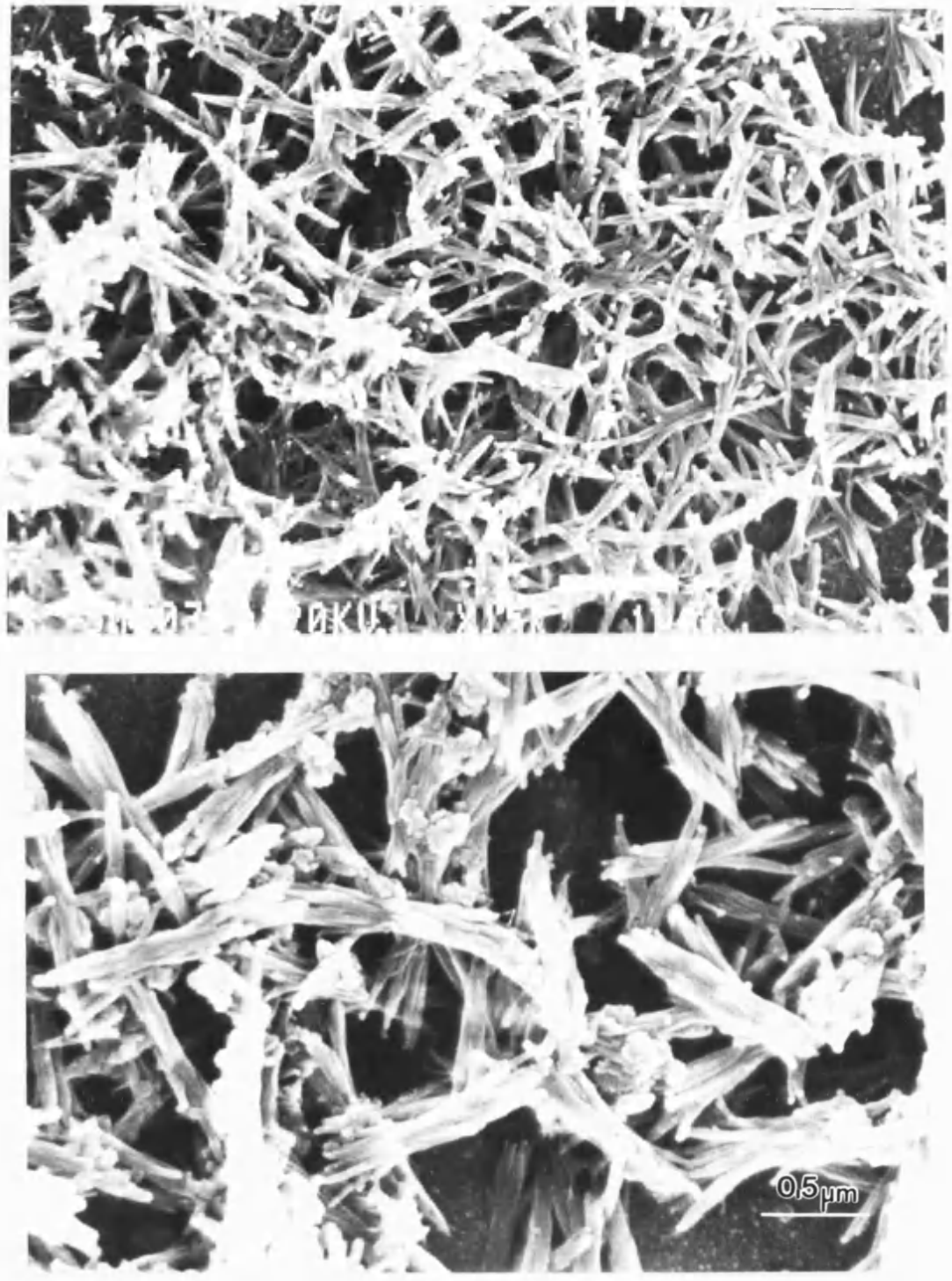

5.10. SEM micrographs of HAP recovered from bicontinuous microemulsion formed by DDAB/ tetradecane supersaturated calcium phosphate solution. (Stored at +2°C for 14 days).

5.11 Preparation of reticulated HAP from bicontinuous microemulsions using DDAB and tetradecane and hexadecane mixtures stored at -25,+2 and +25°C

Method

The product of pure tetradecane based microemulsions indicated that the environment may not have been sufficiently rigid to control the growth of crystals within it. Therefore hexadecane of m.p. +18.1°C was incorporated into the preparation. The long hydrocarbon chain of hexadecane means that it will not penetrate into the surfactant tails, therefore hexadecane itself does not form microemulsions with DDAB at room temperature. However it is known that the addition of shorter chain oils which act as a co-surfactant will readily allow microemulsion formation.

The general preparation described above was followed. In a typical experiment 7ml of supersaturated calcium phosphate solution was added to 8g of DDAB and 5g of alkane oils (table 5.1). An alkane mixture of approximately 1/3 hexadecane was found to produce a clear single phase microemulsion at room temperature. The pre-frozen mixture was stored at -25 and +2-3°C for 3 weeks, or left unfrozen and stored at +25°C for 6 days. The solid residue recovered was characterized by SEM and IR spectroscopy.

Result

TEM reveals the material recovered from the frozen system stored at -25°C for 3 weeks to be composed of strands of amorphous material of 5-10nm diameter, 100-450nm length in a loosely reticulated arrangement, in some areas the strands were associated with ACP spherules (fig. 5.11). SEM examination of material recovered from the system stored at +2-3°C for 3 weeks showed the presence of large reticulated structures composed of single interconnecting crystals, the crystals are in many cases curved and a highly porous structure is visible (fig. 5.12). The crystal wall thickness is 50-130 nm and long curved

crystals form pores of size up to 3μm. The FT-IR spectrum of the recovered material is consistent with HAP (fig. 5.13). The unfrozen system, which was fairly viscous was subjected to the clean-up procedure after 7 days. Upon examination by SEM it was found to consist of reticulated material similar to that from the frozen oil medium except that it comprised straighter crystals and domains of extensive aggregation (fig. 5.14).

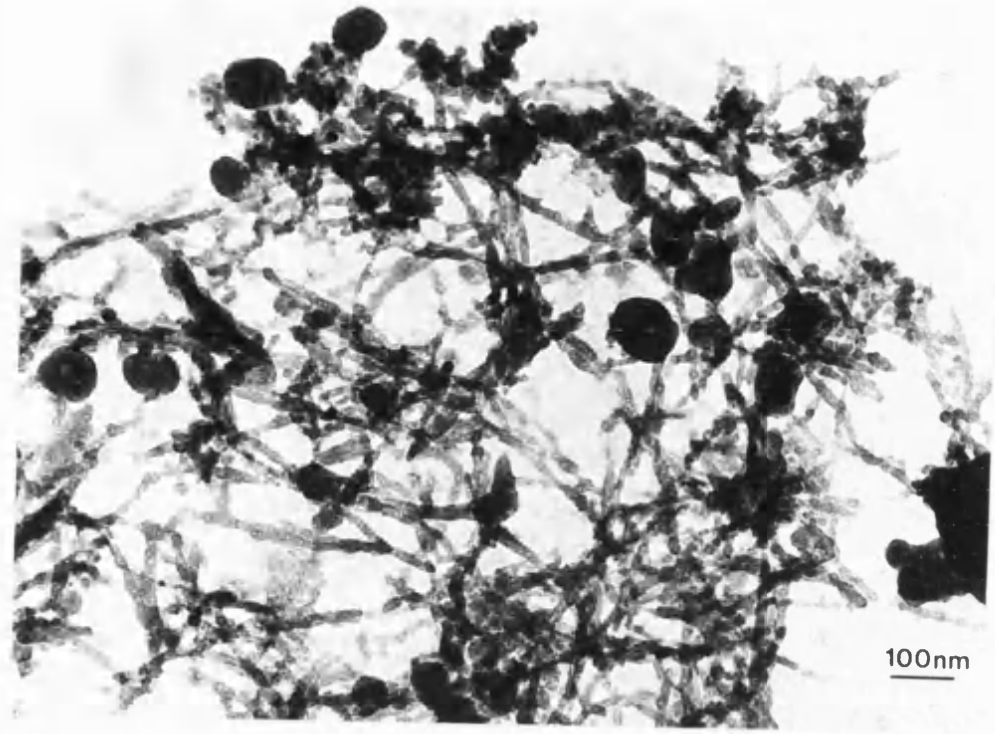

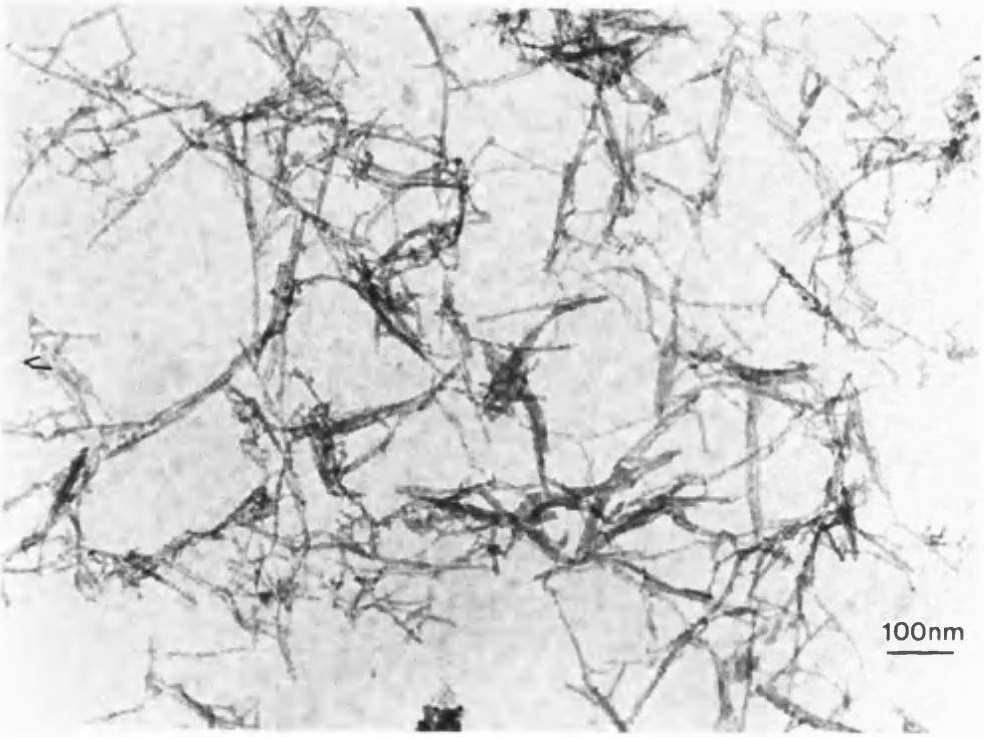

Fig. 5.11. TEM micrographs of poorly developed strands of HAP recovered from DDAB/C_{14}/C_{16} and supersaturated solution system. (Stored at -25°C)

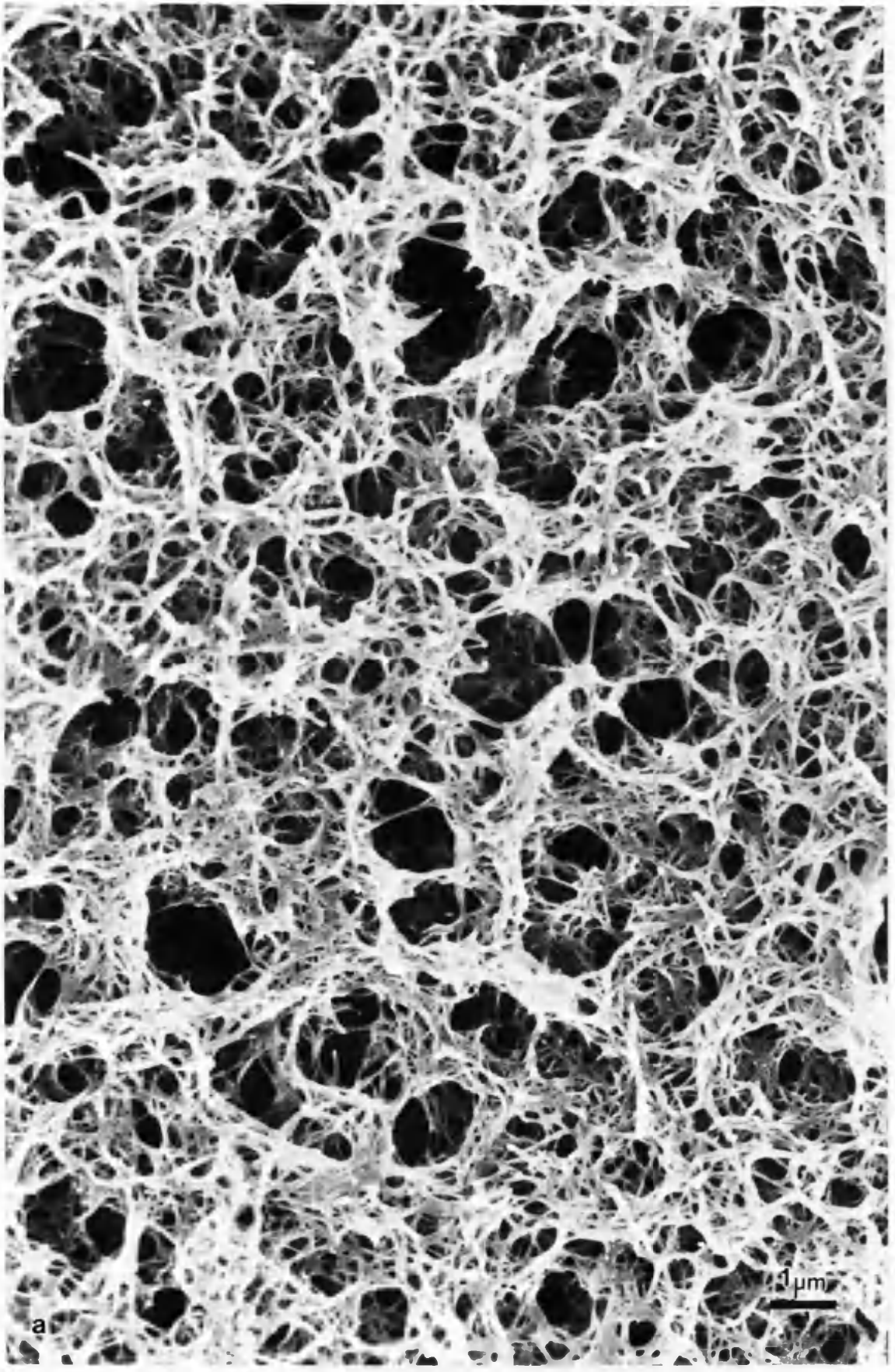

Fig. 5.12. SEM micrographs at (a) medium, (b) low and (c) high magnification of reticulated HAP obtained from DDAB/ C_{14}/C_{16} and supersaturated solution system. (Stored at +2°C).

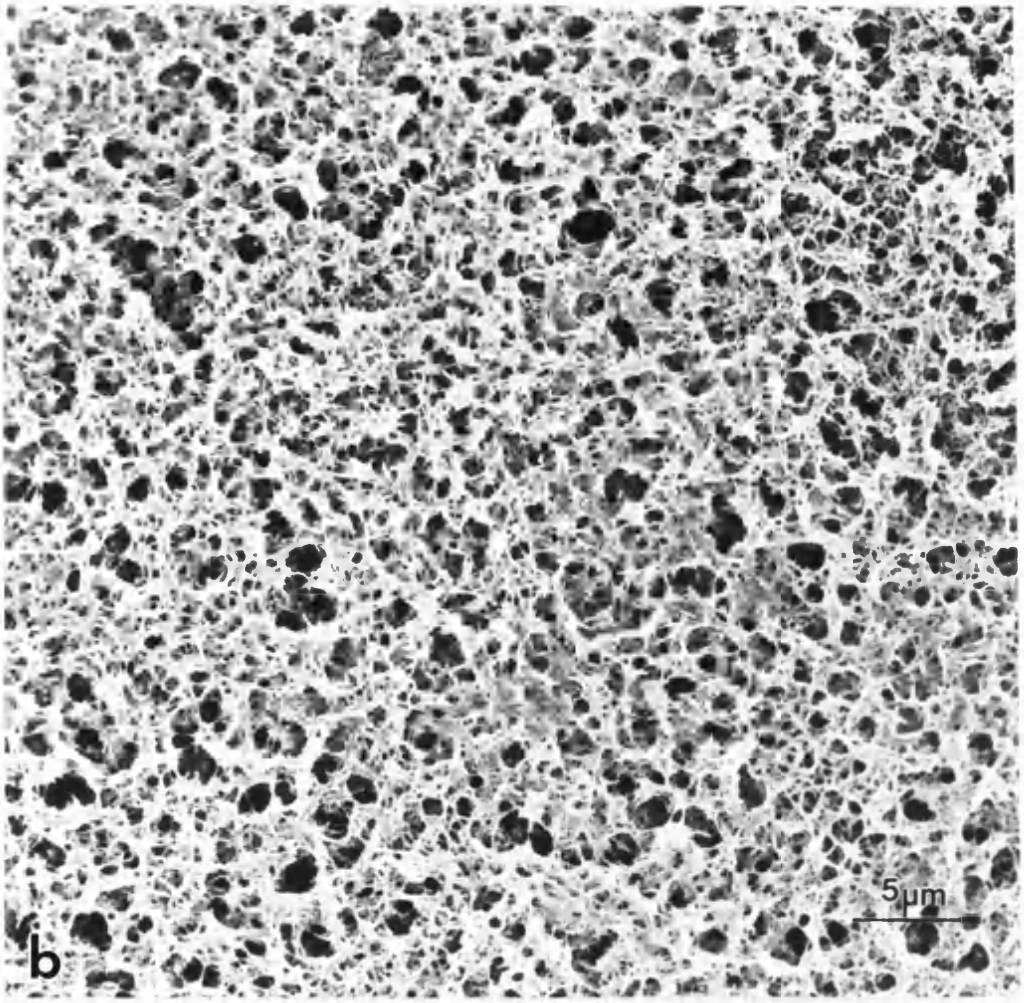
5µm
b

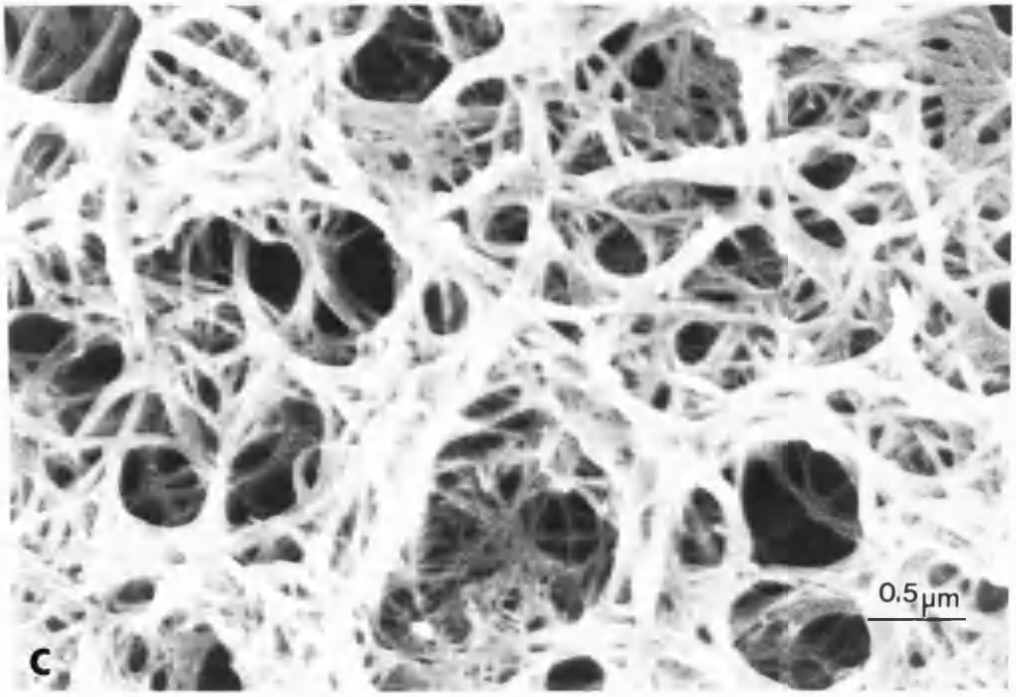
0.5µm
c

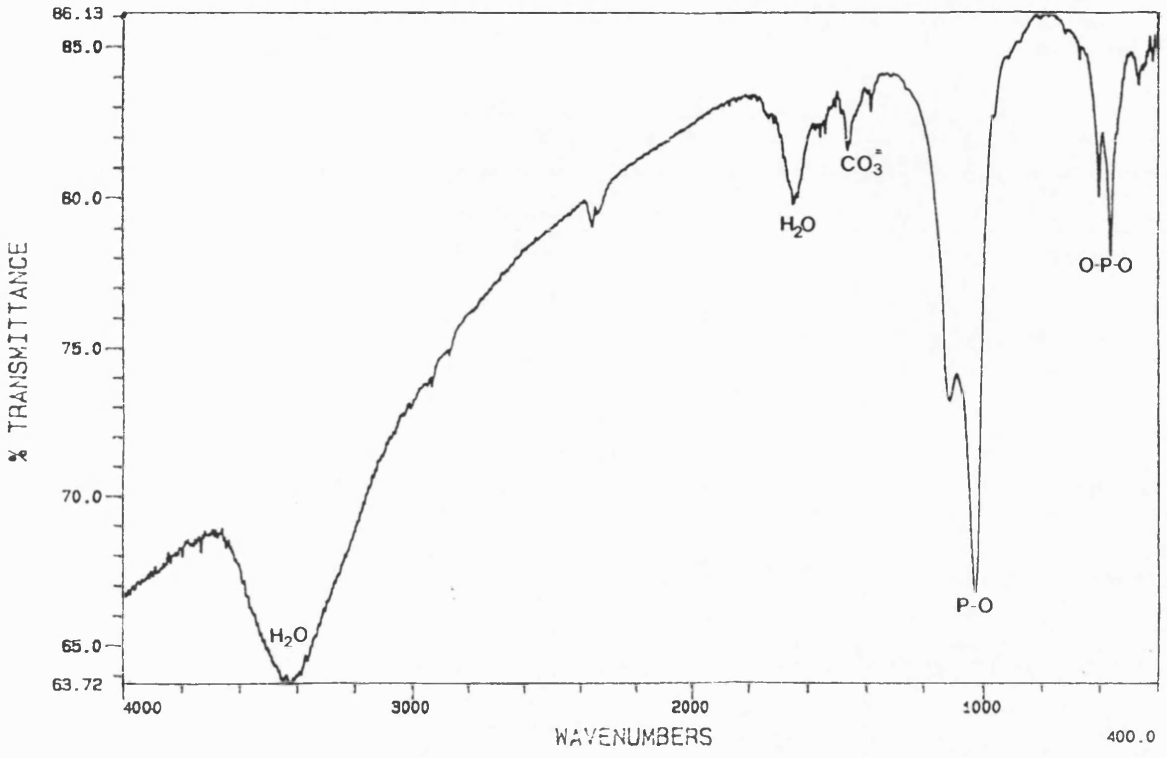

Fig. 5.13. FTIR of HAP recovered from DDAB/ C_{14}/C_{16} / supersaturated solution system. (Stored at +2°C).

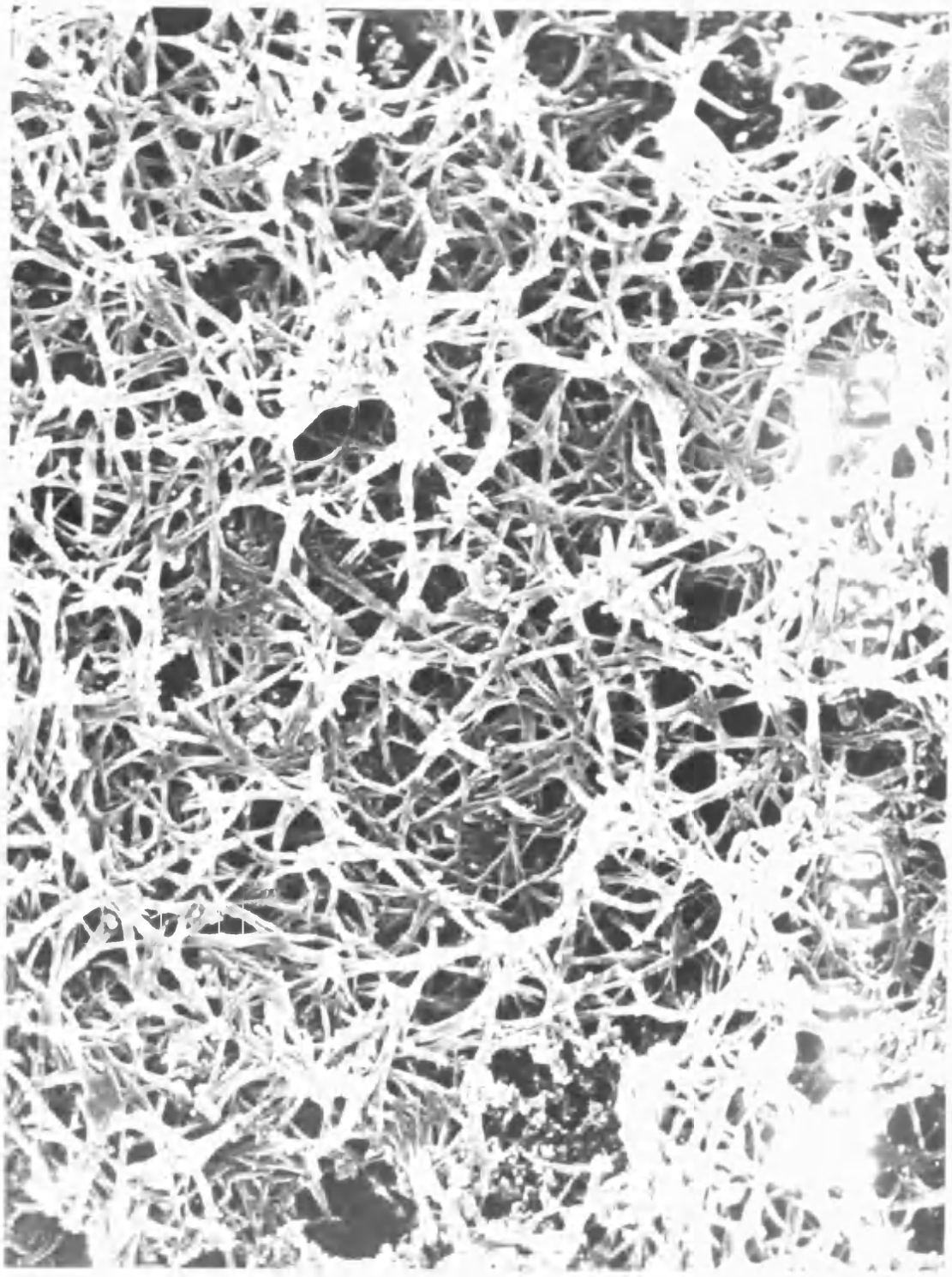

Fig 5.14 SEM micrograph of HAP recovered form DDAB/ C_{14}/C_{16}/ supersaturated solution system (Stored at −25°C)

5.12 Time-course study of growth of HAP in bicontinuous microemulsion using DDAB and tetradecane/hexadecane oils

Method

In order to investigate the growth mechanism that leads to the formation of the macroporous frameworks, samples of a C_{14}-C_{16} microemulsion system stored at +2-3°C (frozen oil) or +25°C (unfrozen oil) were removed at intervals, washed and examined by electron microscopy.

Results

In both cases, at early stages of precipitation (2 to 6 hours at +2°C), filamentous strings of mineral particles down to 1nm in diameter were observed by TEM (fig. 5.15(a)). This seemed to suggest that the native bicontinuous microstructure was not disrupted at this point. However, these aggregates were not visible after 4 to 6 days at +2°C but were replaced by needle-like HAP crystals of 100-500nm in length (fig.5.15(b)). At first the HAP crystals were unconnected, but growth for 10 days at +2-3°C resulted in a loosely held network of relatively straight needles with associated ACP spherules (fig.5.15(c)). The final stage of framework construction up to 3 weeks was characterized by a continued lengthening and thickening of the crystals and an increased curvature of the mineral walls (fig.5.16(d)). The growth pattern was very similar for samples stored at +25°C but greatly accelerated, mature reticulated structures of straighter crystals being formed after 6 days.

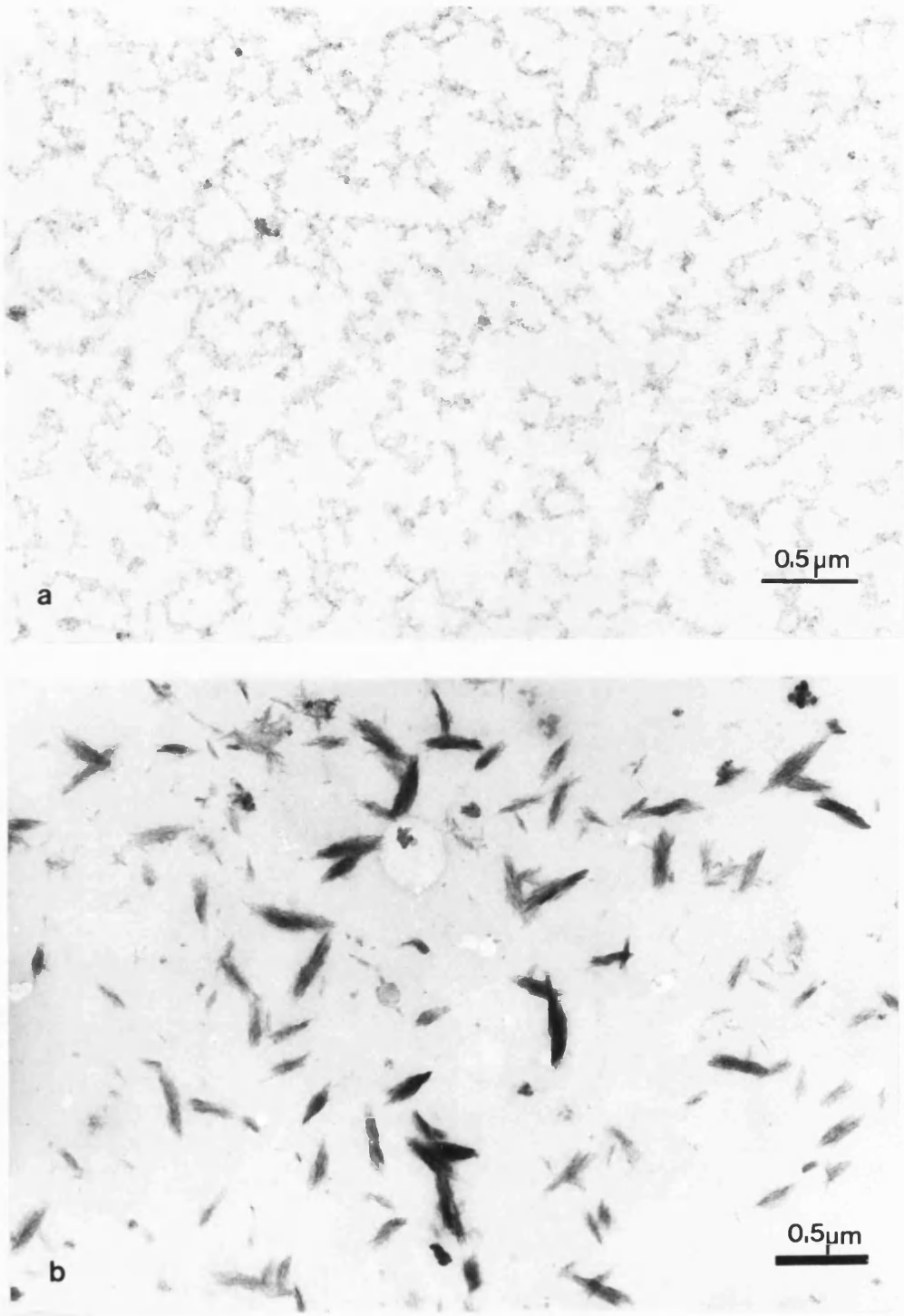

5.15. TEM micrographs of time course of mineralization of mixed oil bicontinuous system stored at +2°C after (a) 2-6 hours; (b) 4-6 days; (c) 10-12 days; (d) 3 weeks.

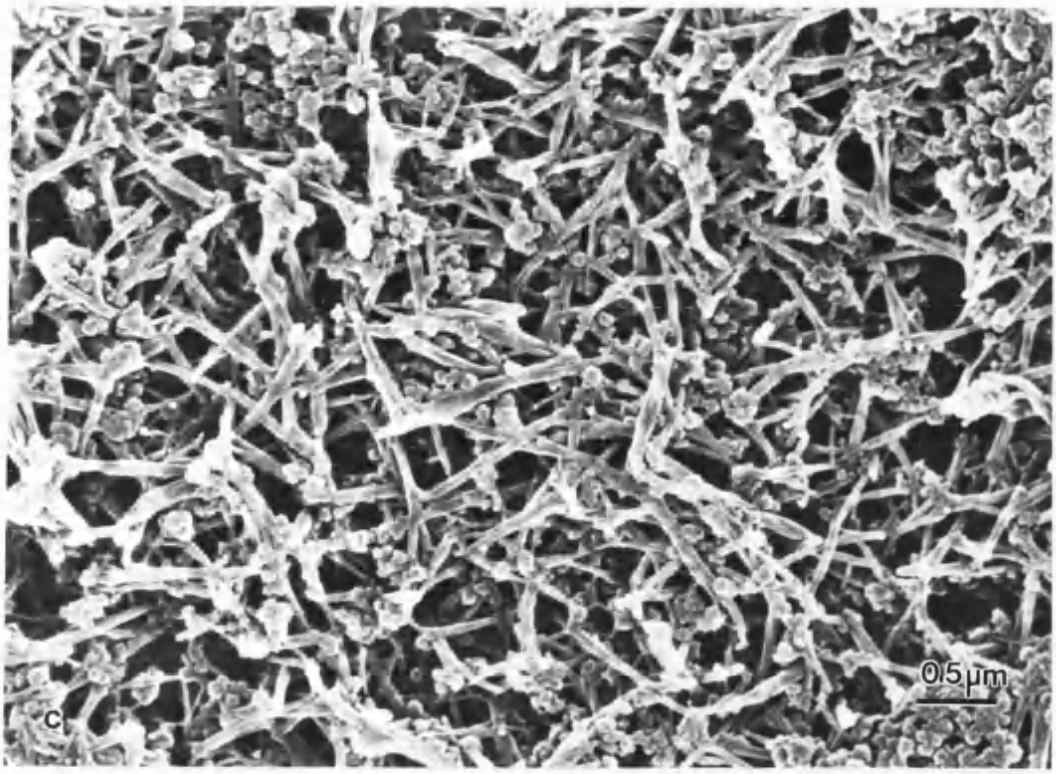
0.5μm
c

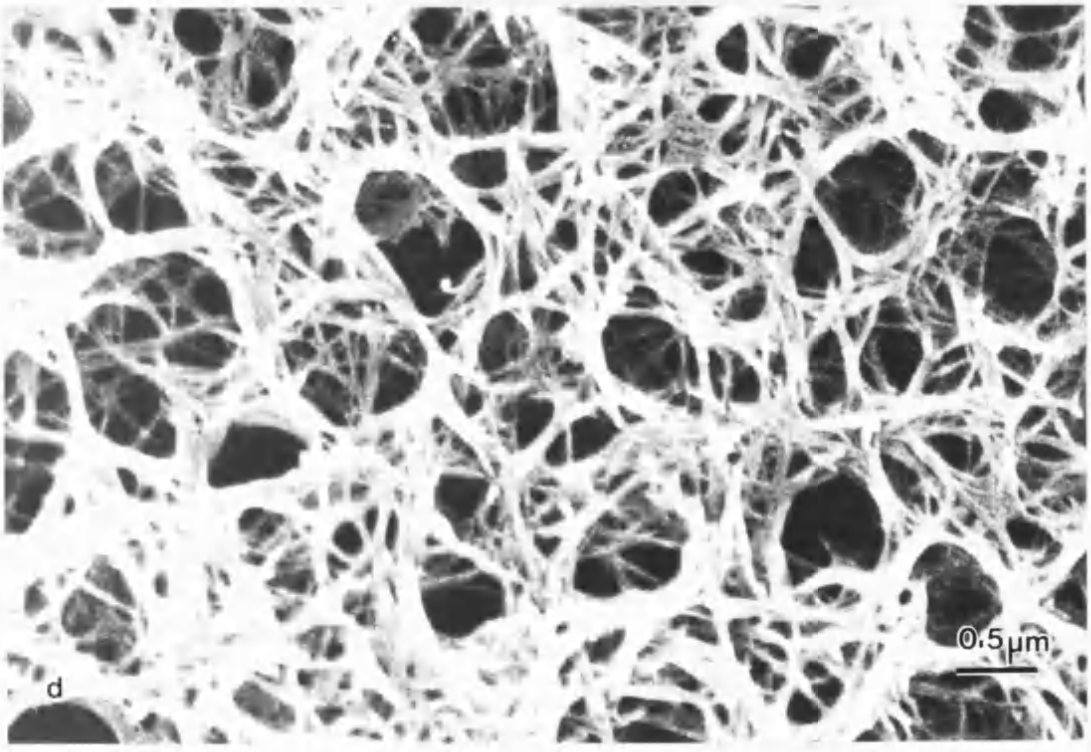
0.5μm
d

5.13 Preparation of HAP using cubic phase of DDAB and dodecane microemulsion

Introduction

Microemulsions prepared at high water and low alkane content form so called cubic phase bicontinuous microemulsions. These are characterized by being optically clear highly viscous gels. Many small-angle X-ray and neutron scattering studies have been conducted on these systems in order to determine their structure (Radiman et al 1990, Maddaford and Toprakcioglu 1993).

Method

A cubic phase bicontinuous emulsion was prepared incorporating a supersaturated HAP solution. The components dodecane, DDAB, and solution were mixed in suitable proportions (fig. 5.16 and table 5.1), which resulted in an optically clear thick gel. In a typical experiment 1.2g of DDAB were mixed with 0.25g of dodecane and 2.5g of supersaturated solution. The mixture was stored at +25°C and samples removed after 3 and 7 days, washed using hot chloroform and TEM and SEM examination of the recovered material conducted.

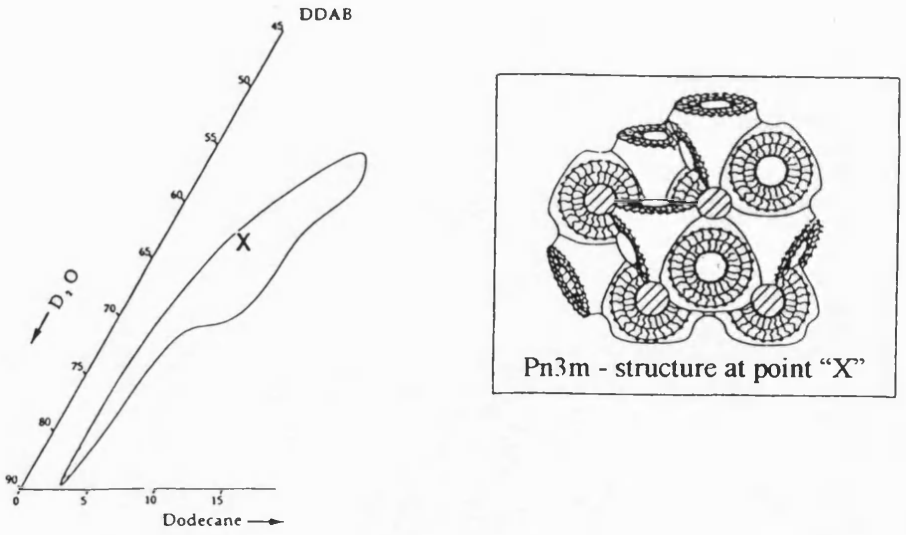

Fig. 5.16. Partial phase diagram for the DDAB, dodecane and water system showing cubic phase at room temperature. Inset shows envisaged structure that exists around "X". Note that a range of different bicontinuous structures are present within the cubic phase.

Results

Observation by TEM after 3 days showed the presence of 50-100nm diameter aggregations of plate-like material that may be composed of a precursor OCP phase (fig. 5.17(a)). SEM examination after 6 days showed the presence of crystals bundles that were not organized into a reticulated structure (fig. 5.17(b)).

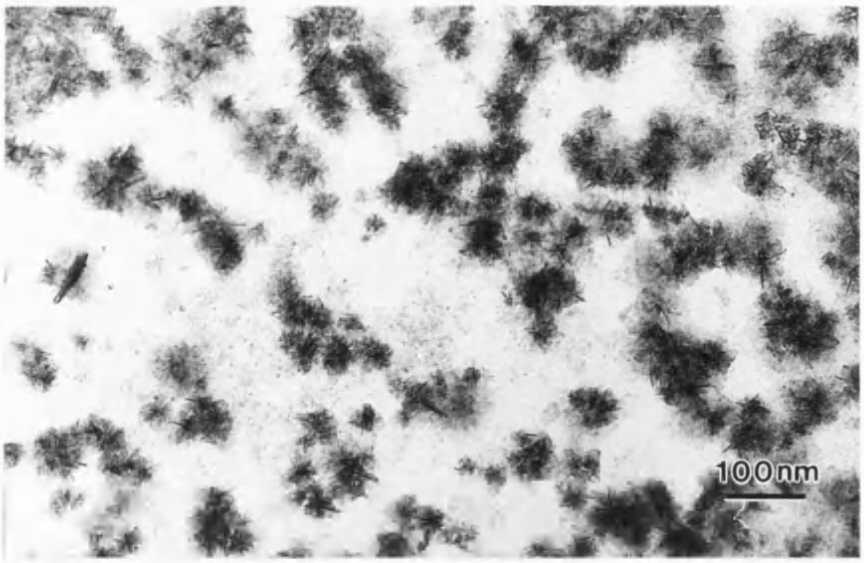

Fig. 5.17(a) TEM micrograph of material recovered from cubic phase microemulsion stored at +25°C for 3 days.

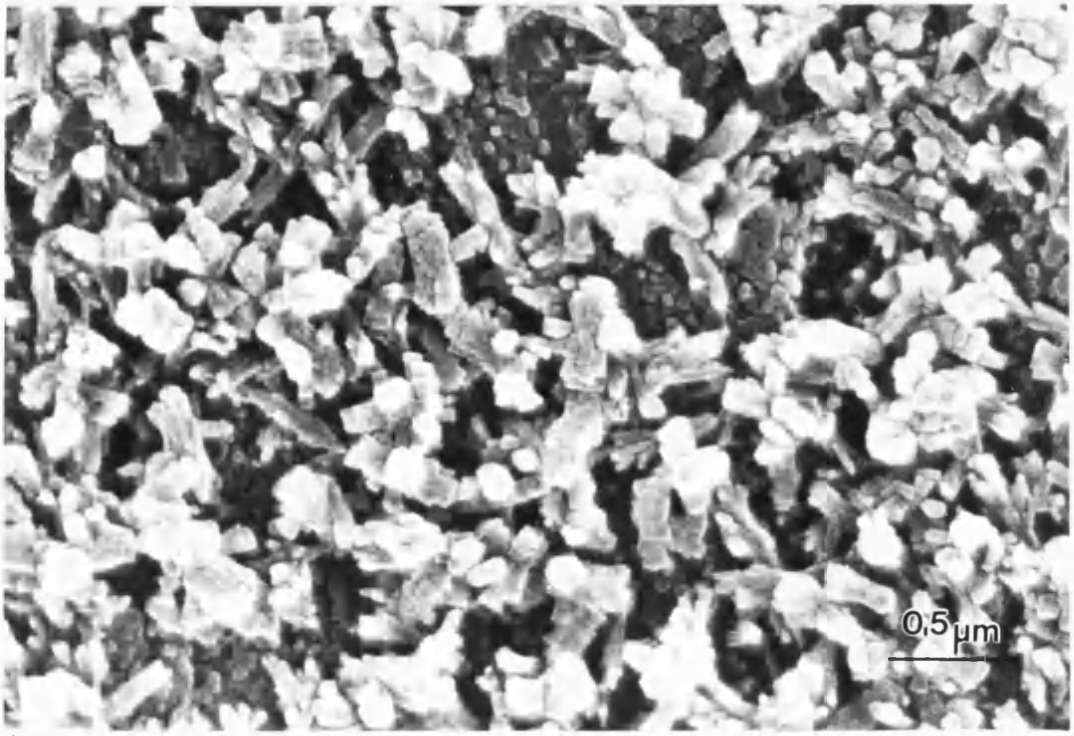

Fig. 5.17(b). SEM micrograph of HAP recovered form cubic phase microemulsion stored at +25°C for seven days. The HAP is of abnormal appearance but non-reticulated.

5.14 Preparation of HAP using bicontinuous microemulsions using pentaethylene glycol dodecylether (C12E5)

Method

The non-ionic surfactant pentaethylene glycol dodecylether (C12E5) forms a bincontinuous network of lamellae interconnected in three dimensions with a suitable proportion of components at around 46°C (fig. 5.18 and table 5.1) (U. Olsson et al 1966). A bicontinuous microemulsion was prepared using a supersaturated HAP solution as described in section 5.5. In a typical experiment 0.67g of C12E5 was mixed with 1.56ml of tetradecane and 1.76ml of calcium phosphate solution. Storage of the frozen microemulsion was made at +2-3°C for 7 days, and unfrozen at +46°C for 3 days, where the mixture was optically clear and believed to be bicontinuous. Samples were obtained by centrifugation as described in section 5.5 and examined by TEM, ED and SEM.

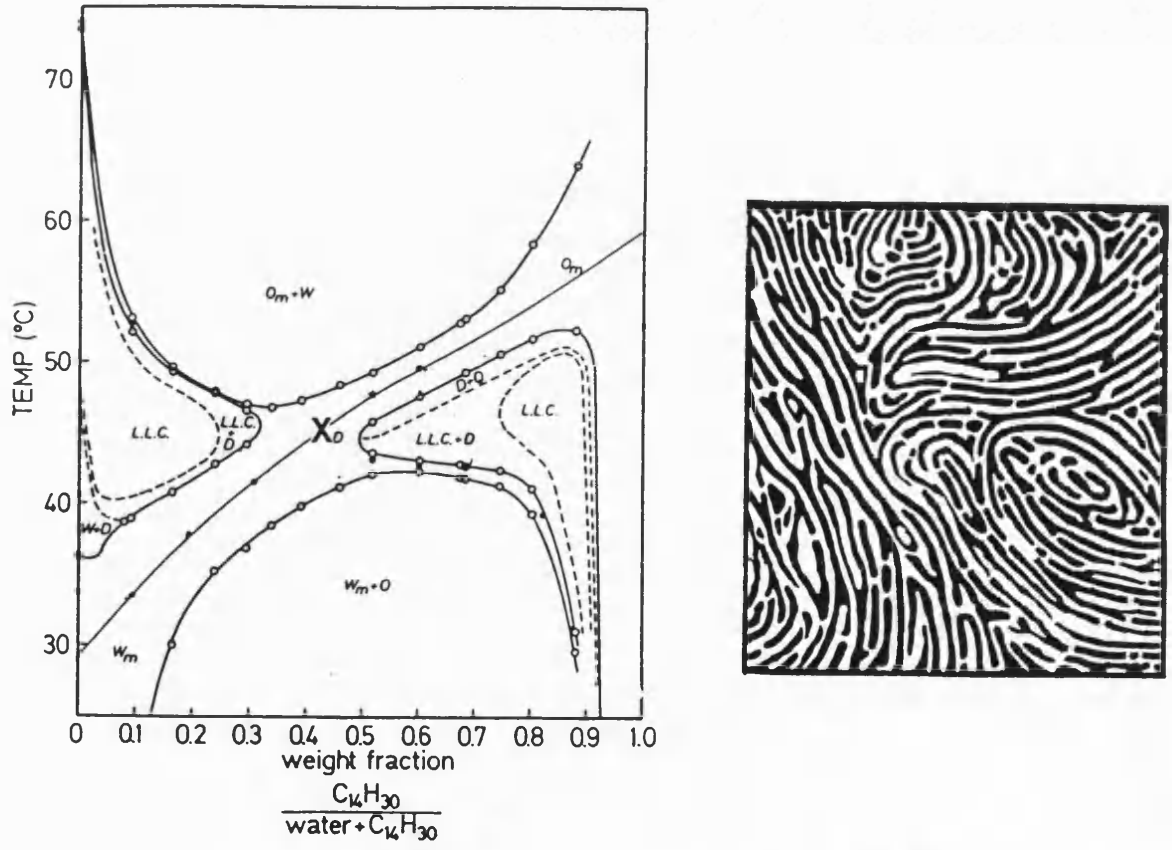

Fig. 5.18. Phase diagram of C12E5/ C_{14}/ supersaturated solution as a function of temperature. Inset shows envisaged structure that exists at X.

5.16 Results

Examination by TEM of material recovered from an unfrozen system revealed the presence of interwoven plates of material that produced an ED pattern consistent with HAP (fig. 5.19). After 3 days material consisting of a network of interconnected mineralized plates was visible by SEM (fig. 5.20). This structure is in accordance with the envisaged lamellar structure of the bicontinuous microemulsion (U. Olsson et al 1986), with the exception of the pores that are visible. The porous nature of the material may have been a reflection of the high mobility of the unfrozen stored microemulsion. A frozen system stored for 7 days was found to consist of a network of smaller plates 50-100nm in size with very few pores present (fig. 5.21). This structure was much more consistent with the envisaged structure for the system.

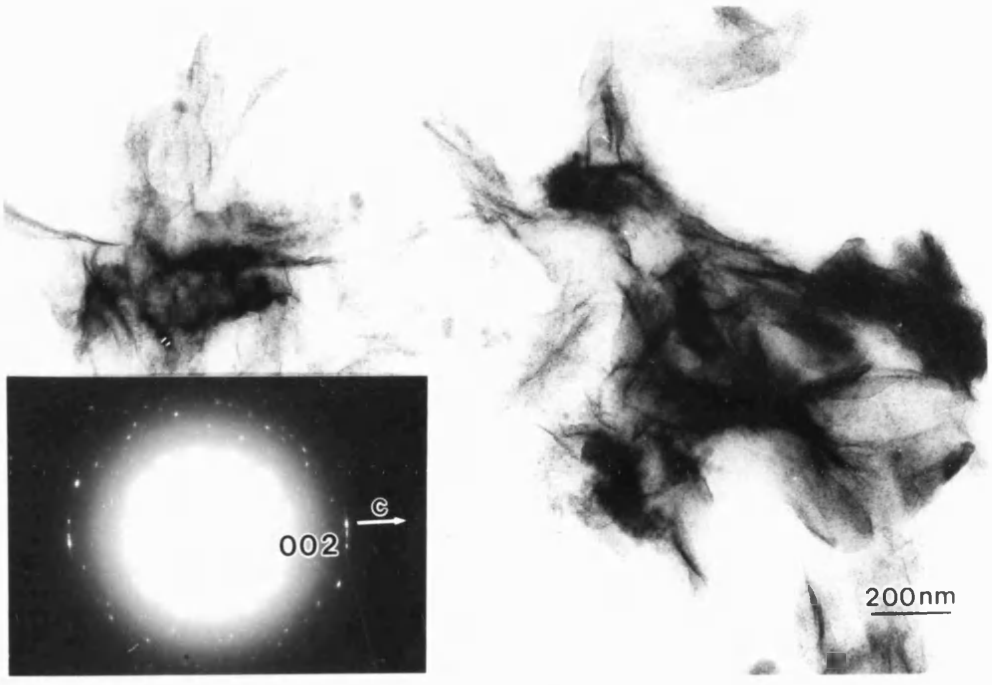

Fig. 5.19. TEM micrograph of HAP material recovered at early stage from C12E5/ C_{14}/ supersaturated solution system. A characteristic (002) HAP ED pattern was produced. (Stored at +46°C).

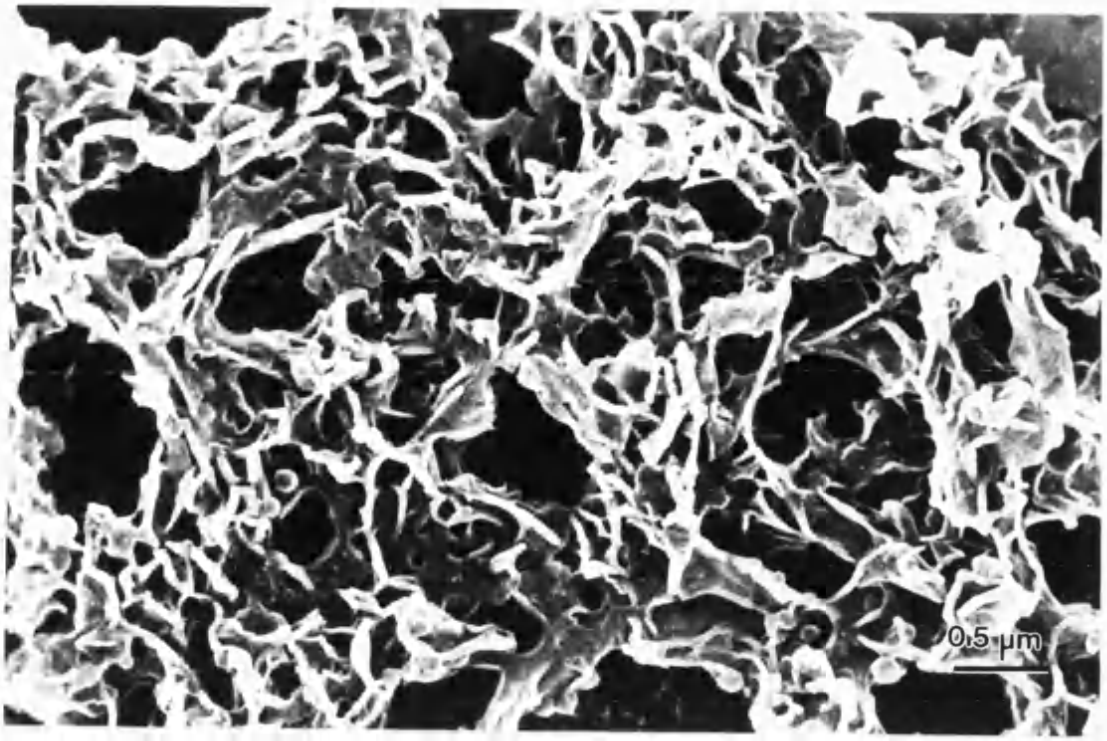

Fig. 5.20. SEM micrograph of HAP recovered form C12E5/ C_{14}/ supersaturated solution stored at +46°C for 3 days.

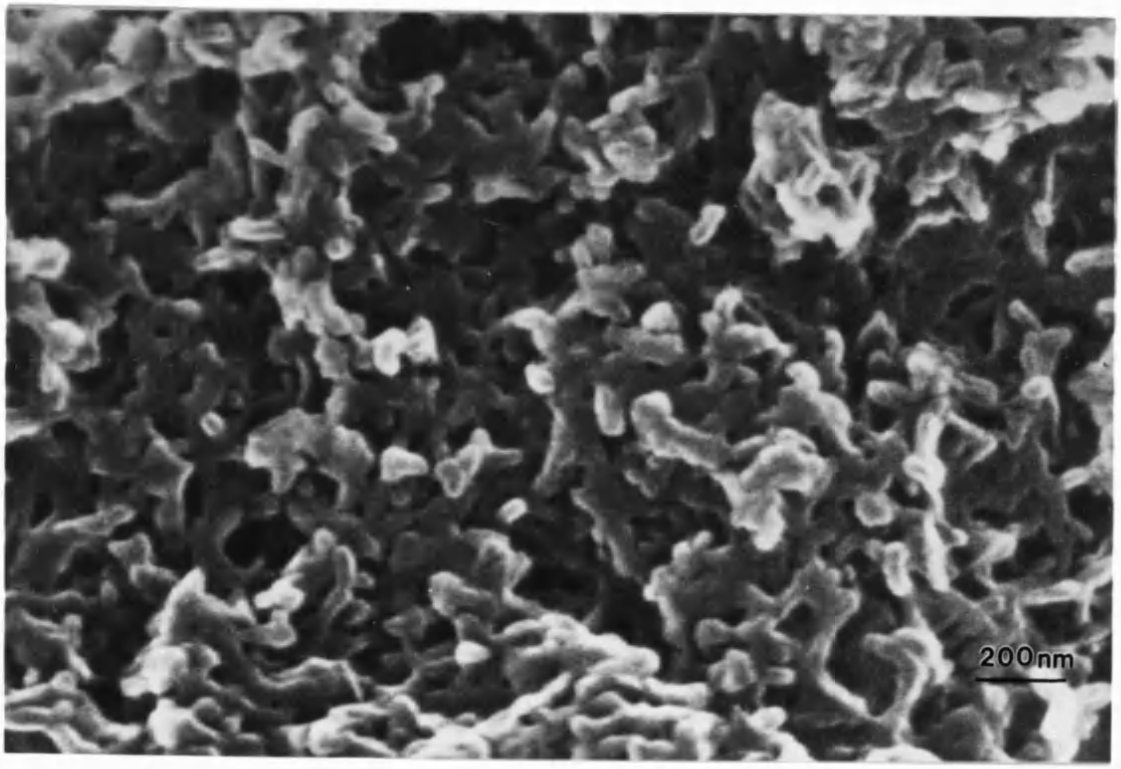

Fig. 5.21. SEM micrograph of HAP recovered form C12E5/ C_{14}/ supersaturated solution stored at +2°C for 7 days.

Alkane	Oil (%)	H_2O (%)	DDAB (%)	Storage Temp. (°C)	Storage time (days)	Pore-size (μm)	Wall size (μm)	Construction unit
C_{14} C_{16}	17 8	35	40	+2	21	0.5 to 2.5	50 to 130	Single and bent crystal needles.
C_{14}	45	30	25	+2	14	0.1 to 2.5	100 to 250	Bundles of crystal needles
C_{12}	40	20	40	-25	21	0.04 to 0.7	50 to 130	Single-crystal needles.
C_{12}	55	30	15	-25	14	0.1 to 0.5	150	Spherical crystals
C_{14}	34	50	16 ($C_{12}E_5$)	+46	3	0.05 to 1.0	-----	Spherical plates
C_{14}	34	50	16 ($C_{12}E_5$)	+2	7	------	-----	Spherical plates

Table 5.1. Summary of HAP mineralization of bicontinuous microemulsions.

5.16 Discussion

A striking feature of the reticulated structures recovered from the microemulsions is that the wall diameters (about 80nm) and pore size (up to 3μm) are not comparable with the 1nm diameter wall channels considered to be present in bicontinuous microemulsions (Hyde et al 1989). Scanning electron micrographs clearly show that the mature networks are intergrown crystal architectures. The time course study suggested that the nucleation of calcium phosphate was initially restricted to the interconnecting water conduits. Subsequent growth of the mineral particles appears to induce changes at the surfactant water interface. A possibility is that the growing crystals retain a hydration layer together with a layer of adsorbed surfactant, maintaining the stability of the microemulsion. Furthermore there may be a net migration of surfactant molecules to the surface of the crystal as it grows. The crystals would no longer be confined to the space delineated by the original bicontinuous structure but form a bicontinuous macroscopic structure of growing crystals bounded by a hydration layer and sheath of surfactant molecules.

The highly viscous cubic phase failed to produce reticulation, at an early stage aggregations material are visible which may be composed of a plate-like OCP phase which subsequently transforms into HAP crystallites. The high proportion of aqueous phase to oil may mean that the relatively thin oil walls were not able to maintain separation between aqueous channels and growth of mineral could not be controlled effectively. It may be that pockets of emulsion separate the large aqueous areas of developing crystal bundles.

The results suggest that a degree of macroscopic flexibility was most successful is producing well defined structures. The highly malleable bicontinuous microemulsions obtained with pure tetradecane at +2°C produced bundles of crystals. Unfrozen mixtures stored at +25°C resulted in structures with areas of aggregation. Storage of preparations with a fairly well frozen mixture of oils at +2°C was most successful in producing well defined structures. It would seem probable that the oil molecules associated with the surfactant tails retained some local mobility, although the bulk molecules are frozen. At -25°C the development of a network appears to cease at an early stage, presumably due to freezing of the water component, the rigid environment may also inhibit development before the water component freezes.

The construction of the frameworks was probably facilitated by the aciculate nature of HAP crystals. This morphology provided effective interlinking and interlocking of the structure as it developed. An interesting feature of the HAP structures obtained with C_{14}/C_{16} at +2°C is the relatively great elongation of the crystals and their highly curved nature compared to control solutions. It may be that the bounding layer of surfactant can control the elongation and growth in a similar way to the apparent tubules of enamelins and other matrix contituents that are believed to guide the growth of HAP crystals in tooth enamel (Jessen 1968). In the past reticulated biominerals such as corals have been used as implant materials because the porous nature of these materials facilitates intergrowth, vasculization and resorption (Holmes et al 1984). Although the pore size of the reticulated structures obtained here is possibly too small to allow extensive vasculization, osteoclastic activity and biocompatibility could be expected. The huge surface area of the material may also allow application as a catalytic material.

References

Allen M., Evans D.F., Mitchell D.J., Ninham B.W. (1987), *Interfacial Tension of Ionic Microemulsion*, J. Phys. Chem. **91**, 2320-2324.

Beck J.S. et al (1992), *A New Family of Mesoporous Molecular Sieves Prepared With Liquid Crystal Templates*, J. Am. Chem. Soc., **114**, 10834-10843.

Bernardi G. (1971), in *Methods in Enzymology*, Grossman I., Moldave K. (Eds), **21**, 95, Academic Press, New York.

Bernardi G. (1971), in *Methods in Enzymology*, Jakoby W.B. (Ed), **22**, 325-342, Academic Press, New York.

Blum F.D., Pickup S., Ninham B., Chen S.J., Evans D.F. (1985), *Structure and Dynamics in 3-Component Microemulsions*, J.Phys. Chem., **89,** 711-713.

Chen S.J., Evans D.F., Ninham B.W., Mitchell D.J., Blum F.D., Pickup S. (1986), *Curvature as a Determinant of Microstructure and Microemulsions*, J. Phys. Chem., **90**, 842-847.

Dubois M., Gulik-Krzywickl Th., Cabane B. (1993), *Growth of Silica Polymers in a Lamellar Mesophase*, Langmiur, **9**, 673-680.

Eastoe J. (1992), *Small-Angle Neutron Scattering from Dilute Didodecyldimethyl ammonium Bromide Water-in-Oil Microemulsions. Evidence for Polymer-Like Aggregates*, Langmuir, **8(6)**, 1503-1506.

Hjerten S. (1957), *Calcium Phosphate Chromatography of Normal Human Serum and Electrophoertically Isolated Serum Proteins*, Biochem. and Biophys. Acta, **31**, 216-235.

Hyde S.T. (1989), *Microstructure of Bicontinuous Surfactant Aggregates*, J. Phys. Chem., **93**, 1458-1464.

Jahn W., Strey R. (1988), *Microstructure of Microemulsions by Freeze Fracture Electron Microscopy*, J. Phys. Chem, **92**, 2294-2301.

Jessen H. (1968), *Elliptical Tubules as Unit Structure of Forming Enamel Matrix in the Rat*, Arch. Oral. Biol., **13**, 351-352.

Krege C.T., Leonowicz M.E., Roth W.J., Vartuli J.C., Beck J.S. (1992), *Ordered Mesoporous Molecular Sieves Synthesized by a Liquid-Crystal Template Mechanism*, Nature, **1(359)**, 710-712.

Maddaford P.J., Toprakcioglu C. (1993), *Structure of Cubic Phases in the Ternary System Didodecyldimethylammonium Bromide/Water/Hydrocarbon*, Langmuir, **9**, 2868-2878.

Makishima A., Aoka H. (1984), in *Bioceramics*, Yamaguchi T., Yamagida H. (Eds), Gihodo, Tokyo.

McDowell H., Gretory T.M., Brown W.E. (1977), J. Res. Natl. Bur.Std. (US) **81A**, 273.

Monnier A. et al (1993), *Cooperative Formation of Inorganic-Organic Interfaces in the Synthesis of Silicate Mesostructures*, Science, **261**, 1299-1303.

Olsson U., Shinoda K., Lindman B. (1986), *Change of the Structure of Microemulsions with the Hydrophile-Lipophile Balance of Non-ionic Surfactant as Revealed by NMR Self-diffusion Studies*, J. Phys. Chem., **90**, 4083-4088.

Radiman S., Toprakcioglu C., Faruqi A.R. (1990), *Symmetry Transition in the Cubic Phase of a Ternary Surfactant System*, J. Phys. (Paris), **51(14)**, 1501-1508.

Sakata K, Kunitake T. (1990), *A Multilayered Film of an Ultrathin Siloxane Network*, J. Chem. Soc. Chem. Commun., 504 - 505.

Tiselius A., Hjerten S., Levin O. (1956), *Protein Chromatography in Calcium Phosphate Columns*, Arch. Biochem. Biophys., **65**, 132-155.

Zemb T.N., Hyde S.T., Derian P-J., Barnes I.S., Ninham B.W., *Microstructure from X-ray Scattering: The Disordered Open Connected Model of Microemulsions*, J. Phys. Chem., **91**, 3814 -3820.

CHAPTER 6.0

GROWTH OF CALCIUM CARBONATE IN BICONTINUOUS MICROEMULSIONS

6.0 Growth of other materials in bicontinuous microemulsions

6.1 Introduction

The approach adopted in the previous chapter was repeated and attempts at growth of calcium carbonates in DDAB based bicontinuous microemulsions conducted.

6.2 Mineralization of DDAB and tetradecane bicontinuous microemulsions with aragonite and calcite

6.3 Introduction

In order to mineralize a bicontinuous microemulsion system with calcium carbonate a suitable means of crystallization was required. A very simple method which gives high yield relative to the ionic strength of the solutions involved is the system used by Kitano (Kitano 1962). A Kitano solution is made by suspending calcium carbonate in water whilst carbon dioxide is bubbled through it. A proportion of the calcium carbonate dissolves to form a solution of calcium bicarbonate, when this solution is left open to the atmosphere CO_2 is evolved, supersaturation rises and precipitation occurs:

$$Ca(HCO_3)_{2\,(aq)} \longrightarrow CaCO_{3\,(aq)} \downarrow + CO_{2\,(g)} \uparrow + H_2O_{\,(l)}$$

The precipitate from this system consists of calcite of rhombohedral morphology and vaterite of plate-like morphology. However, Kitano found that the addition of magnesium to the calcium bicarbonate solution results in the formation of the more soluble aciculate aragonite polymorph only (magnesium is not incorporated into the lattice). It is believed that the magnesium absorbs to the initial more stable calcite and vaterite nuclei and inhibits their development.

This approach involving magnesium was used for the preparation of solutions to be incorporated into bicontinuous microemulsions since it was previously indicated that an aciculate crystal morphology was necessary to produce reticulated networks.

6.4 Aragonite system

Method

A bicontinuous microemulsion was prepared as described in chapter 5.9. The water component consisted of a freshly prepared calcium hydrogen carbonate (Kitano) solution prepared by dissolving 2.5g of calcium carbonate in one litre of distilled water. This was stirred for 1-1.5 hours whilst carbon dioxide is bubbled through at 3 $lmin^{-1}$. The suspension was then filtered, the resulting solution was approximately at 10mM Ca^{2+}. Magnesium chloride was then added to the solution at a $[Ca^{2+}]$:$[Mg^{2+}]$ of 1:5 in order to promote the aciculate aragonite polymorph of calcium carbonate. It was found that the ionic strength of this solution was too high to allow its use directly but dilution by one third or more was successful in allowing the formation of an optically clear bicontinuous mixture. An experiment involved mixing 0.70g DDAB with 0.35g tetredecane and 0.1g hexadecane with 0.6ml of $Ca(HCO_3)_2$ solution. The optically clear mixture was stored at room temperature and also rapidly frozen and stored at +2°C. Before examination a few drops of the melted microemulsion were placed onto a copper SEM stub, the emulsion was washed by repeatedly passing the stub through hot chloroform until it was observed that all the organics had been removed.

Results

Upon examination of the inorganic material from the unfrozen aragonite system after one day, following extensive washing with hot chloroform, a good yield of white crystalline material coated upon the stub was obtained. A sample of this material was analysed by XRD (fig. 6.1) and found to be composed of aragonite, no other calcium carbonate polymorph was detected. Upon examination by SEM a sheet-like cellular structure which completely covered the SEM stub was visible (fig. 6.2). The structure was composed of crystals of 30nm diameter with pore size 150-400nm. It was found that, unlike preparations using HAP solutions, centrifugation was not necessary to extract the mineral

content. SEM examination of the frozen system after 4 days following washing in hot chloroform showed an identical network of crystals. Further examination after 2 and 4 weeks again showed similar network structures. Filtration of the microemulsion using 0.2μm nuclepore polyester filters followed by SEM examination only showed the presence of occasional aragonite crystals however.

Further experiments showed that the cellular structure could be obtained from newly prepared microemulsion systems containing aragonite solution. A sample of the material was then subjected to extensive washing with a range of organic solvents and oven heating to 200°C, re-examination by SEM showed unchanged reticulated structures.

Overall the results indicate that, unlike preparations involving HAP solutions, the network was not the result of a slow growth process within the microemulsion but was the result of rapid precipitation during the washing stage.

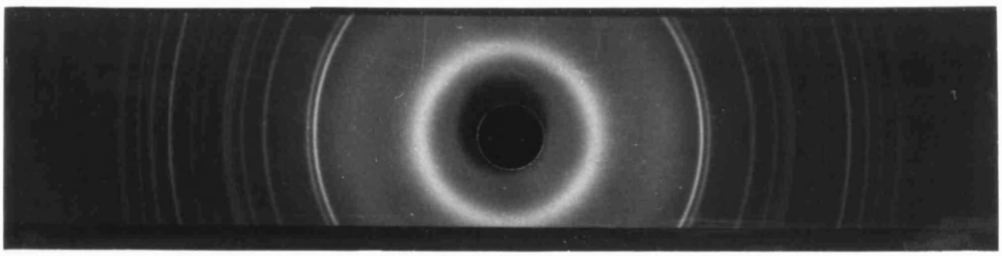

Fig. 6.1. XRD of aragonite obtained from DDAB/ C_{14}/ Mg doped Kitano solution.

d(Å) sample	d(Å) standard	(*hkl*)
8.07	------	----
3.38	3.396	111
3.27	3.273	021
2.70	2.700	012
2.48	2.481	200
1.98	1.977	221
1.55	------	----

Table 6.1. Table of X-ray diffraction data of reticulated aragonite sample compared to standard (Joint Committee on Powder Diffraction Standards 1974).

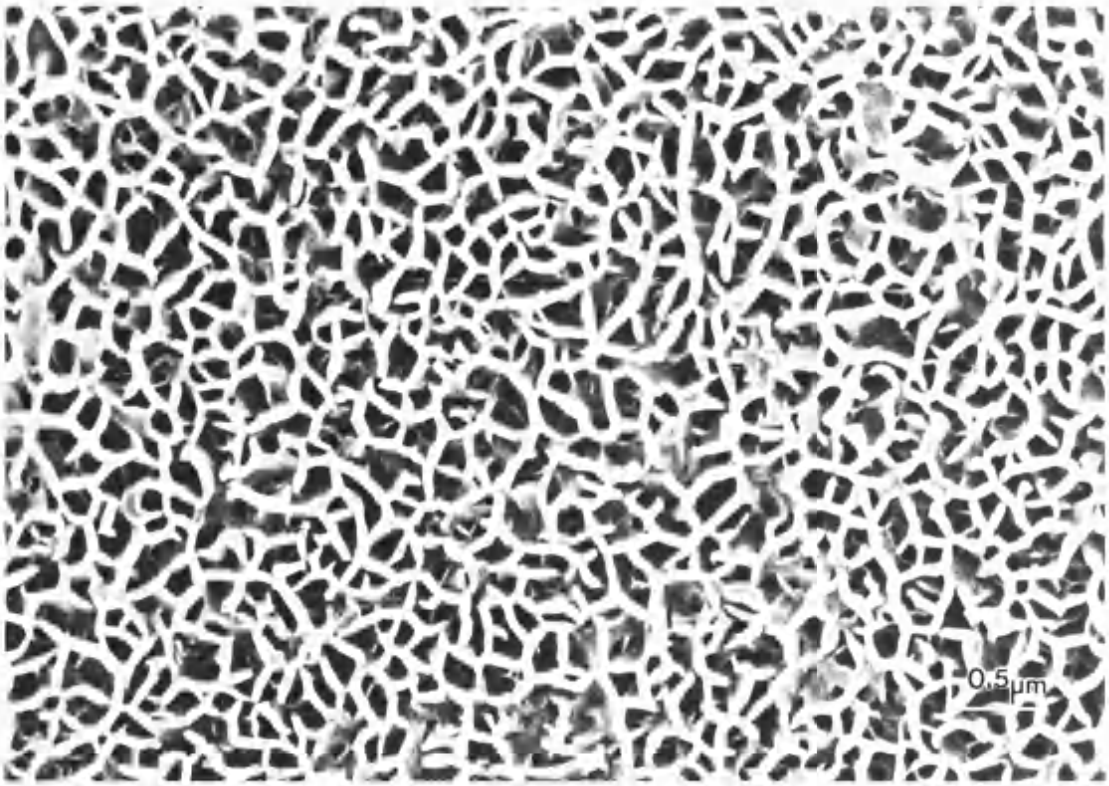

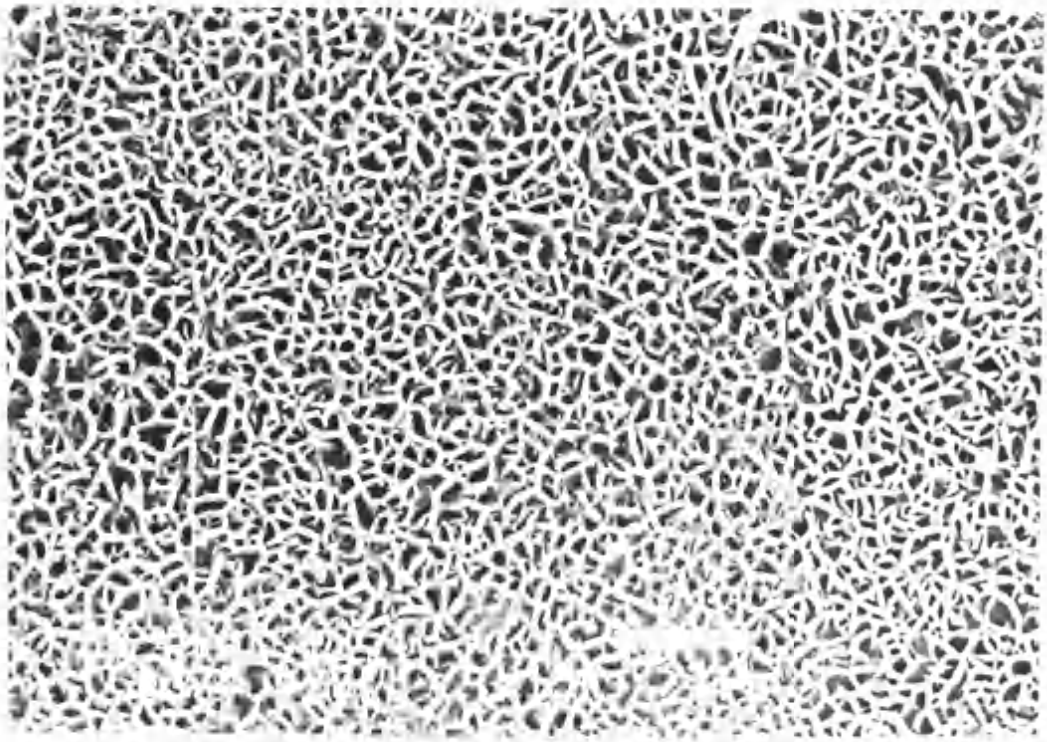

Fig. 6.2. SEM micrographs of cellular-like aragonite obtained from DDAB/ C_{14}/ Mg doped Kitano solution

Fig. 6.3. SEM micrograph of non-organised occasional crystals of aragonite formed on rapid filtration of DDAB/ C_{14}/ Mg doped $Ca(HCO_3)_2$ solution system

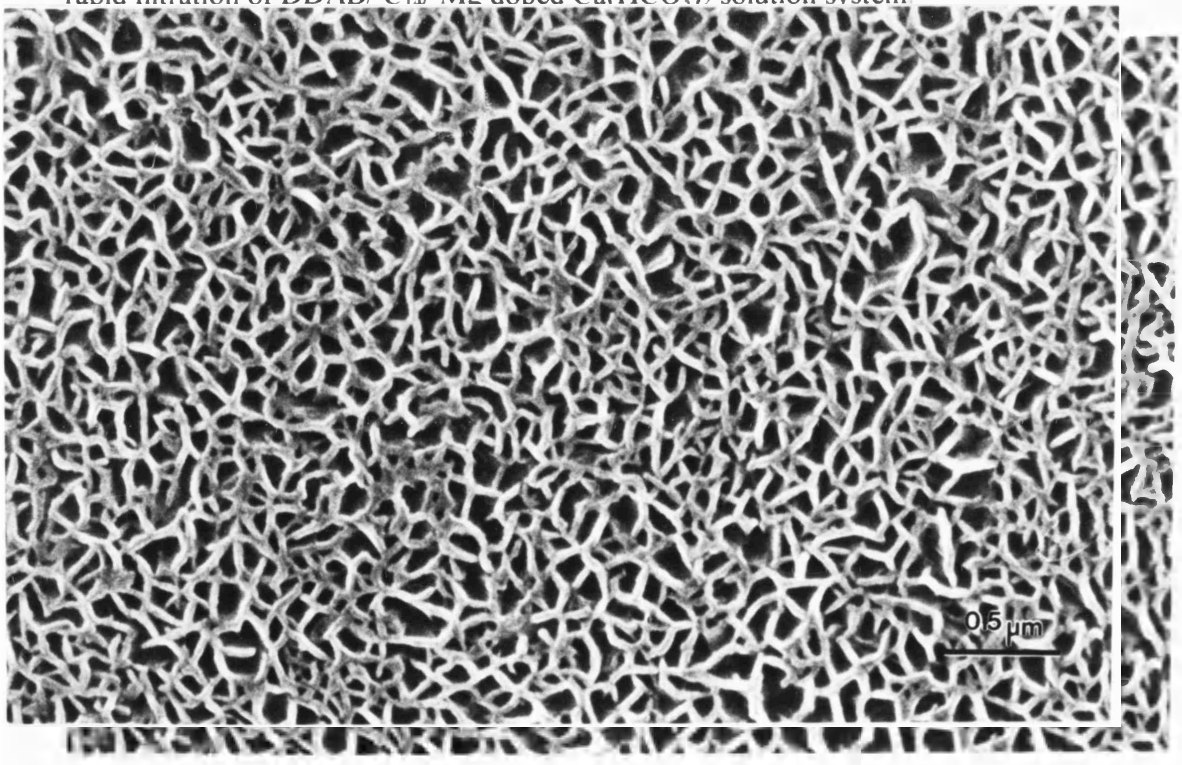

Fig 6.4 SEM micrographs of unchanged cellular-like aragonite obtained from DDAB/ C_{14}/ Mg doped $Ca(HCO_3)_2$ solution system after heating to 200°C

6.5 Calcite system

Method

A bicontinuous microemulsion was prepared as described in chapter 5.9. The water component consisted of a $Ca(HCO_3)_2$ solution prepared as described above. 0.6ml of $Ca(HCO_3)_2$ solution was added directly to 0.70g of DDAB and 0.35g of tetradecane and 0.10g of hexadecane (see table 6.1) and an optically clear bicontinuous emulsion readily formed on mixing. The mixture was then stored at room temperature and also rapidly frozen and stored at +2°C.

Result

Following washing of a sample with hot chloroform a good yield of white crystalline material remained. Analysis of this material by XRD showed it to be composed of calcite and vaterite (fig. 6.5). Examination by SEM revealed the presence of non-reticulated aggregations of calcite rhombs and vaterite plates of 1-10μm in size (fig. 6.6), that were similar to control preparations not involving microemulsions.

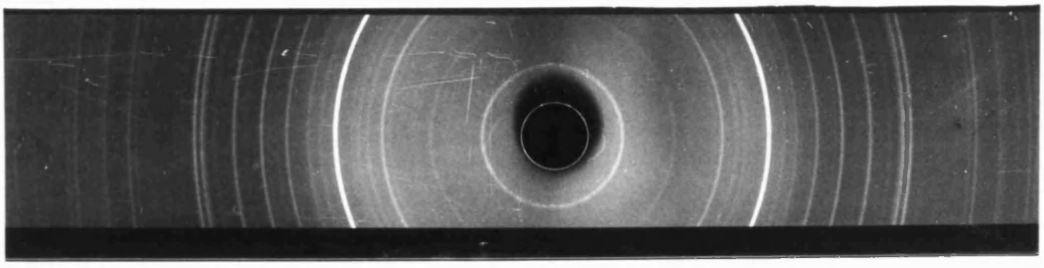

Fig. 6.5. XRD of calcite and vaterite obtained form DDAB /C_{14}/ Kitano solution system.

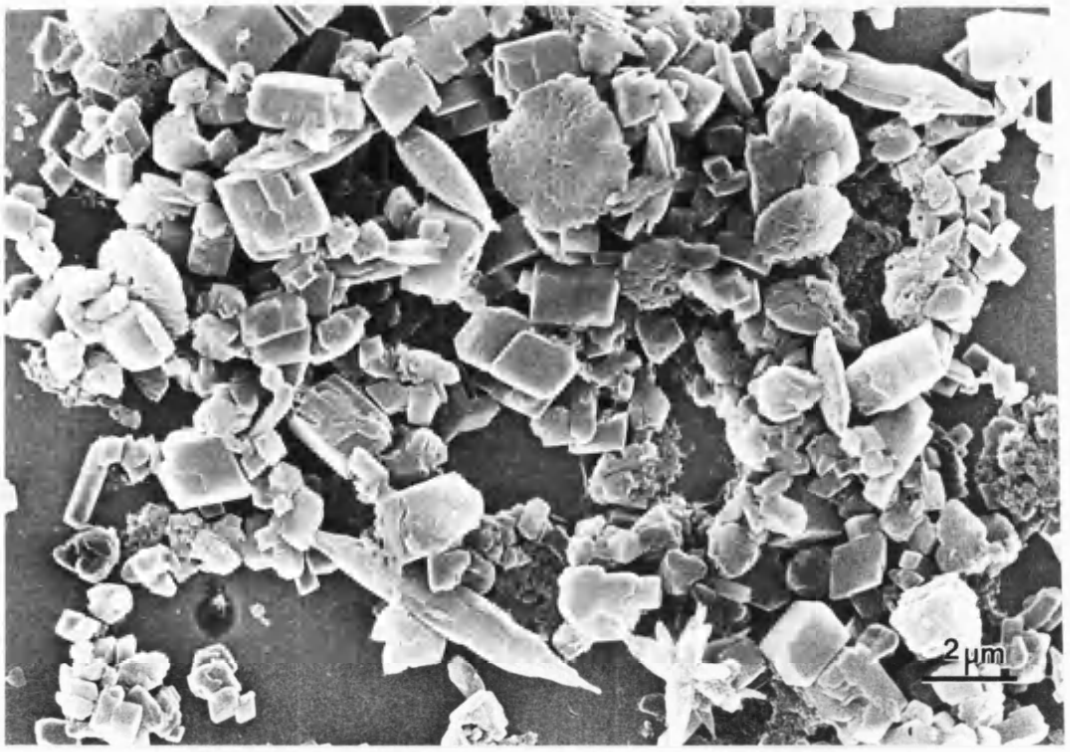

Fig. 6.6. SEM micrograph of non-reticulated calcite and vaterite obtained form DDAB/ C14/ Kitano solution system.

6.6 Effect of microemulsion composition upon mineralization with aragonite.

6.7 Introduction

In order to investigate the effect of the composition of the microemulsion on the formation of aragonite networks, microemulsions at low and high water content were mineralized.

Method

Bicontinuous microemulsions were prepared with a low proportion of solution on the edge of the single phase region using 0.66g DDAB, 0.70g tetradecane and 0.64g of a freshly prepared 5mM Ca2+ $Ca(HCO_3)_2$ solution doped with Mg2+ at a [Ca2+]:[Mg2+] of 1:5 to promote the aciculate aragonite polymorph. Another system at high water as a cubic phase was prepared using 0.64g DDAB, 0.12g tetradecane and 1.2g $Ca(HCO_3)_2$ solution (see table 6.1). Shortly after preparation the microemulsions were placed onto copper SEM stubs and carefully washed with hot chloroform and examined by SEM.

Results

Examination by SEM of a mineralized microemulsion with composition set at low water/ high oil showed the presence of a cellular like structure consisting of 50-100nm aragonite walls bounding irregular spherical spaces of up to 2μm diameter (fig. 6.7). At high water/ low oil an organized structure of relatively small dimensions was obtained, with 20nm aragonite walls bounding spaces of up to approximately 100nm diameter (fig. 6.8).

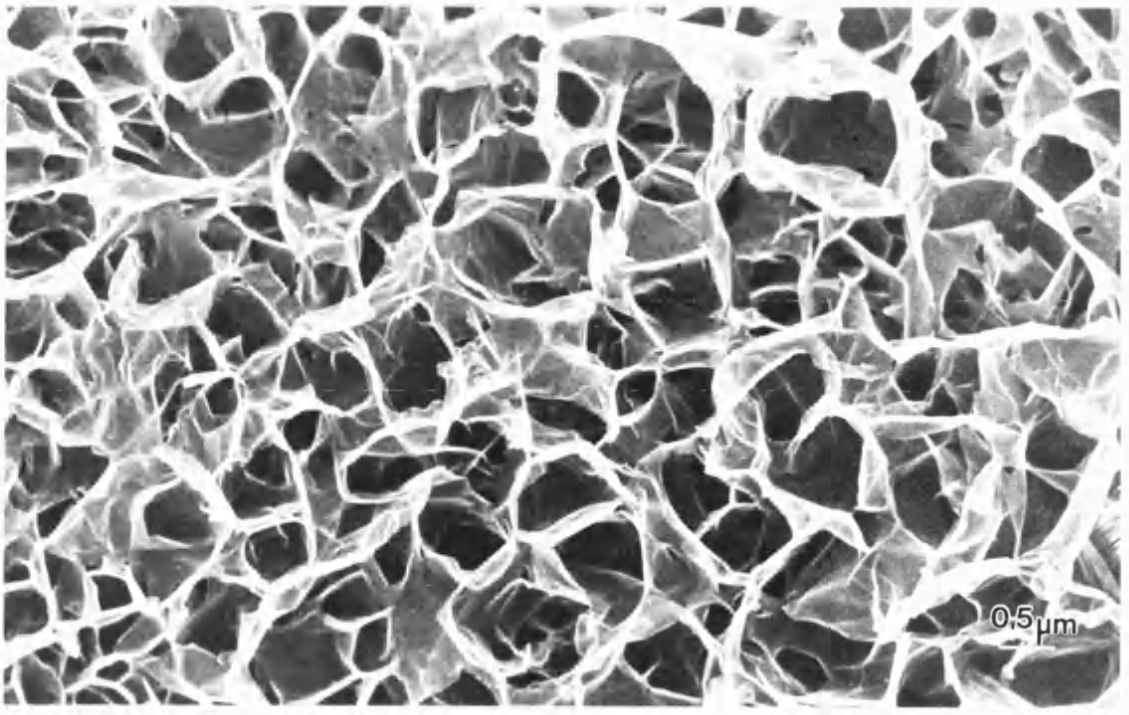

Fig. 6.7. SEM micrograph of aragonite obtained from DDAB /C_{14}/ Mg doped Kitano solution with composition set at low water/ high oil

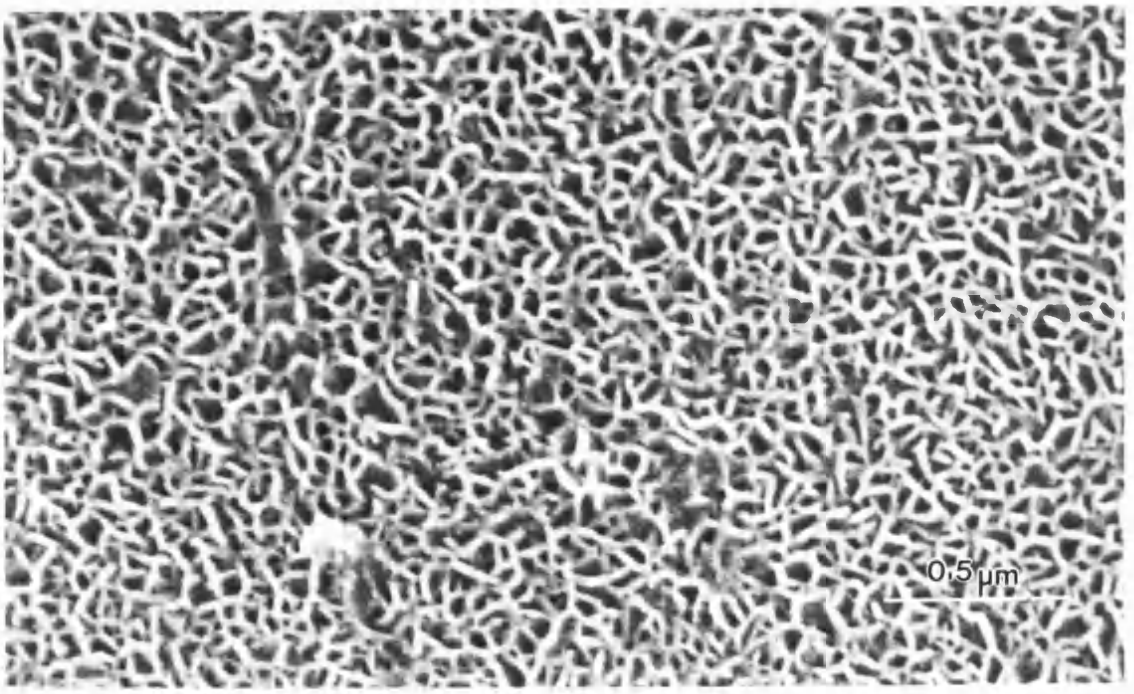

Fig. 6.8. SEM micrograph of aragonite obtained form DDAB/ C14/ Mg doped Kitano solution with composition set at high water/ low oil

Alkane	Oil (%)	Solution (%)	DDAB (%)	Storage Temp(°C)	Cell Size(nm)	Wall Size(nm)	Appearance
$Ca(HCO_3)_2$ solution at a [Ca]:[Mg] of 1:5							
C_{14} C_{16}	17 8	35	40	+2 & +25	150-400	30	Cellular aragonite films
C_{14}	35	32	33	+25	500-2000	50-100	Thin walled, large celled film
C_{14}	6	60	34	+25	100	20	Thin walled, small celled film
$Ca(HCO_3)_2$ solution no Mg added							
C_{14} C_{16}	17 8	35	40	+2	----	----	Non-organized calcite rhombs and vaterite plates

Table 6.1. Table of microemulsion composition for mineralization with calcium carbonate polymorphs.

6.8 Discussion

It was found that preparations involving the aciculate aragonite calcium carbonate polymorph did not produce reticulated structures within the microemulsion. In order for the Kitano solution present in the microemulsion to precipitate, carbon dioxide must be evolved. It is likely that the solubility of CO_2 in the oil component is so low that the diffusion of CO_2 out of the emulsion is greatly inhibited and thus the precipitation of aragonite is extremely slow. However, during the washing process the Kitano solution was able to rapidly outgas CO_2 and therefore rapidly precipitate aragonite. The cellular-like structure may be a result of an initial phase separation during the washing process as the mixture is passed through the hot solvent. The mixture may rapidly self-organize into regularly spaced oil droplets bounded by rapidly mineralizing water, the high surface area presented by the water channels may accelerate the outgassing process greatly. The organics are next removed leaving the mineralized boundaries as a replica of the reorganized structure. This proposed mechanism of formation of mineral cellular structures is summarized in figure 6.9.

a) Bicontinuous microemulsion formed with DDAB/ $Ca(HCO_3)_2$ solution and C_{14}/C_{16}.

b) Phase separation at surface on washing in hot solvent, rapid re-organization into oil droplets surrounded by rapidly mineralizing water channels takes place.

c)Organics are removed on continued washing and mineralization front decends down through the microemulsion.

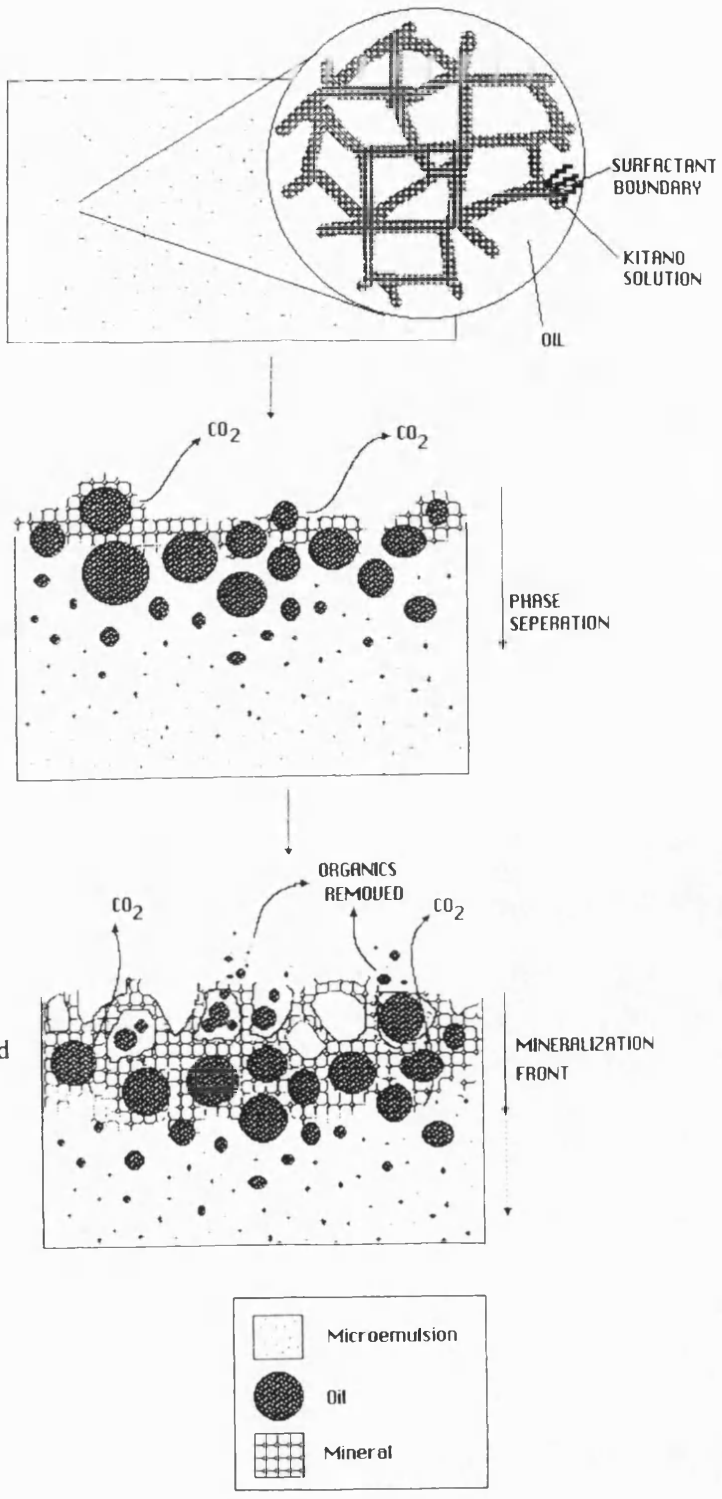

Fig. 6.9. Diagram of proposed mechanism of formation of aragonite cellular films;

A similar phenomenon has been reported in the preparation of porous polymer films by the evaporation of polystyrenes dissolved in carbon disulphide under a flow of moist air (Widawski et al 1994). Foams of the mineral vermiculite which have a similar morphology have been formed from suspensions of exfoliated platelets where bubbles were introduced during evaporation (Ballard et al 1983). Calcium carbonate structures of similar morphology but of much greater dimension (5-50μm) have also been formed from frozen $CaCO_3$ colloidal dispersions formed under pressure (Steytler et al 1993).

The aciculate nature of the precipitated mineral appears to be an essential component since preparation involving other polymorphs of calcium carbonate did not form reticulated structures on washing. When the proportion of the components is varied between low water/ high oil to high water/ low oil the resulting structure appears to vary accordingly. This may be a reflection of the phase separated structure that forms initially during washing. At high oil, larger oil droplets form which results in a relatively large cellular-like structure and vice-versa.

References

Ballard D.G.H., Rideal G.R. (1983), *Flexible Organic Films and Coatings*, J. Mat. Sci., **18**, 545-561.

Kitano Y, Park K., Hood D.W. (1962), *Pure Aragonite Synthesis*, Jr. Geophys. Res., **67(12)**, 4873-4874.

Steytler D.C., Robinson B.H., Eastoe J., Ibel K., Dore J.C., MacDonald I. (1993), *Effects of Solidification of the Oil Phase on the Structure of Colloidal Dispersions in Cyclohexane*, Langmiur, **9**, 903-911.

Widawski G., Rawiso M., Francois B., *Self-organized Honeycomb Morphology of Star-Polymer Polystyrene Films*, Nature, **369**, 387-389.

CHAPTER 7.0

MINERALIZATION OF CEREBROSIDE LIPID TUBULES WITH HAP

7.0 Mineralization of cerebroside lipid tubules with HAP

7.1 Introduction

Another type of self-organized structure is that formed by polymerizable phospholipid molecules. These can be made to form high-axial-ratio tubules of 0.5μm diameter and up to several hundred microns in length (Archibald and Yager 1992, Schnur et al 1987, Rudolph et al 1988). It has been found that it is possible to coat the surface of the tubules with inorganic oxides (Archibald and Mann 1993)

In collaboration with Dr. D. Archibald lipid based hydroxy-fatty-acyl cerebroside (HFA-Cer) tubules were prepared (fig. 7.1a). These possess galactose head-groups which were shown in chapter 3 to have some calcium-binding ability. A small proportion of lipid sulphatide (Sulf) which possess a sulphonate residue at the galactose headgroup was also present, this introduces ionizable groups to the surface of the microstructure (fig. 7.1b) and may also enhance the binding of Ca^{2+}. A calcium phosphate mineralizing solution was used in an attempt to produce tubules that were coated with hydroxyapatite. In principle the organics could then be removed by heating, leaving hollow cylinders of hydroxyapatite.

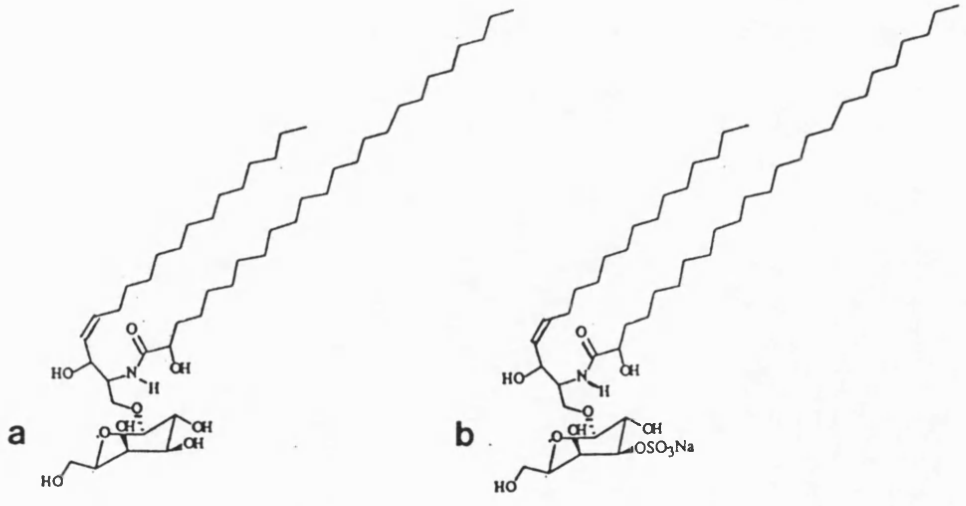

Fig. 7.1. (a) Hydroxy-fatty-acyl cerebroside (HFA-Cer), (b) Sodium sulphatide (Sulf).

Materials

Lyophilized bovine brain HFA-Gal-Cer and sodium sulphatide (Sulf) were obtained from Sigma Chemical Co. (St. Louis, MO) and used as supplied.

Method

In collaboration with Dr. D. Archibald lipid tubules were prepared from HFA-Cer and sulf. The cerebrosides were separately dissolved in a mixture of chloroform and methanol 2:1v/v to form solutions of a known concentration around 5-10mg/ml. Appropriate volumes of cerebrosides solutions were then mixed in a small Teflon sealed vial such that a mixture was formed of 0.9mg/ml HFA-Cer and 0.1mg/ml Sulf of total volume around 250µl. The solvents were then evaporated away under a flow of N_2. 1ml of 1,2-ethanediol (ethylene glycol) was then added to the dried cerebrosides and the sealed vial placed in water at 95-100°C. The vial was held at this temperature for twenty minutes with frequent gentle agitation to aid hydration of the lipids, incubation at this temperature without agitation was continued for a further 15 minutes. The mixture was then slowly cooled to 25°C at <0.5°C/min, tubules are formed spontaneously as the temperature passes through the phase transition from liquid crystal to gel.

300µl (0.3mg) of lipid tubules from the well mixed 1mg/ml preparation was added to a freshly prepared calcium phosphate mineralizing solution of 1.28ml of 1.2mM $CaCl_2.2H_2O$ and 1.28ml of 0.72mM KH_2PO_4 (HAP Ksp=10^{-59}, supersaturation=$3x10^{28}$), this would normally precipitate approximately 0.3mg of HAP and is in a 1:1 weight ratio with the tubules. Samples were removed from this mixture and examined by TEM using a Jeol 2000 FX EM after 3,6 and 10 days.

Results

Upon examination of the lipid tubules obtained from the mineralizing solution after 3 days, 50nm diameter spheroids of ACP were found to be attached to many of the tubules (fig. 7.2a). The degree of coverage varied from near total to occasional. Upon re-examination after 6 days the ACP spheroids had developed into crystalline material and dissolution of the lipid tubules was evident (fig. 7.2b). Most of the crystalline material was not closely associated with tubules but was present as aggregations. After 10 days dissolution of the tubules was complete, occasional tubules were still present stabilized with a coating of HAP material. Also present were large aggregations of crystalline material similar to those formed in a control mineralizing solution.

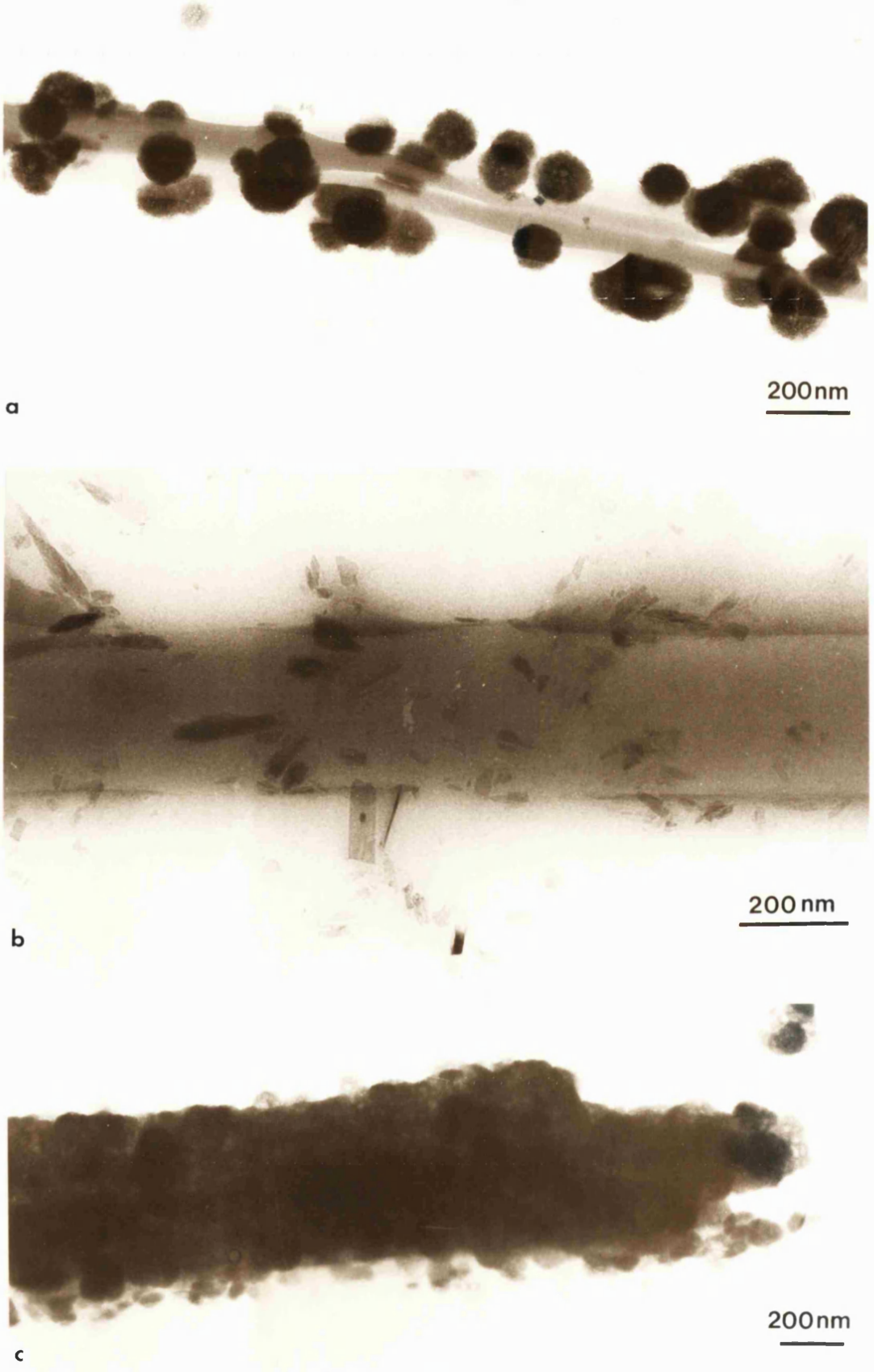

Fig. 7.2. (a) TEM micrographs of lipid tubules after standing in mineralizing solution for 3 days; (b) after 6 days dissolution is evident; (c) after 10 days a few well coated tubules remain.

7.2 Discussion

The approach adopted was found to be only very partially successful in producing HAP coated structures. ACP appeared to have a high nucleation affinity for the S-Cer doped tubules. If a tubule was well coated before dissolution became significant it appeared that it could be stabilized and fully coated tubules formed. A small minority of tubules appeared to follow this pattern, most had a patchy coverage which did not appear to prevent dissolution. Subsequent phase transformation into HAP crystallites was often not associated with the lipid surface. It has been previously suggested that the binding of Ca^{2+} enhances the hydration of the sugar headgroups and destabilizes the cerebroside structures (Boggs et al 1984), this process may have accelerated the breakdown of the tubules. As a result of dissolution the associated HAP material was lost to the solution which may have led to the secondary nucleation of HAP not associated with tubules and the development of characteristic aggregations of HAP crystallites.

References

Archibald D.D., Mann S. (1993), *Template Mineralization of Self-Assembled Anisotropic Lipid Microstructures*, Nature, **364**, 430-433.

Archibald D.D., Yager P. (1992), *Microstructural Polymorphism in Bovine Galactocerebroside and its two Major Subfractions*, Biochemistry, **31**, 9045-9055.

Rudolph A.S., Calvert J.M., Schoen P.E., Schnur J.M. (1988), *Technological Development of Lipid Tubule Microstructures*, from *Biotechnological Applications of*

Lipid Microstructures, Gaber B.P., Schnur J.M., Chapman D. Eds., Plenum Publishing Corporation, 305-320.

Schnur J.M., Price R., Shoen P., Yager P., Calvert M., Georger J., Singh A. (1987), *Lipid-Based Tubule Microstructures*, Thin Solid Films, **152**, 181-206.

8.0 Summary

HAP is an important mineral because it closely matches the inorganic component of bones (as plates) and teeth (as hexagonal needles). The relationship between OCP which is plate-like and plate-like HAP could not accurately be discusssed until recently because it was believed that the large faces of plate-like HAP were (100) faces. However Heywood et al (1990) demonstrated that these are actually (1-10) faces. This finding fitted well with attachment energy calculations of F-faces of OCP (Terpstra and Bennema 1987). These findings suggested that later crystal growth is regulated by a physical constraint rather than specific interactions between a protein matrix and crystal (Heywood 1990). In this study it was found that under certain precipitation conditions the presence of certain (but not all) anions or cations (Cl^- or Li^+) could promote the formation of a plate-like HAP rather than the more usual hexagonal needle form. This may have been brought about by a localized disruption at the surface of ACP/ embryonic nuclei which favours the nucleation of plate-like OCP templates which are hydrolyzed to HAP. Furthermore, the presence of hydroxylated additives weakly bound via non-specific additive-crystal interactions to the developing ACP/HAP crystallites was believed to exclude Cl^- from surface sites inhibiting a plate-like precursor and promoting the formation of hexagonal rods. Well hydroxylated additives were also found to increase the average aspect ratio from 10:1 to 25:1, presumably by a non-specific interaction with the prismatic faces of the developing crystal.

It was noted in the additive experiments and in the presence of the Li^+ ion (often associated with unusual morphological effects) HAP exhibited only plate-like or needle-like morphologies. A more fundamental approach to modification of crystal

environment using the self-organised structure formed by a bicontinuous microemulsion as a medium for the precipitation of slightly supersaturated solutions of HAP was then employed. It was found that nucleation and growth took place within the interconnecting water conduits, bounded by surfactant walls and surrounded by oil. As growth proceeded the crystallizing conduits greatly increased in dimension and a reorganized but stable structure of interconnected crystals with pores up to several microns in diameter developed. The crystals were curved and much more elongated than was found with control precipitations and the surfactant walls may have acted to promote elongation via a physical constraint in a similar way as sheaths of enamelins and other matrix constituents are suggested to in developing teeth.

Mineralization of bicontinuous microemulsions with calcium carbonate was then attempted using solutions of $Ca(HCO_3)_2$ prepared by the Kitano method. Precipitation of calcium carbonate as the calcite and vaterite polymorphs took place as non-organized aggregations. When the $Ca(HCO_3)_2$ solution was doped with magnesium to promote the aragonite polymorph however, sheets of a well organized cellular-like structure were formed on clean-up. It was found that unlike the preparations involving HAP solutions little growth of aragonite took place within the microemulsions, presumably because the evolution of CO_2 from the frozen mixture was inhibited. On washing with hot solvent it may be that the microemulsion undergoes a phase separation, particularly at the surface, CO_2 is rapidly outgassed and aragonite rapidly precipitates around droplets of oil. It was found that the pore-size of the cellular structures could be varied by changing the proportion of the components.

An attempt was then made to mineralize the surface of self-organized cerebroside based lipid tubules. ACP showed a high nucleation affinity for the surface of the tubules, but subsequent phase transformation into HAP crystallites was not usually associated with the tubule surface. Under the reaction conditions occasional well coated tubules developed, however most tubules underwent dissolution before a full coating of HAP was formed.

References

Heywood B.R., Sparks N.H., Shellis R.P., Weiner S., Mann S.(1990), *Ultrastructure, Morphology and Crystal Growth of Biogenic and Synthetic Apatites*, Conn. Tiss. Res., **25**, 1-17.

Terpstra R.A., Bennema P. (1987), *Crystal Morphology of Octacalcium Phosphate: Theory and Observation*, Jr. of Crystal Growth, **82**, 416-426.

9.0 Future work

Further investigation into the role of the Cl^- ion (and other anions and cations) in promoting the formation of plate-like rather than needle-like HAP is necessary. A kinetic effect involving a dynamic interaction at the developing crystal surface is suspected which could be investigated by high resolution TEM and AFM studies of the earliest precipitates.

The formation of porous reticulated HAP structures could be further refined. The pore size may at present be too small to allow vasculization, but the use of a longer chain surfactant (e.g. ditetradecyldimethylammonium bromide) and higher oils may allow the formation of larger reticulated structures. The growth of other suitable materials may also be investigated. Suitable minerals would probably need to meet certain criteria such as low solubility and aciculate morphology (e.g. some oxides of iron, barium carbonate etc).

The ready formation of regular self-organized cellular aragonite films by the precipitation of a magnesium doped $Ca(HCO_3)_2$ solution in a microemulsion system would appear to be a suitable area for further research. Further alteration of the experimental conditions may bring about the formation of other interesting and potentially useful architectures of aragonite films.

Appendix 1 Derivation of Crystal Planes

Crystal planes are known by their *Miller indices,* taking a three dimensional lattice for which the lattice constants are *a,b* and *c*, if a set of planes intersects these axes and divides the a lattice translation into *h* parts, the *b* lattice translation into *k* parts and the *c* lattice translation into *l* parts, the plane is representedby the Miller indices (*hkl*). Also the plane (*hkl*) has intercepts of *a/h*, *b/k* and *c/l* on three crystallographic axes, thus the Miller indices are reciprocals of the fractional intercepts.

A system using four indexes (*hkil*) known as the Miller-Bravais system can be used, this is based on a non-primitive hexagonal cell (hexagonal prism). This endows planes belonging to the same form with indices which are numerically related to each other.
Round brackets (*hkil*) denote a particular plane or face whereas curly brackets {*hkil*} represent a set of symmetry-equivalent planes or faces.

Directions are given by three integers in square brackets [UVW]. The direction [UVW] in a lattice with unit cell base a,b,c is a direction parallel to the vector Ua+Vb+Wc, where U,VW are integers. The set of symmetry related directions [UVW] is designated by different brackets i.e. <UVW>. A set of planes lie in the same *zone* if they are parallel to a common direction [UVW]. The direction [UVW] is called the *zone axis*. This can be visualized in relation to the eight faces of a hexagonal prism. The planes (-100), (-110), (010), (100), (1-10) and (0-10) are all mutually parallel to the direction [001], the *c* axis direction and are said to lie in the zone [001]. All planes (*hk0*) lie in the [001] zone as they do not intersect the *c* axis.

For any crystal system, the condition that a plane *(hkl)* is parallel to the direction [UVW] is given by the Weiss zone law:

$$hU+kV+lW=0$$

If two planes *(hkl)* and *(h'k'l')* lie in the same zone [UVW] then the following equation must also hold:

$$h'U+k'V+l'W=0$$

The zone can be calculated from two planes in the same zone using:

$$U=kl'-k'l$$
$$-V=hl'-h'l$$
$$W=hk'-h'k$$

E.g. taking the (2-22) and (1-12) planes of HAP:

$$U=(-2.2)-(-1.2)=-2$$
$$-V=(2.2)-(1.2)=-2$$
$$W=(2.-1)-(1.-2)=0$$

Thus (2-22) and (1-12) planes lie in the zone [-2-20]=[-1-10]zone = [110] zone.

Appendix 2 Calculation of d spacings and interplanar angles of HAP

Given that $d=\frac{2L}{D}$ where d=d spacing A
L=camera constant
=wavelength electronsx
distance along column
at 200kV
=0.0251A
hence camera constant=800mmx0.0251A
=20.08Amm

Taking the 111 plane

Distance between adjacent spots=10.32mm

$$d=\frac{2L}{D}=\frac{40.16Amm}{10.32mm}$$

$$=3.89A$$

d A measured	d A actual	h k l
3.89	3.88	1 1 1
4.73	4.72	1 1 0
3.44	3.44	0 0 2
2.78	2.78	1 1 2

Table 3. Table of calculated and actual d spacings for hydroxyapatite

Interplaner angles for hexagonal systems

$$\cos\theta=\frac{h_1h_2+k_1k_2+1/2(h_1k_2+h_2k_1)+\frac{(3a)^2}{4c^2}l_1l_2}{\sqrt{(h_1^2+k_1^2+h_1k_1+\frac{3a^2}{4c^2}l_1^2)(h_2^2+k_2^2+h_2k_2+\frac{3a^2}{4c^2}l_2^2)}}$$

		h_1 k_1 l_1				
		100	001	1-10	110	111
	100	---	90	60	30	44.41
h_2	001	90	---	90	90	55.57
k_2	1-10	60	90	---	90	90
l_2	110	30	90	90	---	34.43
	111	44.41	55.57	90	34.43	---

Table of interplanar angles for HAP

Appendix 3 Coordinates and bond lengths and angles of atoms in HAP unit cell

Oxygen I	Value
x	0.372
y	0.487
z	0.25

Calcium II	Value
x	0.2464
y	0.9938
z	0.25

Oxygen II	Value
x	0.5899
y	0.4666
z	0.25

Hydroxyl oxygen	Value
x	0
y	0
z	0.1930

Phosphorus	Value
x	0.3999
y	0.3698
z	0.0736

Hydrogen	Value
x	0
y	0
z	0.0617

Calcium I	Value
x	0.3333
y	0.6666
z	0.0010

Table of coordinates of atoms in unit cell of HAP (space group $P6_3/m$). Determined from X-ray diffraction mapping.

Atoms involved	Distance (Å) or angle
$P\text{-}O_I$	1.538
$P\text{-}O_{II}$	1.547
$P\text{-}O_{III}$	1.529
$O_{III}\text{-}P\text{-}O_{III}'$	107.75°
$O_I\text{-}P\text{-}O_{II}$	111.0°
$O_I\text{-}P\text{-}O_{III}$	111.5°
$O_{II}\text{-}P\text{-}O_{III}$	107.5°
$O_H\text{-}H$	0.957
$Ca_{II}\text{-}O_H$	2.384
$Ca_{II}\text{-}H$	2.692
$Ca_I\text{-}O_I$	2.408
$Ca_I\text{-}O_{II}$	2.454
$Ca_I\text{-}O_{III}$	2.808
$Ca_{II}\text{-}O_I$	2.707
$Ca_{II}\text{-}O_{II}$	2.358
$Ca_{II}\text{-}O_{III}$	2.345
$Ca_{II}\text{-}O_{III}$	2.514

Table of close approaches and angles for bonds in unit cell of HAP.

References

Kay M.I., Young R.A., Posner A.S. (1964), *Crystal structure of hydroxyapatite,* Nature, 204, 1050-1052.

Appendix 4 X-ray diffraction data cards

9-432 MAJOR CORRECTION

d	2.81	2.78	2.72	8.17
I/I$_1$	100	60	60	11

$Ca_5(PO_4)_3(OH)$ $1/2[Ca(OH)_2 \cdot 3Ca_3(PO_4)_2]$ ★

CALCIUM HYDROXIDE ORTHOPHOSPHATE (HYDROXYAPATITE)

Rad. CuKα$_1$ λ 1.5405 Filter Dia. 114.6mm
Cut off 50 I/I$_1$ PHOTOMETER* (GUINIER CAMERA)
Ref. DEWOLFF, TECHN. PHYS. DIENST, DELFT, HOLLAND

Sys. HEXAGONAL S.G. $P6_3/m$ (176)
a_o 9.418 b_o c_o 6.884 A C 0.7309
α β γ Z 2 Dx 3.16
Ref. IBID.

εα nωβ εγ Sign
2V D 3.08 mp Color
Ref.

* I/I$_1$ ARE PEAK VALUES FROM A PATTERN WHICH SHOWS SLIGHT BROADENING OF PRISM REFLECTIONS.
SAMPLE OBTAINED FOLLOWING THE PROCEDURE INDICATED BY HODGE C.S., IND. ENG. CHEM. ANAL. ED. 10 156 (1938).

d Å	I/I$_1$	hkl	d Å	I/I$_1$	hkl
8.17	12	100	2.040	2	400
5.26	6	101	2.000	6	203
4.72	4	110	1.943	30	222
4.07	10	200	1.890	16	312
3.88	10	111	1.871	6	320
3.51	2	201	1.841	40	213
3.44	40	002	1.806	20	321
3.17	12	102	1.780	12	410
3.08	18	210	1.754	16	402,303
2.814	100	211	1.722	20	004,411
2.778	60	112	1.684	4	104
2.720	60	300	1.644	10	322,223
2.631	25	202	1.611	8	313
2.528	6	301	1.587	4	501,204
2.296	8	212	1.542	6	420
2.262	20	310	1.530	6	331
2.228	2	221	1.503	10	214,421
2.148	10	311	1.474	12	502
2.134	4	302	1.465	4	510
2.065	8	113	PLUS ADDITIONAL LINES		

26-1056

26-1056A

d	18.7	2.83	2.82	18.7
I/I$_1$	≈300	100	95	≈300

$Ca_8H_2(PO_4)_6 \cdot 5H_2O$ ★

Calcium Hydrogen Phosphate Hydrate OCP

Rad. CuKα$_1$ λ 1.540598 Filter Mono. Dia.
Cut off I/I$_1$ Diffractometer I/I cor. = 0.5
Ref. NBS Monograph 25, Sec. 13, 21 (1976)[4]

Sys. Triclinic S.G.
a_o 9.529(3) b_o 18.994(4) c_o 6.855(3) A 0.5017 C 0.3609
α 92.53(3)° β 90.13(3)° γ 79.93(2)° Z 2 Dx 2.673
Ref. Ibid.

εα 1.576 nωβ 1.583 εγ 1.585 Sign -
2V ≈50° D mp Color Colorless
Ref. Brown et al., Nature, 196 1050 (1962)

*d=2.83 was assigned I=100, the strongest line d=18.67 is ≈300.
Pattern at 25°C.
To replace 11-184 and 13-391.
W used as internal standard.
Sample made by W. E. Brown et al. at NBS.
See following card

d Å	I/I$_1$	hkl	d Å	I/I$_1$	hkl
18.7	≈300	010	3.660	30	211
9.36	45	100,020	3.492	25	231
9.05	40	110	3.441	50	221
6.10	6	120	3.424	60	002
5.52	25	101	3.378	18	221
5.417	7	111,021	3.311	20	151
5.211	4	111	3.278	18	150
5.101	12	111	3.209	25	102,250+
4.815	6	130	3.180	25	241,310
4.706	5	031	3.132	10	122,300+
4.670	4	040	3.117	7	112,060
4.514	10	031,140+	3.055	14	032 240
4.492	10	121	3.015	8	330
4.294	7	131	2.946	14	122,251
4.111	5	230	2.914	12	151
3.919	16	220,140+	2.873	30	251
3.879	12	201,131	2.833	100	260
3.862	10	201	2.820	95	320,241
3.786	10	041	2.779	45	142,331
3.745	14	221	2.745	35	132,331

FORM M-2
P

5-0586 MINOR CORRECTION

d	3.04	2.29	2.10	3.86
I/I$_1$	100	18	18	12

$CaCO_3$ ★

CALCIUM CARBONATE (CALCITE)

Rad. CuKα$_1$ λ 1.5405 Filter Ni
Dia. Cut off Coll.
I/I$_1$ G.C. DIFFRACTOMETER d corr. abs.?
Ref. SWANSON AND FUYAT, NBS CIRCULAR 539, VOL. II 51 (1953)

Sys. HEXAGONAL S.G. $D_{3D}^6 - R\bar{3}c$
a_o 4.989 b_o c_o 17.062 A C 3.420
α β γ Z 6
Ref. IBID.

εα nωβ 1.659 εγ 1.487 Sign -
2V D_x 2.711mp Color
Ref. IBID.

SAMPLE FROM MALLINCKRODT CHEM. WORKS. SPECT. ANAL.: <0.1% Sr; <0.01% Ba; <0.001% Al,B,Cs, Cu,K,Mg,Na,Si,Sn; <0.0001% Ag,Cr,Fe,Li,Mn.
X-RAY PATTERN AT 26°C

REPLACES 1-0837, 2-0623, 2-0629, 3-0569, 3-0593, 3-0596, 3-0612, 4-0636, 4-0637

d Å	I/I$_1$	hkl	d Å	I/I$_1$	hkl
3.86	12	102	1.297	2	218
3.035	100	104	1.284	1	306
2.845	3	006	1.247	1	220
2.495	14	110	1.235	2	1.1.12
2.285	18	113	1.1795	3	2.1.10
2.095	18	202	1.1538	3	314
1.927	5	204	1.1425	1	226
1.913	17	108	1.1244	<1	2.1.11
1.875	17	116	1.0613	1	2.0.14
1.626	4	211	1.0473	3	404
1.604	8	212	1.0447	4	138
1.587	2	1.0.10	1.0352	2	(0.1.16
1.525	5	214			(1.1.15
1.518	4	208	1.0234	<1	1.2.13
1.510	3	119	1.0118	2	3.0.12
1.473	2	215	0.9895	<1	231
1.440	5	300	.9846	1	322
1.422	3	0.0.12	.9782	1	1.0.17
1.356	1	217	.9767	3	2.1.14
1.339	2	2.0.10	.9655	2	234

CALCULATED PATTERN—INTEGRATED

* 24-30A

See 24-30

24-30

3.30	2.74	3.58	100	67	49

$CaCO_3$

Calcium Carbonate — Vaterite

Ref. Smith et al., Annual Report to the Joint Committee on Powder Diffraction Standards (1973)

Sys. Hexagonal — S.G. $P6_3/mmc$ (194) — Dx 2.644 — Z 2

a_0 4.13 — b_0 — c_0 8.49

α — β — γ

Ref. Kamhi, Acta Cryst., 16 770 (1963)
note: pseudo-cell used for structure analysis

Scale factor (Integrated Intensities) 0.29×10^{-3}

λ 1.54050

d A	I/I_0	h k l	d A	I/I_0	h k l
4.245	5	002	2.122	4	004
3.577	49	100	2.065	38	110
3.296	100	101	1.8569	12	112
2.735	67	102	1.8253	27	104
2.219	2	103	1.7883	2	200

d A	I/I_0	h k l	d A	I/I_0	h k l
1.6481	10	202			
1.3676	2	204			
1.2881	3	212			

FORM CI
B

5-0453 MAJOR CORRECTION

d	3.40	1.98	3.27	4.212
I/I_1	100	65	52	2

$CaCO_3$

CALCIUM CARBONATE (ARAGONITE)

Rad. $CuK\alpha_1$ λ 1.5405 — Filter Ni
Dia. — Cut off — Coll.
I/I_1 DIFFRACTOMETER — d corr. abs.?
Ref. SWANSON AND FUYAT, NBS CIRCULAR 539, VOL. III, (1953)

Sys. ORTHORHOMBIC — S.G. D_{2H}^{16} - PMCN
a_0 4.959 — b_0 7.968 — c_0 5.741 — A 0.622 — C 0.721
α — β — γ — Z 4
Ref. IBID.

ε α 1.529 — n ω β 1.680 — ε γ — Sign −
2V — Dx 2.930 mp — Color
Ref. IBID.

SAMPLE PREPARED AT NBS. SPECT. ANAL.: < 0.1% AL, BA, CU, FE, MG, NI, PB; < 0.001 % AG, MN, SN.
X-RAY PATTERN AT 26°C

REPLACES 1-0268, 3-0405, 3-0425, 3-0670, 3-0893, 3-1067

d Å	I/I_1	hkl	d Å	I/I_1	hkl
4.212	2	110	1.698	3	222
3.396	100	111	1.557	4	311
3.273	52	021	1.535	2	232
2.871	4	002	1.499	4	241
2.730	9	121	1.475	3	321
2.700	46	012	1.466	5	151
2.481	33	200	1.411	5	312
2.409	14	031	1.404	3	330
2.372	38	112	1.365	3	242,331
2.341	31	130	1.358	3	114
2.328	6	022	1.328	2	060
2.188	11	211	1.261	6	332
2.106	23	220	1.240	7	400
1.977	65	221	1.224	5	134
1.882	32	041	1.205	6	243,062
1.877	25	202	1.1892	5	153
1.814	23	132	1.1712	6	162,260
1.759	4	141	1.1599	3	421
1.742	25	113			
1.728	15	231			

Reprint Series
10 June 1994, Volume 264, pp. 1576–1578

SCIENCE

Crystal Tectonics: Construction of Reticulated Calcium Phosphate Frameworks in Bicontinuous Reverse Microemulsions

Dominic Walsh, Jeremy D. Hopwood, and Stephen Mann*

Crystal Tectonics: Construction of Reticulated Calcium Phosphate Frameworks in Bicontinuous Reverse Microemulsions

Dominic Walsh, Jeremy D. Hopwood, Stephen Mann*

The chemical construction of organized architectures is an important aspect of innovative materials synthesis. Bicontinuous water-filled microemulsions can be used as preorganized systems for the fabrication of crystalline calcium phosphate materials with extended reticulated microstructures. These macroporous materials are formed by mineralization reactions located within the interconnecting water channels of the bicontinuous network. The resulting materials represent replicas of the microemulsion architecture, but the pore sizes are incommensurate, suggesting that secondary modifications in the bicontinuous microstructure occur during crystal growth. Synthetic macroporous calcium phosphates could have uses in biomaterial implants.

Although the elucidation of "molecular tectonics" (*1*) is still at a fundamental level, it is clear that there are many parallels between the synthetic requirements of materials chemistry and the biological strategies inherent in biomineralization (*2*). Previously, we have shown that organized assemblies of amphiphilic molecules can be used to provide nanoscale environments for inorganic materials synthesis, anisotropic templates for the production of fibrous inorganic-organic composites, and recognition surfaces for the oriented nucleation of inorganic crystals (*3*). Although this approach has been successful in mimicking aspects of biomineralization involving discrete building units, it has not been forthcoming in fabricating elaborate three-dimensional extended architectures analogous to the tests and shells of biological materials such as diatoms and sea urchins. The technological importance of such a relation is exemplified in the recent discovery involving the use of liquid-crystal surfactant aggregates in the control of the pore size of amorphous aluminosilicate materials formed from aqueous solution (*4*). Here, we report an approach based on "crystal tectonics," in which the nanoscale interconnecting rod-like water conduits of bicontinuous water-filled microemulsions act as an organized medium for the construction of an extended macroporous calcium phosphate material. Our approach differs from previous studies with liquid-crystal aggregates in that aqueous compartments are used and reticulated frameworks comprising crystalline inorganic units are fabricated. Moreover, because the bicontinuous network microstructure rapidly fluctuates in liquid media, we have used frozen oils to generate immobilized frameworks for the construction of inorganic architectures.

Bicontinuous reverse microemulsions (*5*) were prepared from mixtures of the cationic surfactant didodecyldimethyl ammonium bromide (DDAB), a metastable calcium phosphate aqueous solution, and a long chain alkane (*6*). The clear mixture was rapidly frozen in liquid nitrogen (*7*) and stored for up to several weeks at temperatures (−25°C for dodecane, +2°C for tetradecane, and −25°C or +2°C for tetradecane-hexadecane mixtures) at which the alkane oils remained frozen (*8*) but the aqueous phase was liquid (*9*). Extraction of the inorganic component formed by mineralization in the aqueous conduits was achieved by centrifugation of the melted microemulsion at 10,000 rpm for 10 to 15 min, followed by extensive washing of the pellet in hot hexane to remove residual surfactant and oil. Depending on the volumes of metastable calcium phosphate used, product yields of 0.5 to 1.0 g per liter of microemulsion were obtained. Samples were subsequently air-dried and studied by x-ray diffraction, infrared spectroscopy, and electron microscopy (*10*).

Scanning electron micrographs of the extracted mineralized replicas showed the presence of highly reticulated microstructures of interconnecting needle-like crystals (Fig. 1). These architectures were observed in all samples prepared at −25° or +2°C. Infrared spectra, electron and x-ray diffraction patterns, and energy dispersive x-ray analysis spectra were consistent with the crystalline mineral hydroxyapatite [HAP: $Ca_{10}(OH)_2(PO_4)_6$]. The majority of materials studied were macroporous with pore diameters up to several micrometers and wall thicknesses of 50 to 130 nm, depending on the storage time and composition of the microemulsion mixture (Table 1). No evidence of regular interconnecting arrays was observed; in all structures the framework appeared to consist of a randomly arranged network of intergrown crystalline needles (lengths of 0.2 to 1 μm) with a wide range of pore diameters. The largest pores were often formed by curved cylinders of the reticulated material and were possibly artifacts of the washing and drying processes. Some modifications in microstruc-

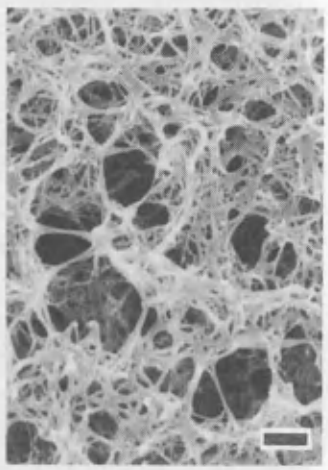

Fig. 1. Scanning electron micrograph showing reticulated framework of needle-like hydroxyapatite crystals formed in bicontinuous microemulsions. The material was prepared from a DDAB-water-tetradecane-hexadecane system at +2°C for 3 weeks. Scale bar, 1.0 μm.

School of Chemistry, University of Bath, Bath, BA2 7AY, UK.

*To whom correspondence should be addressed.

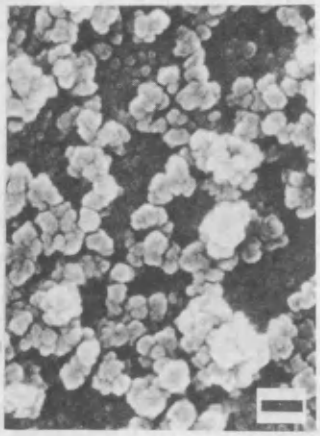

Fig. 2. Scanning electron micrograph of hydroxyapatite synthesized after 2 weeks in DDAB microemulsions at the edge of the bicontinuous phase domain. Note the spherical mineral particles and the absence of a well-defined reticulated architecture. Scale bar, 0.2 μm.

Table 1. Mineralization of reticulated frameworks in bicontinuous microemulsions.

Alkane	Oil (%)	H_2O (%)	DDAB (%)	Storage temp. (°C)	Storage time (days)	Pore size (μm)	Wall size (nm)	Construction unit
C_{14} C_{16}	17 8	35	40	2	21	0.5 to 2.0	50 to 130	Single and bent crystal needles
C_{14}	45	30	25	2	14	0.1 to 2.5	100 to 250	Bundles of crystal needles
	25	50	25	2	14	0.1 to 5.0	100 to 250	
	15	60	25	2	14	0.1 to 8.0	100 to 250	
C_{12}	40	20	40	−25	21	0.04 to 0.7	50 to 130	Single-crystal needles
	55	30	15	−25	14	0.1 to 0.5	150	Spherical crystals
C_{14}	34	50	16 ($C_{12}E_5$)	46	3	0.05 to 1.0	—	Crystal plates

ture were observed with changes in composition. For example, at constant DDAB concentration (25 weight %) increases in the water to tetradecane ratio resulted in larger pore sizes and thicker walls composed of crystal bundles (Table 1). More striking changes in architecture were induced by the preparation of calcium phosphates from microemulsion compositions close to the edge of the single phase region (for example, 55 weight % C_{12}) (Table 1). Under these conditions, the mineralized material was composed of bead-like arrangements of interconnected spherical calcium phosphate particles (Fig. 2). This composition is consistent with the theoretical description of DDAB bicontinuous microemulsions containing alkane oils capable of penetrating the surfactant tails (*11*). In such systems, the rod-like water conduits begin to disconnect into spherical micelles before macroscopic phase separation (*11*).

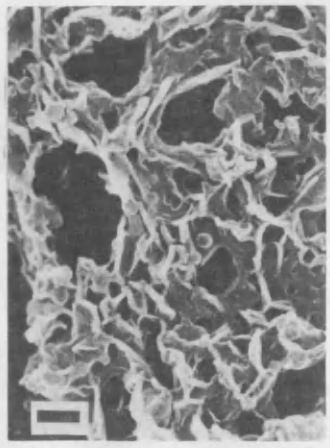

Fig. 3. Hydroxyapatite framework prepared in bicontinuous microemulsions containing the nonionic surfactant pentaethylene glycol dodecylether (46°C for 3 days). The architecture is based on the interlinking of hydroxyapatite sheets. Scale bar, 0.3 μm.

The ability to modify the reticulated inorganic microstructure by secondary changes in the architecture of the associated bicontinuous phase was borne out by the synthesis of calcium phosphate materials in the presence of bicontinuous reverse microemulsions containing the nonionic surfactant pentaethylene glycol dodecylether [$C_{12}H_{25}(OCH_2CH_2)_5OH$ or $C_{12}E_5$] (Table 1). Scanning electron micrographs (Fig. 3) showed the presence of a reticulated material consisting of a network of interconnected mineralized plates, in accordance with the envisaged lamellar structure of the associated bicontinuous microemulsion (*12*).

A striking feature of the reticulated microstructures is that the wall diameters (about 80 nm) are incommensurate with the 1-nm-diameter water channels considered to be present in bicontinuous microemulsions (*13*). Furthermore, the nanometer spacing between branches in the DDAB bicontinuous structure (*13*) is also inconsistent with the micrometer-sized pore diameters observed in the mineralized frameworks. To elucidate aspects of the growth mechanism that could be responsible for the construction of the macroporous inorganic frameworks, samples of a C_{14}-C_{16} microemulsion system stored at +2° (frozen oil) or +25°C (unfrozen oil) were removed at intervals, washed, and examined by electron microscopy. The unfrozen system, which was highly viscous, gave a reticulated material similar to that from the frozen oil medium except that it comprised straighter crystals and domains of extensive aggregation. In both cases, at the early stages of precipitation (2 to 6 hours at +2°C), filamentous strings of mineral particles approximately 1 nm in diameter were visible by TEM. These images suggested that the native bicontinuous microstructure was intact at this stage. However, these aggregates were not present after 4 to 6 days at +2°C but were replaced by needle-like crystals of HAP (100 to 500 nm in length) in association with 100-nm spherules of amorphous calcium phosphate. At first, the HAP crystals were discrete and unconnected, but further growth resulted in a loosely held interconnecting array of relatively straight needles (Fig. 4). The final stage of framework construction (2 to 3 weeks) was characterized by a continued lengthening and thickening of the crystalline units and an increased curvature of the mineral walls.

The results suggest that the nucleation of calcium phosphate is initially restricted to the interconnecting water conduits of the DDAB bicontinuous reverse microemulsion. However, the subsequent growth of mineral particles within the frozen oil medium appears to induce secondary

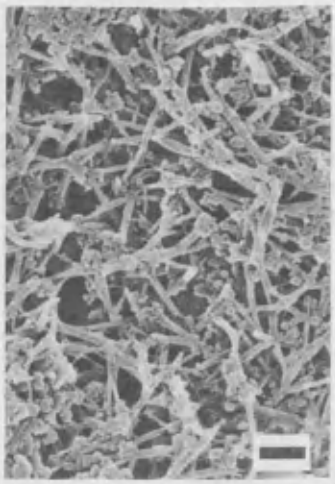

Fig. 4. Scanning electron micrograph of mineralized framework extracted from DDAB bicontinuous microemulsions at an early stage of construction (10 days at 2°C). Note the presence of hydroxyapatite needles and spherules of amorphous calcium phosphate as well as the partially formed reticulated microstructure. Scale bar, 0.5 μm.

changes at the surfactant-water interface. One possibility is that the growing crystals retain a hydration layer together with adsorbed surfactant such that there is a net migration of DDAB molecules toward sites of crystal growth. Therefore, the crystals would no longer be confined to the space delineated by the original water-filled conduits but reshape the microstructure through dynamic changes in the structure of the microemulsion. Although this seems a feasible mechanism in the viscous medium of the liquid oils, it is less obvious that such changes should be associated with microemulsions dispersed in frozen oil. One explanation is that oil molecules associated with the surfactant tails retain some local mobility, although the bulk molecules are frozen. With regard to the construction of the reticulated framework, this construction is probably facilitated by the needle-like morphology of the HAP crystals. This morphology serves to provide effective interlinking and interlocking of the architecture at relatively early stages of formation. Indeed, analogous experiments with CdS, which does not adopt an acicular habit, failed to produce macroporous materials.

Finally, reticulated biominerals, such as corals, have been exploited as biological implants because the macroporosity facilitates intergrowth, vasculization, and the resorption of calcified tissue (*14*). Although the pore size of the reticulated HAP material reported here is possibly too small to allow extensive vasculization, osteoclastic activity and biocompatibility could be expected. In addition, replication of the unperturbed nanoscale microstructure of the DDAB bicontinuous phase might be achieved by minimizing the crystallization forces inherent in systems comprising large crystals such as HAP. Further investigations involving this approach in the synthesis and crystal tectonics of nanoscale cluster materials (for example, CdS) and extended network structures of covalently linked materials (for example, aluminosilicates) are currently being conducted.

REFERENCES AND NOTES

1. S. Mann, *Nature* **365**, 499 (1993).
2. L. Addadi and S. Weiner, *Angew. Chem. Int. Ed. Eng.* **31**, 153 (1992); S. Mann, *J. Chem. Soc. Dalton Trans.* **1993**, 1 (1993).
3. S. Mann *et al.*, *Science* **261**, 1286 (1993), and references therein.
4. C. T. Kresge *et al.*, *Nature* **359**, 710 (1992); A. Monnier *et al.*, *Science* **261**, 1299 (1993).
5. The phase behavior and microstructure of disordered open connected bicontinuous microemulsions have been characterized in numerous studies involving conductivity [S. H. Chen *et al.*, *J. Phys. Chem.* **95**, 7427 (1991)], viscosity (F. D. Blum *et al.*, *ibid.* **89**, 711 (1985)], nuclear magnetic resonance spectroscopy [R. Skurveit *et al.*, *J. Colloid Interface Sci.* **152**, 205 (1992)], fluorescence (*11*), and small angle neutron [J. Eastoe *et al.*, *Langmuir* **8**, 1505 (1992)] or x-ray (T. N. Zemb *et al.*, *J. Phys. Chem.* **91**, 3814 (1987)] scattering measurements.
6. A metastable solution of calcium phosphate was prepared by the mixing of equal volumes of a 5.0 mM solution of calcium nitrate (or calcium chloride) with a 3.6 mM solution of potassium dihydrogen phosphate, and the pH was adjusted to 7.4 by 0.1 M NaOH. In the absence of a microemulsion phase, the onset of calcium phosphate precipitation from this solution occurred within 15 min at room temperature. In a typical experiment, 1.5 cm^3 of this solution was added dropwise to 2.5 cm^3 of a rapidly stirred oil-surfactant mixture at room temperature. Bicontinuous microemulsions formed from a range of oil-water-surfactant compositions were studied (Table 1). In each case, the formation of the bicontinuous phase was accompanied by the formation of an optically clear mixture. DDAB [$(C_{12}H_{25})_2(CH_3)_2NBr$] and the alkane oils dodecane ($C_{12}H_{26}$), tetradecane ($C_{14}H_{30}$), and hexadecane ($C_{16}H_{34}$) were obtained from Aldrich Chemical. The oils were filtered through 0.2-μm membranes before use.
7. Rapid cooling in liquid nitrogen was required to minimize phase changes in the microemulsion system that are known to occur between 5° and 15°C.
8. Freezing points are as follows: dodecane, −9.6°C; tetradecane, +5.9°C; hexadecane, +18.1°C. Mixtures of tetradecane and hexadecane were used (hexadecane does not form bicontinuous microemulsions because of poor penetration of the oil into the surfactant alkyl chains).
9. Bicontinuous microemulsions in dodecane, stored at −25°C, were soft in texture, indicating a supercooled aqueous phase.
10. A few milligrams of extensively washed and dried material was examined by x-ray diffraction with a Debye-Scherrer camera and CuK radiation. Infrared spectra of dried samples were studied with the use of KBr disks with a Nicolet Fourier transform-infrared spectrometer. Samples for scanning electron microscopy and transmission electron microscopy (TEM) were prepared by the mounting of small amounts of the mineralized material extracted after centrifugation and careful washing of the TEM grids with hot hexane followed by air drying. Samples observed by SEM were gold-coated and examined with a Jeol 1200EX electron microscope operating at 120 kV Transmission electron microscopy examination. was conducted with Jeol 1200EX and 2000FX electron microscopes operating at 120 and 200 kV, respectively.
11. V. Chen, G. C. Warr, D. F. Evans, F. G. Prendergast, *J. Phys. Chem.* **92**, 768 (1988).
12. U. Olsson, K. Shinoda, B. Lindman, *ibid.* **90**, 4083 (1986).
13. S. T. Hyde, B. W. Ninham, T. Zemb, *ibid.* **93**, 1464 (1989).
14. R. Holmes *et al.*, *Clin. Orthop.* **188**, 252 (1984).

15. We thank Unilever Research for financial support and T. Douglas for advice with experimental work concerning cadmium sulphide.

14 January 1994; accepted 25 April 1994

Table 2
Non-active additives tested

Additive	Structure
Polyvinyl alcohol	$[-CH_2CH(OH)-]_n$
Ethylene glycol	$HOCH_2CH_2OH$
2,5-hexanediol	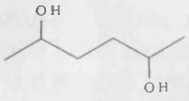
Acetonitrile	CH_3CN

precipitates prepared as KBr disks. X-ray powder diffraction patterns were recorded using a Debye–Scherrer camera and Cu Kα radiation.

3. Results

3.1. HAP crystallization in the presence of chloride

Samples prepared from $CaCl_2$ solutions were shown to be well-crystalline hydroxyapatite (HAP). X-ray diffraction data (not shown) gave *d*-spacings consistent with the hexagonal space group $P6_3/m$, with $a = 0.9432$ nm and $c = 0.6881$ nm [30]. Infrared spectra (fig. 1) were also characteristic of the hexagonal structure of HAP [31,32], showing PO_4^{3-} bands at 1030–1090, 605 and 565 cm^{-1}, and a OH stretch at 3570 $cm^{-1}$and a weak OH librational mode at 630 cm^{-1}. A CO_3^{2-} broad band at 1660–1370 cm^{-1} and bands at 870 and 704 cm^{-1} were also observed indicating that although the crystals were prepared under N_2, incorporation of carbonate (ca. 3 mol%) readily takes place during exposure of the crystals to atmospheric CO_2.

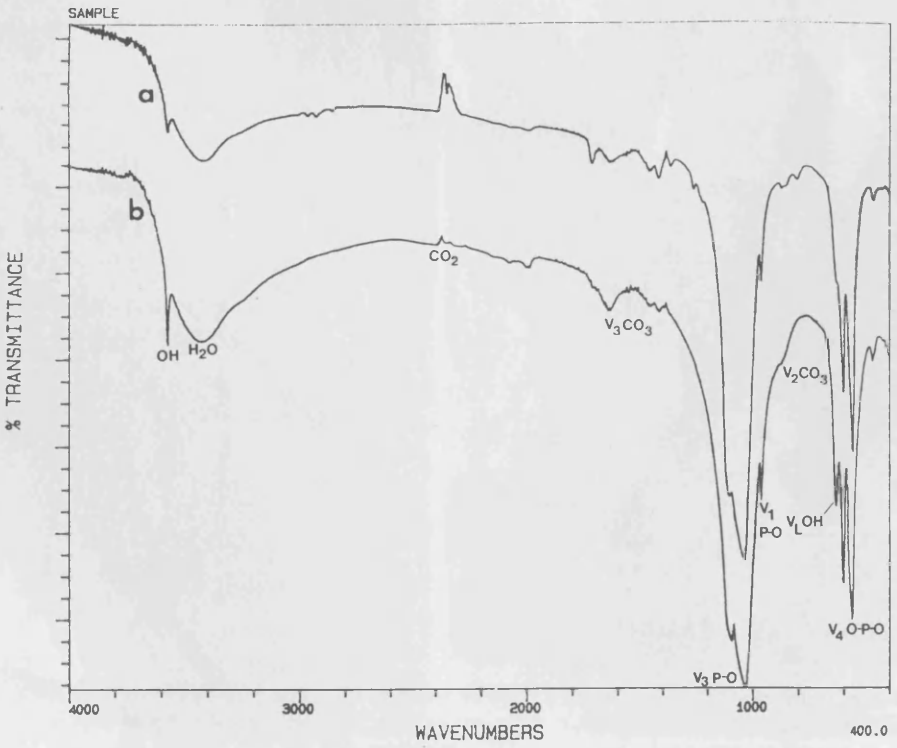

Fig. 1. Infra-red spectra of HAP: (a) precipitated with D-glucose, after reflux; (b) precipitated in absence of an additive, after reflux.

Electron micrographs of the HAP particles showed that the sample largely consisted of thin irregular plates of mean dimensions, length = 500 nm, width = 350 nm and thickness = 5 nm (fig. 2a). Electron diffraction studies indicated that the plate-like particles were single crystals of HAP with two well-developed (100) faces, consistent with previous reports of synthetic and biological HAP [33–37]. A small number of needle-shaped crystals were also observed.

3.2. HAP crystallization in the presence of chloride and additives

Addition of monosaccharides to the $CaCl_2$ reaction mixture had no influence on the crystal structure parameters of the HAP precipitated. X-ray diffraction patterns and infrared spectra (fig. 1) were essentially identical with the control sample. However, imaging of the particles by TEM revealed a dramatic morphological change in which the HAP plates of the control system were replaced by elongated needle-shaped crystals. At a P : D-glucose ratio of 6 : 1, the HAP crystals were generally discrete and longer (550–750 nm) than the plate-like control crystals (fig. 2b). The average aspect ratio was 10 : 1. This morphological effect was apparently optimized at a P : additive ratio of 6 : 1 since a lower concentration of glucose (P : additive = 60 : 1) was less effective, resulting in partially-elongated irregular plate-like crystals, and an increased level of glucose (P : additive = 0.6 : 1) gave ill-defined aggregates of elongated crystals.

Single crystal electron diffraction patterns of HAP were obtained from individual crystals

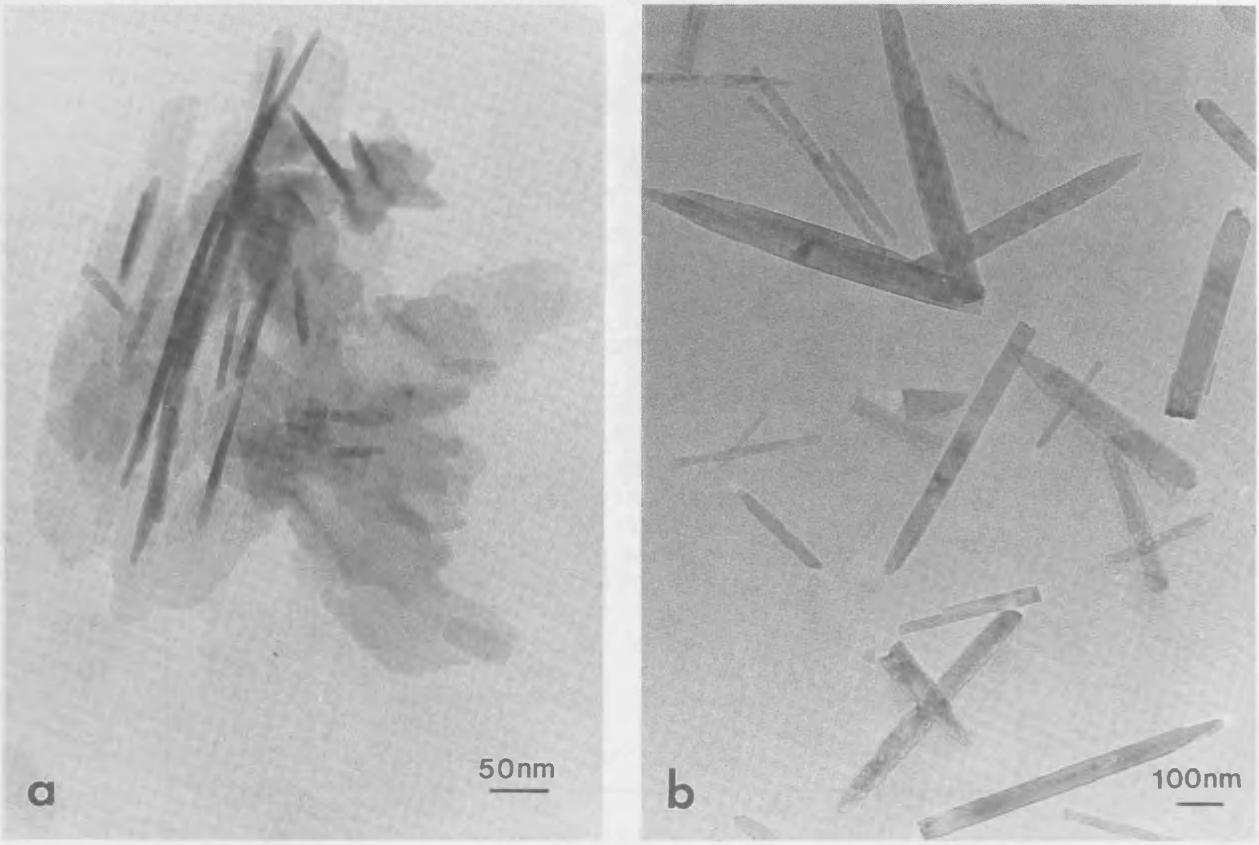

Fig. 2. TEM micrographs of HAP: (a) precipitated in the presence of chloride (note that the apparent needle-shaped crystals are the plate-like particles viewed edge on); (b) precipitated with D-glucose present at PO_4 : D-glucose ratio of 6 : 1.

grown in the presence of D-glucose (fig. 3a). The patterns indicated that the needle axis was parallel to the crystallographic c ([001]) direction of the hexagonal unit cell (fig. 3b). The cross-sectional morphology of the elongated crystals was determined by high resolution TEM of sectioned material. The crystals exhibited a hexagonal profile of six well-defined prismatic faces which were oriented parallel to lattice fringes of 0.82 nm spacing (fig. 3c). These results indicate that the HAP crystals grown in the presence of glucose were hexagonal prisms of {100} faces extensively elongated along the c axis. Many crystals were terminated at one end by a smooth flat edge whilst the other end was noticeably rounded. As this is inconsistent with the centrosymmetric hexagonal space group of HAP, the asymmetry probably originates from the fracturing of individ-

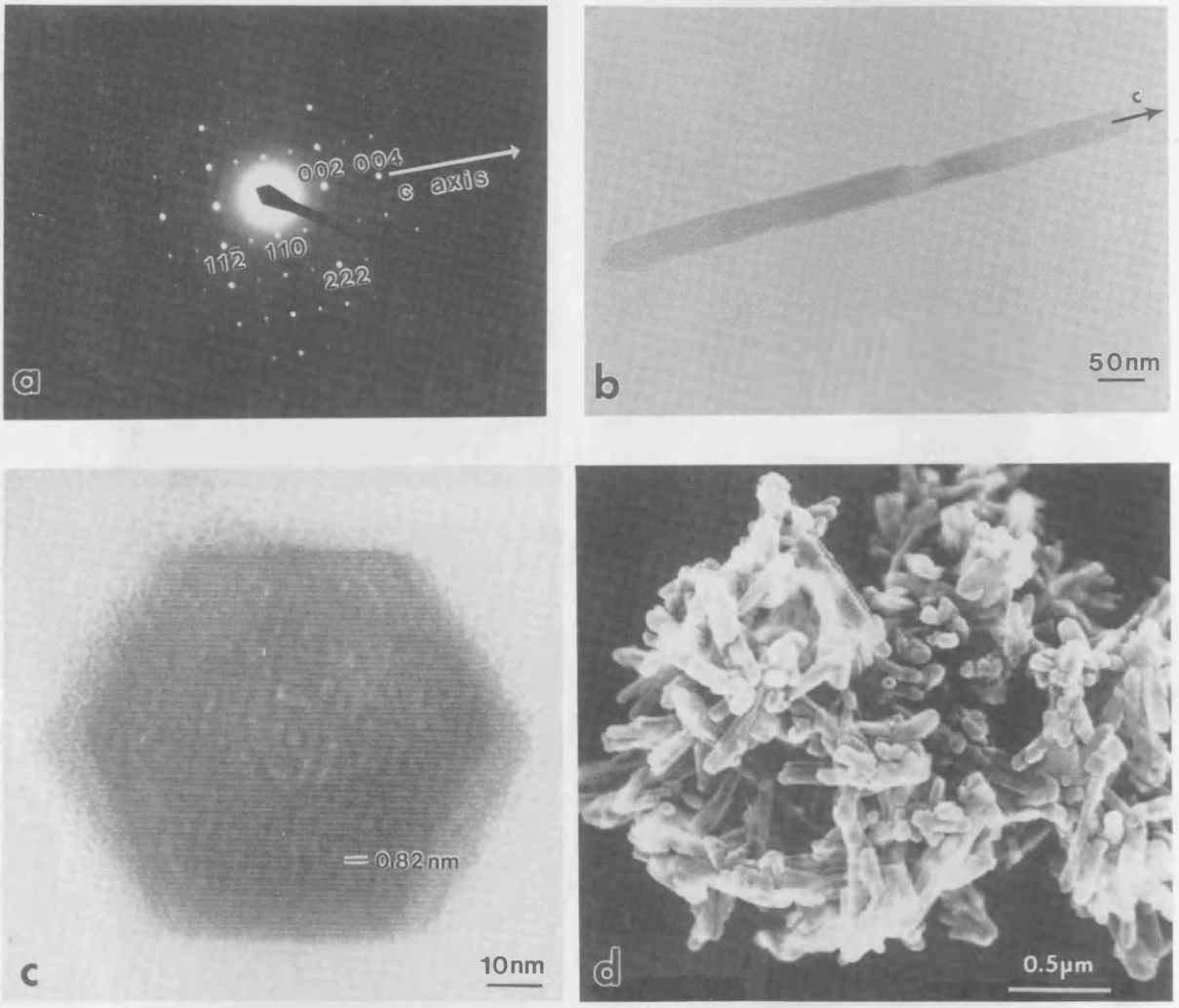

Fig. 3. (a) Single crystal electron diffraction pattern of needle-like HAP crystal (see (b)) formed with D-glucose. The pattern corresponds to the $[1\bar{1}0]$ zone of the hexagonal unit cell; the direction of the c axis is marked; (b) TEM micrograph of needle-like HAP crystal showing elongation along c axis; (c) high resolution TEM micrograph of the cross-section of an elongated crystal showing well defined hexagonal profile of {100} faces and {100} lattice spacings (0.82 nm); (d) SEM micrograph of HAP crystals precipitated with D-glucose.

ual needles present in larger aggregates due to sample preparation. Indeed, dentritic aggregates were often observed by scanning electron microscopy (fig. 3d).

Experiments involving other monosaccharides indicated that the above morphological effects were generic to this class of compounds. Crystallization in the presence of stereoisomers (epimers) of D-glucose, such as D-galactose and D-mannose, which differ in configuration at a single asymmetric carbon centre (C-4 and C-2, respectively), resulted in needle-like HAP single-crystals of similar size distribution as observed in the glucose-containing experiments (fig. 4a). Func-

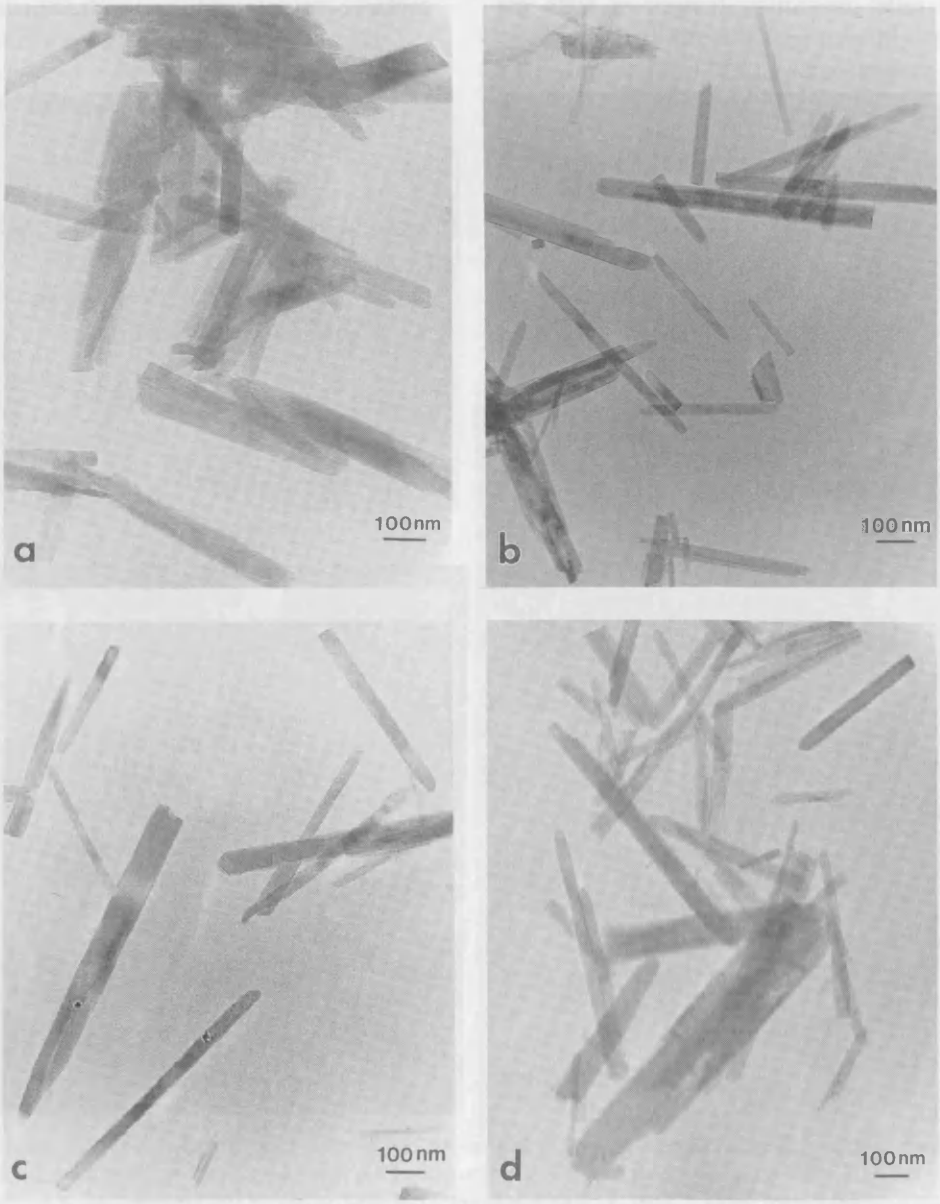

Fig. 4. TEM micrographs of HAP precipitated with monosaccharide additives (at PO_4:additive of 6:1): (a) D-galactose; (b) glucuronic acid; (c) N-acetylglucosamine; (d) fructose.

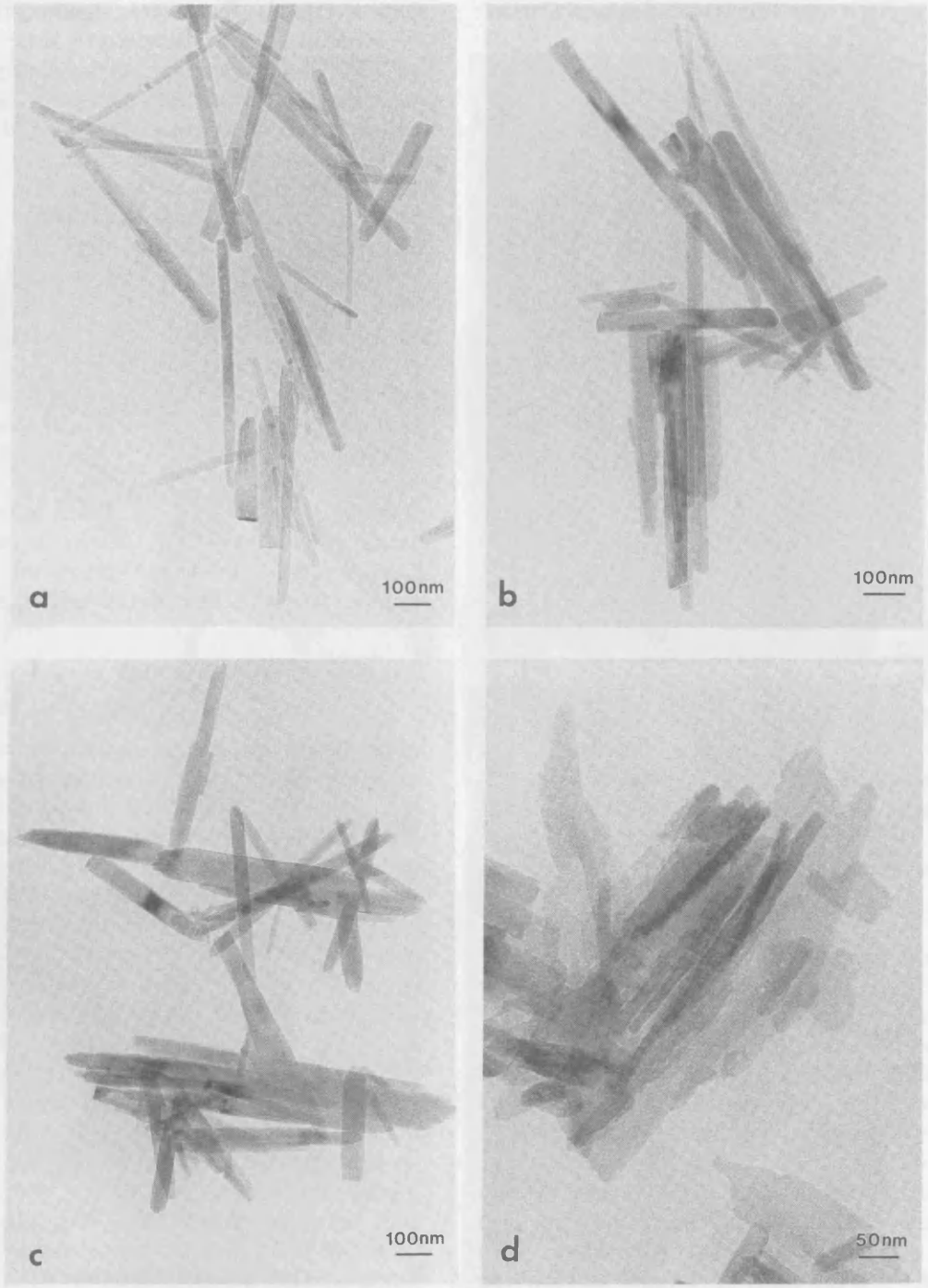

Fig. 5. TEM micrographs of HAP precipitated with non-monosaccharide additives: (a) sorbitol; (b) 1,2-butanediol; (c) ascorbic acid; (d) 2,5-hexanediol.

tionalized derivatives of D-glucose, viz.glucuronic acid and N-acetyl glucosamine, also gave similar results (figs. 4b and 4c). Interestingly, the most effective monosaccharide studied was the keto-hexose, D-fructose, which resulted in needle-shaped crystals that were significantly longer

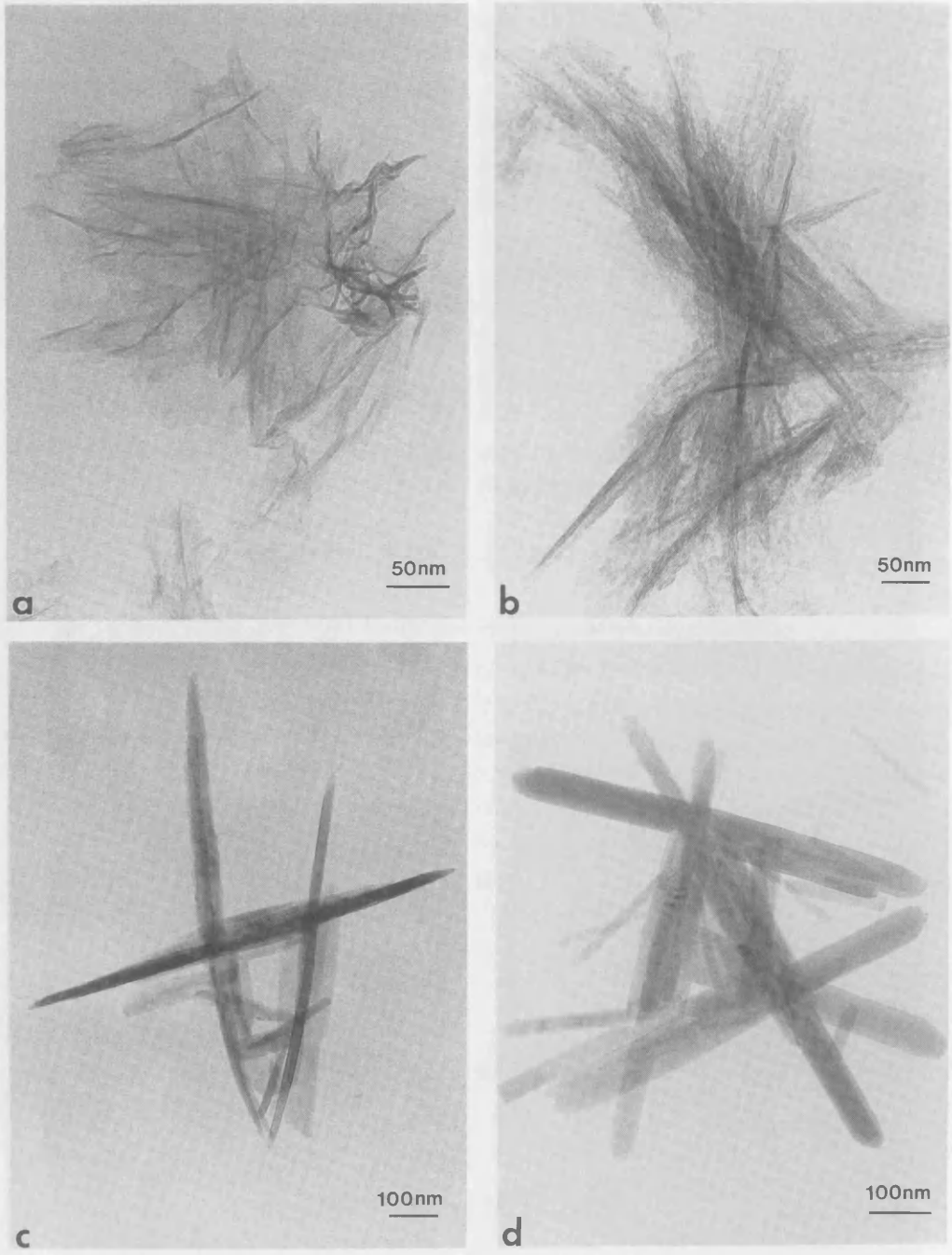

Fig. 6. TEM micrographs of samples removed at intervals from HAP precipitated in the presence of D-glucose: (a) 30 s; (b) 4 min; (c) 10 min; (d) 100 min.

(700–900 nm) and had a higher average aspect ratio (20:1) than the corresponding hexoaldose additives (fig. 4d).

The general importance of the presence of hydroxyl groups in the additives was verified by experiments involving non-sugar additives. Sorbitol, which is an open chain molecule containing six OH groups, produced needle-like crystals that were similar in length (700–950 nm) to the crystals grown in the presence of fructose, but with a higher average aspect ratio (25:1) (fig. 5a). The linear diol, 1,2-butanediol, was similar in potency to sorbitol (fig. 5b) whereas the cyclic molecules, 1,2-cyclohexanediol and 1,3-cyclohexanediol, were less effective than the hexoaldose additives. Ascorbic acid, which contains two adjacent –OH groups connected by a C=C double bond, was less effective than sorbitol, 1,2-butanediol or fructose but similar in activity to the hexoaldoses (fig. 5c). Modifications in the spacing between hydroxyl groups had a significant effect for the linear molecules, for example, 2,5-hexanediol was inactive in producing needle-shaped HAP crystals (fig. 5d).

3.3. Development of HAP crystals in the presence of D-glucose

Electron microscopy studies of HAP crystals, removed at various time intervals from the reaction mixture containing glucose, indicated that the needle-like habit was established in the first few minutes after addition of only 3–5 cm^3 of aqueous $CaCl_2$. After 30 s, spherical particles of amorphous calcium phosphate and sheet-like gel structures of crystalline HAP were observed (fig. 6a). At 4 min, the gel-like structures had transformed into regular elongated HAP crystals of pronounced striated texture consisting of linear arrays of nanometer-size spherical domains (fig. 6b). These particles subsequently developed within 10–15 min after the start of the reaction into smooth-edged filamentous HAP crystals (fig. 6c) which were comparable in maximum length but not width with fully mature particles. The remaining stages of the reaction (20–100 min) were associated with a progressive increase in the width and thickness of the filamentous crystals (fig. 6d).

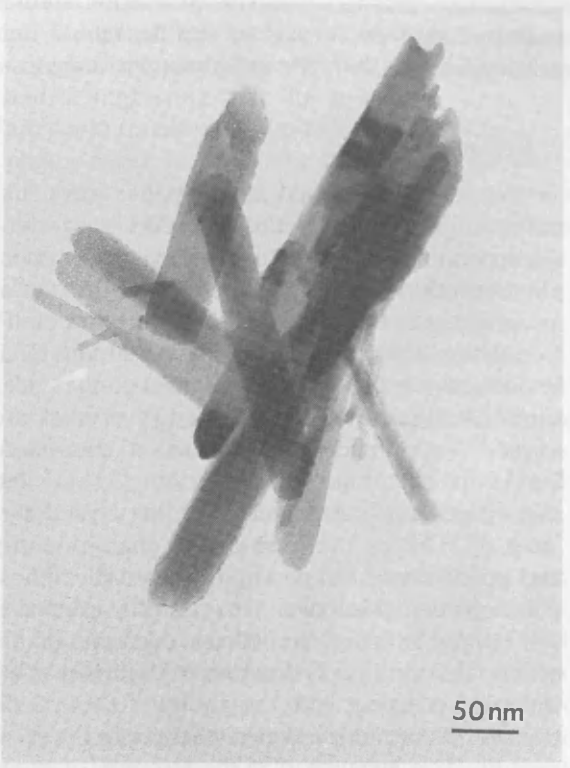

Fig. 7. TEM micrograph of needle-like HAP crystals precipitated in the presence of nitrate.

X-ray diffraction and infrared spectroscopy of samples taken for analysis at various time intervals indicated only the presence of HAP. Minor phases, such as octacalcium phosphate, could not be detected below 5 wt%.

3.4. HAP crystallization in the presence of nitrate

In order to elucidate the role of the above additives on HAP crystallization in the presence of chloride, control experiments were undertaken in calcium nitrate solution. X-ray diffraction patterns and infrared spectra were essentially identical to HAP precipitated in the presence of chloride. However, unlike the chloride-derived crystals, the nitrate-containing solution produced HAP crystals that were needle-like (fig. 7). In general, the lengths of these crystals (350–550 nm) and average aspect ratio (9:1) were reduced compared with those formed in the glucose-con-

taining experiments. Electron diffraction studies indicated that the *c* axis of the hexagonal unit cell was aligned with the morphological long axis.

4. Discussion

The results presented in this paper show that the introduction of monosaccharides into chloride-containing supersaturated calcium phosphate solutions dramatically influences the crystal morphology of the hexagonal polymorph of HAP. Interaction of the monosaccharides with the HAP lattice restricts growth perpendicular to the *c* axis such that thin hexagonal needle-like crystals are formed. Sugar molecules are known to coordinate Ca^{2+} ions in various configurations [39–41] and this effect could be enhanced at the crystal surfaces of HAP by the high spatial charge density and possibility of H-bonding to the surface phosphate groups. Moreover, the stability constants for Ca polyhydroxyl complexes decrease in the order, D-sorbitol > D-fructose > D-glucose [38], which is consistent with the ability of these additives to induce morphological changes in the HAP crystals. This suggests that the strength of interaction with surface Ca ions could be an important factor in determining the size and aspect ratio of the needle-like crystals formed from chloride-containing solutions

The expression of well-defined HAP {100} faces in the presence of sugar molecules could indicate some selectivity in surface binding. However, these surfaces are also stable in the absence of additives, implying that kinetic rather than structural factors could be responsible for the adoption of the hexagonal needle-like morphology. This is borne out by the fact that changes in structure (ring verses open-chain), stereochemistry or functionalization often had negligible effect, suggesting that the extent of molecular recognition present at the crystal/additive interface is limited to multiple polar interactions involving cooperative binding of hydroxyl residues. In this regard, the increased morphological efficacy of sorbitol can be attributed to the presence of six hydroxyls. However, 1,2-butanediol was equally effective suggesting that the 1,2-diol moiety of a linear molecule interacts strongly with the crystal surfaces. This group is less effective when present in a cyclic molecule, possibly due to increased steric hindrance arising from the ring conformation. This may explain why fructose was more effective than the hexaldoses since the greater conformational flexibility of the envelope form of the furanose ring, as compared with that of the $^4C_1$ chair form of the β–D-glucopyranose ring, would reduce the degree of steric hindrance associated with additive adsorption.

Further support for a general kinetic, rather than structural mechanism for the modification of HAP crystallization in the presence of monosaccharides, is indicated by the formation of needle-like crystals in the presence of nitrate-containing solutions. Although these crystals were not as elongated as the additive-grown samples, their presence clearly indicates the important role of Cl^- in promoting the plate-like morphology of HAP. Thus, it appears that the efficacy of the polyhydroxyl additives in inducing high axial ratio crystals is dependent on their ability to override the effect of Cl^-. The morphological influence of Cl^- has been previously observed [20] and can be attributed to surface incorporation at defect sites. More information is required to elucidate how these interactions give rise to a plate-shaped crystal consisting of only two of the possible six symmetry-related {100} faces. The supersaturation conditions appear to be important since we have observed (unpublished data) that a slow continuous dropwise addition of aqueous $CaCl_2$ to a phosphate solution at 70°C, rather than the pulse addition used above, results in needle-like and not plate-like HAP crystals. We suggest that the effect of Cl^- involves a dynamic exchange at the surface of the amorphous calcium phosphate (ACP) that exists transiently upon each pulse addition. The localized disruption due to Cl^- incorporation into the ACP surface could possibly increase the local supersaturation by increasing the solubility of the precursor phase. This could kinetically favour the nucleation of thin plates of octacalcium phosphate (OCP) which serve as templates for HAP overgrowth. In this regard, polyhydroxyl additives could bind strongly to the surfaces of the incipient ACP phase, thereby excluding Cl^- from surface sites and

inhibiting the OCP plate-like precursor. Nucleation of HAP would then be followed by a normal growth pattern involving preferential elongation along the *c* axis and expression of six {100} faces, as predicted by theoretical considerations [38]. Moreover, differences in the lability of Ca–sugar complexes [39] could account for the variations observed in the aspect ratios of HAP crystals grown in the presence of different additives due to changes in the affinity of polyhydroxyl additives at the developing crystal surfaces.

A further possibility is that the observed differences in morphological potency could be due to differences in the thermal and chemical stability of the additives at 70°C and pH 9.3–9.8. For example, α and β anomers, epimers, fructose, open-chain structures, dissaccharides, polysaccharides and a variety of saccharinic acids are known to coexist in alkaline glucose solutions [42,43]. Indeed, NMR spectra of solutions of monosaccharides subjected to our reaction conditions were invariably complex (data not shown). Further work is in progress to elucidate the nature of these species but it seems likely that many open chain polyhydroxyl derivatives (such as sorbitol) will produce HAP crystals extensively elongated along the *c* axis.

In order to circumvent the problems associated with high temperature, we undertook a series of analogous experiments in which HAP crystals were grown in the presence of monosaccharides but at 40°C. In all cases, plate-like HAP crystals were observed and no morphological effects were apparent (unpublished observations). These results suggest that the rapid transformation of the initial gel-like precipitate into filamentous HAP crystals (fig. 6) is kinetically inhibited at lower temperature. Presumably, adsorption of sugar molecules onto the primary precipitate can stabilize this phase unless sufficient thermal energy is provided to overcome the activation energy barriers associated with desorption and subsequent crystal growth in the presence of the additives. This could explain why P : additive ratios lower than 6 : 1 were not as selective in producing the needle-like habit at 70°C, since an increased sugar concentration could stabilize the initial gel by extensive surface adsorption.

The first stage in the transformation of the gel-like structures involves the formation of linear arrays of spherical domains within the ill-defined matrix suggesting that this process is essentially an in situ transformation within the calcium phosphate/sugar network. The subsequent rapid crystal growth along the *c* axis could be a consequence of both chemical and physical properties of the surrounding gel matrix. Growth perpendicular to the c axis becomes more pronounced as the reaction proceeds possibly because of increasing thermal degradation and transformation of the sugar molecules. Indeed, we have observed that the continuous addition of monosaccharide solutions to the reaction medium results in increased *c*-axis elongation of the HAP crystals compared with those in the above experiments (unpublished observations).

Finally, we note that the observations presented in this paper may have significance in the field of biological calcification. Although the HAP crystals were grown under conditions far-removed from the physiological environment, there are striking similarities between the crystals produced in the presence of chloride and bone mineral, and the sugar-induced needle-shaped crystals and enamel HAP. Whilst we accept that the presence of spatially-delineating organic structures could be responsible for extreme c axis elongation of enamel crystals, we postulate that the covalently-bound polysaccharide residues of the acidic enamelin proteins could act in a similar manner to the monosaccharides used in the above experiments. Moreover, the combination of polyhydroxyl and negatively charged glutamate and aspartate residues of enamelins might have a role in chloride exclusion from developing tooth enamel and augment the growth of needle-shaped HAP crystals under conditions of physiological temperature and pH.

Acknowledgements

This study was supported in part by Unilever Research, Port Sunlight, UK. We thank Drs. S. Carr and A. Waller (Unilever Research Labora-

tories) for helpful discussions and Miss S. Peters for assistance in the preparation of sections.

References

[1] A. Bigi, L. Campostella, A.M. Fichera, E. Foresti, M. Gazzano, A. Ripamonti and N. Roveri, J. Inorg. Biochem. 34 (1988) 75.
[2] S.V. Chiranjeevirao, J. Heemmerle, J.C. Voegel and R.M. Frank, Inorg. Chim. Acta 67 (1982) 183.
[3] R.Z. LeGeros, Progr. Crystal Growth Characterization 4 (1981) 1.
[4] J.C. Elliot, Clin. Orthop. 93 (1973) 313.
[5] A.S. Posner, Physiol. Rev. 49 (1969) 760.
[6] C.A. Baud, S. Bangs and J.M. Very, J. Buccale 5 (1975) 105.
[7] J.C. Eanes, J. Dental Res. 58 (1973) 829.
[8] H. Fleisch and S. Bisaz, Am. J. Physiol. 203 (1962) 671.
[9] A. Bigi, G. Falini, E. Foresti, M. Gazzano, A. Ripamonti and N. Roveri, J. Inorg. Biochem. 49 (1993) 69.
[10] R.Z. LeGeros, Science 155 (1967) 1409.
[11] P.G. Werness, J.R Bergert and K.E. Lee, Clin. Sci. 61 (1981) 487.
[12] M.D. Francis, W.W. Briner and J.A. Gray, in: Hard Tissue Growth, Repair and Remineralization, Eds. R.F. Sognnanes and J.M. Vaughn (Elsevier, Amsterdam, 1973).
[13] E.C. Moreno and K. Varoghese, J. Crystal Growth 53 (1981) 20.
[14] J. Garnett and P. Dieppe, Biochem. J. 266 (1990) 863.
[15] C.C Chen, A.L. Boskey and L.C. Rosenberg, Calcif. Tissue Intern. 36 (1984) 285.
[16] D.D. Dziewiatkowski, Calcif. Tissue Intern. 40 (1987) 265.
[17] G.K. Hunter, M.D. Grynpas, P.T. Cheng and K.P.H. Pritzker, Calcif. Tissue Intern. 41 (1987) 164.
[18] R.W. Romberg, P.G. Werness, B. Riggs and K.G. Mann, Biochemistry 25 (1986) 1176.
[19] M.R. Christoffersen and J. Christoffersen, Calcif. Tissue Intern. 36 (1984) 659.
[20] P.G. Koutsoukos and G.H. Nancollas, J. Crystal Growth 55 (1981) 369.
[21] M. Okazaki, Biomaterials 13 (1992) 749.
[22] R.Z. LeGeros, J.P. LeGeros, O.R. Trautz and W.P. Slurra, Advan. X-Ray Anal. 14 (1971) 57.
[23] G.H. Nancollas and P.G. Koutsoukos, Colloids and Surfaces 17 (1986) 361.
[24] G.H. Nancollas, P.G. Koutsoukos, J. Am. Chem.Soc. 85 (1981) 2403.
[25] H.A. Lowenstam and S. Weiner, On Biomineralization (Oxford University Press, Oxford, 1989).
[26] A. Tiselius, S. Hjerten and O. Levin, Arch. Biochem. Biophys. 65 (1956) 132.
[27] G. Bernardi in: Methods in Enzymology. Vol. 21, Eds. L. Grossman and K. Moldave (Academic Press, New York, 1971) p. 95.
[28] S. Hjerten, Biochem. Biophys. Acta 31 (1959) 216.
[29] A. Makishima and H. Aoka, in: Bioceramics, Eds. T. Yamaguchi and H. Yamagida (Gihodo, Tokyo, 1984).
[30] A.S. Posner, A. Perloff and A.F. Diorio, Acta Cryst. 11 (1958) 308.
[31] D.G.A. Nelson and J.D.B. Featherstone, Calcif. Tissue Intern. 34 (1982) S69.
[32] B.O. Fowler, E.C. Moreno and W.E. Brown, Arch. Oral Biol. 11 (1966) 477.
[33] K. Selvig, Calcif. Tissue Res. 6 (1970) 227.
[34] J. Moradian-Oldak, S. Weiner, L. Addadi, W.J. Landis and W. Traub, Connect. Tissue Res. 25 (1991) 219.
[35] E.F. Bres, J.C. Barry and J.L. Hutchison, J. Ultrastruct. Res. 90 (1985) 261.
[36] F. Cuisinier, E.F. Bres, J. Heinmerle, J.C. Voegel and R.M. Frank, Calcif. Tissue Intern. 40 (1987) 332.
[37] B.R. Heywood, N.H.C. Sparks, R.P. Shellis, S. Weiner and S. Mann, Connect. Tissue Res. 25 (1990) 1.
[38] R.A. Terpstra, P. Bennema, P. Hartmann, C.F. Woensdregt, W.G. Perdok and M.L. Senechal, J. Crystal Growth 78 (1986) 468.
[39] K.K. Makinen and E. Soderling, Calcif. Tissue Intern. 36 (1984) 64.
[40] W.J. Cook and C.E. Bugg, J. Am. Chem. Soc. 95 (1973) 19.
[41] W.J. Cook and C.E. Bugg, Biochim. Biophys. Acta 389 (1975) 428.
[42] S.J. Angyal, Australian J. Chem. 25 (1972) 1957.
[43] L. Hough and A.C. Richardson, in: Comprehensive Organic Chemistry, Eds. D. Barton and W.D. Ollis (Pergamon, Oxford, 1979) pp. 687–748.
[44] G. Machell and G.N. Richards, J. Chem. Soc (1960) 1924.

REPRINTED FROM:

JOURNAL OF

CRYSTAL GROWTH

Journal of Crystal Growth 133 (1993) 1–12
North-Holland

Influence of monosaccharides and related molecules on the morphology of hydroxyapatite

Dominic Walsh, Joanne L. Kingston, Brigid R. Heywood [1] and Stephen Mann [2]
School of Chemistry, University of Bath, Bath BA2 7AY, UK

Received 22 May 1993; manuscript received in final form 6 July 1993

NORTH-HOLLAND

US mailing notice – Journal of Crystal Growth (ISSN 0022-0248) is published monthly by Elsevier Science Publishers, Molenwerf 1, P.O. Box 211, 1000 AE Amsterdam, Netherlands. Annual subscription price in the USA is US $4774 (subject to change), including air speed delivery. Second class postage paid at Jamaica NY 11431.

USA POSTMASTERS: Send address changes to Journal of Crystal Growth, Publications Expediting, Inc., 200 Meacham Avenue, Elmont NY 11003. Airfreight and mailing in the USA by Publications Expediting.

PUBLISHED MONTHLY | Library of Congress Catalog Card Number 68-26537 | PRINTED IN THE NETHERLANDS

Journal of Crystal Growth 133 (1993) 1–12
North-Holland

JOURNAL OF CRYSTAL GROWTH

Influence of monosaccharides and related molecules on the morphology of hydroxyapatite

Dominic Walsh, Joanne L. Kingston, Brigid R. Heywood [1] and Stephen Mann [2]
School of Chemistry, University of Bath, Bath BA2 7AY, UK

Received 22 May 1993; manuscript received in final form 6 July 1993

The influence of monosaccharides and related molecules on the crystal morphology of hydroxyapatite (HAP) precipitated from chloride-containing supersaturated solutions has been studied by transmission electron microscopy. Pulse addition of aliquots of $CaCl_2$ to Na_2HPO_4 solutions resulted in the formation of plate-like HAP crystals. In contrast, the presence of the monosaccharides D-glucose, D-galactose, D-mannose, glucuronic acid, N-acetyl glucosamine and D-fructose (phosphate:additive = 6:1) induced the precipitation of needle-shaped HAP crystals elongated along the *c*-axis. Other molecules, such as sorbitol and 1,2-butanediol, also showed this morphological effect. The order of decreasing aspect ratios was; sorbitol = 1,2-butanediol (25:1) > fructose (20:1) > glucose = galactose = mannose = glucuronic acid = N-acetyl glucosamine (10:1). Expression of the needle-like morphology is discussed in terms of kinetic factors involving nucleation and growth. The former is dependent on the exclusion of Cl^- from HAP nuclei due to additive interactions with an amorphous calcium phosphate precursor phase. The latter is related to the strength of additive binding with the subsequent development of {100} HAP crystal faces.

1. Introduction

Bone, enamel, dentine and cementum consist of a mineral phase that closely resembles hydroxyapatite ($Ca_{10}(PO_4)_6(OH)_2$, HAP) together with an assemblage of organic macromolecules. Biogenic hydroxyapatites are often associated with a wide variety of trace constituents such as Mg^{2+} [1,2] Na^+, CO_3^{2-}, and Cl^- [3], Sr^{2+} [4,5], F^- [6,7], and $P_2O_7^{4-}$ [8], and are therefore both structurally and compositionally complex materials. Some of these ions can enter the crystal lattice whilst others remain adsorbed only at surface sites. The presence of extraneous ions may play an important role in determining the nucleation, crystal growth, morphology, aggregation, ion-exchange, adsorption and dissolution properties of biological and synthetic HAP.

A number of kinetic studies of HAP crystal growth in the absence and presence of additives such as Mg^{2+} [9], CO_3^{2-} [10], citrate [11], pyrophosphate [12], polyphosphates and polyphosphonates [13], albumin [14], proteoglycans [15,16], glycosaminoglycans [17], oesteocalcin and osteonectin [18] and ATP [19] have been reported. In contrast, few studies have been undertaken on the effect of soluble additives on the crystal morphology of HAP. Inorganic ions such as Cl^- [20], F^- [21], CO_3^{2-} [22], Li^+ [23] and Sr^{2+} [24] have been shown to produce morphological effects but there are few counterpart studies involving organic additives. This is surprising since the morphology of HAP can be significantly different in contrasting biological tissues such as bone (plate-like) and enamel (needle-like hexagonal prisms) [25]. Moreover, many of the properties of synthetic HAP will be influenced by crystal size, shape and surface area, and the ability to tailor these characteristics could be relevant to the use of HAP in chromatography, catalysis and ion-exchange [26–28], orthopaedics and dentistry [29].

[1] Present address: Department of Chemistry, University of Salford, Salford M5 4WT, UK.
[2] Author to whom correspondence should be addressed.

In this paper, we describe the influence of monosaccharides and related molecules on the crystal morphology of HAP grown from chloride-containing solutions. Although these additives are not directly relevant to biological systems, we note that extensively glycosylated molecules such as proteoglycans and glycosoaminoglycans are considered to play important roles in the regulation of bone and cartilage calcification processes.

2. Materials and methods

Hydroxyapatite was prepared under N_2 at 70°C by the pulse addition of 100 cm^3 (3.5 cm^3 aliquots at 4 min intervals) of either 0.1M $CaCl_2$ or 0.1M $Ca(NO_3)_2$ to 100 cm^3 of 0.06M Na_2HPO_4. The reaction mixture was stirred continuously and maintained at pH 9.3–9.8 by the addition of small quantities of 1.5M NaOH. After ca. 120 min the mixture was allowed to cool, and the white precipitate filtered and washed several times with distilled water to remove residual anions. The sample was then washed with acetone, dried under vacuum and oven dried at 80°C. The precipitates were stored at room temperature in vials under N_2.

The above procedure was repeated except that a known weight of the additive was dissolved in the Na_2HPO_4 solution prior to addition of aqueous $CaCl_2$. Unless stated otherwise, all experiments were performed at total phosphate : additive mole ratios of 6 : 1. The additives used are listed in tables 1 and 2. In some experiments involving D-glucose, crystals were removed at various time intervals during the reaction and examined by transmission electron microscopy (TEM).

Samples for electron microscopy were prepared by air-drying a drop of a sonicated suspension of the dried precipitate in ethanol onto carbon-coated, Formvar-covered copper electron microscope grids. The samples were characterized by bright field imaging, selected area electron diffraction (SAED) and energy dispersive X-ray analysis (EDXA). Samples were dried onto a copper mount and gold coated for scanning electron microscopy (SEM). A small quantity of the crystals was embedded in 100% TAAB premix resin and polymerized at 60°C for 24 h. Thin sections (60–100 nm) were cut using a diamond blade and mounted onto carbon-coated mesh grids for TEM examination. Fourier transform infrared spectroscopy was performed on dried

Table 1
Additives that promote needlelike HAP crystals

Additive	Structure
D- Glucose	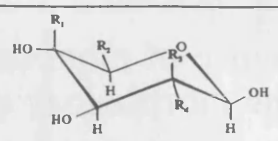 R_1=H, R_2=CH_2OH, R_3=H, R_4=OH
D(+)-Galactose	R_1=OH, R_2=CH_2OH, R_3=H, R_4=OH
D(+)-Mannose	R_1=H, R_2=CH_2OH, R_3=OH, R_4=H
D- Glucuronic acid	R_1=H, R_2=COOH, R_3=H, R_4=OH
N-acetyl glucosamine	R_1=H, R_2=CH_2OH, R_3=H, R_4=$NHCOCH_3$
Glucose-6-phosphate	R_1=H, R_2=$CH_2PO_4^{2-}$, R_3=H, R_4=OH
Glucose-6-sulphate	R_1=H, R_2=$CH_2SO_4^{1-}$, R_3=H, R_4=OH
D(-)-fructose	R_1=H, R_2=OH, R_3=OH, R_4=H + 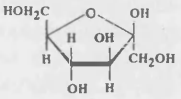
Ascorbic acid	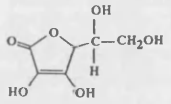
Sorbitol	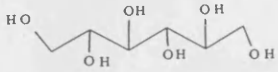
1,2-butanediol	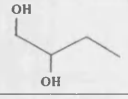
1,2-cyclohexanediol	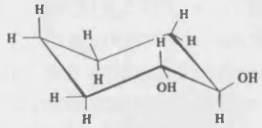
1,3 cis/trans cyclohexanediol